Molecular analysis of the Ccr4-Not Deadenylase: relevance to human disease

Blessing Airhihen

Thesis submitted to the University of Nottingham for the degree of Doctor of Philosophy

June 2017

Abstract

In eukaryotes, the removal of the poly (A) tail of cytoplasmic mRNA (deadenylation) is a crucial step in post-transcriptional gene regulation. A major enzyme involved in regulated mRNA deadenylation is the Ccr4-Not deadenylase, which contains two catalytic subunits: the Caf1 and Ccr4 ribonucleases. For both enzymes, two Mg^{2+} ions are required in the active site for activity. These enzymes in addition to six other non-catalytic subunits of the Ccr4-Not complex are possible drug targets in diseases such as metastatic cancer, osteoporosis and obesity. To facilitate the discovery, development and characterisation of small drug-like inhibitors of these enzymes, a biochemical approach was used. First, we investigated the biochemical characteristics of the highly similar CNOT6 and CNOT6L enzymes. Next, we evaluated two biochemical assays for characterisation of Ccr4-Not catalytic subunits and evaluation of *N*-hydroxyimide inhibitors of CNOT7. A chemiluminescence-based detection assay of AMP was used as the basis of a method and thermal shift assays were also used to characterize binding of compounds to deadenylase enzymes. In addition, cell based assays were used to study interactions between BTG2 variants and CNOT7 and CNOT8 in lymphoma.

Our findings demonstrate that the CNOT6 and CNOT6L though highly similar, display different biochemical characteristics *in vitro*. The deadenylase activity of CNOT6 was higher compared to CNOT6L. The results also indicate that AMP detection is a highly sensitive assay that can be used as a secondary assay to the previously developed substrate-based assay for compound screening and IC_{50} determination. We conclude that thermal shift assays can be used to determine the binding mode of inhibitory compounds, specifically regarding the presence of the Mg^{2+} ions in the active site. Finally, we identified BTG2 variants that potentially regulate mRNA abundance in lymphoma via interaction with the Ccr4-Not deadenylase.

Acknowledgements

I would like to thank my supervisor, Dr Sebastiaan Winkler for the guidance, training, and continuing support to enable me complete my PhD. I would also like to thank all past and present members of the Winkler lab for their contributions at different stages of my study. I thank Dr Loyin Olotu-Umoren and Dr Ishwinder Kaur for their immense support and sign posting during my PhD. I would like to appreciate Dr Maryati for the nice collaboration especially during the characterisation of the Ccr4-Not Deadenylase and screening of compound inhibitors of CNOT7. I also thank Dr Maryati for the gift of plasmids used for expression of the trimeric nuclease complex. I would like to appreciate Ben, Dario and Hibah for the yeast-two hybrid CNOT7 data. Many thanks to Lorenzo for the kind support and help to surmount challenges especially with the final set of experiments.

I would like to thank Prof. David Heery, Dr Cornelia and all members of the Gene regulation and RNA Biology group for their support through my work. I thank Bismoy, Johnny, Lin and Cintia for being so helpful. The laughter and support in various ways are much appreciated. I thank Hilary, Masar, Patrick, Aimee and Sadaf for all the support. I appreciate Barbara for all the kindness and support which will be truly missed. I would like to appreciate the Schlumberger foundation for funding my PhD, for bringing out the best in me and making my dreams a reality. I also thank the Niger Delta University, friends and colleagues for their support. Prof Lanre, Lucky Nwidu, Vaikosen amongst others.

Finally, I sincerely thank my numerous friends and family members who have constantly stood by me in various ways. I would like to thank my mum and mother-in law for being an anchor. I thank my siblings and inlaws. Most importantly I appreciate my husband Ewere Airhihen, my children Efesombia and Samuel. We have weathered every storm through the past four years. I am convinced there is nothing we can't achieve together. The best is yet to come.

Table of Contents

List of Figures

Chapter 1

Chapter 3

Chapter 4

Chapter 5

Chapter 6

List of Tables

Abbreviation list

AD	Activation domain
Ago	Argonaute
AMP	Adenosine monophosphate
ARE	Adenylate Uridylate rich element
ARE-BP	ARE binding protein
ATP	Adenosine triphosphate
BSA	Bovine serum albumin
BTG	B-cell translocation gene
CCR4	Carbon catabolite repression 4
COSMIC	Catalogue of somatic mutations in cancer
CPEB3	Cytoplasmic polyadenylation element-binding protein 3
Dcp1	Decapping enzyme 1
Dcp2	Decapping enzyme 2
DMSO	Dimethyl sulfoxide
DNA	Deoxyribonucleic acid
DSF	Differential Scanning Fluorimetry
E. coli	Escherichia coli
EDTA	Ethylene diamine tetraacetic acid
EDC3	Enhancer of decapping-3
EEP	Exonuclease-endonuclease-phosphatase
eIF4	Elongation initiation factor 4
FEN 1	Flap Endonuclease-1
Flc	Fluorescein
FRET	Förster resonance energy transfer
GST	Glutathione S-transferase
HIV	Human immunodeficiency virus
IMAC	Immobilised metal affinity chromatography
IRE1	Inositol requiring enzyme 1
IPTG	Isopropyl β-D-1-thiogalactopyranoside

LB	Lysogeny Broth
LRR	Leucine-rich repeat
MCS	Multiple cloning sites
m^7G	7-methyl-guanosine
mRNA	Messenger RNA
miRNA	MicroRNA
miRISC	MicroRNA induced silencing complex
NHL	Non-Hodgkins Lymphoma
NMD	Nonsense mediated decay
NSD	Nonstop mediated decay
NGD	No go decay
NAR	Not Anchoring Region
ORF	Open reading frame
PABP	Poly (A) binding protein
PAN	Poly (A) specific nuclease
PAN2	Poly (A) specific ribonuclease subunit 2
PAN3	Poly (A) specific ribonuclease subunit 3
PAP	Poly (A) polymerase
PABN1	Poly (A)-binding protein nuclear 1
PARN	Poly (A) specific ribonuclease
PCR	Polymerase Chain Reaction
PMR1	Polysomal ribonuclease 1
Poly (A)	Poly adenosine tail
PTC	premature termination codon
RNA	Ribonucleic acid
RNAP II	RNA polymerase II
rRNA	Ribosomal RNA
RRM	RNA recognition motif
SDS-PAGE	Sodium dodecyl sulphate polyacrylamide gel electrophoresis
SEC	Size exclusion chromatography

SIFT	Selecting intolerant from tolerant
siRNAs	short interfering RNAs
snRNA	Small nuclear RNA
TAMRA	Tetramethylrhodamine
TSA	Thermal shift assay
TTP	Tristetraprolin
UTR	Untranslated region
UPF	Up-frameshift

Chapter 1

Introduction

Chapter 1 Introduction

1.1 Genetic basis of human disease and gene regulation

The human genome encodes about 25,000 genes or more. Human diseases are often caused by genetic defect, environmental factors, or a combination of both. Many common diseases may be classified based on the underlying genetic contribution which could be monogenic, chromosomal abnormalities or quantitative traits which include polygenic disorders with phenotypic characteristics due to multiple genes. Other classifications include mitochondrial or somatic mutations and cancers. Eukaryotes respond to environmental signals by regulating their genes. This regulation is in two levels: transcriptional control which involves a limitation of the production of mRNA from a gene and post-transcriptional occurrences that control mRNA translation to proteins. Understanding eukaryotic gene expression, regulation and DNA function is a starting point for exploring new fields of medicine.

The regulation of genes in eukaryotes involves various processes in a cell. The first step is transcription which is one of the most highly regulated processes. Transcription involves the synthesis of messenger RNA (mRNA) from a DNA strand by RNA polymerase (RNAP). In eukaryotes, transcription can be grouped into three main steps: initiation – the recruitment of RNAP to the DNA; elongation – the lengthening of the mRNA molecule; and termination which is the removal of the RNA polymerase and release of the newly synthesised mRNA. Eukaryotes have three different classes of RNA polymerase, RNAPI, RNAPII, and RNAPIII. All mRNA molecules are synthesised by RNAPII (Kornberg, 1999, Sims et al., 2004). The immature mRNA produced by RNA polymerase II (RNAPII) is known as pre-mRNA. The pre-mRNA is processed in the nucleus to convert it to mature mRNA. The processes include capping, splicing and polyadenylation (Bentley, 2005). Capping involves modification of the 5' ends of eukaryotic mRNAs. The 7-methylguanosine cap which functions in stabilising mRNAs is attached to the

5' end of the pre-mRNA and connected to the rest of the mRNA by a 5' to 5' triphosphate bridge (Cowling, 2009). The next modification involves splicing which is the removal of the introns leaving the protein coding exon sequences. This is catalysed by spliceosome, a multi subunit complex of proteins and small nuclear (SnRNA) molecules (McManus and Graveley, 2011). The final process is the modification of the 3' end of mRNA referred to as polyadenylation. It involves the addition of several adenosine nucleotides to the 3' end of the mRNA. The poly (A) tail protects the mature RNA from degradation. Mature mRNA is exported through the nuclear pores into the cytoplasm and translated into proteins or undergoes degradation (Figure 1.1). Gene expression control is primarily at the level of transcription initiation and post-transcriptional regulation.

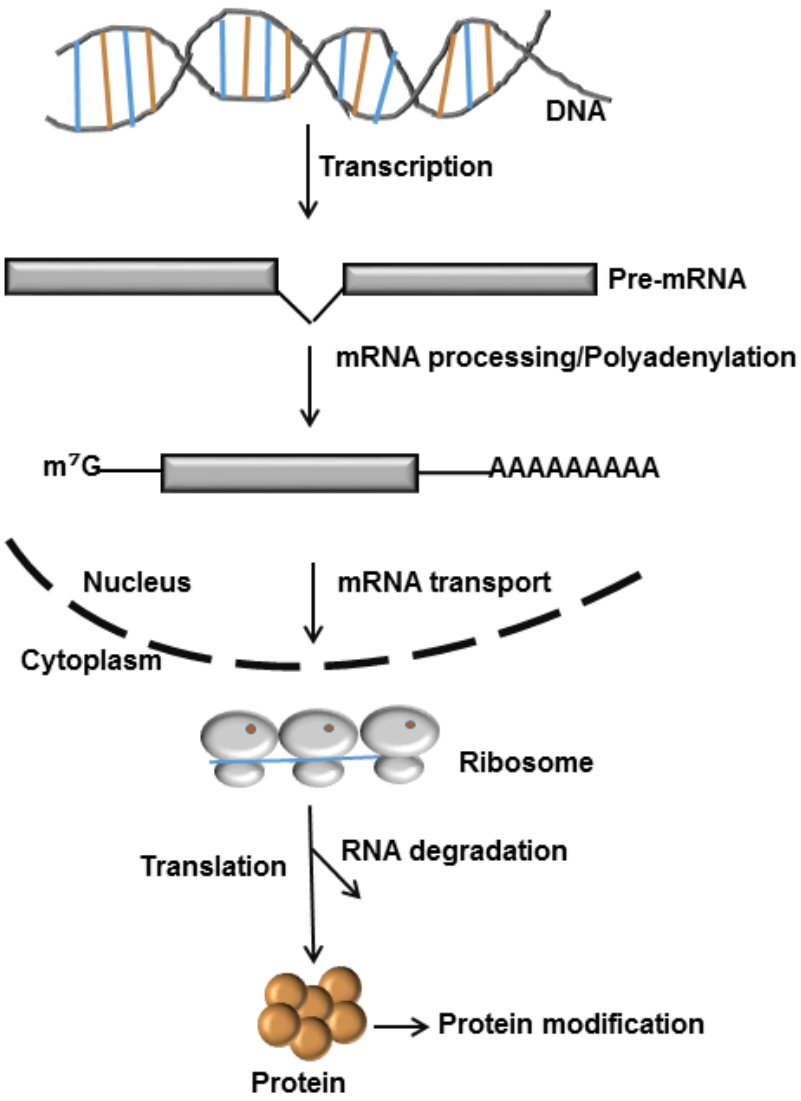

Figure 1.1 Overview of gene regulation in eukaryotes. The expression and regulation of genes in eukaryotes involves various processes. The first step in gene expression is transcription. A messenger RNA is synthesised from a DNA strand and processed in the nucleus to convert it to mature mRNA. The processes include capping, splicing and polyadenylation. Mature mRNA is exported through the nuclear pores into the cytoplasm and translated into proteins or degraded.

1.2 Post transcriptional mechanisms and messenger RNA turnover

Post transcriptional regulation mechanisms are vital for various biological events as they modulate the number of gene product that is synthesised (Morita et al., 2011). Amongst the post transcriptional points of control of gene expression include splicing, capping, poly-A tail addition, messenger RNA stability or Messenger RNA (mRNA) translation. Of these, the regulation of mRNA stability is critical as it determines the amount of mRNA available for translation (Ross, 1995, Fan et al., 2002, Cheadle et al., 2005a). Many diseases are often as a result of dysregulation of mRNA decay (Schoenberg and Maquat, 2012a). The abundance of mRNAs overall is influenced majorly by the rate of mRNA synthesis and its decay (Wu and Brewer, 2012). Microarray studies have shown that about 50% of the changes that take place in gene expression in response to cellular signalling occur at the level of mRNA decay (Fan et al., 2002, Cheadle et al., 2005b). In eukaryotes, most mature mRNAs have a 5' untranslated region (5' UTR) or cap structure, an open reading frame (ORF) and a 3 poly (A) tail up to 200 adenosine residues in length. These impact on translational efficiency, mRNA stability and turnover. The 5’ cap interacts with the cytoplasmic proteins eIF4E and the 3’ poly (A) tail interacts with the poly (A) binding protein (PABP), conferring stability on mRNA. Messenger RNA decay is initiated when either the 5′ cap or 3′ poly (A) tail or both structure is compromised or when it is cleaved internally by endonuclease enzymes (Garneau et al., 2007a). In eukaryotes, there are two main pathways for mRNA decay (Figure 1.2). In both pathways, deadenylation is the first and often rate-limiting step (Parker and Song, 2004, Goldstrohm and Wickens, 2008, Wahle and Winkler, 2013). Deadenylation is the shortening or removal of the poly (A) tail and is catalysed by deadenylases. Following the removal of the poly (A) tail mRNA degradation can occur via two mechanisms: either decapping which is followed by 5′→3′ degradation or a 3′ to 5′ decay. In the first pathway, the Lsm1→7 complex makes a connection with the 3′ end of the mRNA transcript and triggers off the cap removal by the decapping (Dcp1–Dcp2) complex. The mRNA is then prone to exonucleolytic

degradation of the 5' end by Xrn1 or alternatively the exosome complex is degraded from 3'-5' end while the remaining cap structure is disintegrated by the scavenger-decapping enzyme DcpS (Parker and Song, 2004, Garneau et al., 2007a, Houseley and Tollervey, 2009). Messenger RNA degradation mechanisms can be broadly divided into two: regulations that control the length or shorten the half-life of the mRNA. These mechanisms may affect the abundance of functional proteins and quality control mechanisms that eliminate the production of toxic proteins (Schoenberg and Maquat, 2012b).

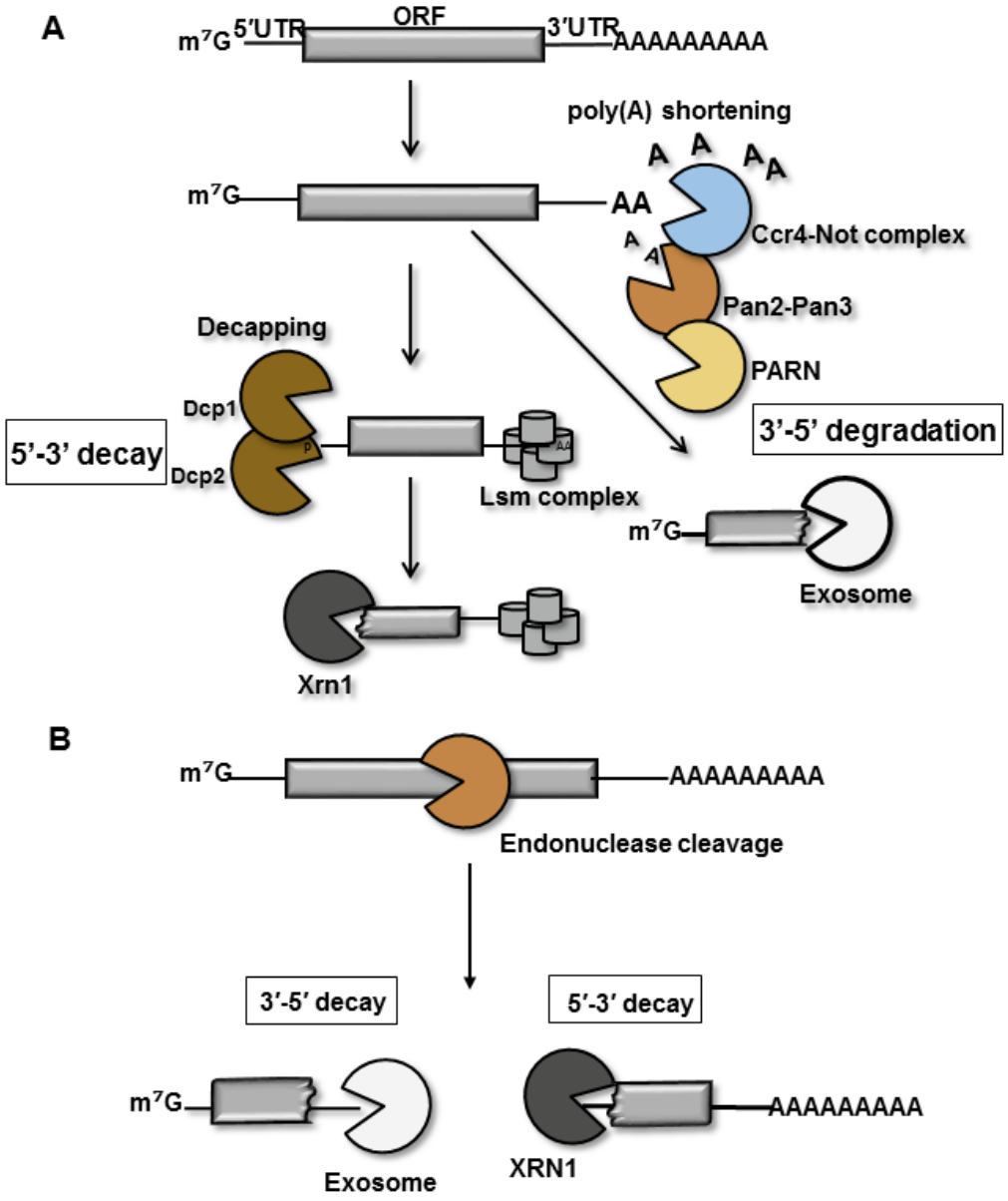

Figure 1.2 The main mRNA degradation pathways. (A) Most mRNAs are degraded exonucleolytically either by a 5′→3′ or 3′→5′ decay pathway. In both pathways, deadenylation is the first step. The poly (A) tail is removed by the Ccr4-Not complex, Pan2-Pan3 complex or PARN. In the first pathway following deadenylation, the Lsm complex connects with the 3′ end of the mRNA transcript and triggers decapping by the Dcp1/Dcp2 complex. The mRNA is then prone to exonucleolytic degradation of the 5′ end by Xrn1. Alternatively, deadenylation leads to a 3′→5′ decay by the exosome complex. (B) In some mRNAs, degradation is initiated by endonuclease cleavage of the mRNA body. This generates cleavage products with one unprotected end which are degraded by the exosome complex and XRN1.

1.2.1 mRNA decay pathways and enzymes

1.2.1.1 Deadenylation

Deadenylation takes place both in the nucleus and the cytoplasm (Bartlam and Yamamoto, 2010) making it an ideal point of control in mRNA regulation. There are several enzyme complexes involved. Examples of these are the conserved Pan2-Pan3 complex which consists of a Pan2 catalytic subunit associated with a Pan3 dimer, the poly (A) ribonuclease PARN, which is not found in single cellular eukaryotes (Wahle and Winkler, 2013, Winkler and Balacco, 2013, Wolf and Passmore, 2014) and the multisubunit Ccr4-Not complex (Tucker et al., 2001, Meyer et al., 2004, Yamashita et al., 2005).

Pan2-Pan3 dimer was the first deadenylase identified in yeast. Pan2–Pan3 dimer is dependent on a poly (A) binding protein (PABP). It removes the poly (A) tails of mRNAs to the 60–80 nucleotides in *S. cerevisiae* (Brown et al., 1996). In mammals, it is thought, though unclear, that there are two phases of deadenylation. Pan2–Pan3 is involved in the initial shortening of the poly (A) tail from the 200 to about 80 nucleotides. Thereafter, the CCR4–NOT complex shortens the poly (A) tail.

PARN was first isolated from calf thymus due to its ability to preferentially hydrolyse poly (A) (Korner and Wahle, 1997). It is a magnesium dependent enzyme that requires a free 3 hydroxyl group. It belongs to the RNase D family of exoribonuclease (Körner et al., 1998). Its deadenylation activity is cap-dependent and is inhibited by cap-binding proteins (Dehlin et al., 2000, Gao et al., 2000, Martinez et al., 2001). In addition, PARN has an RNA recognition motif (RRM)-type RNA-binding domain and a nuclear localization signal (Copeland and Wormington, 2001). Asp-28, Glu-30, Asp-292 and Asp-382 amino acids are directly involved in co-ordinating the divalent ions at the active site of PARN (Ren et al., 2002, Ren et al., 2004). Of these, Asp-28 is the most essential for binding to the magnesium ions (He et al., 2011). PARNL, ANGEL, ANGEL2, Nocturin and 2′PDE12 deadenylases are also encoded in the human genome. PARN is found in many higher eukaryotes including mammals and various insect species (Dehlin et al., 2000). In *S. cerevisiae* or

Drosophila melanogaster, no PARN homologue has been found (Meyer et al., 2004). However, in all systems examined, the Ccr4-Not complex is widely deduced as the main deadenylase (Tucker et al., 2001, Meyer et al., 2004, Yamashita et al., 2005). The deadenylase enzymes involved in mRNA degradation are shown in Table 1.1.

Complex	**Human homologs**	**Information/function**
Deadenylase enzyme	CNOT7	DEDD-type deadenylases, member of Ccr4-Not complex
	CNOT8	DEDD-type deadenylases, member of Ccr4-Not complex
	TOE1(Caftz)	DEDD-type deadenylases, member of Ccr4-Not complex
	PARN	DEDD-type deadenylases, member of Ccr4-Not complex
	PAN2	DEDD-type deadenylase that exists as dimer with PAN3.
	CNOT6	EEP-type deadenylase, member of Ccr4-Not complex
	CNOT6L	EEP-type deadenylase, member of Ccr4-Not complex
	Nocturin	EEP-type deadenylase
	Angel	EEP-type deadenylase
	Angel2	EEP-type deadenylase
Decapping enzyme	Dcp1a, Dcp1b	Member of decapping complex with Dcp2
	Dcp2	Catalytic pyrophosphatase subunit of decapping complex
	Lsm 1-7	Member of Lsm complex with subunits 1-7
Cytoplasmic exonuclease enzyme	XRN1	Cytoplasmic 5'-3' exonuclease
	XRN2	Multisubunit exonuclease

Table 1.1 Enzymes involved in mRNA degradation

1.2.1.1.1 Human deadenylase enzymes

Deadenylases are nuclease enzymes which degrade mRNA by removal of poly (A) tail in a 3' to 5' direction. The end product of deadenylation is the release of 5'-Adenosine monophosphate (AMP) products. The hydrolysis of the terminal adenylate residues requires two metal ions for catalysis, usually magnesium ions. . In recent times, approximately 11 deadenylase enzymes have been identified in humans and are categorised into two main classes based on their nuclease domains (Table 1.1). The first group are the DEDD (Asp-Glu-Asp-Asp) type deadenylases. They are characterised by the presence of four conserved acidic amino acids: three aspartates (D) and one glutamate (E) in the order DEDD that form the core domain. These acidic residues that form a highly negatively charged cavity, bind or co-ordinate metal ions involved in catalysis. Substitution of any of these amino acid residues will abolish enzymatic activity (Thore et al, 2003; jonstrup et al, 2007; Horiuchi et al, 2009). The main families of the DEDD-type deadenylases include POP2 (also referred to as CNOT7, CNOT8, TOE1/CAF1Z)(Thore, 2003; Collart and Panasenko, 2012a), PARN and PAN2 in complex with PAN3. An illustration of the S. Pombe POP2 core catalytic domain representing the DEDD conserved amino acid coordination with magnesium is shown in figure 1.3.

The second group of deadenylases are the EEP (endonuclease-exonuclease-phosphatase) family which have conserved catalytic Asp and His residues in their catalytic site. Two magnesium ions are required for hydrolysis. The residues essential for coordination of Mg (II) ions, are clustered within the negatively charged pocket around the metal ions. Thus, they provide a suitable environment to carry out hydrolysation. Enzymatic activity is abolished on substitution of amino acids involved in coordination of metal ions (Chen et al, 2002; Wang et al, 2010). Members of the EEP family include Nocturin, a circadian regulated deadenylase (Baggs and Green, 2003), PDE12 (phosphodiesterase 12), a mitochondrial deadenylase involved in antiviral defence mechanisms (Rorbach et al., 2011, Doidge et al., 2012b), Angel, and

the highly similar CNOT6 and CNOT6L deadenylases which interact with the CNOT7 and CNOT8 enzymes and make up the catalytic subunit of the Ccr4-Not complex (Dupressoir et al., 2001, Collart and Panasenko, 2012b). The deadenylases vary among species. In all eukaryotes, POP2, CCr4, PAN2 and Angel families are present. However, PAN and CAF1Z deadenylases are both absent from *Drosophila melanogaster* and also less conserved (Bartlam and Yamamoto, 2010).

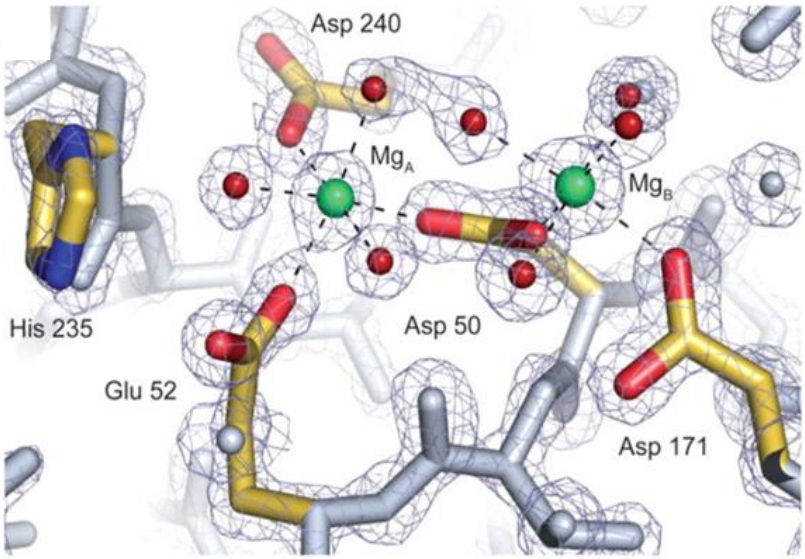

Figure 1.3. Active site of S. Pombe POP2 deadenylase showing coordination of magnesium ions by the DEDD amino acid residues. Amino acid residues are coloured by element and magnesium ions are shown in green, waters involved in coordination of the active site ions are coloured in red, and the octahedral coordination of the active site magnesium ions is indicated by dashed lines. Figure as originally published in Anette Thyssen Jonstrup, Kasper R.Andersen, Lan B.van, Ditlev E. Brodersen (2007). The 1.4-Å crystal structure of the *S. Pombe* POP2p Deadenylase subunit unveils the configuration of the active enzyme. The figure was reproduced under the terms of the creative commons attribution license (CC-BY3.0)

1.2.1.2 Decapping and 5'-3' mRNA degradation pathway

Following deadenylation, the 5′→3′ mRNA degradation pathway starts with the cap removal. In yeast, the enzyme responsible for decapping is a dimer made up of Dcp1 and Dcp2 proteins (Dcp1/Dcp2). Dcp2 has RNA binding properties and is the main enzyme involved in decapping. It is a member of the Nudix hydrolase family, conserved among eukaryotes (Song et al., 2010, Piccirillo et al., 2003). Dcp2 has an MutT domain which is responsible for the catalytic activity (Steiger et al., 2003). In higher organisms, a third component exists, Hedls or Ge-1, and it forms a bridge Dcp2 and Dcp1 interaction influencing their decapping activity (Fenger-Gron et al., 2005, Yu et al., 2005). The reaction products of decapping are m^7GDP and 5' monophosphate RNA. The decapping complex prefers substrates ≥25 nucleotides. For efficient decapping, several factors are essential. First, the Lsm1–7 complex forms an association with the 3′ end of mRNAs that have undergone deadenylation and promotes decapping (Tharun et al., 2000, Tharun and Parker, 2001). Other Lsm proteins, such as Lsm16, the S. cerevisiae PABP-binding protein-1 (Pbp1) and mammalian RAP55 (RNA associated protein of 55 kDa; also referred to as Lsm14), have been implicated in mRNA regulation (Garneau et al., 2007b, Mangus et al., 1998, Yang et al., 2006). Other decapping proteins include enhancers of decapping proteins, the DExD/H-box RNA helicase Dhh1 and Pat1 (Bonnerot et al., 2000). Decapped mRNA is susceptible to a 5' to 3' degradation by Xrn1. The degradation by Xrn1 is regulated by decapping efficiency since there is a direct interaction with Hedls (Braun et al., 2012).

1.2.1.3 3'-5' decay pathway

Messenger RNA can be degraded in a 3' to 5' direction by the exosome. The exosome is a highly conserved complex that exists in both the nucleus and cytoplasm. In addition to cytoplasmic mRNA decay, the exosome is involved in processing of noncoding RNAs in the nucleus. The human exosome responsible for this has been extensively studied and consists of 9 core subunits and enzymatically active ribonuclease (Chlebowski et al., 2013). In yeast, the exosome is functionally associated with the Ski complex which modulate the RNA-binding and ATpase properties of Ski2. In humans, enzymatic activity is similar to what occurs in yeast. Following degradation of the messenger RNA body by the exosome complex, the remaining 5' cap is metabolised by the scavenger decapping enzyme DcpS. DcpS forms a homodimer and decaps substrates with no more than 10 nucleotides (Liu et al., 2002).

1.2.2 Endonucleolytic-cleavage mediated mRNA decay

In some eukaryotes, the degradation of mRNA is triggered by endonucleolytic cleavage within the mRNA body. This results in two fragments that are prone to degradation by the exosome and Xrn1 (Figure 1.2B). Endonucleases that target mRNA include polysomal ribonuclease1(PMRI); inositol-requiring enzyme 1(IREI), some nucleolar ribosomal RNA (rRNA)-processing enzyme RNase2 MRP some short interfering RNAs (siRNAs) that initiate mRNA decay by cleavage, and some unidentified endonucleases involved in aberrant mRNA decay (Gatfield and Izaurralde, 2004). PMRI and IREI target actively translating mRNAs and are activated only when needed (Hollien and Weissman, 2006). While PMRI is polysome associated, IREI targets transcripts in the endoplasmic reticulum.

1.3 Signals and proteins that control mRNA degradation

1.3.1 Protein mediated decay

Studies have shown that many proteins mediate mRNA degradation by binding to sequence motif such as the Adenylate uridylate-rich elements (AREs), which are important signals that control mRNA turnover. The AREs are the most studied group of factors that destabilise mRNAs and are found in the 3'UTR in tightly regulated mRNA that encode proto-oncogene, proteins and inflammatory mediators such as interleukins and cytokines (Chen and Shyu, 1995, Wilusz et al., 2001, Shim and Karin, 2002). AREs have sequence regions rich in adenosine and uridine residues which often include one or more copies of the AUUUA pentamer that are embedded in a Uridine rich context (Chen and Shyu, 1995, Wilusz et al., 2001). This sequence has an overall influence on mRNA stability. The proteins which mediate mRNA decay include tristetraprolin (TTP) protein, pumilio and Nanos proteins (Inada and Makino, 2014, Blackshear, 2002), Roquin, Y^{th} domain proteins (Zhang et al., 2010, Leppek et al., 2013), amongst others. They function through interaction with other related proteins (Moraes et al., 2006) to recruit one or more of the decay enzymes responsible for mRNA degradation (Lykke-Andersen and Wagner, 2005). (Figure 1.4). The first step in the decay of mRNA containing ARE is deadenylation (Yamashita et al., 2005) which is followed by degradation of the mRNA body via the 5' to 3' or 3' to 5' exonuclease.

TTP binds to AREs and triggers mRNA degradation, by acting as a bridge to recruit the mRNA decay enzymes (Lykke-Andersen and Wagner, 2005). Nanos2 associates with the Ccr4-Not complex to initiate suppression of specific RNAs. Nanos1–3 is known to associate with CNOT1 via a short CNOT1interacting motif conserved in all vertebrates and some invertebrate species (Bhandari et al., 2014). Roquin controls mRNA decay with conserved CDE stem-loop motifs via recruitment of Ccr4-Not complex to initiate deadenylation (Leppek et al., 2013).

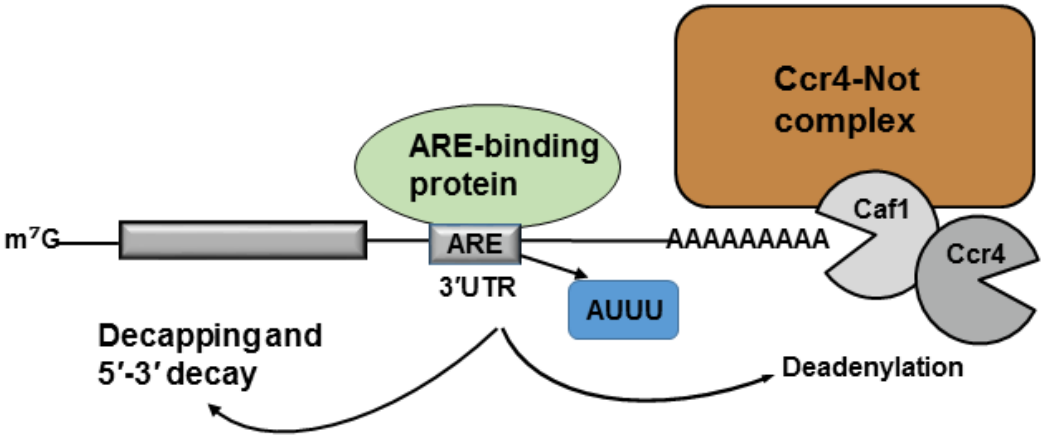

Figure 1. 4 ARE-mediated decay. ARE-binding proteins which regulate specific mRNAs, bind directly to the 3′ untranslated region (UTR) and recruit the mRNA decay machinery. The Ccr4-Not complex initiates poly (A) tail removal which is catalysed by the Caf1-Ccr4 deadenylases. Deadenylation is followed by decapping of the mRNA in a 5' to 3' direction.

1.3.2 MicroRNA mediated decay

MicroRNAs are a large family of small non-coding RNAs of about 21-nucleotide length that play key roles in post-transcriptional regulation of gene expression. MicroRNAs form imperfect matches with target mRNAs mainly found in the 3′ UTR of the mRNA. Thus, they mediate translational repression or mRNA degradation by a breakage of the mRNA strand into two pieces, destabilization of the mRNA through deadenylation or by reduced translational efficiency of the mRNA into proteins by ribosomes. In eukaryotes, microRNAs are predicted to regulate the activity of nearly 30% of all protein-coding genes, and are involved in the regulation of almost every cellular process. Dysregulation of miRNA expression is associated with different kinds of diseases, such as cancer (Filipowicz et al., 2008, Hesse and Arenz, 2014, Jackson and Standart, 2007). Recent evidence indicates that miRNA-mediated mRNA decay starts by poly (A) tail removal, followed by decapping and 5′ to 3′ exonucleolytic decay (Jonas and Izaurralde, 2015, Giraldez et al., 2006). During mRNA biosynthesis, newly formed single stranded microRNAs (miRNAs) bind to an Argonaute (AGO) protein in miRNA-induced silencing complexes (miRISCs) (Figure 1. 5) The AGO family protein, form the core of the miRISCs. AGO proteins recruit and interact with a GW182 protein (Eulalio et al., 2009, Wu and Brewer, 2012). When AGO proteins interact with GW182, this facilitates the interaction with poly (A) binding protein (PABP) and with deadenylase enzyme complexes Pan2/Pan3 and CCR4–NOT. The deadenylase complexes (Pan2/Pan3 and CCR4–NOT complex) trigger the poly (A) tail removal of the mRNA. Deadenylated mRNAs are decapped and degraded by XRN1 exonuclease. Alternatively, if there is a near perfect complementary strand between the mRNA and the microRNA a direct endonucleolytic cleavage occurs which generates products for 5′ to 3′ decay by XRN1 and the exosome complex.

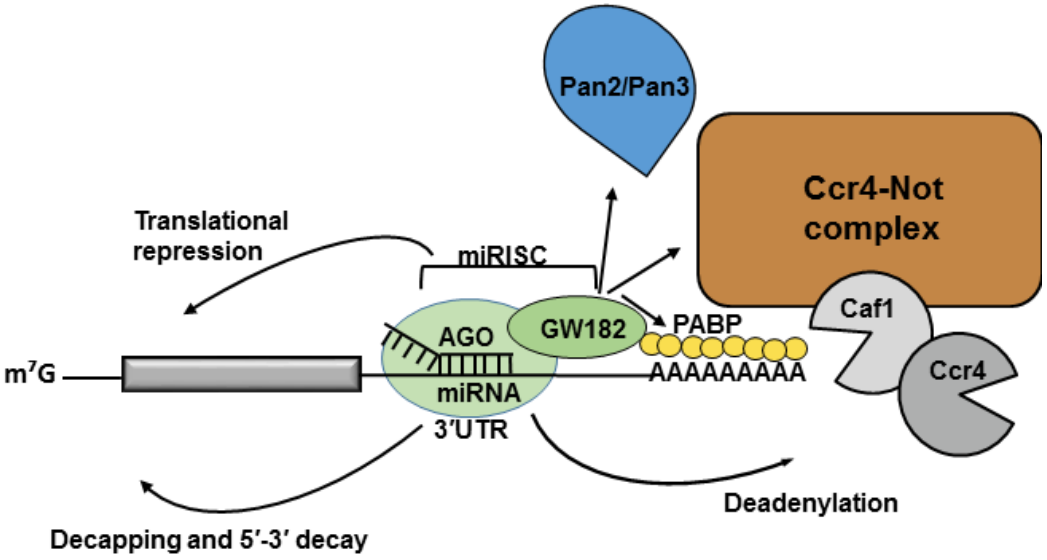

Figure 1. 5 MicroRNA-mediated mRNA decay. Destabilization of target mRNAs by recruitment of the Ccr4-Not complex to mRNA. When miRNAs bind to AGO proteins, they recruit and interact with GW182 to form the miRISC. This facilitates interaction with PABP, PAN2/PAN3 and CCR4–NOT deadenylases which trigger poly (A) tail removal. Deadenylated mRNAs are decapped and degraded by Xrn1 exoribonuclease in a 5′ to 3′ direction. The miRISC complex may also repress translation independently.

1.4 mRNA surveillance mechanisms

Every step in mRNA processing and maturation has a potential of introducing errors (Garneau et al., 2007a, Shyu et al., 2008). The detection and degradation of aberrant messenger RNA is therefore vital. To avoid production of toxic protein products, the cell detects and degrades faulty transcripts by surveillance and this occurs in the nucleus. However, other mechanisms control the quality of mRNA in the cytoplasm and these include; Nonsense mediated decay (NMD), Nonstop mediated decay (NSD) and a No-Go-decay mechanism.

1.4.1 Nonsense mediated decay

Nonsense-mediated decay (NMD) has been extensively studied and is found in all eukaryotes (Figure 1.6). It is a mechanism by which cells detect and degrade mRNA transcripts that have premature termination codons (PTCs). The PTCs may be as a result of mutations, frameshifts and other abnormalities on the 3'UTRs (Garneau et al., 2007a). NMD is reported to be triggered by mutations found in many human inherited diseases (Frischmeyer and Dietz, 1999). It has been estimated that approximately 30% of human disease alleles cause NMD, and in many of these case, NMD is a major factor that contributes to the disease phenotype (Holbrook et al., 2004). The main proteins involved are the upshift frame 1, 2 and 3 (UPF1, UPF2 and UPF3) (Conti and Izaurralde, 2005). Of these three protein factors, the biochemical function of Upf1 is vital (Czaplinski et al., 1995). In a normal mRNA, the translating ribosome and displace these proteins so that they cannot initiate NMD (Figure 1.6). However, if a ribosome encounters a premature stop codon (PTC) it recruits UPF1 and SMG1 by association with the eRF1 and eRF3 release factors to form the SURF complex (Kashima et al., 2006) . In the presence of UPF2 and UPF3, which may be bound to downstream exon junction complex on the mRNA, the ribosome eRF1 and eRF3 are released. The phosphorylation of UPF1 by SMG1 triggers the recruitment of SMG5, SMG6, and SMG7. The SMG5–SMG7 heterodimer recruit the mRNAs decay

factors leading to mRNA degradation by interaction with Caf1, a subunit of Ccr4-Not complex (Loh et al., 2013, Zhang et al., 1998).

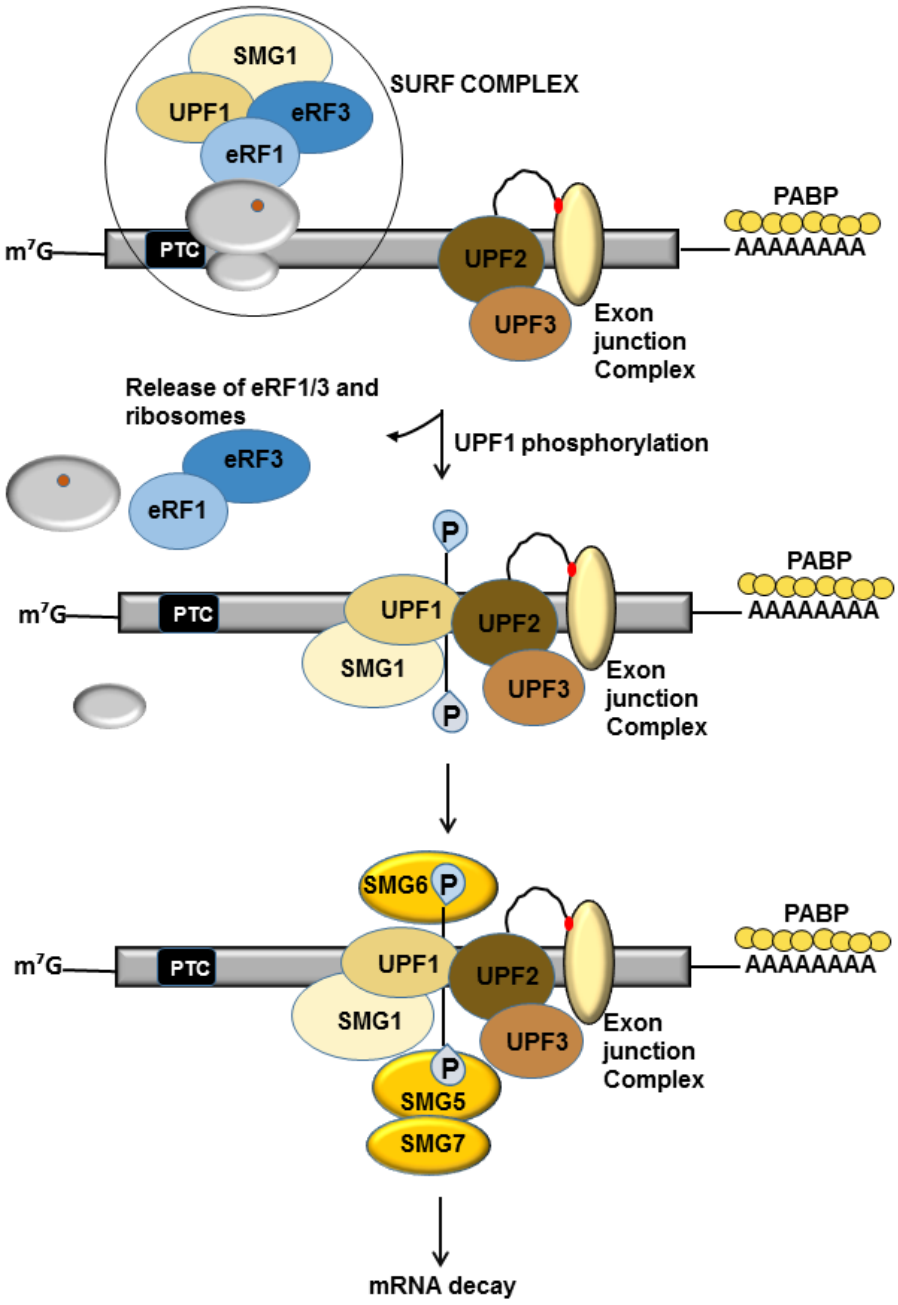

Figure 1.6 Nonsense mediated mRNA decay (NMD). If a ribosome encounters a premature termination codon (PTC) it recruits UPF1 and SMG1 by association with the release factors (eRF1 and eRF3) to form the SURF complex. In the presence of UPF2 and UPF3, which may be bound to downstream exon junction complex on the mRNA, the ribosome eRF1 and eRF3 are released. The phosphorylation of UPF1 by SMG1 triggers the recruitment of SMG5, SMG6, and SMG7. The SMG5–SMG7 heterodimer recruit the mRNAs decay factors leading to mRNA degradation.

1.4.2 Non-stop decay

Non-stop decay (NSD) surveillance mechanism targets mRNAs lacking a stop codon. This occurs when there is breakage or an in-frame stop codon is absent leading to translation proceeding along the poly (A) tail. NSD protects cells from faulty proteins and enhances the release of the ribosomes. Two distinct pathways of NSD include the SKI7 and non-SKI7 pathways. The NSD mechanism requires the SKI complex (SKI2, SKI3 and SKI8) and SKI7 which serves as adaptor protein (van Hoof et al., 2002, Frischmeyer et al., 2002). During translation, of a mRNA lacking a stop codon, the ribosomes displaces poly (A) binding protein (PABP) and stalls. The stalled ribosome at the 3′ end of the mRNA transcript, triggers NSD in two models: In the presence of SKI7 protein (that mimics tRNAs), its C terminus binds to the empty A site of the ribosome, thus releasing the ribosome. Ski7 then recruits the exosome and the associated SKI complex (SKI2, SHI3 and SKI8) to remove the poly (A) tail and then degrade the mRNA in the 3′ to 5′ direction. The second model described in yeast occurs in the absence of SKI7 (Inada and Aiba, 2005). The displacement of PABP by the ribosome render transcripts prone to decapping and a 5′-3′ decay by Xrn1 exoribonuclease (Figure 1.7).

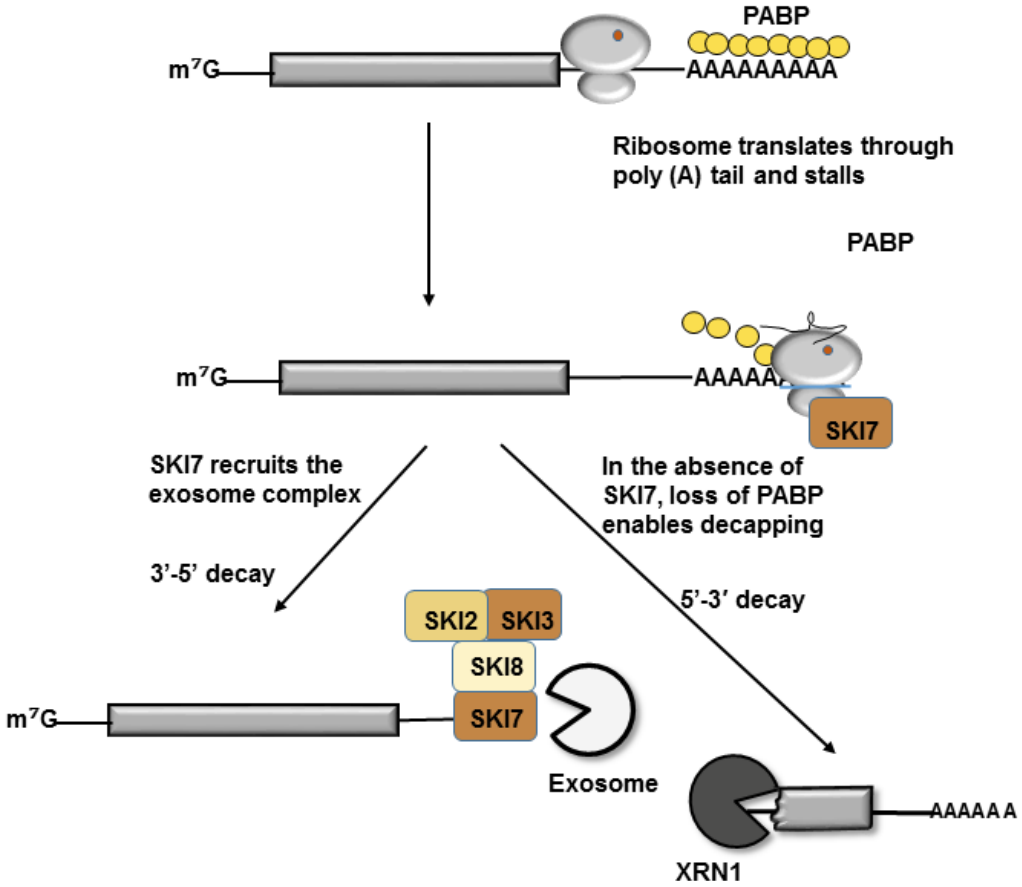

Figure 1.7 Non-stop decay. The translation of a mRNA lacking a stop codon leads to ribosomes displacing poly (A) binding protein (PABP) and stalls. The stalled ribosome at the 3′ end triggers non-stop decay in two models. First, when SKI7 is present, it associates with the empty A site of the ribosome, thereby releasing the ribosome. Ski7 then recruits the associated SKI complex (SKI2, SKI3 and SKI8) to deadenylate and the exosome to degrade the mRNA in the 3′ to 5′ direction. The second model described in yeast occurs in the absence of SKI7. The displacement of PABP by the ribosome allows decapping and a 5′-3′ decay by Xrn1 exoribonuclease.

1.4.3 No-go decay

This decay mechanism was recently identified in yeast and a lot is still unclear. This mechanism prevents translation factors from sequestering to faulty mRNA transcripts. It detects stalled ribosomes on a mRNA and then cleaves the mRNA endonucleolytically near the stall site. The stalled ribosome is released and mRNA fragments are degraded by the exosome and Xrn1 nuclease (Doma and Parker, 2006).

1.5 The human Ccr4-Not complex

1.5.1 Overview of the Ccr4-Not complex

The Ccr4-Not complex is a large protein complex with multi-subunits, conserved from yeast to humans (Collart and Timmers, 2004) and plays multifunctional roles in gene regulation. Studies done on the yeast identified the Ccr4-Not complex to be about 0.9-1.2 MDa in size (Liu et al., 1998). It contains five NOT proteins (Not1, Not2, Not3 Not4 andNot5), Caf40, Caf130 subunit and two catalytic subunits, Ccr4 and Caf1 (Pop2). In humans, the core Ccr4-Not complex was found to be similar to yeast and also Drosophila (Table 1.2)) (Mahadevan and Struhl, 1990, Maillet and Collart, 2002, Lee et al., 1998, Viswanathan et al., 2003, Collart, 2016). Other additional subunits in the human Ccr4-Not complex include the RQCD1 (CNOT9/Not9/Rcd1/Caf40), CNOT10 (Caf130, Not10), CNOT11 and TAB182 (Lau et al., 2009, Bawankar et al., 2013, Mauxion et al., 2013). A list of the Ccr4-Not components in Drosophila, yeast and humans is shown in Table 1.2. The subunits are known under different alternatively used names. In this thesis, the gene names shown on Table 1.2 will be used throughout. Interaction studies have unravelled in both yeast and in humans that the complex is centred on a scaffold protein Not1 (homologous to CNOT1) and interacts with various proteins which include CNOT2 which associates with CNOT3 and the CNOT7 or CNOT8 deadenylases in humans) (Lau et al., 2009). Despite the similarities between the yeast and human Ccr4-Not complex, several differences exist amongst the complexes. The yeast Not11 and human CNOT1 were shown to be vital for cell viability however, the human CNOT1 is essential for cell proliferation but not cell viability in MCF7 cells (Maillet et al., 2000, Ito et al., 2011, Mittal et al., 2011). The human CNOT4 unlike yeast Not4 is not found in the conserved core of the Ccr4-Not complex (Lau et al., 2009). The Not4 protein consists of two functional domains, the N-terminal RING domain which makes an interaction with the UbcH5b E2 enzyme and provides ubiquitin protein ligase activity and a conserved RRM which provides RNA binding activity (Albert et al., 2002, Dominguez et al., 2004). Extensive

studies on the properties of the Ccr4-Not complex in yeast and humans has unravelled the architecture of the complex. The first description of its architecture using a low-resolution electron microscopy (EM) reconstruction reported an L shaped structure with two arms of approximately similar length (Nasertorabi et al., 2011). Predictions from this report were that the Not1-Ccr4-Caf1 is found in the hinge region connecting the two arms (Figure 1.8) where an accessible point could make room for interaction with RNA or other factors that regulate it. In another description by Bawankar et al, 2013 which is the most extensive till date, the complex consists of a deadenylase module and a NOT module. The deadenylase module consists of two subunits: Ccr4 and Caf1. The nuclease module is formed between the N-terminal region of NOT1, Ccr4 and Caf1. The Ccr4 subunit forms an interaction with Caf1 through its Leucine rich repeat (LRR) domain (Figure 1.9). The NOT module on the other hand consists of CNOT1, CNOT2 and CNOT3 in humans. In yeast, it is NOT1, NOT2 and either Not3 or Not5 (Bawankar et al., 2013). The scaffold protein CNOT1 which serves as a base for assembling the NOT and deadenylase module is made up of three regions. An N-terminal, middle and C terminal region. The deadenylase module binds to the middle region through an MIF4G domain in NOT1 with CNOT7 acting as an adaptor protein between NOT1 and CNOT6L. There is a neighbouring DUF3819 domain located at the middle region which serves as the binding site for CAF40/CNOT9 (Bawankar et al., 2013). The NOT module interacts with the C-terminal region of CNOT1/NOT1. CNOT2 interacts with CNOT1, whereas CNOT3 interacts with CNOT2 through their respective NOT boxes and have no direct interaction with CNOT1. Studies in D. melanogaster complexes have also shown that the N-terminal residues of CNOT1 interact with CNOT10 and CNOT11 which currently have no orthologs in yeast. In addition to the deadenylase and NOT modules, the Ccr4-Not complex consists of other subunits whose functions are yet still not understood. They are either peripheral to the core complex or specific to species. The function of CNOT9 is still unknown, however it is located closely to the deadenylase module in

the Ccr4-Not complex (Nasertorabi et al., 2011, Bawankar et al., 2013) and may play a role in deadenylation.

Core name	**Drosophila Gene name**	**Yeast (Saccharomyces cerevisiae)**	**Homo sapiens Gene name**
Not1	Not1	Not1/CDC39	CNOT1
Not2	Regena	Not2/CDC36	CNOT2
Not5	Not3	Not5	CNOT3
Caf1	Pop2	Caf1/Pop2	CNOT7 and CNOT8
Ccr4	twin	Ccr4	CNOT6 and CNOT6L
Caf40	Rcd1	Caf40	CNOT9/Rcd1/Caf40/RQCD1
Not4	Not4	Not4	CNOT4
Not10	Not10		CNOT10
Not11	Not11		CNOT11
Caf130		Caf130	
Not3		Not3	
TAB182			TAB182

Table 1.2 Names of the Ccr4-Not components in Drosophila, Yeast and Humans.

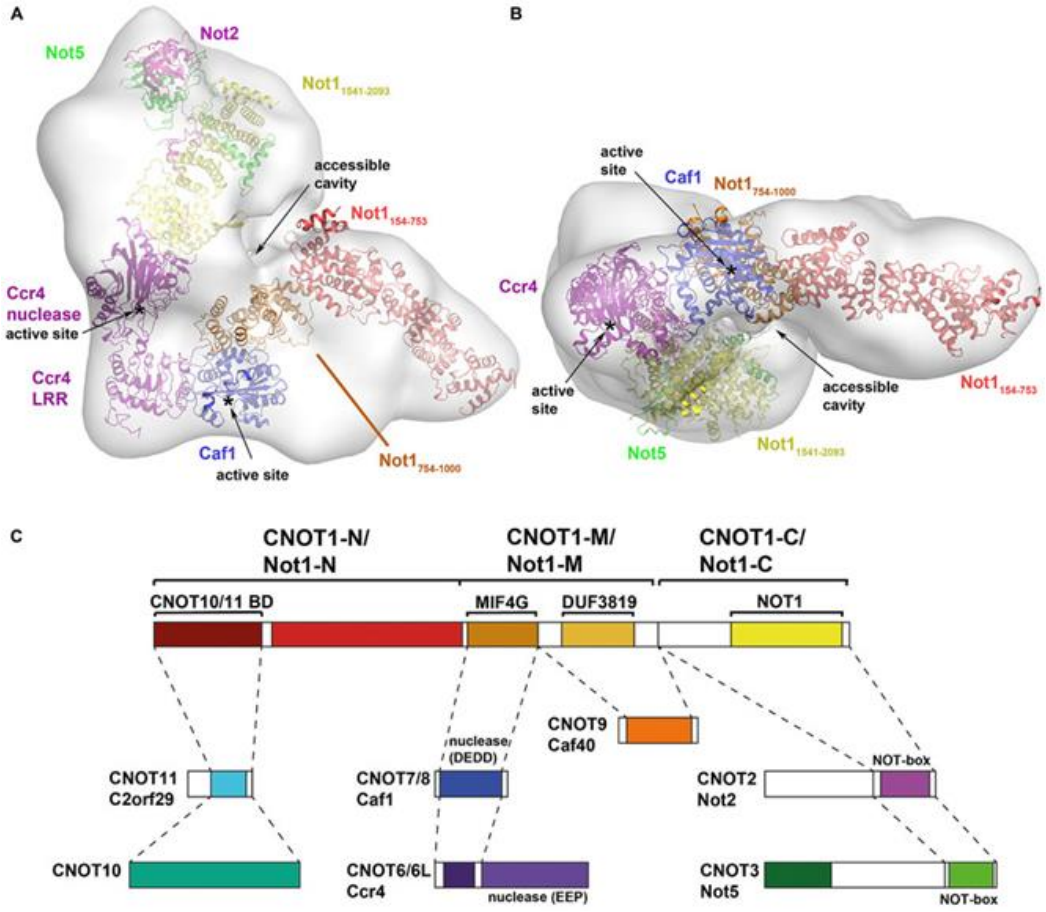

Figure 1.8 Structure of the Ccr4-NOT complex. (A, B) A representation of the architecture of the Ccr4-NOT complex using X-ray crystal structures docked into a negative stain EM map using UCSF Chimera software based on size and shape considerations. (C) Interactions of the Ccr4-NOT complex. Subunits are coloured in accordance with structures in (A, B). Figure as originally published in Xu k, Bal Y, Zhang A, Zhang Q and Bartlam MG (2014). Insights into the structure and architecture of the Ccr4-Not complex. Front. Genet 5: 137.doi:10.3389/fgene.2014.00137. The figure was reproduced under the terms of the creative commons attribution license (CC-BY3.0).

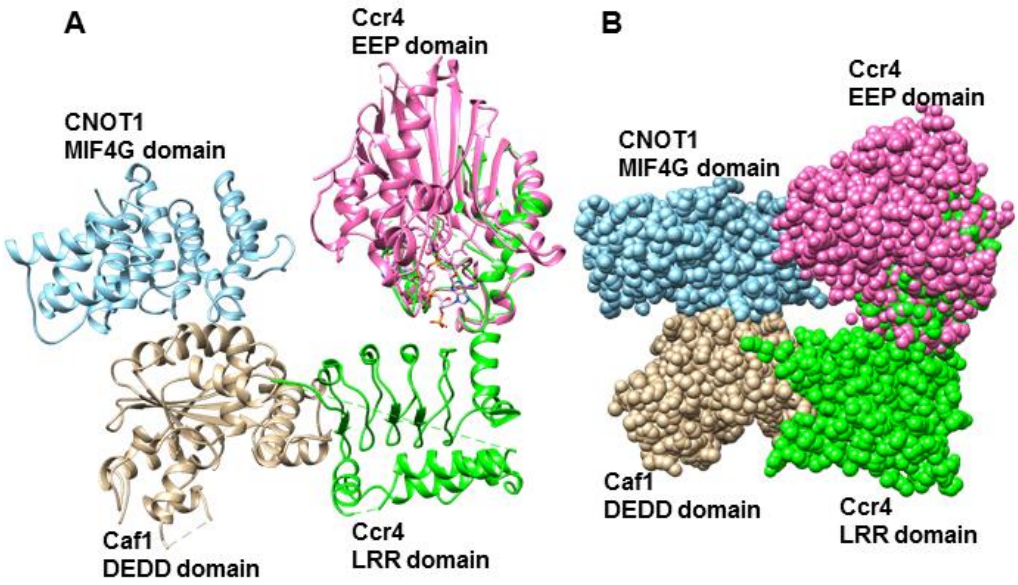

Figure 1.9 A structural representation of the Ccr4-Not nuclease complex. (A) Crystal structure of the nuclease sub-complex. The MIF4G domain of the human CNOT1 is indicated in blue, the catalytic EEP domain of human Ccr4 (pink), the LRR domain of Ccr4 (green) and CNOT7 (tan). (B) A surface representation of the nuclease sub-complex. The model was generated by superimposition of the M1F4G domain of human CNOT1 in complex with CNOT7 (PDB accession number 4GMJ) and the EEP nuclease domain of human CNOT6L (PDB accession number 3NGO) on the structure of the yeast-Not1-Caf1-ccr4 complex (PDB accession number 4B8C). Structures were visualised using UCSF Chimera package.

1.5.1.1 The nuclease module

The Ccr4-Not nuclease complex is characterised by two main subunits which are involved in ribonuclease activity: the Ccr4 and Caf1 subunits. These enzymes belong to either the DEDD-type family or EEP-type family. The Ccr4-Not complex comprises of one deadenylase enzyme from each family. In yeast, the Ccr4 and Caf1 are involved in mRNA degradation however the Ccr4 has been shown to be the main deadenylase (Malvar et al., 1992, Draper et al., 1994, Chen et al., 2002, Tucker et al., 2001). The human Ccr4-Not complex has two orthologues conserved from yeast. The Ccr4 and Caf1 deadenylases (Albert et al., 2000, Dupressoir et al., 2001). The CNOT6 and the CNOT6L are the two human orthologues of yeast Ccr4. These have been shown to have different functions in cells though similar and identical structurally (Mittal et al., 2011). The two orthologues of yeast Caf1 are CNOT7 and CNOT8 also known as POP2/CALIF. The Caf1 orthologues share high sequence similarity and have partially overlapping roles (Aslam et al., 2009, Lau et al., 2009).

1.5.1.1.1 The Ccr4 subunit

The Ccr4 subunit has two domains, an endonuclease exonuclease-phosphatase (EEP) domain (Tucker et al., 2002, Wang et al., 2010b) and an amino-terminal leucine-rich repeat (LRR) domains (Malvar et al., 1992, Dupressoir et al., 2001). Its amino-terminal leucine-rich repeat domain binds directly to an interaction surface with the Caf1 catalytic subunit (Dupressoir et al., 2001, Clark et al., 2004). The EEP domain on the other hand is associated with its ribonuclease activity. Studies have shown that the Ccr4 nuclease has a strong preference for poly (A) residues *in vitro* (Chen et al., 2002, Wang et al., 2010b). The Ccr4 proteins encoded by the CNOT6 and CNOT6L are 78% identical and 88% similar at the amino acid level. The surface residues in the catalytic sites are totally conserved. The CNOT6L structure reveals a two-layered α and β sandwich with two interior β-sheets that are embedded between outer layers of α-helices. The active site pocket features two magnesium ions which are important for activity (Figure 1.10). The metal

ions are coordinated by an asparagine, glutamate, two aspartate and a histidine typical of the EEP-type enzyme family. The substitution of amino acid that affect the coordination of metal ions will potentially abolish enzyme activity (Chen et al., 2002, Wang et al., 2010a).

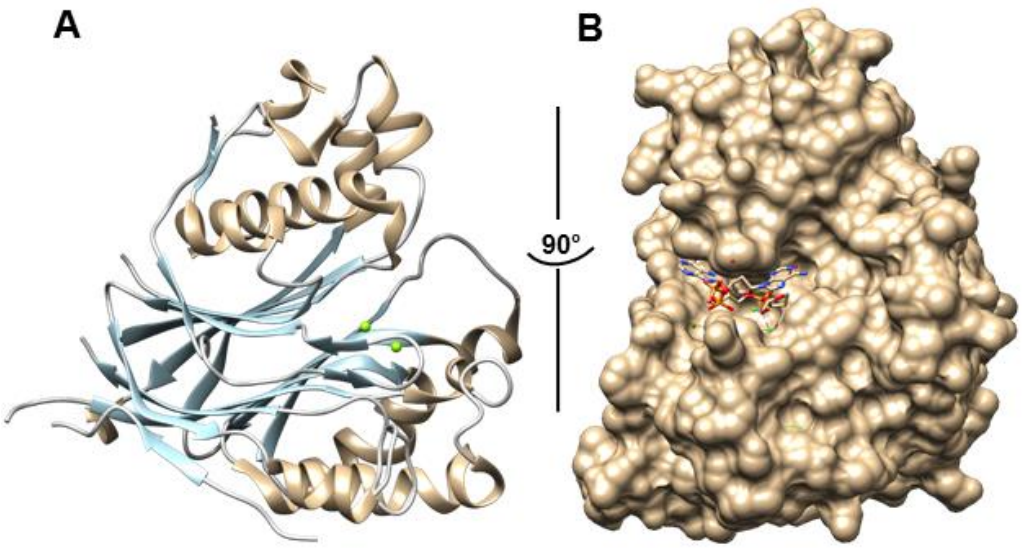

Figure 1.10 The Ccr4 catalytic subunit. (A) The structure of the human CNOT6L catalytic domain. (PDB accession number 3NGO). The Mg^{2+} at the active site are shown as green spheres, α-helical regions, tan, β strands in blue. (B) Binding of Poly (A) DNA substrate by human CNOT6L. Poly (A) DNA is shown as blue stick, Mg^{2+} at the active site are shown as green spheres. Structures were visualised using UCSF Chimera package.

1.5.1.1.2 The Caf1 subunit

The Caf1 crystal structure was initially identified from *S. cerevisiae* in 2003 (Thore et al., 2003). The structure is a kidney-like shape with α helices and β sheets (Figure 1.11). When the human CNOT7 structure in complex with Tob was reported, it shared a high similarity with Caf1 from the yeast. The CNOT7 subunit is characterised by an RNase D domain and belongs to the DEDD (Asp-Glu-Asp-Asp) superfamily of proteins (Thore et al., 2003, Jonstrup et al., 2007). Similar to the Ccr4 subunits, the human Caf1 proteins consist of two magnesium ions which are essential for enzyme activity. The metal ions are coordinated by a single glutamate and three aspartate residues. The substitution of these amino acids will abolish enzyme activity (Thore et al., 2003, Jonstrup et al., 2007). There are other bivalent cations which may modulate enzyme activity at the active site (Andersen et al., 2009b). Caf1 is structurally similar to DNA polymerase III and the exonuclease domain of DNA polymerase I though there is low similarity in sequence. In vertebrates, the CNOT7 and CNOT8 are two related paralogs of the Caf1 subunit. Studies show that AMP is released as a reaction product of Caf1 enzymatic activity (Bianchin et al., 2005). The Caf1 proteins are 76% identical and 89% similar at the amino acid level.

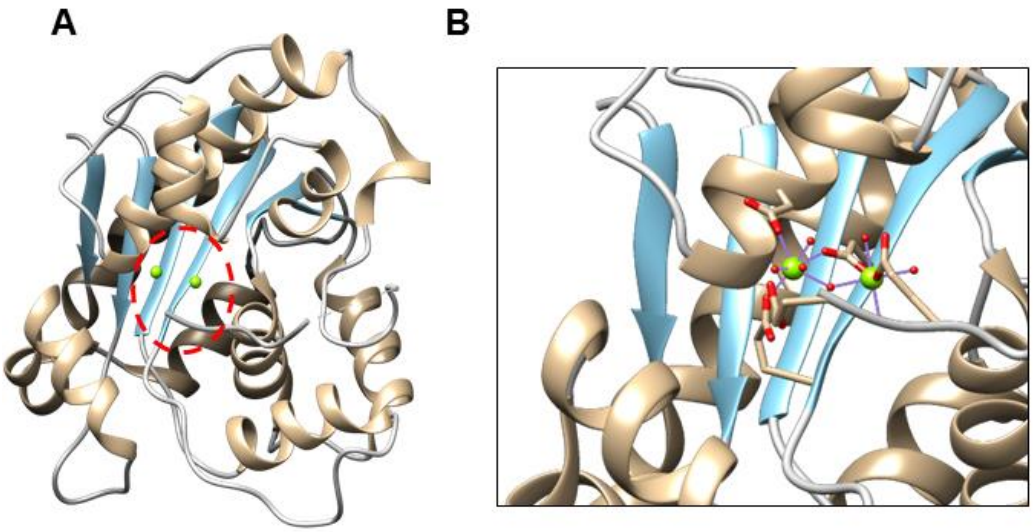

Figure 1.11 The Caf1 catalytic subunit. The structure of the human CNOT7 active site. (PDB accession number 4GMJ). The Mg^{2+} at the active site are shown in green, α-helical regions, tan, β strands in blue. (B) Enlarged view of the CNOT7 active site indicating the catalytic residues in stick representation. Mg^{2+} are indicated as green spheres. Structures were visualised using UCSF Chimera package.

1.5.2 The Ccr4-Not complex interactions and recruitment to mRNA

It has been shown that the Ccr4-Not complex interacts with various proteins including RNA-binding proteins, miRNA-induced silencing complexes (miRISCs) and the BTG/TOB protein family (Doidge et al., 2012b). The anti-proliferative activity of BTG/TOB proteins and the regulation of mRNA abundance has been shown to be mediated through interactions with the CNOT7 and CNOT8 deadenylase enzymes. The Ccr4-Not complex regulates specific mRNAs by its interaction with these proteins which may recruit the complex to target mRNAs. The recruitment of Ccr4-Not complex to target mRNA could be either by direct interactions with poly (A) binding protein or with targeted sequence specific RNA binding proteins or via microRNA decay machinery (Wahle and Winkler, 2013). Regulated recruitment of the Ccr4-Not complex also occurs via binding to ARE elements. RNA binding proteins that interact with the Ccr4-Not and suppress mRNA targets include Nanos, Pumilio, fem-3 binding factor proteins, Tristrapolin (TTP), Roquin, Y^{th} domain proteins and Bicaudal-C (Bic-C) (Semotok et al., 2005, Goldstrohm et al., 2007, Fabian et al., 2013, Leppek et al., 2013) interact with Ccr4-Not complex and target specific mRNAs. Other RNA binding proteins including Cytoplasmic polyadenylation element-binding protein (CPEB) recognise U-rich RNA sequence through two RRM motifs in the C-terminal. CPEB binds to specific mRNAs and requires TOB as an adaptor protein to enhance the recruitment of the Ccr4-Not complex to degrade the mRNA (Hosoda et al., 2011, Ogami et al., 2014). TOB recruits the Ccr4–Not complex to PABPC that is bound to the mRNA poly (A) tail (Ezzeddine et al., 2012, Stupfler et al., 2016). The Ccr4-Not is also involved in the microRNA mediated deadenylation of mRNAs through interaction with the AGO and GW182 proteins (Behm-Ansmant et al., 2006, Braun et al., 2011). AGO recruits the GW182 proteins which binds to the large CNOT1 of the Ccr4-Not complex (Braun et al., 2012) (Figure 1.12).

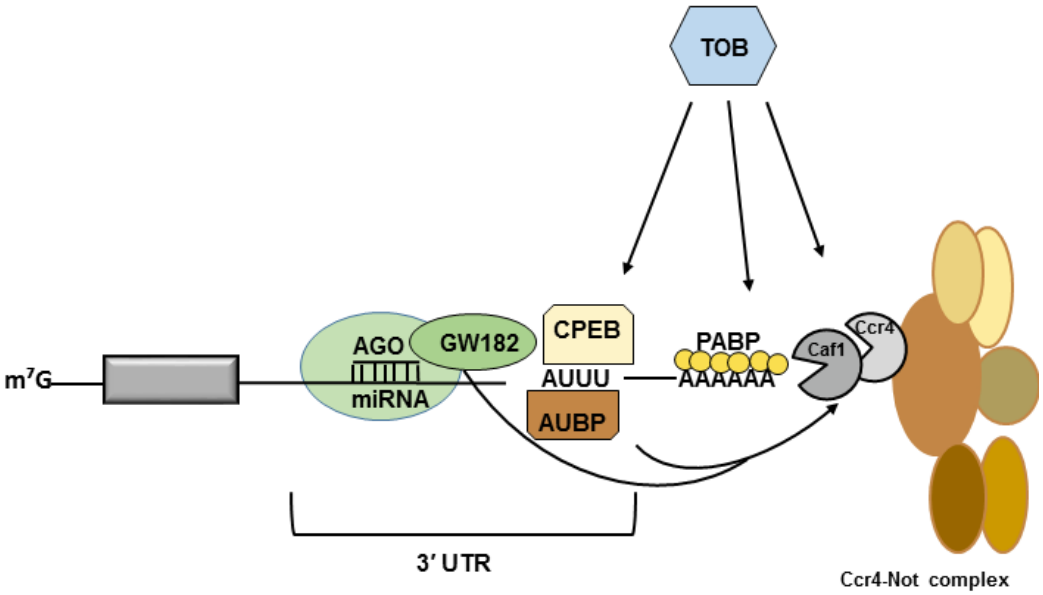

Figure 1.12. Schematic showing recruitment of the mammalian Ccr4-Not complex for initiating deadenylation. (A) The Ccr4-Not complex is recruited to the 3' UTR of specific mRNAs by direct interactions with poly (A) binding proteins (PABP). It is also recruited by AU-rich RNA binding proteins (AUBP). These include tristetraprolin (TTP), AGO proteins which associate with GW182 together with miRNA. These interactions initiate deadenylation. TOB1 enhances the recruitment of the Ccr4-Not complex to specific mRNA by interaction with the C terminal domain of PABP via the PAM2 motif. TOB1 also enhances recruitment of the Ccr4-Not complex to the polyadenylation element binding protein (CPEB) by an interaction with the Caf1 sub-unit.

1.5.3 The role of the Ccr4-Not complex in physiological function and human disease

The Ccr4-Not complex is implicated in physiological processes and plays distinct roles in various human diseases (Collart, 2003, Ito et al., 2011). While the complex exists in both the cytoplasm and nucleus, its localisation determines its role (Collart and Panasenko, 2012a). The main role of the Ccr4-Not complex is deadenylation thus regulating mRNA abundance. Recent studies using mammalian cell culture and genetically modified mice have shown the roles of the Ccr4-Not subunits in various physiological processes. A deviation in Ccr4-Not expression has been found in various diseases based on clinical specimen analysis (shirai, yamamoto, 2014). Studies show that Ccr4 and Caf1 deadenylase allow for specific targeting and regulation of deadenylation (Collart et al., 2013). A deficiency of CNOT7 results in physiological abnormalities in mice. In CNOT7 knockout mice, the males were found to be apparently normal but had a high bone mass phenotype and CNOT7 was identified as a potential regulator of bone morphogenesis (Washio-Oikawa et al., 2007). In CNOT7 males knock out mice it was observed that the males were defective in spermatogenesis associated with oligo-astheno-teratozoospermia (Berthet et al, 2004; Nakamura et al, 2004; shirai et al, 2014). This phenotype is intriguing considering that CNOT7 is one of the subunits of the CCr4-Not complex that is ubiquitously expressed in adult mouse. CNOT7 was also identified to be a therapeutic target in cancer metastasis. Using mouse models, breast cancer cells were engineered to express similar amounts of the wild type and inactive mutant D40A. It was observed that there was a dramatic reduction in pulmonary metastatic events (ref). A recent study identified CNOT7 as a potential therapeutic target for anti-metastatic therapy (Faraji et al., 2016). The findings show that a high expression of CNOT7 is a driver of tumour cell autonomous metastatic events, requiring its deadenylase activity.

Further studies reveal that the non-catalytic subunits of the Ccr4-Not complex have been implicated in various physiological processes and disease.

They were shown to be essential for embryonic development in higher eukaryotes (Collart et al., 2013). In addition to the catalytic subunits, CNOT1 and CNOT2 subunit affect cell proliferation and or cell death (Aslam et al., 2009, Yang et al., 2008, Mittal et al., 2011). CNOT1 knock out mice died during embryonic development. Research done in HeLa cells show that a depletion of CNOT1 affects poly (A) tail removal and reduces the number of P-bodies, in which mRNA decay is thought to occur (Ito et al., 2011). CNOT2 and CNOT3 have been shown to affect cell cycle progression in mammalian cells through regulation of mRNA turnover (Ito et al., 2011). CNOT2 was also shown to be pertinent for susceptibility of breast cancer to metastasis (Faraji et al., 2014). Using genome-wide RNAi screen conducted in mouse cells, CNOT3 was identified as vital for cells to self-renew (Hu et al., 2009). CNOT3 was also identified to be important for heart function (Morita et al., 2011). In heterozygous CNOT3 null mice to evaluate the importance of CNOT3 in heart function, there was an expression of half the amount of CNOT3 but normal amounts of the subunits of the Ccr4-Not complex. Dysregulation of CNOT3 expression is closely connected to a various human diseases (Shirai et al., 2014). SNP analytical reports show that there is a correlation between CNOT3 polymorphism and cardiac repolarization duration (Neely et al, 2010). In mammals, a deficiency in CNOT3 resulted in lethality of mice at early embryonic stages. This implies that CNOT3 is essential for embryonic viability (Neely et al;2010; Morita et al, 2011). CNOT3 is shown to be essential in metabolic regulation. In a recent study, CNOT3 +/- mice were lean and displayed resistance to high fat diet induced obesity compared to control mice due to enhanced metabolic rates and glucose tolerance (Morita et al., 2011). A reduction in CNOT3 expression affects specific mRNA stability that encode proteins involved in energy metabolism. In the study, CNOT3 was also discovered to be involved in the recruitment of the Ccr4–Not deadenylase to mRNAs

1.6 The BTG/TOB protein family

The BTG/TOB family are an antiproliferative gene family that consists of six members in human cells. These include BTG1, BTG2/PC3/Tis21, BTG3/Ana, BTG4/PC3B, TOB/TOB1 and TOB2 (Winkler, 2010, Mao et al., 2015). These proteins regulate cell cycle progression in various cell types and are characterised by a conserved N-terminal BTG domain that extends from 104-106 amino acids (Matsuda et al., 2001, Tirone, 2001). Amongst the members of the BTG/TOB family, BTG1 and BTG2, TOB1 and TOB2 are highly similar (Figure 1.13). BTG3 and BTG4 are more distantly associated. Structurally, the conserved domain of BTG N-terminus consists of two regions: box A and box B regions which is highly conserved compared to the other domains (Boiko et al., 2006b, Horiuchi et al., 2009, Zhang et al., 2011, Winkler, 2010). Box A and box B regions mediate interaction with Caf1 catalytic subunit of the Ccr4-Not deadenylase complex (Duriez et al., 2004, Yang et al., 2008, Horiuchi et al., 2009, Aslam et al., 2009, Winkler, 2010). The conserved BTG domain is shown to mediate protein-protein interactions as illustrated by the crystal structure of TOB1 in complex with CNOT7 (Horiuchi et al., 2009). CNOT7 interacts with TOB1 through the amino-terminal BTG domain of TOB1. An alignment of the crystal structure of TOB1 in complex with CNOT7 (PDB accession number 2D5R) and human BTG2 (PDB accession number, 3DJU) shows that the BTG domain of TOB1 and BTG2 are very similar (Figure 1.13). The CNOT7 and BTG2/TOB protein interaction mediates the recruitment of the Ccr4-Not complex to target mRNA. In addition, the two highly similar TOB proteins, TOB1 and TOB2 contain a (Poly (A)-binding-protein-interacting Motif 2) PAM2 motif in their C-terminal regions which mediate interactions with poly (A)-binding protein PAPB (Ezzeddine et al., 2007, Mauxion et al., 2008, Funakoshi et al., 2007) Unlike the other family members, BTG1 and BTG2 have an additional box C region and reports show that they bind to the poly (A)-binding protein PABPC1 via the box C region (Yang et al., 2008, Stupfler et al., 2016). This interaction is enough to trigger Caf1 deadenylase activity *in vitro* in the absence of other CCR4–NOT complex subunits. The interaction

also plays a vital role in the control of cell proliferation and translational repression. Interaction studies done *in vitro* show that mutants of BTG2 can retard the activity of Caf1 although the conserved BTG2 domain of TOB1 does not affect the activity of Caf1 (Yang et al., 2008, Horiuchi et al., 2009). Research based on reporter genes show that BTG2, TOB1 and TOB2 promote deadenylation and mRNA decay in cell-based assays (Ezzeddine et al., 2007, Mauxion et al., 2008, Doidge et al., 2012b, Ezzeddine et al., 2012).

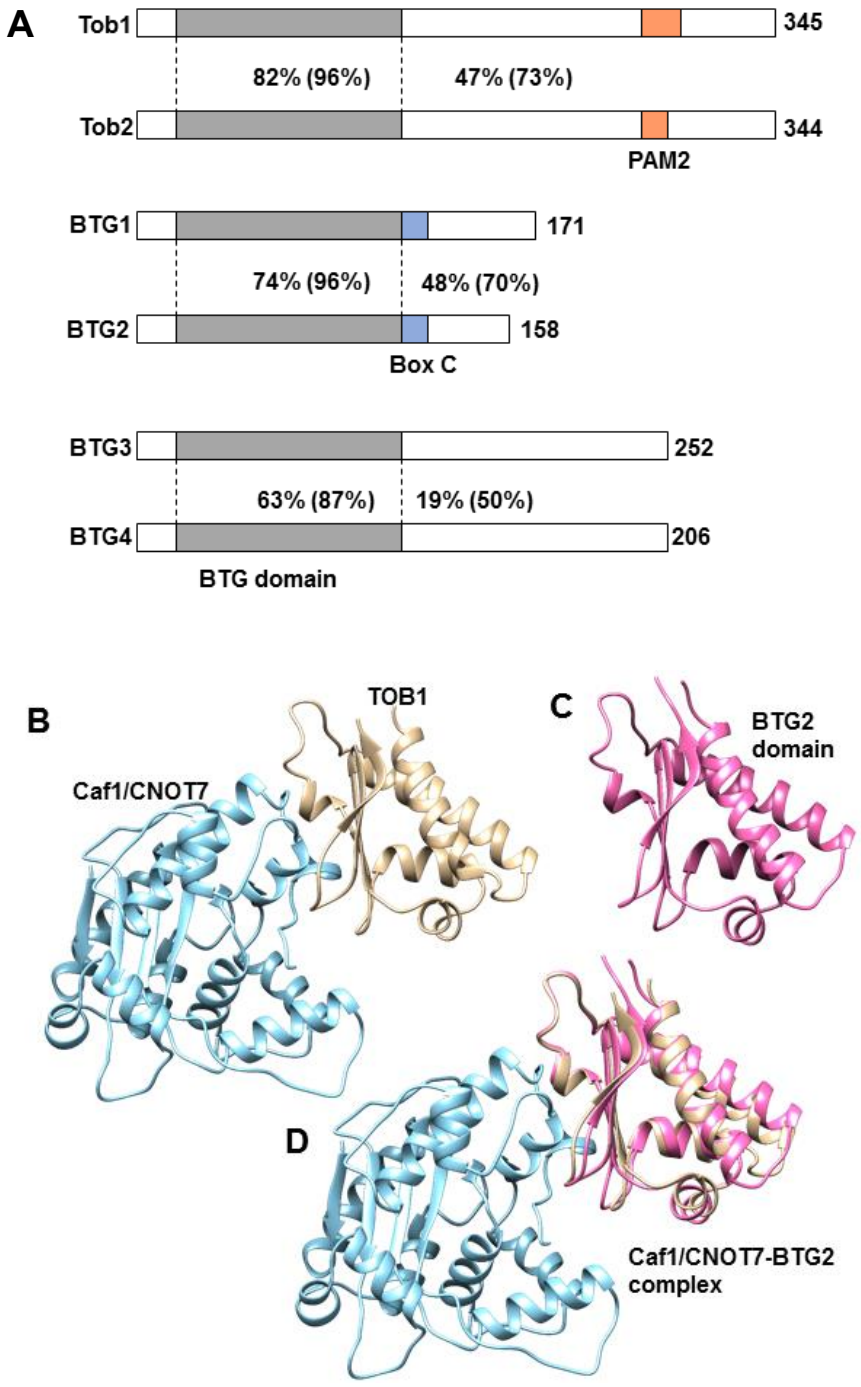

Figure 1.13 A representation of BTG/Tob protein family. (A) Diagram is based on amino acid sequences. BTG domain is shown in grey, the conserved PAM motif in orange and the Box C is shown in blue. The size of amino acids and percentage of identical amino acids are also represented. (B)Caf1/Tob1 crystal structure. (C) BTG2 domain. (D) Caf1/BTG2 complex. Caf1 is shown in blue, Tob1 BTG domain in complex with Caf1 (Khaki) and BTG2 (pink). This model was generated by the alignment of the Tob1-Caf1 structure (PDB accession number 2D5R), and BTG2 (PDB accession number 3DJU). Structures were visualised using UCSF Chimera package (http://www.cgi.ucsf.edu/chimera;Pettersen et al, 2004).

1.6.1 BTG2 and mRNA deadenylation.

In humans, the BTG2/TOB protein interaction with CNOT7CNOT7is the most characterised. All BTG/TOB proteins except BTG4 can interact with the Caf1 paralogues (CNOT7 and/or CNOT8) (Collart and Panasenko, 2012a, Doidge et al., 2012a, Goldstrohm and Wickens, 2008, Bartlam and Yamamoto, 2010). Previous studies indicated that BTG2 could function as transcription cofactor (Guardavaccaro et al., 2000, Prevot et al., 2000, Passeri et al., 2006), however, the ability of BTG/TOB to interact with CNOT7 deadenylase indicates that BTG/TOB proteins could also play a role in mRNA deadenylation. Consistent with that, overexpression of TOB and BTG2 proteins triggered deadenylation of reporter and endogenous transcripts (Ezzeddine et al., 2007, Mauxion et al., 2008). Through bioinformatic analysis of the structure of TOB1/CNOT7 complex and BTG2, the Box A and Box B regions appear close to CNOT7 and may be required for interaction. Research findings show that amino acid substitutions within box A and box B regions can disrupt interactions with CNOT7 (Yang et al., 2008, Horiuchi et al., 2009). In addition, the interaction is away from the active site of CNOT7 and therefore leaves the C terminal domain of BTG/TOB available to interact with other possible RNA binding protein. The mechanism by which BTG2 protein increase mRNA deadenylation remains unclear. Studies show TOB1 may increase mRNA deadenylation and co-localise to P-bodies indicating its role in mRNA turnover (Ezzeddine et al., 2007). The ability of TOB proteins to associate concurrently to Caf1 and the MLLE domain of PABPC gave an indication that TOB would recruit the CCR4–NOT complex to PABPC that is bound to the mRNA poly (A) tail. It also implied that the PABPC1 serves as a docking protein for binding to target mRNA. However, the dependence on PABPC1 binding of TOB-enhanced deadenylation/decay can be bypassed if TOB is directly tethered to the target mRNA. This notion was established by studies where it was observed that the requirement for PABPC binding was abolished when TOB was tethered directly to mRNA. TOB mutants unable to bind PABP promoted rapid deadenylation and decay only if tethered to the target mRNA

(Ezzeddine et al., 2012). The lack of a PAM2 motif in BTG2 was suggestive of an alternative model by which BTG2 stimulates mRNA decay. BTG2 may interact directly or indirectly with other conserved features of mRNAs such as the cap, bound ribosomes or translation factors. Studies in mammalian cells suggest that BTG2 may be involved in general activation of mRNA decay (Mauxion et al., 2008).

1.6.2 BTG/TOB proteins, role in tumorigenesis and cancer

Studies have proposed that BTG/TOB family is a potential biomarker for prognosis in cancer patients (Wagener et al., 2013, Zhang et al., 2013, Takahashi et al., 2011). TOB1 is shown to inhibit cell growth by suppressing the expression of Cyclin D1. The phosphorylation of TOB1 via Ras signalling component Erk1/Erk2 is shown to result in the loss of TOB1 antiproliferative activity (Suzuki et al., 2002, Boiko et al., 2006b). Mice that lack TOB1 were shown to be prone to cancer with high frequencies in liver, lung and lymph nodes (Yoshida et al., 2003). Other reports have also suggested that BTG/TOB proteins may be directly involved in cancer. BTG2 is shown to be closely associated with tumour suppressor genes including p53, p73 and RB (Melamed et al., 2002, Zhang et al., 2011, Boiko et al., 2006a, Rouault et al., 1996). The frequency of tumours is shown to increase in the absence of p53 (Yoshida et al., 2003). Expression of BTG3 is shown to be relatively high in normal lung cells however, its expression in human cancer cell lines is reduced (Yoneda et al., 2009). Based on the analysis of clinical samples from various tumour types, a reduction in BTG expression or inactivation by phosphorylation gave an indication that the event contributes to carcinogenesis and tumour growth (Winkler, 2010). Research show that BTG2 protein expression is downregulated in laryngeal carcinoma (Liu et al., 2009). While BTG2 expression in patients with pancreatic cancer is suppressed in tumour tissues compared to non-cancerous tissues (Mao et al., 2015), It is reported that BTG2 expression is reduced in clear renal cell carcinomas (Struckmann et al., 2004). A reduction in BTG2 is related to tumour size, grade, metastasis and poor survival in patients with breast cancer (Mao et al., 2015). In human kidney and breast cancer cells, BTG2 expression is shown to be reduced significantly (Boiko et al., 2006b). Analysis of human clinical samples show that BTG1 and BTG2 are mutated in NHL (Morin et al., 2011). Recently, mutations in the BTG1 and BTG2 were identified in about 10-15% of Non-Hodgkin's lymphoma (NHL) cases (Morin et al., 2011, Lohr et al., 2012, Love et al., 2012), suggesting a direct

involvement of BTG1 and BTG2 in lymphoma. However, the underlying mechanism of BTG2 function in cancers is not fully understood. Taken together, the observation of an impaired expression or inactivation of BTG/TOB proteins in clinical samples of patients indicates that the loss of BTG/TOB expression enhances cancer growth.

1.7 Aim of study

Over the years, studies have revealed distinct roles of the Ccr4-Not complex subunits in regulation of a wide range of physiological and disease phenomena. However, the involvement of the Ccr4-Not deadenylase in the onset and progression of these diseases remains unclear. The overall aim of this study is to characterize the Ccr4-Not deadenylase as a potential drug target focussing on the catalytic subunits of the Ccr4-Not complex. This would be useful as pharmacological intervention in human disease. To facilitate the discovery, development, and characterisation of small drug-like inhibitors of the Ccr4-Not deadenylase enzymes, I used a biochemical approach. In addition, a cell-based approach was used to characterise lymphoma associated variants of the Caf1-interacting protein BTG2. The specific aims are:

1. To purify and investigate the biochemical properties of the highly similar CNOT6 and CNOT6L enzymes.

2. To evaluate the potential use of AMP detection as the basis of a method to determine the activity of the Ccr4-Not catalytic subunits and characterise *N*-hydroxyimide inhibitors of CNOT7.

3. To evaluate the use of thermal shift assays (TSAs) for the characterization of the binding mode of drug-like inhibitors.

4. To determine the ability of BTG2 variants found in lymphoma to interact with the Caf1 subunit of the Ccr4-Not complex and the ability of BTG2 variants to induce mRNA degradation using a reporter mRNA.

1.8 Experimental approaches

1.8.1 Protein purification and biochemical characterisation of Ccr4-Not deadenylases

Using a biochemical approach, I aim to first purify and investigate the biochemical properties of the highly similar CNOT6 and CNOT6L enzymes as a starting point for the characterisation of the Ccr4-Not deadenylase activity. An analytical purification based on immobilised metal affinity chromatography will be performed. Typically, plasmids containing the gene of interest will be transformed into bacteria for expression of His-tagged proteins in pQE80L plasmids. Thereafter proteins will be purified and analysed (Figure 1.14A). Affinity-based purification are specific for the proteins to be separated, however some bacteria native proteins may also contaminate the proteins. To eliminate this, and to ensure maximum purity, further purification by ion exchange chromatography will be carried out.

Once a procedure for the purification of the Ccr4 proteins is established, the enzymatic activities of the CNOT6 and CNOT6L proteins will be investigated using an established fluorescence-based assay Figure 1.14B). The fluorescence-based assay is a substrate detection method based on fluorescence resonance energy transfer (FRET) which has been well characterised (Maryati et al., 2014). The assay involves incubation of a 5´ Flc-labelled RNA oligonucleotide substrate with the deadenylase enzyme. At a specified time point, the reaction is stopped by the addition of a 3´TAMRA–labelled DNA oligonucleotide probe which is complementary to the RNA substrate. When there is no activity, Flc fluorescence of the intact substrate is quenched as the DNA probe hybridizes with the RNA. On the contrary, when there is deadenylase activity, the TAMRA probe cannot hybridize to the Flc-labelled reaction product due to substrate degradation thus allowing for detection of fluorescence (Figure 1.15) Thereafter, an evaluation of activity measurements in a plate-based format will be carried out using both proteins. For controls, the inactivating amino acid substitutions at the catalytic site will be used.

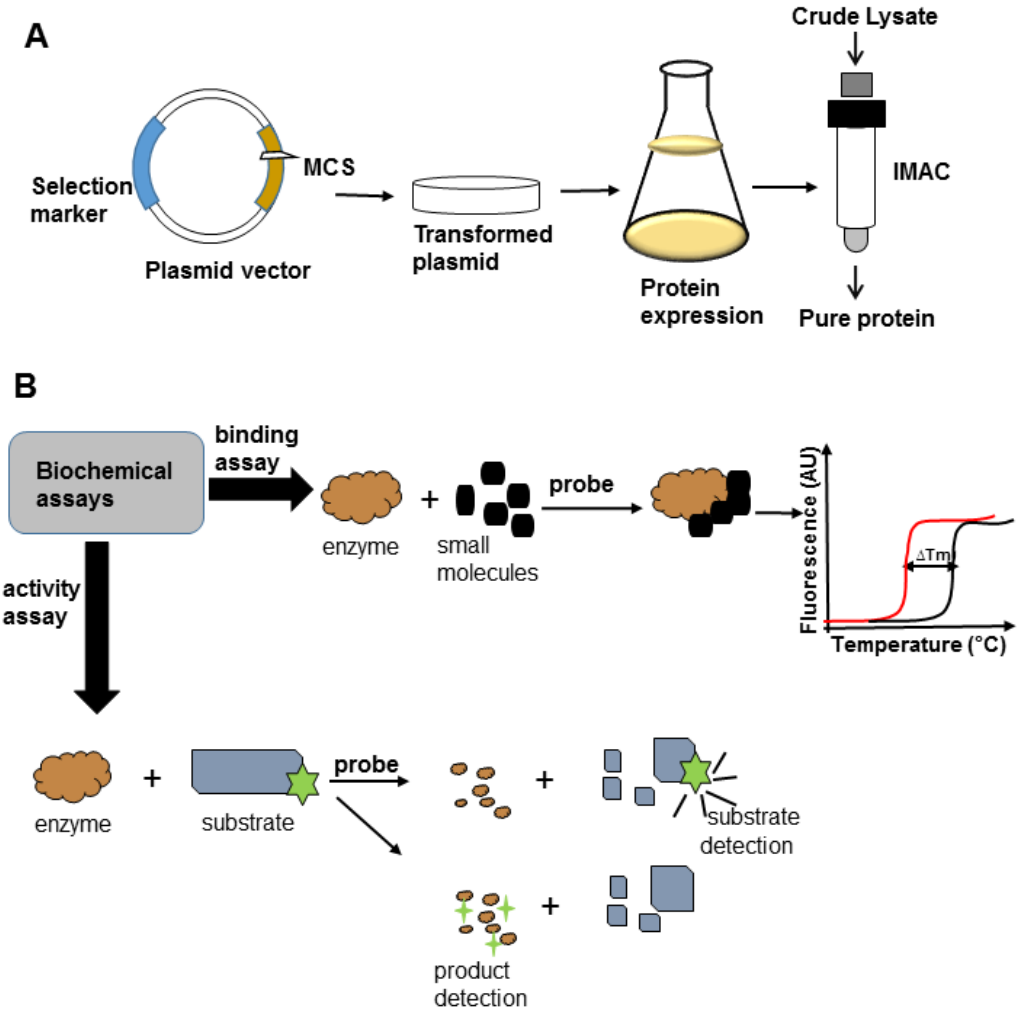

Figure 1.14. An overview of experimental approaches used in this thesis. (A) Expression and purification of proteins for use in assays. Plasmids containing genes for expression were transformed into bacteria, *E.coli*, expressed and purified by immobilised metal affinity chromatography. (B) Schematic showing biochemical assays used for deadenylase enzyme characterisation. Assays were either discontinuous activity assays based on substrate or product detection (left panel) or biochemical binding assays (thermal shift assays) (right panel).

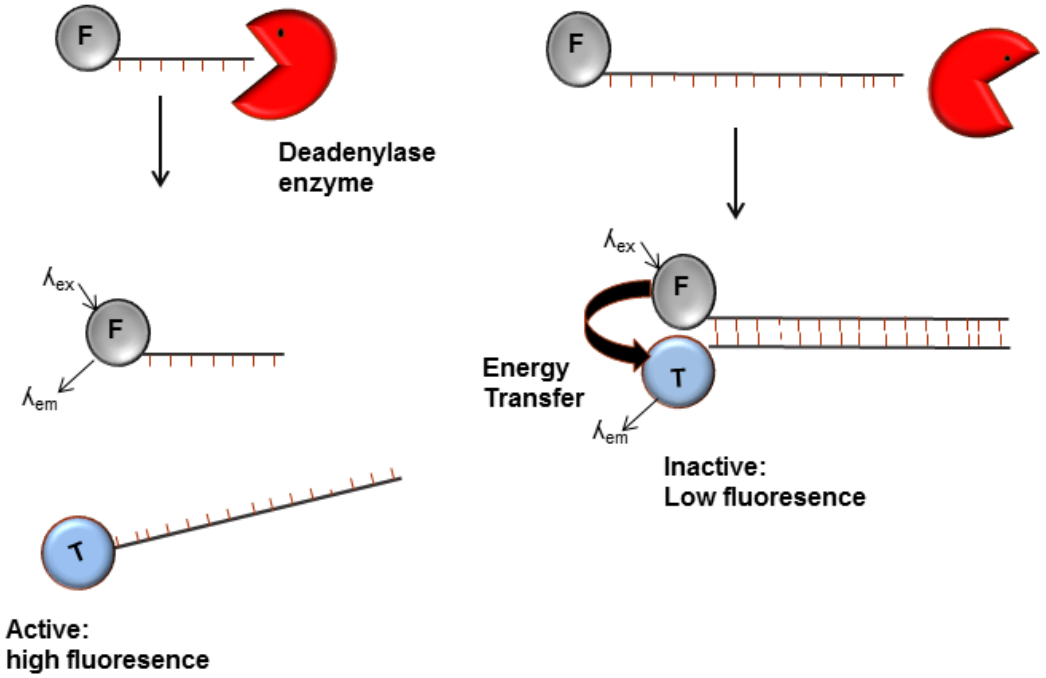

Figure 1. 15 The principle of fluorescence-based assays.
A schematic representation of the substrate fluorescence-based assay. The assay involves the incubation of a 5´ Flc-labelled RNA oligonucleotide substrate with the deadenylase enzyme. The reaction is terminated by adding SDS and a 3´labelled DNA oligonucleotide probe which is complementary to the RNA substrate. When the enzyme is active, the probe cannot hybridize to the Flc-labelled RNA product which allows the detection of fluorescence (left). On the contrary, in the presence of inactive enzyme, the fluorescence labelled substrate is intact and is quenched when the probe hybridises (right).

1.8.2 Evaluation of biochemical assays for characterization of Ccr4-Not deadenylases

This section is aimed at evaluating the potential use of two biochemical assays for characterisation of the Ccr4-Not deadenylase. These include the use of AMP detection as the basis of a method to determine the activity of the Ccr4-Not catalytic subunits and characterise *N*-hydroxyimide inhibitors of CNOT7. It will also involve the use of thermal shift assays (TSAs) for the characterization of the binding mode of drug-like inhibitors. These are discontinuous assays performed in multiwall plate format which are widely applicable. The evaluation of these assays would determine their complementarity to a substrate fluorescence-based assay previously established and their usefulness for counter screening of deadenylase enzyme activity and compounds. The AMP-based detection assays will involve biochemical reactions which was based on AMP, a reaction product of deadenylation. It is a homogenous assay that generates light signal from any reaction that produces AMP as a reaction product. AMP-based assays quantitatively monitor the concentration of AMP in a biochemical reaction in a high-throughput format. Enzymatic activities will be measured by AMP chemiluminescence. The assay involves two steps: First, the termination of enzymatic reaction, simultaneous removal of adenosine triphosphate (ATP) and conversion of AMP produced to ADP by the enzyme polyphosphate AMP phosphotransferase (PAP). The second step involves the conversion of ADP to ATP by a second enzyme adenylate kinase (AK) and determining the amount of the ATP produced using a bioluminescent reaction utilizing a luciferase enzyme and a substrate for the luciferase enzyme. (Figure 1.16). The amount of ATP produced determines the amount of AMP present in the original solution. The amount of AMP produced by the reaction is proportional to the light measured and can be extrapolated using a standard curve.

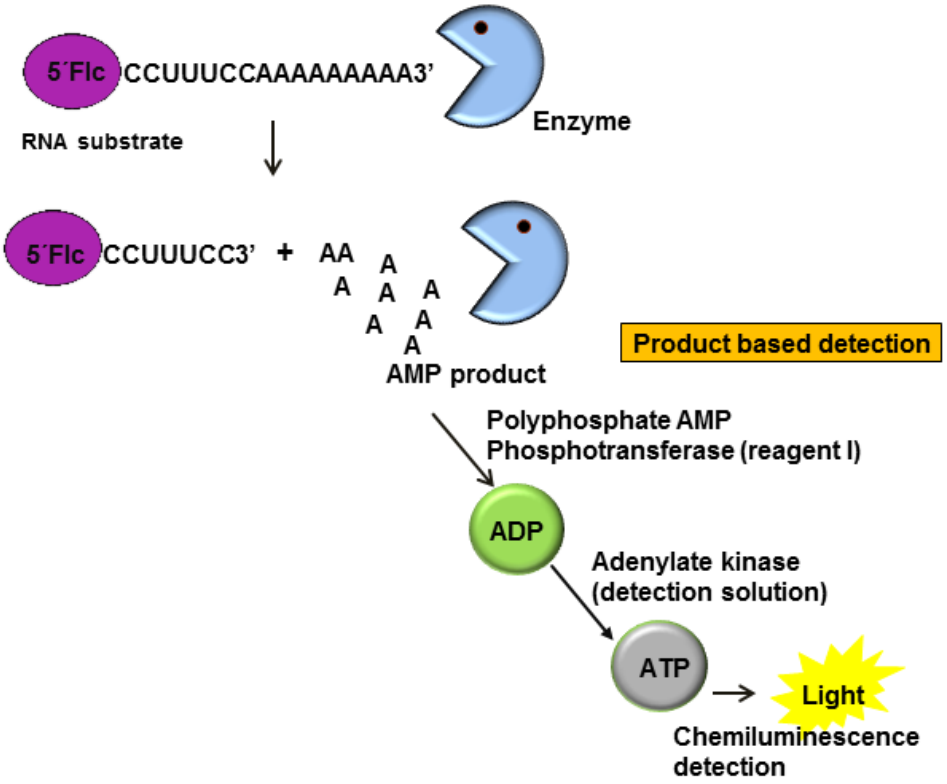

Figure 1.16 Principle of AMP-based deadenylase assay. A schematic representation of AMP product-based measurements of enzyme activity. Deadenylase enzymes are incubated with 5´ Flc-labelled RNA oligonucleotide substrate for 60 minutes at 30^0C. Reactions for AMP product-based measurements are terminated by the addition of AMP-Glo reagent I containing the enzyme polyphosphate AMP phosphotransferase (PAP) for conversion of AMP to ADP. Then an AMP detection solution containing adenylate kinase enzyme is added for conversion of ADP to ATP and the amount of ATP produced is determined by chemiluminescence. The amount of ATP produced is proportional to the light measured and determines the amount of ATP in the original solution. In the absence of enzymatic activity, there are no AMP products.

Next, thermal shift assays will be used to screen small molecular inhibitors as an alternative assay. Protein stability is a common property that can be modulated by binding of small molecules and thermal shift assays are established tool for the assessment of protein stability and their interactions with ligands. TSAs monitor unfolding of proteins from the native to denatured form in the presence of a fluorescence dye which shows enhanced fluorescence in a hydrophobic environment and serves as a reporter to monitor thermal unfolding of the protein. Proteins in their native form are folded, when exposed to a range of temperature the protein unfolds. As the protein unfolds, the hydrophobic pockets become exposed allowing binding of the SYPRO Orange dye, resulting in increased fluorescence (λ_{ex} = 492 nm, λ_{em} = 610 nm) and thus acts as reporter to monitor thermally induced protein unfolding. A gradual fall is observed following the peak fluorescent intensity mainly due to protein aggregation, precipitation and dye dissociation (Figure 1.17). This assay method requires relatively low sample amounts and can be used to measure many conditions in parallel on one multiwell plate. TSAs therefore will be explored as a means to unravel the binding mode of some small molecular inhibitors of CNOT7 deadenylase (more details to follow). Thermal shift assays are typically conducted with a real-time PCR where the protein samples are mixed with other additives, and a fluorescent dye (Figure 1.17).

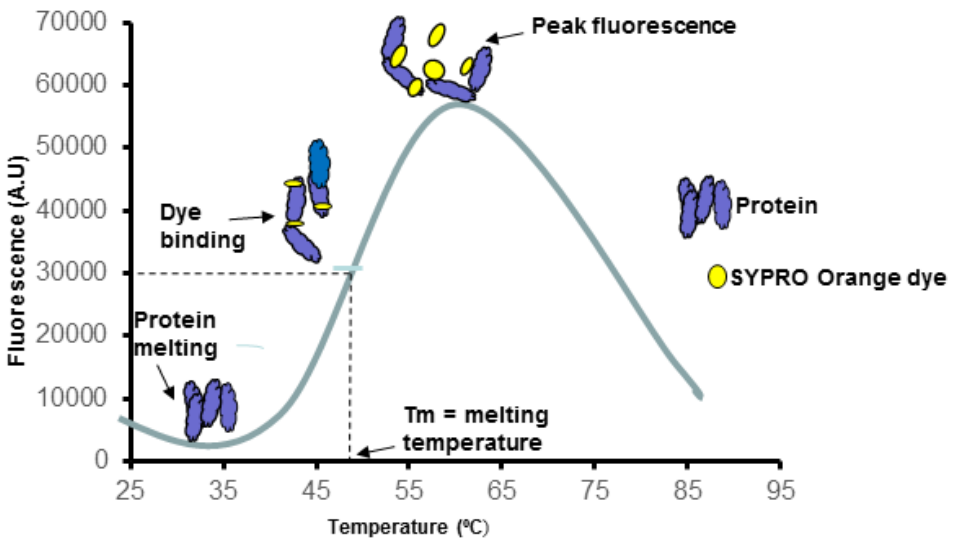

Figure 1.17 Principle of Thermal Shift Assay (TSA). A schematic showing typical unfolding of protein in the presence of the dye SYPRO orange. As the protein unfolds, hydrophobic pockets become exposed allowing binding of the SYPRO orange and resulting in increased fluorescence (λ_{ex} = 492 nm, λ_{em} = 610 nm). A gradual fall is observed following the peak fluorescent intensity mainly due to protein aggregation, precipitation and dye dissociation. The melting temperature (Tm) of the protein is determined by the transition midpoint between the native and unfolded state.

1.8.3 Yeast two hybrid analysis and RNA tethering assay

To determine the ability of BTG2 variants found in lymphoma to interact with the Caf1 subunit of the Ccr4-Not complex, yeast-two hybrid analysis will be used. The transcriptional and post translational protein modifications of budding yeast *Saccharomyces cerevisiae* are well conserved in higher organisms. This method is easily conducted in budding yeast *Saccharomyces cerevisiae* and is useful for studying eukaryotic protein interactions. This method takes advantage of the ability to disengage the DNA binding domain (DBD) and transcriptional activation domain (AD) of transcription factors. The DBD can bind to DNA without activating transcription; the AD domain cannot bind to DNA and recruit RNA Pol II by itself. Both the DBD and AD domains must be brought together onto the promoter to initiate transcription, normally of a reporter gene like β-Galactosidase. The AD and DBD domains are fused to two target proteins. If the target proteins interact they bring together the DBD and AD domain onto the β-Galactosidase promoter and initiate transcription (Figure 1.18A) (left panel). If there is no interaction between the two target proteins or if that interaction has been disrupted by amino acid substitutions, then there will be no transcription because the AD domain will not be brought to the promoter (Figure 1.18A) (right panel). The primary limitation to the yeast two-hybrid system is the high incidence of intrinsic transcriptional activation caused by the protein being tested. To address this all proteins will be tested individually to ensure they are not capable of stimulating β-Galactosidase transcription alone. In this project, the yeast two-hybrid system will be used to screen amino acid substitutions of BTG2 implicated in lymphoma and disrupt the interaction between BTG2 and the deadenylases CNOT7 and CNOT8. To correlate the yeast-two hybrid findings in human cells to determine the ability of BTG2 variants to induce mRNA degradations, RNA tethering assay will be performed in HEK293T cells.

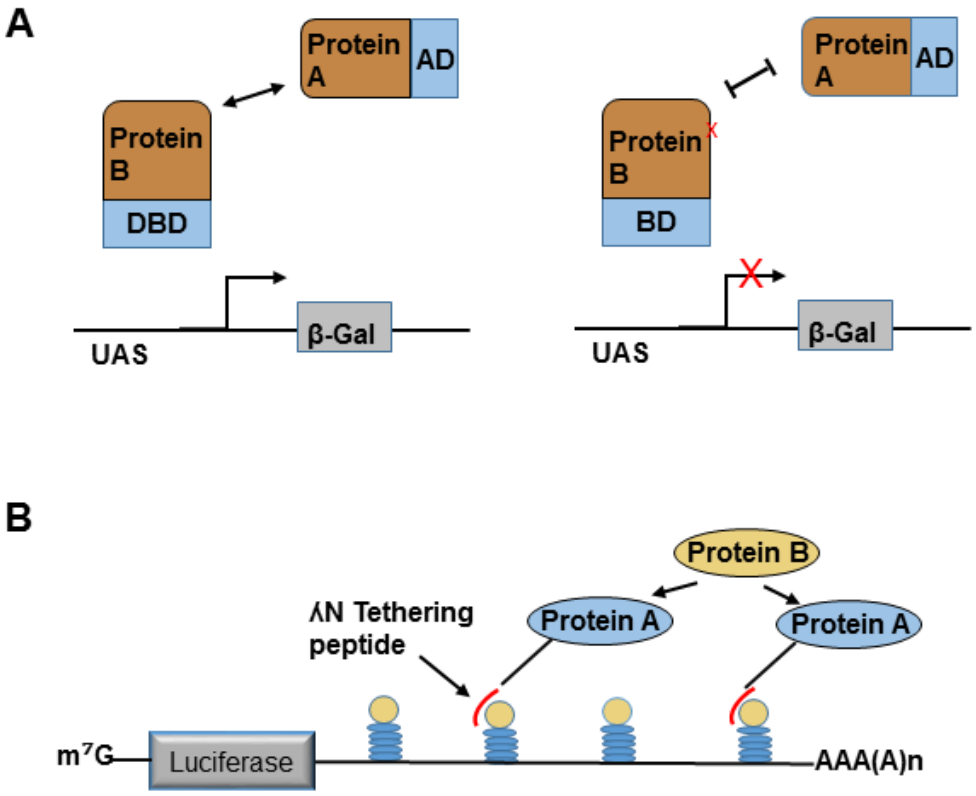

Figure 1.18 A representation of experimental approaches used in this thesis. (A) Yeast two hybrids**.** When there is an interaction between protein A and protein B, the Gal4-binding domain (Gal4-BD) and the Gal4 activation domain (Gal4-AD) are brought in close proximity on the β-Galactosidase promoter triggering transcription (left panel). In the absence of interaction between protein A and protein B, there is no transcription initiation (right panel). (B) RNA tethering assay. When protein A fused to the ʎN peptide is expressed, it will bind to the 5 Box B motifs located in the renilla luciferase mRNA 3' UTR. This enables protein A to recruit other factors to the 3'UTR that may affect mRNA stability or translation.

The assay uses the RNA binding properties of the bacteriophage lambda-antiterminator protein N (lambda N-peptide). This 22-amino acid peptide is fused to a target protein of interest (here the BTG proteins) allowing it to bind to specific RNA motifs. A renillia luciferase plasmid was modified to include the corresponding RNA motifs in its 3' UTR. These Box B sequences form hairpin loop structures that bind to the lambda N-peptide and therefore cause the target protein to be tethered to the luciferase mRNA 3' UTR (Figure 1.18B). This reporter system can be used to identify changes in translation and mRNA stability in response to the presence of BTG proteins bound to mRNA.

Chapter 2

Materials and Methods

Chapter 2 Materials and Methods.

2.1 Bacterial growth and transformation

2.1.1 Reagents, stock solutions and buffers

Lysogeny broth (LB) media and agar: 10 g/L tryptone, 5 g/L yeast extract, 5 g/L NaCl, pH 7.2 (NaOH), LB agar included 15 g/L bacteriological agar. The medium was sterilised by heat using a Prestige medical 2100 classic bench-top autoclave and stored at room temperature.

Ampicillin 1000 x stock solution: 100 mg/ml in 50% ethanol/water. Sterilised by filtration (0.22 μM pore size). Stored at -20°C

Chloramphenicol 1000 x stock solution: 34 mg/ml in 100% ethanol. Sterilised by filtration (0.22 μM pore size). Stored at -20°C

1M IPTG: Isopropyl β-D-1-thiogalactopyranoside, in H_2O. Sterilised by filtration (0.22 μM pore size). Stored at -20°C.

2.1.2 Culture of Escherichia coli

The bacterial strain *E. coli* DH5α was used for all DNA manipulations. To obtain single colonies the bacteria were streaked onto agar plates (containing the appropriate antibiotics) and grown at 37°C. Once colonies had formed the plates were stored at 4°C for a few weeks. Liquid cultures were prepared by inoculating LB medium (in universal screw-cap tubes containing the appropriate antibiotics) with a single colony of bacteria and incubated at 37°C, 200 rpm for 12-24 h. For cultures grown on large scale, glass conical flasks were used.

2.1.3 Transformation of competent cells

Competent bacterial cells (50 µl) were used for plasmid transformation and 100 µl of competent cells were used for ligation or mutagenesis transformation. When transforming plasmids, 10 -100 ng of DNA was used to give a good transformation yield, when transforming ligations or mutagenesis reactions, 10 µl of ligation reaction mix was used. Competent *E. coli* cells and DNA were mixed in pre-chilled round bottomed universal tubes and incubated on ice for 5-20 minutes. The transformation mix was heat shocked by incubation at 42°C for 90 seconds followed by incubation on ice for 2 minutes. One millilitre of LB medium (pre-warmed at 37°C) was added to the cells and they were incubated at 37°C, 200 rpm for 1 hour. For plasmid transformation 100 µl of the cell suspension was spread onto LB agar plates (containing the appropriate antibiotic). For ligations or mutagenesis transformations the cells suspension was centrifuged at 3000 g for 2 minutes, 900 µl of supernatant removed and the cells re-suspending in the remaining 100 µl of LB. All the re-suspended cells were then spread onto LB agar plates (containing the appropriate antibiotic).

2.2 Molecular biology

2.2.1 Reagents, stock solutions and buffers

5 x TBE: 40 mM Tris base, 40 mM boric acid, 1 mM EDTA, pH 8.0, stored at room temperature

6 x Ficoll loading dye: 16% Ficoll, 0.2% Orange G in H_2O, stored at room temperature.

TE Buffer: 10 mM Tris-HCl pH 8.0, 1 mM EDTA

Oligonucleotides: Lyophilised primers were dissolved in TE to give a 100 mM solution and stored at -20^{0}C.

2.2.2 DNA plasmid purification

Plasmid mini prep kits obtained from Macherey-Nagel (Cat# 740588.250) were used for DNA plasmid purification. For small scale preparation, a single bacterial colony was picked and used to inoculate 2 ml LB in appropriate antibiotic. It was grown overnight in orbital shaker 200 rpm, at 37°C. The overnight culture was then spun in a micro centrifuge for 1-2 minutes at 6000 rpm until pellet form. The plasmid DNA was then extracted using Macherey-Nagel plasmid mini prep kits. Details of manufacturer's instructions can be found in the Macherey-Nagel plasmid mini prep handbook. Plasmids were eluted in 50 µl of elution buffer pre-warmed to 65°C. Plasmid DNA concentration was measured using a Nanodrop ND-1000 spectrophotometer, then stored at -20°C.

2.2.3 Determination of DNA concentration/quantification

Plasmid DNA concentration was determined using the NanoDrop ND-100 UV-Vis Spectrophotometer (NanoDrop Technologies). The A_{260}/A_{280} ratio values were calculated to estimate sample purity. A ratio between 1.8 and 2.0 was judged as acceptable for DNA samples.

2.2.4 Agarose gel electrophoresis

DNA samples were separated using agarose gels (0.8-2% w/v) as appropriate to the size of the DNA fragment being resolved. A 0.8% agarose gel (w/v) was prepared by dissolving 0.4 g of agarose in 50 ml of 0.5 X TBE. 0.5 µg/ml of ethidium bromide was added to the slurry and poured into a tank with appropriate comb. DNA samples were mixed with a six-fold Ficoll dye and loaded onto appropriate wells. 5 µl of NEB standard 1 kb DNA ladder marker diluted to 0.2 µg/µl was loaded alongside samples. DNA gels were run at 80 V for between 45 minutes and 2 hours depending upon the sample being run. Following electrophoresis, gels were visualised by transillumination with ultraviolet light and documented using a Gel-Doc 2000 (Bio-Rad) and BioRad Quantity One computer software.

2.2.5 Restriction enzyme digestion of DNA

DNA plasmids were digested using restriction enzymes to create compatible ends for cloning and to verify newly created plasmids. All restriction enzymes and buffers were supplied by NEB and the instructions provided were followed.

For verification of new plasmids from ligation products, 100 ng of plasmid DNA was digested in 20 µl total reaction volume. To digest large amount of DNA for cloning, 5 µg of plasmid DNA was digested for 2 hours at 37°C.

2.2.6 Extraction and purification of DNA from agarose gel

To purify DNA fragments from gels, DNA bands were excised from the agarose gel using a surgical scalpel. Purification was performed according to the manufacturer's protocol provided in the Macherey-Nagel Gel/PCR purification kit (Cat# 740609.50). Briefly, the gel slice was dissolved at 65°C in binding buffer (100 µl of binding buffer per 100 µg of gel). Samples were applied to the spin columns, centrifuged briefly in a bench top microfuge and the flow-through discarded. Columns were washed twice with Wash Solution I and subsequently, the DNA was eluted in 50 µl of the pre-heated 65°C elution buffer provided. For small DNA fragments (< 500 bp) used in cloning the DNA was eluted in 30 µl of pre-heated 65°C elution buffer to increase the DNA concentration.

2.2.7 Annealing of DNA oligos

To anneal complementary DNA oligos 1µl of each oligo (100 µM stock in TE buffer) was incubated with 3 µl of 10 x T4 DNA ligase buffer (NEB) and 25 µl of H_2O. The sample was placed into the peqlab Primus 96 advanced thermal cycler at 85°C and allowed to cool slowly at 1°C per minute until the temperature reached 20°C. The oligos were used in restriction digests or blunt end ligation reactions.

2.2.8 DNA fragment ligation

To create recombinant plasmids, ligation of DNA fragments using T4 DNA ligase (NEB) was carried out. Ligation of vector to insert used was approximately 100 ng of digested vector DNA and a 3-fold excess insert concentration (Table 2.1). The reaction was carried out overnight at room temperature.

Reaction component	**Volume (µl)**
100ng template DNA	x
3-fold excess insert DNA	y
10x T4 DNA Ligase buffer	1.5
T4 DNA Ligase enzyme	1.0
RNase-free H_2O	Up to 15 µl (12.5 – (x+y))

Table 2.1 Standard Ligation reactions

2.2.9 DNA transformation and colony screening

Competent cells (100 µl) were added to 10 µl of DNA (ligation product), and incubated on ice for 15- 30 minutes. Thereafter, cells were subjected to a heat shock in a 42°C water bath for 90 seconds and then placed on ice for 2 minutes. LB media (1 ml) was added to the competent cell before incubating for an hour at 37°C incubator shaking. The culture was then spun for 1-2 minutes at 6000 rpm until pellet form, the media was removed, and the pellet was resuspended in the remaining media. Finally, the resuspended pellet was plated on LB plate containing antibiotic followed by overnight incubation at 37°C.

2.2.10 Polymerase Chain Reaction (PCR)

PCR was carried out using a Peqlab Primus 96 advanced thermal cycler. A standard reaction set up is indicated in Table 2.2 and Table 2.3. Samples were initially denatured at 95°C for 5 minute followed by 30 cycle of a denaturing step 95°C for 15 seconds, annealing at 50°C for 30 second, then elongation at 72°C for 2 minutes. At the end of this process, a final elongation step for 10 minutes at 72°C was done. The primers used are shown in Table 2.4 and Table 2.7-2.10. To check the PCR product was the correct size, some of the reaction was loaded onto an agarose gel of appropriate percentage.

Reagent	Volume (µl)
10 mM dNTPs	2.0
Phusion enzyme	1.0
5× Phusion Buffer HF	20.0
10 µM forward primer (Sigma), 100 µM stock in TE	1.0
10 µM reverse primer (Sigma), 100 µM stock in TE	1.0
100 ng DNA template	X
Nuclease free H_2O	Up to 100

Table 2.2 Standard PCR reaction set up using the Phusion DNA polymerase

Reagent	Volume (µl)
10 mM dNTPs	1.0
Taq DNA polymerase	0.25
10 × Taq pol Buffer	2.5
10 µM forward primer (Sigma), 100 µM stock in TE	0.5
10 µM reverse primer (Sigma), 100 µM stock in TE	0.5
Bacterial culture	4.0
Nuclease free H_2O	16.25

Table 2.3 Standard PCR reaction set up using Taq DNA polymerase

Primer Name	Sequence (5'-3')
CNOT6ΔLRRFW	AAAAAGGATCCCTGCTGGATAACCTGAGTGGTAC
pQE30RV	GTTCTGAGGTCATTACTGG

Table 2.4 Primer sequence used for amplification of CNOT6ΔLRR cDNA

Primer Name	Sequence (5'-3')
CNOT6E240A FW	CGTGAGTCTGCAGGCAGTTGAAACCGAAC
CNOT6E240A RV	GTTCGGTTTCAACTGCCTGCAGACTCACG

Table 2.5 Primer sequence used for site directed mutagenesis (CNOT6E240A)

Primer Name	Sequence (5'-3')
Strep-tag Top	AATTCATTAAAGAGGAGAAATTAACTATGGCTAGCT GGAGCCACCCGCAGTTCGAGAAAGGTGGAGGTTCCG GAGGTGGATCGGGAGGTGGATCGTGGAGCCACCCGC AGTTCGAAAAAG
Strep-tag Bottom	GATCCTTTTTCGAACTGCGGGTGGCTCCACGATCCAC CTCCCGATCCACCTCCGGAACCTCCACCTTTCTCGAAC TGCGGGTGGCTCCAGCTAGCCATAGTTAATTTCTCCT CTTTAATG

Table 2.6 Primer sequence used for annealing Strep-tag oligonucleotide

Primer Name	Sequence (5'-3')
NcoI-STREP FW	AAAAACCATGGCTAGCTGGAGCCAC
pQE30RV	GTTCTGAGGTCATTACTGG

Table 2.7 Primer sequence used for the amplification of Strep-CNOT6L or Strep-BTG2 fragment

Primer Name	Sequence (5'-3')
T5 promoter FW	CCCGAAAAGTGCCACCTG
pQE30RV	GTTCTGAGGTCATTACTGG

Table 2.8 Primer sequence used for the amplification of modified pQE80L-Strep plasmids

Primer Name	Sequence (5'-3')
pACYCDuetUP1	GGATCTCGACGCTCTCCT
DuetDown1	GATTATGCGGCCGTGTACAA
DuetUP2	TTGTACACGGCCGCATAATC

Table 2.9 Primer sequences used for amplification and DNA sequencing of MCS1 and MCS2 of pACYCDuet-1

Primer Name	Sequence (5'-3')
PCI-Xhol-HA-BTG2 (FW)	CCACTGCTGGGCCTGGACAGCACCctcgagTACCCATACGATGTTCCAG
PCI-BTG2 (RV)	ggtcgactctagaggtaccacgcgtgaattCTAGCTGGAGACTGCCATCACG

Table 2.10 Primer sequences used for amplification of pCI

2.2.11 Site-directed mutagenesis

For site-directed mutagenesis, overlapping primers with the desired mutations (Table 2.5) were designed by using the PrimerX programme (http://www.bioinformatics.org/primerx.) and also, using the primer design protocol optimised for the Stratagene Quickchange protocol. Reactions were set up as shown in Table 2.2. Reactions were initially incubated at 95°C for 3 min followed by 30 cycles consisting of a denaturing step of 95°C for 10 seconds, annealing for 30 seconds, then elongation at 68°C for 1 min/0.5 kb. A final elongation step for 10 minutes at 68°C was included at the end. The annealing temperature was varied between 40 and 60°C to optimise the reaction efficiency.

To remove template DNA from site directed mutagenesis reactions, the enzyme DpnI was used. 1 µl of DpnI was added to each 50 µl mutagenesis reaction and was incubated at 37°C for 2 hours. 10 µl of the reaction was then loaded and run on a 1% agarose gel. The remaining sample was then used to transform *E. coli* DH5α before DNA isolation and sequencing to confirm the presence of the desired mutations.

2.2.12 List of new plasmids

	Abbreviation	MCS1	MCS2
1.	pQE80L	-	-
2.	pQE80L-Strep	-	-
3.	pQE80L-Strep•BTG2	Strep•BTG2	-
4.	pQE80L-Strep•CNOT6L	Strep•CNOT6L	-
5.	pACYCDuet-1BA	Strep•CNOT6L	CNOT7
6.	pACYCDuet-1 BA2	Strep•CNOT6LE240A	CNOT7D40A
7.	PCIλN-S39N	HA-BTG2 (S39N)	
8.	PCIλN-L46F	HA-BTG2 (L46F)	
9.	PCIλN-H49Y	HA-BTG2 (H49Y)	
10.	PCIλN-I70M	HA-BTG2 (I70M)	
11.	PCIλN-L100P	HA-BTG2 (L100P)	
12.	PCIλN-G117D	HA-BTG2 (G117D)	
13	PCIλN-S158C	HA-BTG2 (S158C)	
14	PCIλN-S158I	HA-BTG2 (S158I)	

Table 2.11 List of generated plasmids in this work

2.2.13 Structural and computational analysis of genes

Protein structures were analysed and molecular graphics were performed by using UCSF chimera package (http://www.cgi.ucsf.edu/chimera)(Pettersen et al., 2004). Computational analysis of proteins and variants were done using web-based platforms as described (Morin et al., 2011, Lohr et al., 2012, Yates et al., 2014, Ng and Henikoff, 2003, Forbes et al., 2008): COSMIC, Selecting intolerant from tolerant (SIFT) http://blocks.fhcrc.org/sift/SIFT.html and SuSPect analysis tools, http://www.sbg.bio.ic.ac.uk/suspect were used. SIFT and SuSPect analysis were based on the degree of conservation of amino acid

residues in sequence alignment derived from closely related sequences collected through PSI-BLAST. Normalised probabilities for all possible substitutions at each position from the alignment are calculated.

2.3 Protein expression and purification

2.3.1 Reagents, stock solutions and buffers

Lysogeny Broth (LB) media and agar: 10 g/L tryptone, 5 g/L yeast extract, 5 g/L NaCl, pH 7.2 (NaOH)

Ampicillin 1000 × stock solution: 100 mg/ml in 50% ethanol/water. Stored at -20°C.

Chloramphenicol 1000 × stock solution: 34 mg/ml in 100% ethanol, stored at -20°C.

IPTG (Isopropyl β-D-1-thiogalactopyranoside)

NaCl (Sodium chloride)

β-mercaptoethanol

Tris-HCl pH 7.8

Imidazole

2.3.2 Protein Expression: His-Tagged CNOT7, CNOT6ΔLRR and CNOT6L ΔLRR Expression

Plasmids pQE80L-CNOT7, pQE80L-CNOT6 ΔLRR and pQE80L-CNOT6L ΔLRR and the corresponding inactive mutant versions (CNOT7D40A, CNOT6 E240A, CNOT6L E240A) were transformed into *E. coli* BL21 (DE3) respectively. A single colony was grown into 1 ml of LB containing 100 μg/ml ampicillin for 6 hours at 37°C, the starter culture was used to inoculate LB (100 ml) containing 100 μg/ml ampicillin and then incubated at 37°C overnight. The pre-culture was diluted to 2 L of LB at 37°C until the OD_{600} was between 0.6 and 0.8. Protein expression was then induced by adding 0.2 mM isopropyl β-D-1-thiogalactopyranoside for 3 hours at 30°C. The cells were harvested by centrifugation (6000 rpm) using a Sorvall SLC-6000 SUPER-LITE rotor at 4°C for 15 minutes or by using a TX-1000 SL 40R rotor (Thermo scientific) at 4200 rpm for 30 minutes. The supernatant was discarded, and then the

bacterial pellet was resuspended in 30 ml of ice-cold extraction buffer (20 mM Tris-HCl pH 7.8, 500 mM NaCl, 10% glycerol, 1 mM β-mercaptoethanol). Cells were frozen and keep at -80°C until further use. The bacterial suspension was thawed and then lysed on ice using a Qsonica XL2000, using five 30s on/30s off cycles. The crude lysate was transferred into Sorvall tubes and then centrifuged in an SS-34 rotor at 10,000 rpm at 4°C for 30 minutes to remove insoluble material. The supernatant was collected and further purified.

2.3.3 Purification of His-Tagged CNOT7, CNOT6 ΔLRR and Ccr4 /CNOT6L ΔLRR Proteins

The histidine-tagged CNOT7, CNOT6 ΔLRR and CNOT6L ΔLRR proteins were purified in a single step using His-Trap column (GE Life Science; 1ml bed volume). Before use, 1 ml His-Trap HP columns were washed with 5 column volumes of distilled water, then equilibrated with 5 column volumes of extraction buffer (20 mM Tris-HCl pH 7.8, 500 mM NaCl, 10% glycerol, 1 mM β-mercaptoethanol). The soluble lysate was then applied to the column. Thereafter, the column was washed with 10 ml wash buffer (20 mM Tris-HCl pH 7.8, 500 mM NaCl, 10% glycerol, 1 mM β-mercaptoethanol, 10 mM imidazole). Finally, elution buffer (20 mM Tris-HCl pH 7.8, 500 mM NaCl, 10% glycerol, 1 mM β-mercaptoethanol, 250 mM imidazole) was added to the column (approximately 5-6 ml) to elute the protein and 1 ml fractions were collected. Elution fractions were analysed by sodium dodecyl sulphate polyacrylamide gel electrophoresis (SDS-PAGE) and Coomassie staining (Invitrogen Bio-Safe Staining Kit). The protein concentrations were quantified using Bio-Rad Protein Assay Reagent and stored in aliquots at -80°C until further use.

2.3.4 Protein Expression: recombinant Human BTG2-CNOT7-CNOT6L protein complex

Plasmids pACYCDuet-1 CNOT6L/CNOT7 and pQE80L-Strep•BTG2 or pQE80L-His•BTG2 and pACYCDuet-1-Strep•CNOT6L-CNOT7 were co-transformed into *E.coli* BL21 (DE3) using selection with the chloramphenicol and ampicillin antibiotics. The full length CNOT6L was used for the expression of the recombinant nuclease protein complex. A single colony containing the pACYCDuet-1 CNOT6L/CNOT7 and pQE80L-Strep•BTG2 plasmid or pACYCDuet-1-Strep•CNOT6L-CNOT7 and pQE80L-His•BTG2 plasmid was used to inoculate a starter culture for protein expression. The pre-culture, was then grown in the presence of chloramphenicol (34 μg/ml) and ampicillin (100 μg/ml) at 37°C until the OD_{600} was between 0.6-0.8. Protein expression of the trimeric nuclease complex was induced by adding IPTG (final concentration of 0.1 mM) to the culture and incubated overnight at room temperature. The cells were harvested by centrifugation (6000 rpm) using a Sorvall SLC-6000 SUPER-LITE rotor at 4°C for 15 minutes or by using a TX-1000 SL 40R rotor (Thermo scientific) at 4200 rpm for 30 minutes. The supernatant was discarded, and then the bacterial pellet was resuspended in 30 ml of ice-cold extraction buffer (20 mM Tris-HCl pH 7.8, 250 mM NaCl, 5 % glycerol, 1 mM β-mercaptoethanol). Cells were frozen and keep at -80°C until further use. Subsequently, the bacterial suspension was thawed and cells were lysed on ice using a Qsonica XL2000, by a five 30s on/30 s off cycles. The crude lysate was made clear by centrifugation using a SS-34 rotor spun at 10000 rpm at 4°C for 30 minutes to remove insoluble material. The supernatant was collected and stored until further use at -80°C.

2.3.5 Purification of Human BTG2-Caf/CNOT7-CNOT6L protein complex

Purification of Strep•BTG2-CNOT7-His•CNOT6L or His•BTG2-Strep•CNOT6L-CNOT7 was done by a single step using a 1 ml gravity column (GE Life Science; 1ml bed volume). Before use, the column was equilibrated with 5 column volumes of extraction buffer (20 mM Tris-HCl pH 7.8, 250 mM NaCl, 10% glycerol, 1 mM β-mercaptoethanol) and the flow through was discarded. Next, 10 ml of the soluble lysate was applied to the column and the flow through was collected. Subsequently, the column was washed using 10 ml extraction buffer (20 mM Tris-HCl pH 7.8, 250 mM NaCl, 10% glycerol, 1 mM β-mercaptoethanol). Finally, 6 ml elution buffer (20 mM Tris-HCl pH 7.8, 250 mM NaCl, 10% glycerol, 1 mM β-mercaptoethanol, 2.5 mM D-Desthiobiotin) was used to elute the protein and 1 ml fractions were collected. Elution fractions were analysed by SDS-PAGE and Coomassie staining (Invitrogen Bio-Safe Staining Kit). The protein concentrations were assessed using Bio-Rad Protein Assay Reagent and stored until further use at -80°C.

2.4 Protein analysis

2.4.1 Reagents, stock solutions and buffers for use in protein analysis

Upper buffer (4×): 0.5 M Tris base, 0.4% SDS, pH 6.8; store at room temperature

Lower buffer (4×): 1.5 M Tris base, 0.4% SDS, pH 8.8; store at room temperature

Running buffer (10×): 0.25 M Tris Base, 1.0% SDS, 1.92 M glycine, store at room temperature

Transfer buffer (10×): 0.25 M Tris Base, 1.92 M glycine, stored at room temperature

SDS loading buffer (4×): 50% upper buffer, 40% glycerol, 1% β-mercaptoethanol, 1.25% Bromophenol Blue (0.1%), 0.25% H_2O; store stock at -20°C. Small aliquots were stored at -4°C

Tris buffered saline supplemented with 0.05% Tween-20 (TBST):
50 mM Tris-HCl pH7.8, 150 m NaCl, and 0.1% Tween-20. Store at room temperature

10% APS: 10% ammonium persulphate (APS) in H_2O stored at 4°C or - 20°C.

2.4.2 Determination of protein concentration by Bradford assay

For Bradford assays, the Bio-Rad protein reagent (Bio-Rad Laboratories) was used. The reagent was diluted 1:5 with water before use. Bovine serum albumin (BSA) was used as standard. BSA dissolved in water was used to plot a standard curve. 10 µl of protein sample was added to 990 µl of 1x Bradford reagent, vortexed and incubated for 1 minute at room temperature. Samples were transferred to 1 ml cuvettes and the absorbance was read at OD_{600}. The standard curve was obtained by linear regression analysis using Microsoft Excel and the protein concentration was calculated based on intrapolation from the curve.

2.4.3 Separation of proteins by Sodium dodecyl sulphate polyacrylamide gel electrophoresis (SDS-PAGE)

Protein samples were analysed by SDS-PAGE using the Invitrogen X-Cell sureLock Mini cell system. SDS-PAGE gels were prepared to the appropriate percentage resolving gel (Table 2.12) based on the molecular mass of the protein of interest. Separating gels were cast in gel cassettes (Invitrogen) leaving 1.5 cm room at the top for the stacking gel to be cast. The separating gel was cast first and allowed to set for 30 minutes before the stacking gel was applied, and then the appropriate comb inserted and the gel left to set for further 30 minutes. The wells were washed with 1x running buffer before use. Protein extract were denatured by boiling for 5 minutes in 4 x SDS sample buffer (50% Upper buffer, 40% glycerol, 1% β-mercaptoethanol, 1.25% Bromophenol Blue (0.1%), 0.25% H_2O) immediately before loading. Gels were run in 1x running buffer diluted from a 10x stock (10× 0.25 M Tris Base, 1.0% SDS, 1.92 M glycine) at 180 V for approximately 1-1.5 hours.

	Resolving gel			**Stacking gel**
	10%	**12%**	**14%**	**4%**
Protein MW range, kDa	30-200	20-150	10-80	
40% acrylamide: Bisacrylamide (29:1)	2.0 ml	2.4 ml	2.8 ml	300 µl
4x Lower buffer	2.0 ml	2.0 ml	2.0 ml	-
4x Upper buffer	-	-	-	750 µl
H_2O	4.0 ml	3.6 ml	3.2 ml	1950 µl
10% APS	80 µl	80 µl	80 µl	60 µl
TEMED	8 µl	8 µl	8 µl	6 µl

Table 2.12 Recipe for SDS-PAGE preparation

2.4.4 Visualisation of proteins by Coomassie blue

To analyse protein purity, Coomassie Blue staining was used. After protein separation by gel electrophoresis, gels were placed in water for 15 minutes shaking on an orbital shaker and then incubated with Coomasie Blue stain (Invitrogen Cat#LC6060, UK) for 0.5-1 hour with gentle rocking. Thereafter, gels were destained in water for >30 minutes. Gels were visualised on a Fujifilm LAS-4000 digital imaging system and analysed using ImageJ software.

2.4.5 Visualisation of proteins using SYPRO Ruby dye

To analyse the purity of proteins and visualise proteins of low molecular weight such as human BTG2, SYPRO Ruby staining was used. After gel electrophoresis, the gel was placed into a clean container with 100 mL fix solution (50% methanol, 7% acetic acid) and agitated on an orbital shaker for 30 minutes. The gel fixing step was repeated with fresh solution. Thereafter, the gel was stained with 60 ml SYPRO Ruby dye (S12001 SYPRO) and agitated overnight on an orbital shaker. After staining, the gel was transferred into a clean container and washed in 100 ml wash solution (10% methanol, 7% acetic acid) for 30 minutes to minimise background staining irregularities and stain speckles on the gel. Before imaging, the gel was rinsed in ultrapure water a minimum of two times for 5 minutes to prevent possible corrosive damage to the imager. Flc-labelled RNA was visualised by epifluorescence using a Fujifilm LAS-4000 imager equipped with an Epi-Blue illuminator (460 nm).

2.4.6 Storage of proteins

All proteins were stored in small volume aliquots at -80^{0}C.

2.4.7 Western Blot Analysis

To analyse proteins by western blotting, proteins were first separated on SDS-PAGE gels transferred to nitrocellulose (Whatman Protran 0.45 μm) membranes using the Invitrogen X-Cell SureLock Mini Cell system for 1 hour at 25 V in 1x transfer buffer diluted from 10x stock (0.25 M Tris Base, 1.92 M glycine). The membrane was then blocked using dried milk in 1x TBST (TBS, supplemented with 0.05% Tween20) for 1 hour at room temperature while mixing on a shaker. The membrane was transferred to a 5 ml falcon tube containing 5 ml of the appropriate primary antibody solution (Table 2.13) and incubated overnight at 4°C on a rotating shaker. Membranes were then washed 3 times for 5 minutes in each round with TBST, transferred to the secondary antibody solution (Table 2.14) and incubated at room temperature for 1 hour on a shaker. The membrane was washed again 3 times with TBST, placed between the sheets of a plastic wallet before adding a chemiluminescence detection reagent (Pierce). After 1 minute incubation, signals were detected immediately using a Fujifilm LAS-4000 digital imaging system and image was analysed and processed using ImageJ.

2.4.8 Antibodies used for western blotting

Primary antibodies	Dilution	Supplier
Anti-HA	1/1000	Roche (1 867 423)
Anti-Gal4 TA	1/1000	Santa Cruz (sc-1663)
Anti-γtubulin	1/1000	Santa Cruz (sc-7396)

Table 2.13 Primary antibodies used for western blotting

Secondary antibodies	Dilution	Supplier
Anti-Rat HRP	1/1000	Santa Cruz (sc-2006)
Anti-Mouse HRP	1/1000	Santa Cruz (sc-2314)
Anti-Rabbit HRP	1/1000	Santa Cruz (sc-2004)

Table 2.14 Secondary antibodies used for western blotting. Antibodies were diluted in TBST containing 5% dried milk powder

2.5 *In vitro* analysis of deadenylase activities

2.5.1 Reagents, stock solutions and buffers

Purified deadenylase enzyme in elution buffer (20 mM Tris-HCl pH 7.8, 500 mM NaCl, 10% glycerol, 1 mM β-mercaptoethanol, 250mM imidazole)

Fluorescent RNA substrate (5'- Flc-CCUUUCCAAAAAAAAA -3') 100 mM in TE stock (Eurogentec).

Fluorescent DNA probe (5'- TTTTTTTTTGGAAAGG-TAMRA -3') 100 mM in TE stock (Eurogentec)

5× reaction buffer: 100 mM Tris-HCl pH 7.8, 25% glycerol, 5 mM β-mercaptoethanol

20 mM $MgCl_2$

Nuclease-free water

384-well low volume black plates (Greiner Bio-One)

96-well white or black plates (flat bottom) suitable for luminescence measurements

AMP-Glo reagent (Promega catalogue# V5011)

SDS (Sodium dodecyl sulphate)

RNA Loading buffer (95% formamide, 0.025% SDS, 0.025% Bromophenol Blue, 0.025% Xylene Cyanol FF, 0.025% SDS, 5 mM EDTA)

40% Acrylamide: bisacrylamide (19:1) solution

10% Ammonium persulphate (APS) in H_2O

Urea

TEMED (Tetramethylethylenediamine).

2.5.2 Fluorescence-based deadenylase assay

For analysis of deadenylase activity by substrate fluorescence-based, assays were done as described (Maryati et al., 2014).The standard reaction condition was a final volume of 10 µl containing the indicated amount of protein (0-1 µM), 20 mM Tris-HCl pH 7.9, 50 mM NaCl, 2 mM $MgCl_2$, 10% glycerol, 1 mM β-mercaptoethanol and 1.0 µM 5' Flc-labelled RNA substrate in nuclease free water. The reactions were incubated for 60 minutes at 30°C and stopped by adding 10 µl of stop/probe mix containing 10 mM Tris-HCl, pH 8, 0.1 mM EDTA, 1% SDS and 5 µM of DNA probe). Subsequently, the fluorescence intensity was measured using a 96 or 384 well plate on a Biotek Synergy HT plate reader at 25^0C (sensitivity setting 70; filter sets used were: Excitation: 485/20 nm, Emission: 528/20 nm, Optics position: Top. Data analysis and curve fitting were done using Microsoft Excel 2007 and Graphpad Prism 7.

2.5.3 Gel based analysis by denaturing polyacrylamide gel electrophoresis (PAGE)

For visualisation and analysis of deadenylase reaction products, 6 µl of RNA loading buffer (95% formamide, 0.025% SDS, 0.025% Bromophenol Blue, 0.025% Xylene Cyanol FF, 0.025% SDS and 5 mM EDTA) was added to 5 µl of reaction sample. The reaction samples were then heated for 3 minutes at 85°C and part of the RNA mixture (3 µl) of each sample was analysed by denaturing PAGE using a 20% acrylamide: bisacrylamide (19:1)/50 % (w/v) urea gel. Poly acrylamide gels were pre-run for 30 minutes at 200 V before loading the samples. The gel was run using the Invitrogen X-Cell SureLock Mini cell system, at 200 V for approximately 1.5 hours or until the loading dye was ¾ or at the bottom of the gel. Flc-labelled RNA was visualised by epifluorescence using a Fujifilm LAS-4000 imager equipped with an Epi-Blue illuminator (460 nm).

2.5.4 AMP product-based deadenylation assay

For analysis of deadenylase activity by AMP-product, all reactions were done in 384 well plates (Greiner Bio-one) following Promega standard protocol with some modifications (https://www.promega.com/-/media/files/resources/protocols/technical-manuals/101/amp-glo-assay-protocol). The standard reaction condition was a final volume of 10 µl containing the indicated amount of protein, 20 mM Tris-HCl pH 7.9, 50 mM NaCl, 2 mM $MgCl_2$, 10% glycerol, 1 mM β-mercaptoethanol and 1.0 µM 5' Flc-labelled RNA substrate in nuclease free water. The reactions were incubated for 60 minutes at 30°C and 10 µl AMP-Glo reagent I (Tris pH 7.5, Calmodulin, 2U/ml pyrophosphate, 0.1mg/ml prionex, 60U/ml HQ-tagged Adenylate cyclase, 10mM $MgCl_2$, 8ug/ml HQ tagged polyphosphate AMP phosphotransferase (PAP)) was added to terminate the reaction and simultaneously remove ATP while converting AMP produced to ADP. The reaction was spun at 1000 rpm for a minute to ensure samples were at the bottom of the plate and further incubated for 60 minutes at room temperature. Thereafter, 15 µl of the reaction from each well was transferred to a white 96-well flat bottom plate. 15 µl of AMP detection solution

containing AMP-Glo reagent II (2KU/ml of Adenylate kinase (AK), 4mM polyphosphate, 3.2 mM Ammonium sulfate pH 6.0 and 1mM EDTA) and Kinase-Glo solution (Kinase-Glo substrate and buffer containing protein methyltransferases substrate (S-adenosylmethionine) (Promega) was dispensed into each well and incubated for another 60 minutes. AMP-chemiluminescence was measured using a Glo-Max luminometer by Kinase-Glo Promega settings.

2.5.5 Determination of the IC_{50} value of compounds

Inhibitory concentrations of compounds were determined as described (Jadhav et al., 2015). Serial dilutions of the compound were made using 100% DMSO. Aliquots of the compound (1µl) were transferred to black U-well, 384-well plates (Greiner Bio-One) and pre-incubated with the indicated amount of protein for 15 minutes at room temperature. After addition of RNA substrate (final concentration of 1.0 µM), the reaction mixture was incubated for 60 minutes at 30°C. For substrate fluorescence-based assays, the reactions were stopped by adding an equal volume of solution containing 1% SDS and a fivefold molar excess of DNA probe. For AMP-product based assay, the reaction was terminated by adding AMP-Glo reagent I and thereafter, AMP detection solution following manufacturer's instructions. Data analysis and curve-fitting were carried out using Microsoft Excel 2007 and Graphpad Prism 7.0. By using non-linear regression, x-axis data was transformed into Log and curve fittings were done by non-linear regression using dose-response inhibition, variable slope. IC_{50}s values were then determined from graphs.

2.6 Characterization of drug-like small molecule inhibitors of CNOT7 CNOT6 and CNOT6L by thermal shift assays

2.6.1 Reagents, stock solutions and buffers

Thin-wall 96 multiwell plates or thin-wall 8-well microtubes with optically clear caps

Real time qPCR machine; Agilent (Stratagene) MX3005p

SYPRO orange dye (5000× concentrate in DMSO; Thermo Fischer Scientific; cat no: S6650)

20 mM $MgCl_2$

Purified protein in elution buffer (20 mM Tris-HCl pH 7.8, 500 mM NaCl, 10% glycerol, 1mM β-mercaptoethanol, 250 mM imidazole)

Test compound (in 20% DMSO)

5× reaction buffer: 100 mM Tris-HCl pH 7.8, 25% glycerol, 5 mM β-mercaptoethanol

Nuclease-free water

DMSO (100%)

2.6.2 Determination of the influence of MgCl2 on CNOT7, CNOT6 and CNOT6L thermal stability.

The reaction conditions were as described in (Niesen et al., 2007) with a few modifications. Standard assay conditions were: 20 mM Tris-HCl pH 7.8, 10% glycerol, 2 mM $MgCl_2$, SYPRO Orange dye (5000x) and the purified enzyme contained in elution buffer (20 mM Tris-HCl pH 7.8, 500 mM NaCl, 10% glycerol, 1 mM β-mercaptoethanol and 250mM imidazole) shown in Table 2.15. Reactions were performed in 96-well PCR plates in a 20 µl reaction volume. The dye was first diluted in water or elution buffer (1:1,000) before adding the indicated amount of protein in the presence or absence of $MgCl_2$ (controls). The PCR plates were sealed with optical seal, centrifuged for 1 minute at 1000 g at 4^0C and then placed in real time qPCR machine. Thermal

scanning was carried out at a temperature gradient from 25°C to 95°C at 1°C per minute using filter settings: excitation/ 492 nm and emission/610 nm. Triplicate readings were taken and data analysis was done using custom calculation software based on Macros in Excel, Graphpad prism software and DSF analysis manual v.3.0. (ftp://ftp.sgc.ox.ac.uk/pub/biophysics) (Niesen et al., 2007).

Reaction component	**Volume**
Purified enzyme	2-10 µM in 2 µl
$MgCl_2$ (20 mM)	2 µl
SYPRO Orange (1:1000)	0.1 µl
1 x Reaction buffer	Up to 20 µl

Table 2.15 Standard reaction set up for thermal shift assays

2.6.3 Small molecule screening by thermal shift assay

Small molecule screening by thermal shift assay was performed as described in section 2.6.2. First, the reaction set up shown in Table 2.16 was prepared. The compounds were diluted to the indicated concentration using DMSO and distributed on each well on PCR plate. Next, the protein solution mixed with SYPRO Orange dye was added to the PCR plate in the presence or absence of $MgCl_2$ (controls). The PCR plates were sealed with optical seal, centrifuged for 1 minute at 1000 g at 4^0C and then placed in real time qPCR machine (Agilent technologies, Mx 3005). Thermal scanning was carried out at a temperature gradient from 25°C to 95°C at 1°C per minute using filter settings: excitation/492 nm and emission/610 nm. Triplicate readings were taken and data analysis was done using custom calculation software based on Macros in Excel, Graphpad prism software and DSF analysis manual v.3.0. (ftp://ftp.sgc.ox.ac.uk/pub/biophysics) (Niesen et al., 2007).

Reaction component	**Volume (µl)**
Purified enzyme	2-10 µM in 2 µl
$MgCl_2$ (20 mM)	2 µl
SYPRO Orange (1:1000)	0.1 µl
Compound (20% DMSO)	1 µl
1 x Reaction buffer	Up to 20 µl

Table 2.16 Reaction set up for compound screening by thermal shift assay

2.7 Yeast-two hybrid analysis

2.7.1 Reagents, stock solutions and buffers for use in yeast culture

YPD medium*:* 10 g/L yeast extract, 20 g/L glucose, 20 g/L bacteriological peptone. For YPD agar, 20 g/L bacteriological agar was added. The medium was sterilised by heat using a Prestige medical 2100 classic bench-top autoclave and stored at 4°C.

Yeast selective complete (SC) medium: 6.7 g/L yeast nutrient broth, 20 g/L glucose, 1.4 g/L amino acid drop out mix (minus histidine, uracil, tryptophan and leucine). For selective agar plates, 20 g/L bacteriological agar was added. The medium was sterilised by heat using a Prestige medical 2100 classic bench-top autoclave and stored at 4°C.

Histidine solution*:* stock 20 mg/ml in H2O (add 4.3 ml per 1 L of medium). After sterilisation by filtration (0.22 µm pore size), the solution was stored at room temperature.

Uracil*:* stock 5 mg/ml in H_2O (add 17.2 ml per 1 L of medium). After sterilisation by filtration (0.22 µm pore size), the solution was stored at room temperature.

Single-stranded *DNA:* Herring Sperm single-stranded DNA (2 mg/ml, Abcam, ab46666) was heated to 98°C for 5 minutes and placed on ice before use. Stored at -20°C.

Lithium acetate solutions*:* LiAc solutions (1 M and 0.1 M; Sigma) were prepared and sterilised by filtration (0.22 µm pore size). Stored at room temperature.

PEG-3350 solution*:* a solution containing 50% (w/v) polyethylene glycol (PEG-3350; Sigma) was sterilisation by filtration (0.22 µm pore size). The solution was stored at room temperature for up to several months.

NaOH 0.2 M: After sterilisation by filtration (0.22 µm pore size), the solution was stored at room temperature

2.7.2 Culture of Saccharomyces cerevisiae strain YRG2

For yeast two–hybrid experiments, the yeast strain *S. cerevisiae* YRG2 (Stratagene; stored at -80^{0}C in YPD containing 50% glycerol) was used. To obtain single colonies the yeast was streaked onto YPD agar plates and grown at 30°C. Once colonies had formed (2-4 days) the plates were stored at 4°C for several weeks. Liquid cultures were inoculated with a large, single colony and grown in universal screw-cap tubes containing YPD or SC medium and incubated at 30°C, 200 rpm for 12-24 hours.

2.7.3 Transformation of YRG2 cells

Yeast YRG2 cells were first made competent by a heat shock treatment. The competent yeast cells were always used on the day they were made. One large single colony was used to inoculate 10 ml of YPD medium, grown overnight at 30°C and at 200 rpm. The culture was then used to inoculate 50 ml of YPD medium to give an OD_{600} of 0.2. This culture was incubated at 30°C, 200 rpm until the OD_{600} was 0.8 (3-5 hours). Thereafter, the culture was centrifuged to pellet the yeast cells at 3000 g for 5 minutes. The supernatant was removed and the cells were carefully re-suspended in 25 ml of sterile water followed by another centrifugation step of 3000 g for 5 minutes. The water was removed and the yeast cells re-suspended in 1 ml of 0.1 M lithium acetate and transferred to a 1.5 ml microfuge tube before being centrifuged at 4000 g for 15 seconds to remove the remaining Lithium acetate. The cells were re-suspended to a final volume of 500 µl in 0.1 M lithium acetate (requiring the addition of approximately 350 µl 0.1 M lithium acetate). One 50 ml culture provided enough cells for ten transformations. The cell suspension was equally divided (50 µl) into ten 1.5 ml microfuge tubes, the cells pelleted and the supernatant removed.

Next, 50% PEG solution was first pipetted onto the yeast cell pellet followed by a mixture containing the other transformation components. Herring sperm ssDNA, (Abcam, ab46666) was boiled for 5 min and quickly chilled on ice before use. After adding all components (pBD-Gal4 250ng, pAD-Gal4 250ng,

Lithium acetate, single stranded DNA and polyethylene glycol) as shown on Table 2.17, the transformation mix was vortexed until the pellet was completely resuspended. The mix was then incubated for 30 minutes at 30°C, 200 rpm followed by 20 minutes incubation at 42°C in a water bath. The samples were then centrifuged at 4000 g for 15 seconds and the yeast pellet was re-suspended in 500 µl of sterile H_2O. From this cell suspension 100 µl was placed on SC selective plates (without tryptophan and leucine) and incubated at 30°C for 3-5 days until colonies formed. Derivatives of plasmids pBD-GAL4 Cam and pAD-GAL4-2.1 (Stratagene) were used for yeast two-hybrid assays

Reaction Component	**Volume (µl)**
plasmid DNA (pBD-Gal4 250ng, pAD-Gal4 250ng) diluted in water	50
50% w/v polyethylene glycol (PEG-3350)	240
1M Lithium acetate	36
Single-stranded DNA (2 mg/ml)	25
H_2O	50

Table 2.17 Yeast transformation mixture per reaction sample

2.7.4 Yeast two-hybrid β-galactosidase assay

Three independent clones were analysed for every transformation. Yeast colonies were streaked into small rectangles (approximately 0.5 x 1.0cm) on SC selective medium agar plates. After 48-72 h the yeast from each rectangle was used to inoculate 2 ml of YPD medium. After incubation at 30°C, 200 rpm for 24 hours, 1 ml of the yeast culture was used to obtain the optical density of the culture (OD_{600}). For dense cultures with an OD_{600} >1, the sample was diluted tenfold with yeast (SC) selective medium. 25 µl from the remaining culture was pipetted into a white 96 well flat bottom plate. Thereafter, 25 ul of β-Glo reagent (Promega) was added to each well. The plate was incubated in the dark for 30 minutes at room temperature. β-Galactosidase luminescence was measured for 1 second using a Berthold Orion microplate

luminometer and Simplicity 4.02 software. For each yeast culture, the β-galactosidase activity was tested in triplicate. The β-galactosidase activities were normalised using the OD_{600} values.

2.7.5 Western blot analysis of yeast cell lysates

To confirm expression of AD-CNOT7, AD-CNOT8 and BD-HA-BTG2 respectively, protein lysates were prepared from yeast cells and subjected to western blot analysis. First, single yeast colonies were streaked into small rectangles and grown in 2 ml to SC yeast selective medium. 1 ml of yeast culture was transferred to a 1.5 ml microfuge tube and centrifuged at 3000 g for 2 minutes. The resulting cell pellet was re-suspended in 100 µl of H_2O. Thereafter, 100 µl of 0.2 M NaOH was added to the cells, vortexed and incubated for 5 minutes at room temperature. The cells were then centrifuged at 3000 g for 2 minutes, the supernatant was removed and the pellet re-suspended in 50 µl of 1x SDS loading buffer. The samples were boiled at 98°C for 5 minutes and were stored at -80°C until required or analysed by SDS-PAGE and western blotting.

2.8 Cell culture

2.8.1 Reagents, stock solutions and buffers for use in cell culture

Phosphate buffered saline: 137 mM NaCl, 2.7 mM KCl, 4.3 mM Na2HPO4, 1.47 mM KH2PO4 (1x PBS without Ca^{2+}, Mg^{2+}; PAA, H15-002)

HEPES-buffered saline: 50 mM HEPES-KOH, 280 mM NaCl, 1 mM NA2HPO4, pH 7.1

DMEM complete: DMEM (Sigma, D6546) 10% fetal calf serum (FCS; Biosera S1900-500, lot-S0611951900), 100 units/ml penicillin and 100 units/ml streptomycin (PAA, P11-010), glutamine (200mM; Lonza, BE17-60SE)

Trypsin/EDTA solutions: 10 x concentrated solutions of phosphate-buffered saline containing 0.5% trypsin and 0.2% EDTA were purchased from (PAA, L11-003) stored at -20°C. 1x solutions obtained by the addition of PBS were stored at 4°C.

Human embryonic kidney cells (HEK293T)

2.8.2 Routine maintenance of cell lines

Cell culture was performed in a Class II biological safety cabinet under aseptic conditions. The cell line used were Human embryonic kidney cells (HEK293T). Adherent cells were maintained in Dulbecco's modified Eagles medium (DMEM) supplemented with 10% foetal calf serum (FCS), 2 mM glutamine, 100 units/ml penicillin and 100 units/ml streptomycin (complete DMEM), in a humidified incubator at 37°C and 5% CO_2. When cells were 70-80% confluent, they were washed with phosphate buffered saline (PBS; pre-warmed at 37°C) and incubated with 1-2 ml of trypsin/EDTA for 1-5 min at 37°C. Trypsin was deactivated by the addition of 10 ml complete DMEM and the cells were resuspended into a single cell suspension. The cell suspension was centrifuged at 250 x g for 5 minutes to pellet the cells, the supernatant removed and then the pellet re-suspended in complete DMEM for dilution and plating.

2.9 RNA tethering assay

2.9.1 Reagents, stock solutions and buffers for use in RNA tethering assays

PCIλN Plasmids (Table 2.10)

TE Buffer: 10 mM Tris-HCl pH 8.0, 1mM EDTA

Cell lysis buffer (NEB) containing 0.2% NP-40*:* 50 mM 1M Tris-HCl pH8.0, 150 mM NaCl, 5 mM MgCl2, 0.5 mM EDTA, 5% glycerol, 0.2% NP-40, 1 mM DTT.

DMEM complete: DMEM (Sigma, D6546), 10% fetal calf serum (FCS; Biosera S1900-500, lot-S0611951900), 100 units/ml penicillin and 100 units/ml streptomycin (PAA, P11-010), glutamine (200 mM; Lonza, BE17-60SE)

Serum free media: DMEM (Sigma, D6546)

HEPES-buffered saline: 50 mM HEPES-KOH, 280 mM NaCl, 1 mM NA2HPO4, pH 7.1

Phosphate buffered saline: 137 mM NaCl, 2.7 mM KCl, 4.3 mM Na2HPO4, 1.47 mM KH2PO4 (1x PBS without Ca^{2+}, Mg^{2+}; PAA, H15-002)

BioLux Gaussia Luciferase Assay Kit, (NEB) E3300S/L

2.9.2 Cell seeding and transfection for RNA tethering assay

Working in a class II biological safety cabinet, H293T cells were seeded into 12-well culture plates at 80,000 cells per well. After 24 hours, cells were at 70% confluency and co-transfected using calcium phosphate transfection method. For each transfection 1 µg of pRL-5boxB, 1 µg of pCIλN plasmid, 6 µl of 2 M Calcium chloride and HEPES-buffered saline (HBS) was used. The DNA/Calcium chloride mixture was incubated for 20 minutes before being added drop wise to the cells. Sixteen (16) hours after transfection, cell medium was removed, cells were washed with PBS and replaced with fresh medium to reduce cell toxicity. Twenty four hours after transfection, cells were harvested for the luciferase assay.

2.9.3 RNA tethering reporter assay

Twenty four hours after transfection, cells were harvested for the luciferase assay. First, cells were washed with 1 ml PBS and then 100 µl of 1 x cell lysis buffer (Luciferase cell lysis buffer, NEB B3321S) was added directly to the cells in the 12-well culture plate. The plates were then placed at -80°C for 15 minutes until completely frozen. Samples were then thawed and mixed by pipetting to aid the lysis process before transfer into 1.5 ml microfuge tubes. Samples were centrifuged at 16,000 g for 5 minutes at 4°C using an Eppendorf centrifuge (5810R) and stored at -80°C or used immediately.

The BioLux Gluc assay solution (BioLux Gaussia Luciferase Assay Kit, NEB E3300S/L) was prepared according to the manufacturer's instructions. The BioLux GLuc substrate mix was prepared by diluting with BioLux Gluc buffer (1:100) and mixed by gentle inverting. Thereafter, 10 µl of cell lysate was added to a white opaque flat bottom 96 well plate, and the plate was placed into a Berthold Orion microplate luminometer. After injection of 50 µl of GLuc assay solution, chemiluminescence was measured for 2 sec after a 5 sec delay. Each sample was tested in duplicate. A Bradford assay (section 2.4.2) was conducted for all samples to determine total protein concentrations, which was used to normalise the luciferase activity.

2.9.4 Cell seeding and transfection for protein expression analysis

Working in a class II biological safety cabinet, H293T cells were seeded into 6-well culture plates at 180,000 cells per well. After 24 hours, cells were at 70% confluency and subjected to DNA transfection using Calcium phosphate. For each transfection, 1 µg of pCIλN plasmid, 1 µg of DNA and 6 µl of 2 M Calcium chloride, was used. The DNA/Calcium phosphate mixture was incubated for 20 min before being added drop wise to the cells. Sixteen (16) hours after transfection, cell medium was removed, cells were washed with 1 ml PBS and replaced with fresh medium (2 ml) to reduce cell toxicity. Forty eight hours after transfection cells were harvested and total proteins were extracted. First, cell media was removed and cells were collected by scraping using a 1 ml tip in 500 µl cold (4^0C) PBS and transferred into a pre-chilled 1.5 ml microfuge tube. The cell suspension was centrifuged at 16,000 g for 3 minutes at 4^0C and resuspended in 100 µl of 0.2% NP-40 lysis buffer. Thereafter, the cells were frozen at -80^0C and thawed before a second centrifugation at 16,000 g for 5 minutes at 4^0C. Aliquots of the cell lysate and 4 x SDS loading dye were made in a ratio (3:1). The mixture was heated at 95^0C for 5 minutes and subjected to SDS-PAGE and western blot analysis.

Chapter 3

Expression, purification and comparative analysis of the human CNOT6 and CNOT6L ΔLRR deadenylase enzymes

Chapter 3. Expression, purification and comparative analysis of the human CNOT6 and CNOT6L ΔLRR deadenylase enzymes

3.1 Introduction

The human Ccr4-Not complex consists of catalytic and non-catalytic subunits. The catalytic subunits are Ccr4 (CNOT6 and CNOT6L) and Caf1 (encoded by the paralogues CNOT7 and CNOT8) (Lau et al., 2009). Ccr4 is characterized by two domains: the amino–terminal leucine rich-repeat (LRR) domain and a carboxy-terminal endonuclease-exonuclease–phosphatase (EEP) domain (Dupressoir et al., 2001, Tucker et al., 2001, Tucker et al., 2002, Chen et al., 2002) (Figure 3.1). The EEP domain is associated with ribonuclease activity while the amino-terminal leucine rich domain provides an interaction surface with the CNOT7 subunit (Draper et al., 1994, Dupressoir et al., 2001, Clark et al., 2004)The EEP domain is associated with ribonuclease activity while the amino-terminal leucine rich domain provides an interaction surface with the (Draper et al., 1994, Dupressoir et al., 2001, Clark et al., 2004). The CNOT7 nuclease subunit is bound to the non-catalytic subunits of the Ccr4-Not complex by interactions between CNOT7 and the central MIF4G domain of the large CNOT1 subunit (Basquin et al., 2012, Petit et al., 2012b)CNOT7 subunit (Draper et al., 1994, Dupressoir et al., 2001, Clark et al., 2004). The CNOT7 nuclease subunit is bound to the non-catalytic subunits of the Ccr4-Not complex by interactions between CNOT7 and the central MIF4G domain of the large CNOT1 subunit (Basquin et al., 2012, Petit et al., 2012b). In yeast, the LRR domain of Ccr4 is vital for its function in vivo (Clark et al., 2004). By contrast, the LRR domain of the human Ccr4 (CNOT6/CNOT6L) is not critical for deadenylase activity *in vitro* (Wang et al., 2010a, Mittal et al., 2011).

Despite the high similarity and identity between the CNOT7 and CNOT8 paralogues (76% identical and 88% similar at the amino acid level), and the fact that the surface residues around the active site are completely conserved

(Horiuchi et al., 2009, Jonstrup et al., 2007, Shirai et al., 2014, Thore et al., 2003, Winkler and Balacco, 2013, Xu et al., 2014) (Figure 3.2), the enzymatic activities of purified CNOT7 and CNOT8 proteins differ significantly (Bianchin et al., 2005). Although both proteins show selectivity for poly (A), the CNOT8 seems to have a higher turnover rate (Bianchin et al., 2005). By contrast, cell studies using human breast cancer cells show that CNOT8 plays a more limited role compared to CNOT7 though their roles in the regulation of mRNA levels are identical (Aslam et al., 2009). Similarly, the human CNOT6 and CNOT6L are 78% identical and 88% similar at the amino acid level. Their surface residues in the active site are totally conserved (Figure 3.1). In cells, the CNOT6 and CNOT6L have been shown to have identical properties using a knockdown approach in combination with microarray-based expression profiling (Mittal et al., 2011). Relatively little is known about their biochemical properties. Based on their cellular roles, it can be hypothesised that the highly similar CNOT6 and CNOT6L may be biochemically interchangeable. However, given the differences observed with the Caf1 subunits despite their high conservation, it is of interest to investigate the biochemical properties of the CNOT6 and CNOT6L. In this chapter, the enzymatic activities of the human CNOT6 and CNOT6L were compared *in vitro*. Studies show that the Ccr4 (CNOT6/CNOT6L) is active as a monomer and remains active in the absence of CNOT7 (Chen et al., 2002, Bianchin et al., 2005). Therefore, monomeric human CNOT6 and CNOT6L proteins lacking the leucine-rich region (ΔLRR) were expressed and purified. The wild type proteins with a histidine tag fused at the N-terminal were expressed in bacterial cells. The findings of this study revealed that CNOT6 displays higher activity as an isolated EEP compared to CNOT6L. Based on these results, the assay was then adapted for use with a plate-based format, which allows the comparison of many reactions in parallel and may be useful for the screening of compound libraries or libraries of proteins with amino acid substitutions.

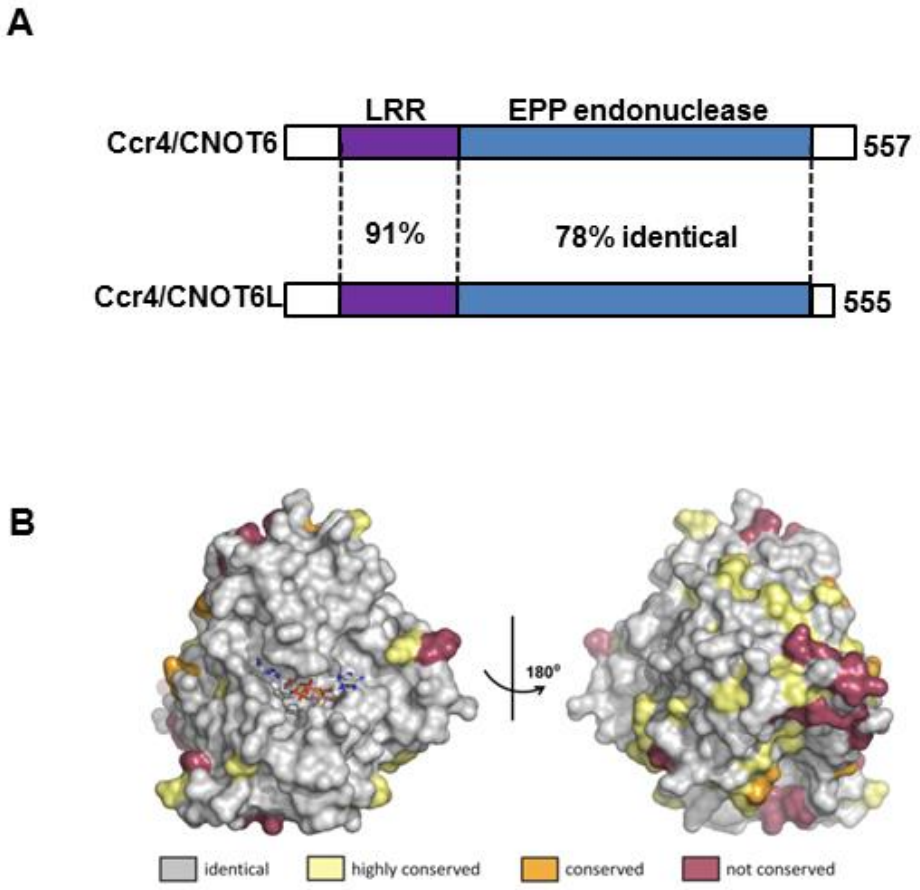

Figure 3.1. Similarity of the human Ccr4 paralogues. (A) A schematic representation showing similarity of the human Ccr4 subunits that consists of the CNOT6 and CNOT6L genes. The LRR domain is shown in purple and the conserved EPP domain is indicated in blue. (B) A representation showing conserved surface residues between the human CNOT6 and CNOT6L subunits. Identical residues in CNOT6 and CNOT6L are indicated in grey, conserved residues are in tan or dark yellow and non-conserved residue in purple. Figure as originally published in Winkler and Balacco (2013). Heterogeneity and complexity within the nuclease module of the Ccr4-Not complex. Frontiers in genetics doi.10.3389/fgene.2013.00296. The image was reproduced under the terms of Creative Common Attribution License, (CC-BY 3.0).

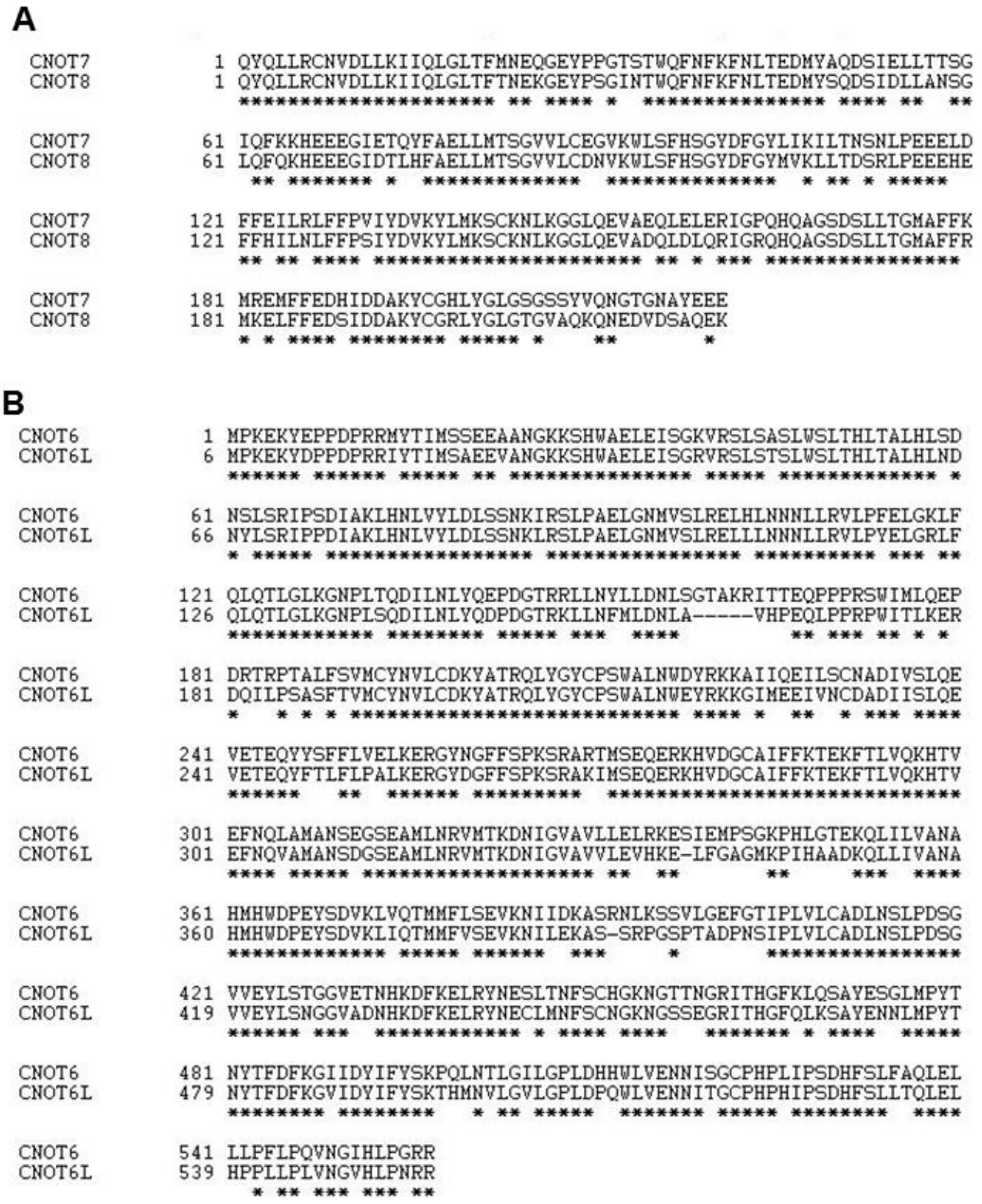

Figure 3.2 Sequence alignment of Caf1(CNOT7/CNOT8) and Ccr4 (CNOT6/CNOT6L) proteins. (A) Human CNOT7 and CNOT8 amino acid sequence. (B) Full length CNOT6 and CNOT6L amino acid sequence. The sequence conservation is indicated in stars (*) below the aligned sequences indicating complete amino acid conservation between the two sequences.

3.2 Protein expression of human CNOT6 and CNOT6L lacking the leucine rich repeat domain

3.2.1 Cloning of human CNOT6 cDNA lacking the Leucine rich region (LRR)

The CNOT6L wild type and catalytic mutant plasmids lacking the LRR region were readily available in our laboratory. Here, the CNOT6 wild type and catalytic mutant plasmids lacking the LRR domain was cloned. Plasmids lacking the leucine rich region were cloned because previous studies had demonstrated that the full length CNOT6 and CNOT6L with the leucine rich region were insoluble (Maryati et al., 2015). However, the truncated protein lacking the leucine rich region (ΔLRR) was easily expressed in bacterial cells and soluble. Therefore, CNOT6 plasmids lacking the LRR domain was cloned for expression in *E. coli*. First, primers were designed based on comparison of the full length human CNOT6 parent cDNA sequence with the LRR region in alignment with the CNOT6 lacking the LRR domain (Figure 3.3). Using standard PCR technique, the gene pQE80L-CNOT6 containing the full length CNOT6 was amplified and the PCR product, CNOT6ΔLRR was ligated to the BamHI and SaII restriction sites of expression vector pQE80L (Figure 3.4). Cloning was confirmed by DNA sequencing.

For controls in enzyme characterisation, the catalytic inactive mutants E240A plasmid lacking the LRR domain was also cloned. A site directed mutagenesis on the amino acid residue responsible for activity was done (Figure 3.5). The glutamic acid (E) at position 240 was mutated to alanine (A). Expression vector pQE80L-CNOT6ΔLRR was the template used for the mutagenesis. Primers were designed using PrimerX (http://www.bioinformatics.org/primerx/) based upon the cDNA sequence of human CNOT6. Plasmid pQE80L-CNOT6 was amplified by using the mutagenic forward and reverse primers obtained (Table 2.1). After amplification, DpnI was added to the reaction to remove methylated template DNA. Site directed mutations were verified by DNA sequencing.

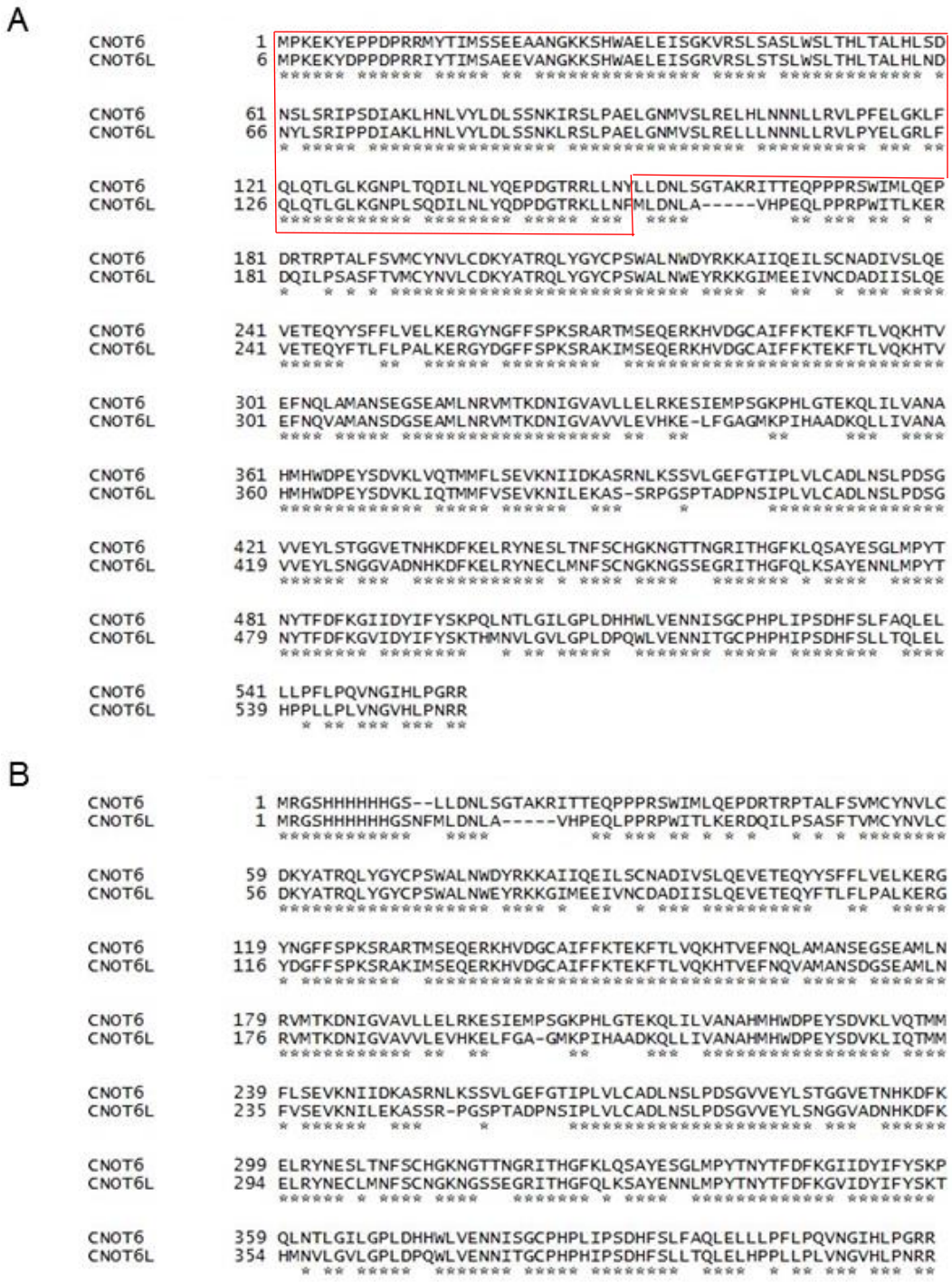

Figure 3.3. Sequence alignment of the CNOT6 and CNOT6L proteins. (A) Full length Ccr4 (CNOT6/CNOT6L). The LRR region is indicated in red box. (B) Truncated Ccr4 lacking the LRR region. Sequences were aligned with http://web.expasy.org/sim tool. The sequence conservation is indicated in stars (*) below the aligned sequences indicating complete amino acid conservation between the two sequences.

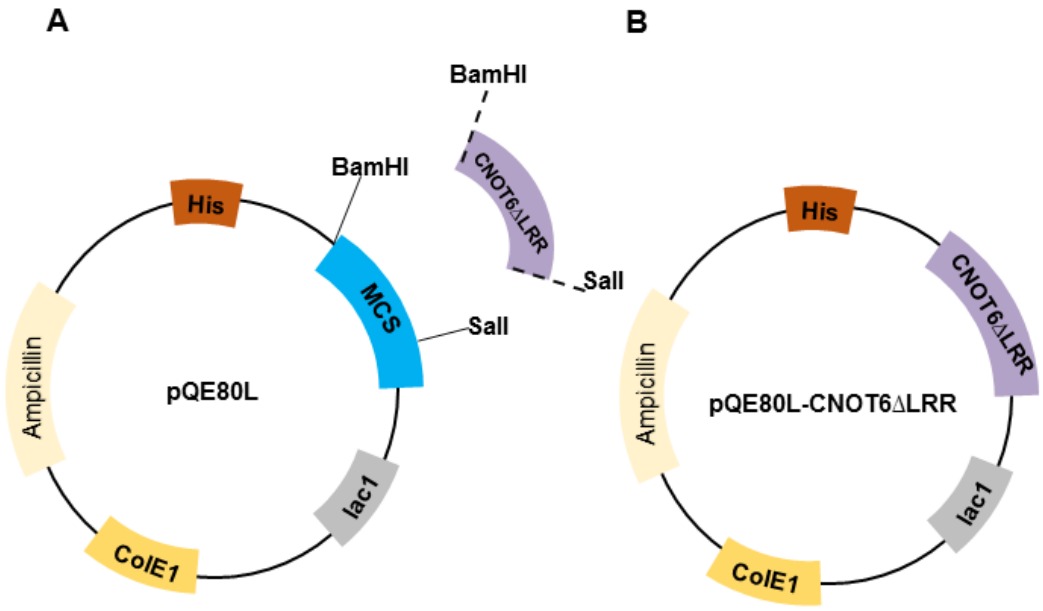

Figure 3.4 Generation of modified bacterial expression vector pQE80L-CNOT6ΔLRR. Plasmid pQE80L containing CNOT6ΔLRR was constructed using standard PCR techniques. Full length CNOT6 cDNA was amplified and ligated into the BamHI and SalI restriction sites of expression vector pQE80L

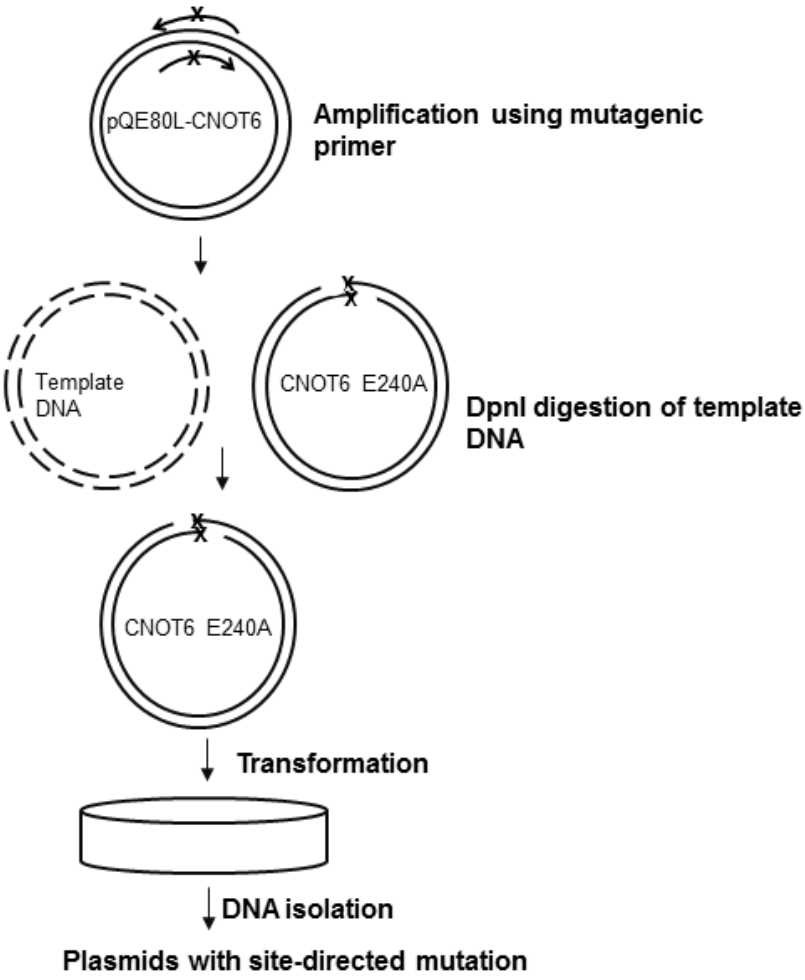

Figure 3.5. Site directed mutagenesis of human CNOT6ΔLRR. (A) Schematic showing mutagenesis of the human CNOT6 gene to generate catalytically inactive variant CNOT6 E240A. Plasmid pQE80L-CNOT6 was amplified to introduce mutations (x) using the forward and reverse primers. After amplification, DpnI was added to the mutagenesis reaction to remove methylated template DNA. The synthesised mutagenic plasmid was transformed into *E.coli* DH5α cells and the repaired plasmid DNA was extracted and purified.

3.2.2 Protein expression and purification of human CNOT6ΔLRR and CNOT6LΔLRR

To purify enzymes for use in defined assays, His-tagged CNOT6 and CNOT6L lacking the LRR region were expressed in *E.coli* BL21. Proteins were expressed using pQE80L expression vector containing CNOT6 (pQE80L-CNOT6) and CNOT6L (pQE80L-CNOT6L) cDNA respectively. The wild type proteins and catalytic inactive variant E240A were expressed and purified under same conditions. A single colony of *E.coli* BL21 containing plasmid pQE80L-CNOT6 or pQE80L-CNOT6L and the corresponding catalytic inactive variant E240A was used to inoculate a starter culture for protein expression. The pre-culture was expanded into 1L Lysogeny Broth (LB) and grown at 37°C until the OD_{600} was between 0.6-0.8. A final concentration (0.5 mM) of Isopropyl-β-D-1-thiogalactopyranoside (IPTG) was added to the culture to induce protein expression and bacterial cultures were incubated further at 30^0C for 3 hours or at room temperature overnight.

Proteins were harvested and purified by immobilised-metal affinity chromatography. A 1 ml Hi-trap HP column was used (GE healthcare). The soluble lysate was applied to the column using a syringe and the column was washed with 10 ml wash buffer (20 mM Tris-HCl pH 7.9, 1 mM β-mercaptoethanol, 10% glycerol, 500 mM NaCl and 10 mM Imidazole) to remove unspecific proteins. Bound proteins were eluted with buffer containing 250 mM imidazole and collected in 0.5 ml fractions (Figure 3.5A). Peak elution fractions were analysed on 10% Sodium-Dodecyl Sulphate Poly-Acrylamide Gel Electrophoresis (SDS-PAGE) to ascertain purity and then visualised by staining with Coomassie blue. Protein concentration was measured with Bio-Rad protein assay reagent. The result of a purification round of CNOT6ΔLRR and CNOT6LΔLRR is shown in Figure 3.6B and Figure 3.6C. To assess the level of protein purity, equal amounts (300 ng) of the wild type and inactive variant protein E240A were then analysed on SDS-PAGE respectively (Figure 3.6D). SDS-PAGE analysis shows the CNOT6ΔLRR and CNOT6LΔLRR were of comparable purity.

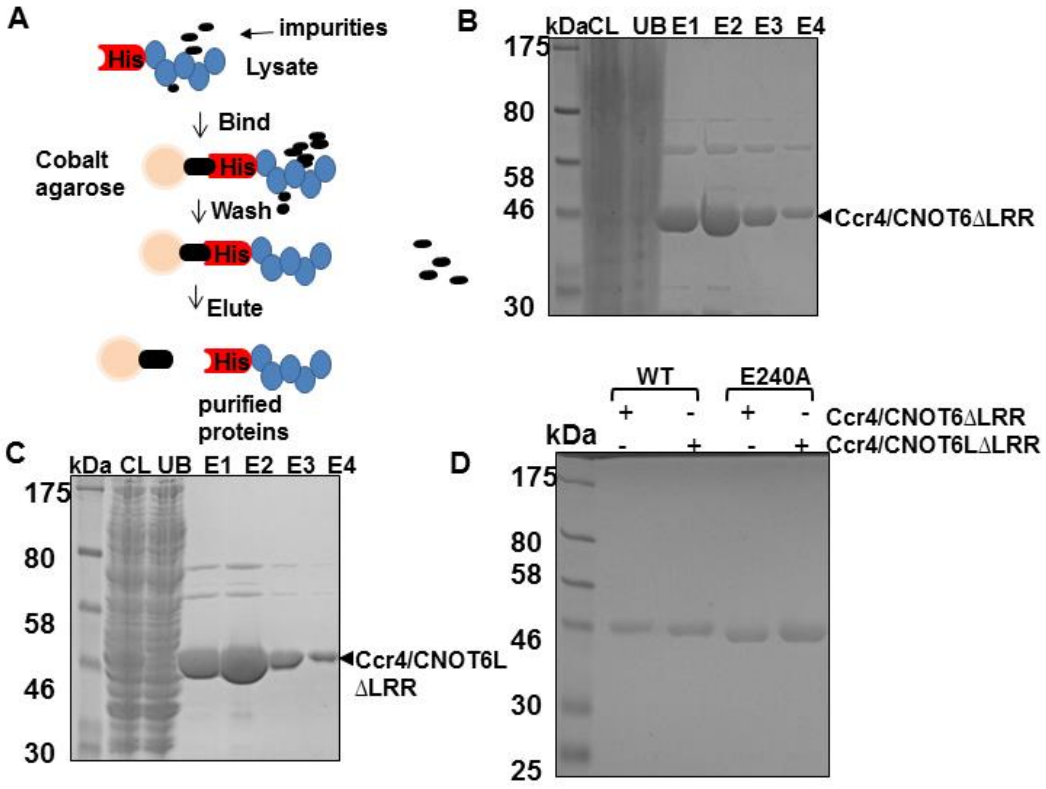

Figure 3.6. SDS-PAGE analysis of purified human Ccr4ΔLRR proteins
(A) Schematic showing protein purification strategy based on expression of His-tagged human Ccr4 proteins in bacteria. Proteins were purified by immobilised metal affinity chromatography using cobalt agarose. The lysate was applied to a column, washed to remove unspecific proteins (black ovals) and pure proteins were eluted. (B and C) Purified human CNOT6 (right panel) and CNOT6L (left panel). Overnight cultures of *E.coli* BL21 induced with 0.5 mM final concentration of IPTG were used to purify human Ccr4 proteins using a 1 ml Hi-trap column. The column was washed with buffer containing 10 mM imidazole and bound protein was eluted with buffer containing 250 mM imidazole. Protein purity was analysed on 10% SDS-PAGE and visualised by Coomassie staining. CL, clear lysate; UB, unbound; E1-E4, elution fractions 1 to 4. (D) 10% SDS-PAGE analysis of equal amounts of purified human CNOT6ΔLRR and CNOT6LΔLRR. The concentration was determined using a Bradford assay. Wild type and inactive mutant proteins (300 ng) were analysed.

3.3 Optimisation of human Ccr4 purification by ion exchange chromatography

3.3.1 Purification of human CNOT6LΔLRR using Hi-trap Q column

During His-tag affinity purification, there were some contaminants on the purified proteins (Figure 3.6B and C). To further purify the Ccr4 proteins, we optimised purification by ion exchange chromatography taking advantage of their overall protein charge. This was done as a second step after a His-affinity purification. First, we expressed the CNOT6L. The Ccr4 proteins have an isoelectric point of (6.26/CNOT6L and 6.82/CNOT6) and overall negative charge at pH 7.9. Therefore, an anionic exchanger (Hi-trap Q column) was chosen for use in the purification step. First, we expressed the Ccr4/CNOT6CNOT6L in *E.coli BL21* cells and purified proteins by immobilised metal affinity chromatography using cobalt agarose. Peak elution fractions were pooled and desalted in buffer A (20 mM Tris-HCl pH 7.9, 10% glycerol, 1 mM β-mercaptoethanol and 50 mM NaCl) using a PD-10 column. A Hi-trap Q column was equilibrated with buffer A (20 mM Tris-HCl pH 7.9, 10% glycerol, 1 mM β-mercaptoethanol and 50 mM NaCl). Protein samples were applied to the Hi-trap Q column (GE healthcare) using a syringe and the column was washed with five column volumes of buffer A. The CNOT6L protein was eluted in twenty (20) column volumes by an initial gradient (0-1 M) NaCl collecting 0.5ml fractions and thereafter a 100% step elution with buffer B containing (20 mM Tris-HCl pH 7.9, 10% glycerol, 1 mM β-mercaptoethanol and 2 M NaCl). Peak fractions were desalted in buffer A using PD-10 column. The protein yield was quantified by Bradford protein assay, protein purity was analysed on 10% SDS-PAGE and visualised by Coomassie blue staining. Figure 3.7 shows the purity of eluted CNOT6L purified by ion exchange chromatography. The purification step worked efficiently with high yields of pure CNOT6LΔLRR protein.

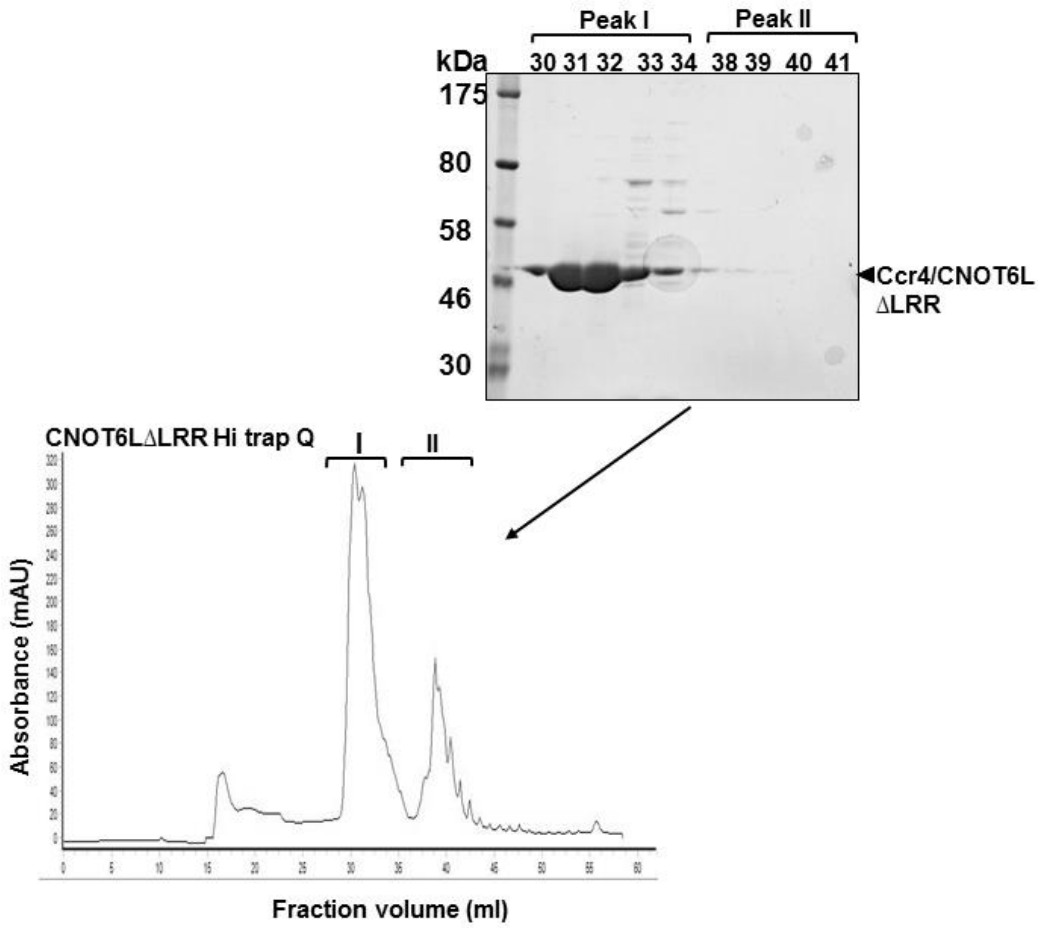

Figure 3.7. Purification of CNOT6LΔLRR by ion exchange chromatography. Chromatograph showing human CNOT6LΔLRR ion exchange purification profile. Peak fractions of Cobalt agarose affinity purified proteins (2.5 ml) were loaded onto a Hi-trap Q column. The column was washed with buffer A containing 20 mM Tris-HCl pH 7.9, 10% glycerol, 1mM β-mercaptoethanol and 50 mM NaCl. Proteins were eluted using a linear gradient (0-50%) followed by a step elution using 100% buffer B containing 20 mM Tris-HCl pH 7.9, 10% glycerol, 1mM β-mercaptoethanol and 2 M NaCl. Elution fractions (2.5 ml) are indicated on the horizontal axis. 0.5 ml elution fractions were collected. The inset represents elution peak fraction I and II analysed on a 10% SDS-PAGE and stained with Coomassie Blue.

3.3.2 Optimisation of human CNOT6ΔLRR purification using Hi-trap Q column

Next, attempts were made to further purify the CNOT6ΔLRR by ion exchange chromatography following the same conditions used for the CNOT6LΔLRR purification. CNOT6 was expressed in *E.coli BL21* cells and purified by immobilised metal affinity chromatography using cobalt agarose. Peak elution fractions were pooled and desalted in buffer A (20 mM Tris-HCl pH 7.9, 10% glycerol, 1 mM β-mercaptoethanol and 50 mM NaCl) using a PD-10 column. A Hi-trap Q column was equilibrated with buffer A (20 mM Tris-HCl pH 7.9, 10% glycerol, 1 mM β-mercaptoethanol and 50 mM NaCl). Protein samples were applied to the Hi-trap Q column (GE healthcare) using a syringe and the column was washed with five column volumes of buffer A to remove unbound proteins. The CNOT6 protein was eluted in twenty (20) column volumes by an initial gradient (0-1 M) NaCl collecting 0.5 ml fractions and thereafter a 100% step elution with buffer B containing 20 mM Tris-HCl pH 7.9, 10% glycerol, 1 mM β-mercaptoethanol and 2 M NaCl. Peak fractions were further desalted in buffer A using a PD-10 column. The protein yield was quantified by Bradford protein assay, protein purity was analysed by SDS-PAGE and visualised by Coomassie staining. The elution profile of CNOT6 purified by ion exchange using a Hi-trap column is shown in Figure 3.8. SDS-PAGE analysis of peak CNOT6ΔLRR protein fractions revealed high and low molecular weight bands indicating impurities with trace amounts of the CNOT6ΔLRR protein. It appeared that the CNOT6ΔLRR was weakly bound or did not bind to the Hi-trap Q column as shown on the chromatograph.

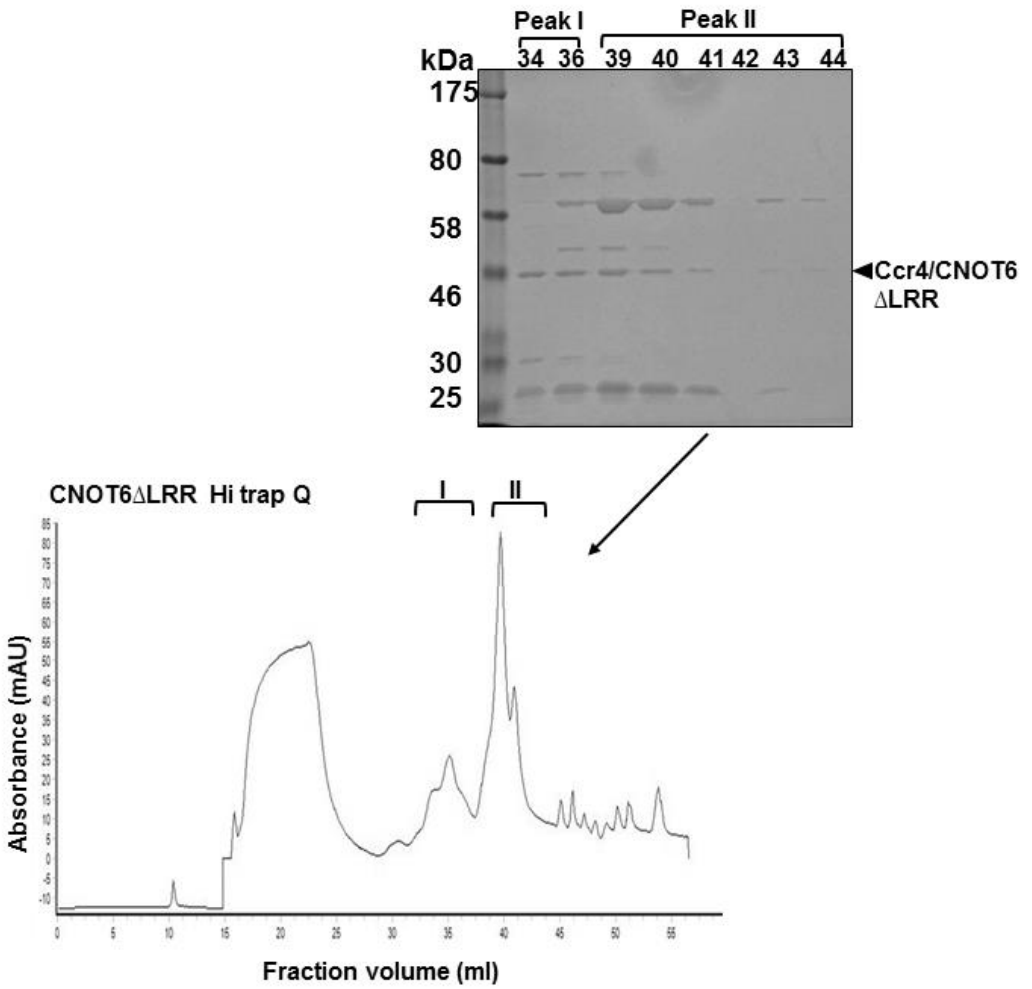

Figure 3.8. Optimisation of CNOT6ΔLRR purification by ion exchange chromatography. A chromatograph showing ion exchange purification profile of CNOT6ΔLRR using a Hi-trap Q column. Pooled peak fractions of Cobalt-agarose affinity step purified CNOT6ΔLRR (2.5 ml) were loaded onto a Hi-trap Q column. The column was washed with buffer A containing 20 mM Tris-HCl pH 7.9, 10% glycerol, 1mM β-mercaptoethanol and 50 mM NaCl. Proteins were eluted using a linear gradient (0-50%) followed by a step elution using 100 % buffer B (20 mM Tris-HCl pH 7.9, 10% glycerol, 1mM β-mercaptoethanol and 2 M NaCl). Elution fractions (ml) are indicated on the horizontal axis. 0.5 ml elution fractions were collected. The inset represents elution peak fraction I and II analysed on a 10% SDS-PAGE and stained with Coomassie Blue.

3.3.3 Human CNOT6ΔLRR is not retained on a Hi-trap SP XL column

To further optimise the purification of CNOT6ΔLRR by ion exchange chromatography, a Hi-trap SP XL column, a strong cationic exchanger was used. Peak elution fractions from the His-purification step were pooled and desalted in buffer A (20 mM Tris-HCl pH 7.9, 10% glycerol, 1 mM β-mercaptoethanol and 50 mM NaCl) using a PD-10 column. A Hi-trap SP XL was equilibrated with buffer A (20 mM Tris-HCl pH 7.9, 10% glycerol, 1 mM β-mercaptoethanol and 50 mM NaCl). Protein samples were loaded onto the Hi-trap SP XL column (GE healthcare) using a syringe and the column was washed with five column volumes of buffer A. The CNOT6ΔLRR protein was eluted in twenty (20) column volumes by an initial gradient (0-1 M) NaCl collecting 0.5 ml fractions and thereafter a 100% step elution with buffer B containing 20 mM Tris-HCl pH 7.9, 10% glycerol, 1 mM β-mercaptoethanol and 2 M NaCl. Peak fractions were desalted in buffer A using a PD-10 column. The protein yield was quantified by Bradford protein assay and success of the protein purification was analysed based on the chromatographic chart and SDS-PAGE. Figure 3.9 shows the results of the ion exchange purification. Clearly, the CNOT6ΔLRR was not retained on the column. Interestingly, SDS-PAGE analysis indicated that the pure protein was found in the unbound and wash fractions compared to the peak fractions. However, this was not further explored.

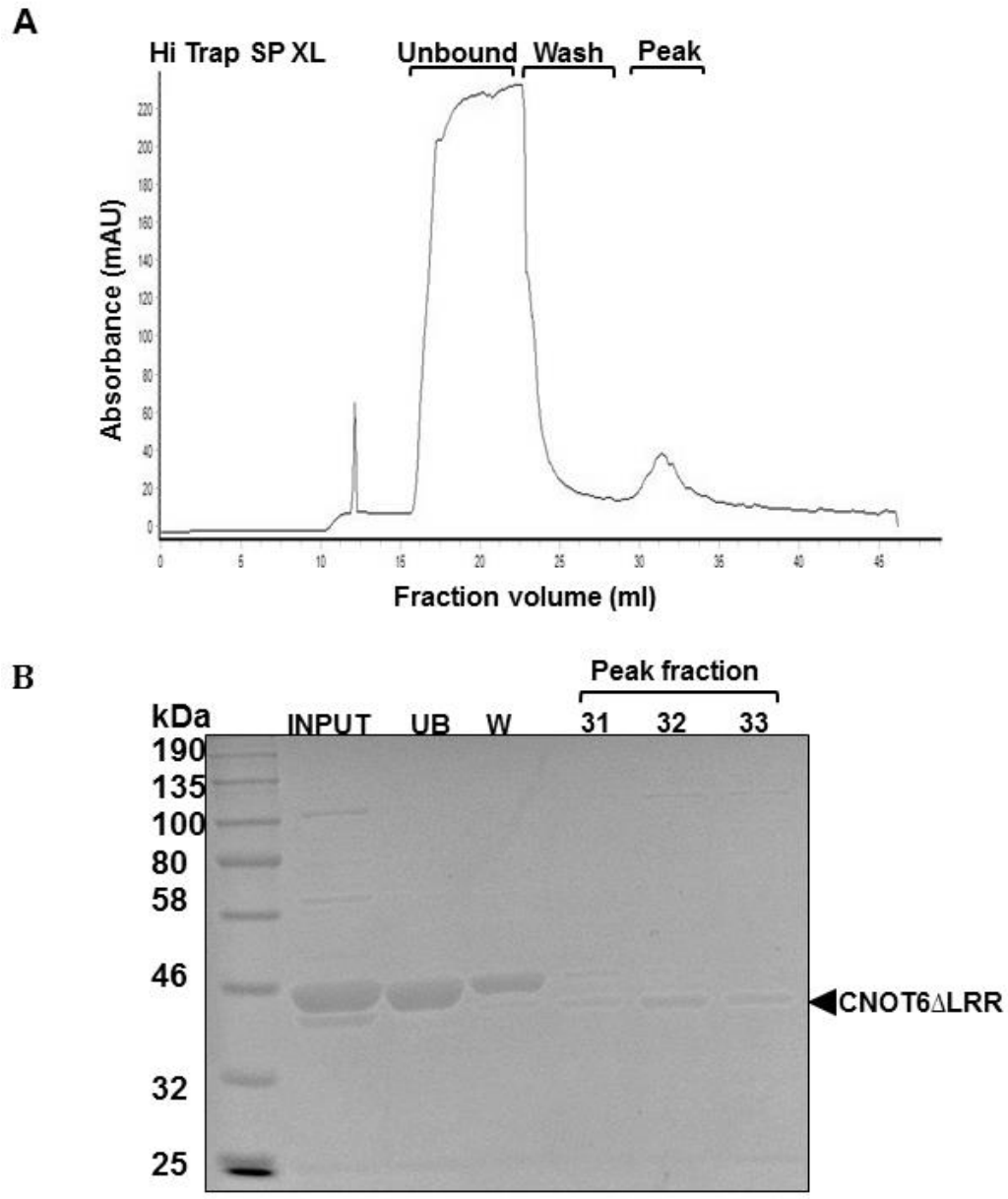

Figure 3.9. CNOT6ΔLRR is not retained on a Hi-trap SP XL column
(A) A Chromatograph showing CNOT6ΔLRR elution profile using Hi trap SP XL ion exchange column. (B) SDS-PAGE analysis showing the fractions as in chromatogram. The input, unbound fraction (UB), wash fractions (W) and peak elution fractions are indicated.

3.3.4 Human CNOT6ΔLRR does not bind the Hi-trap DEAE column

Finally, a DEAE sepharose column, a weak anionic exchanger suitable for proteins of a wide variety of pI values, we used to further optimise the purification of CNOT6ΔLRR. Peak elution fractions from the His-purification step were pooled and desalted in buffer A (20 mM Tris-HCl pH 7.9, 10% glycerol, 1 mM β-mercaptoethanol and 50 mM NaCl) using a PD-10 column. A Hi-trap DEAE was equilibrated with buffer A (20 mM Tris-HCl pH 7.9, 10% glycerol, 1 mM β-mercaptoethanol and 50 mM NaCl). Protein samples were loaded onto the Hi-trap DEAE column (GE healthcare) using a syringe and the column was washed with five column volumes of buffer A. The CNOT6 protein was eluted in twenty (20) column volumes by an initial gradient (0-1 M) NaCl collecting 0.5 ml fractions and thereafter a 100% step elution with buffer B containing 20 mM Tris-HCl pH 7.9, 10% glycerol, 1 mM β-mercaptoethanol and 2 M NaCl. Peak fractions obtained were desalted in buffer A using a PD-10 column. The result is shown in Figure 3.10. The chromatogram suggested that there was binding of proteins to the DEAE column. However, SDS-PAGE analysis indicates that the CNOT6ΔLRR does not bind to the Hi-trap DEAE column.

Other purification methods such as size exclusion chromatography may have been used for further purification but were not explored. As a result of the setback in further purifying the CNOT6ΔLRR by ion exchange, we therefore used the CNOT6ΔLRR and CNOT6LΔLRR proteins purified by one-step His-purification for the characterisation and development of biochemical assays.

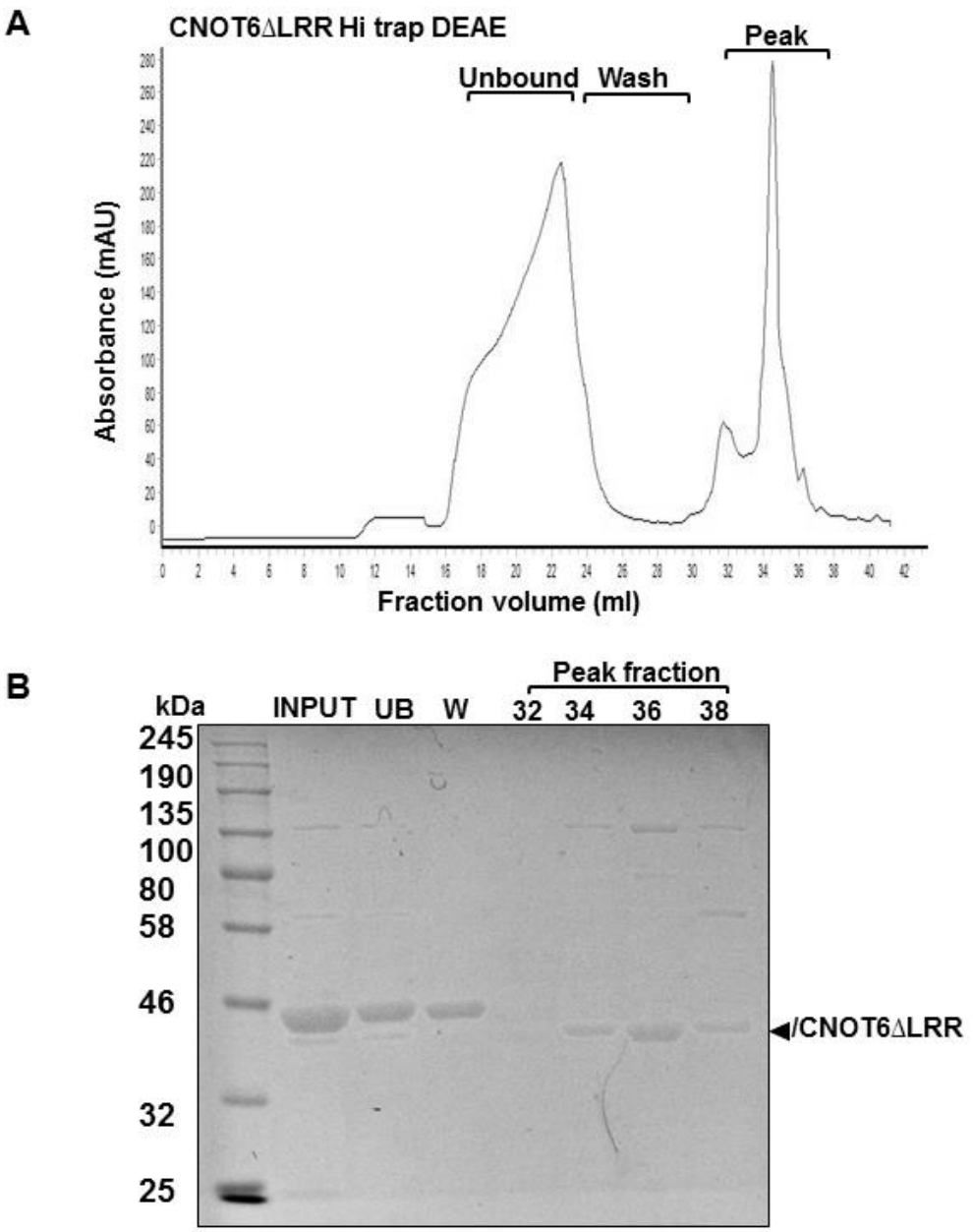

Figure 3.10. CNOT6ΔLRR does not bind the Hi-trap DEAE column
(A) Chromatograph showing CNOT6ΔLRR elution profile using DEAE ion exchange column. (B) SDS-PAGE analysis showing the fractions as in chromatogram. The input, unbound fraction (UB), wash fractions (W) and peak elution fractions are indicated.

3.4 Characterisation of the Ccr4 deadenylases by fluorescence-based method

A substrate detection method based on fluorescence resonance energy transfer (FRET) which has been well characterised (Maryati et al., 2014) was used to determine and compare the activities of the CNOT6 and CNOT6L. The two-stage assay involved the incubation of a 5′ Flc-labelled RNA oligonucleotide substrate with the enzyme. At specified time points, the reaction is stopped by the addition of a 3′TAMRA–labelled DNA oligonucleotide probe which is complementary to the RNA substrate. When there is no activity, Flc fluorescence of the intact substrate is quenched as the DNA probe hybridizes with the RNA. On the contrary, when there is deadenylase activity, the TAMRA probe cannot hybridize to the Flc-labelled reaction product due to substrate degradation thus allowing for detection of fluorescence (Figure 3.11). A fluorescent RNA oligonucleotide containing nine adenosine residues at the 3′ (5′- Flc-CCUUUCCAAAAAAAAA-3′) was used as the substrate. The total reaction volume was 10 µl. The reaction which contained 20 mM Tris-HCl, pH 7.9, 10% glycerol, 1mM β-mercaptoethanol, 2 mM $MgCl_2$ and RNA substrate (1 µM) was incubated for 60 minutes at 30^0C. Next, the reaction was stopped by the addition of an equal volume of stop mix containing 1% SDS and a 5-fold molar excess of DNA probe.

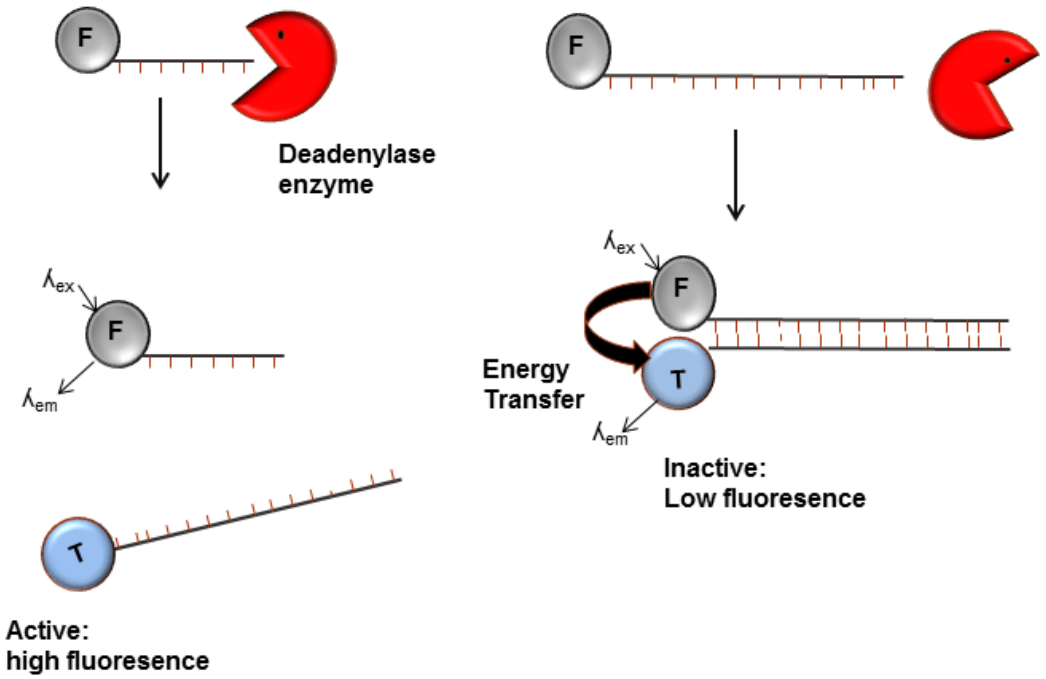

Figure 3.11. The principle of fluorescence-based deadenylation assay (A) A schematic representation of the substrate fluorescence-based assay. The assay involves the incubation of a 5´ Flc-labelled RNA oligonucleotide substrate with the deadenylase enzyme. The reaction is terminated by adding SDS and a 3´labelled DNA oligonucleotide probe which is complementary to the RNA substrate. When the enzyme is active, the probe cannot hybridize to the Flc-labelled RNA product which allows the detection of fluorescence (left). On the contrary, in the presence of inactive enzyme, the fluorescence labelled substrate is intact and is quenched when the probe hybridises (right).

3.4.1 Comparison of the deadenylase activities of the human CNOT6ΔLRR and CNOT6LΔLRR

As a first step to evaluate the biochemical properties of CNOT6 and CNOT6L enzymes, their deadenylase activities were compared. We performed a series of time course assays using different enzyme concentrations (500, 600, 800 and 1000 nM) of CNOT6 and CNOT6L respectively. As controls, the catalytic inactive variant E240A was used. The enzymes were incubated with RNA (1 μM) at 30^0C for one hour and the reaction was quenched by the addition of stop mix containing 1% SDS, and a 5-fold molar excess of DNA probe. Deadenylase activity was determined by measuring substrate fluorescence.

Using this assay, it was observed that CNOT6ΔLRR and CNOT6LΔLRR both displayed deadenylase activity as expected when compared to the controls, which were inactive. In addition, CNOT6ΔLRR displayed significantly higher activity compared to CNOT6LΔLRR as judged by the minimal amount of enzyme required for activity and the substrate fluorescent signal. (Figure 3.12). This observation appeared to be different from their characteristics *in vivo* as established from previous report of both enzymes having identical properties in cells (Mittal et al., 2011). The results also showed that 60 minutes incubation was optimal for the assays. Therefore, 600 nM enzyme concentration was chosen for use in further assays.

To confirm the differences in enzyme activity observed, deadenylase activity products of the CNOT6ΔLRR and CNOT6lΔLRR were analysed by denaturing polyacrylamide gel electrophoresis. Enzyme concentrations (0, 0.4, 0.6, 1 and 2 μM) were used. Again, the CNOT6ΔLRR showed higher activity compared to the CNOT6LΔLRR indicating that these observations were not due to artefacts of the fluorescence based assay (Figure 3.13). Enzyme activity was observed at 2.0 μM concentration of the inactive CNOT6E240A, albeit at reduced levels as compared to the wild type enzyme.

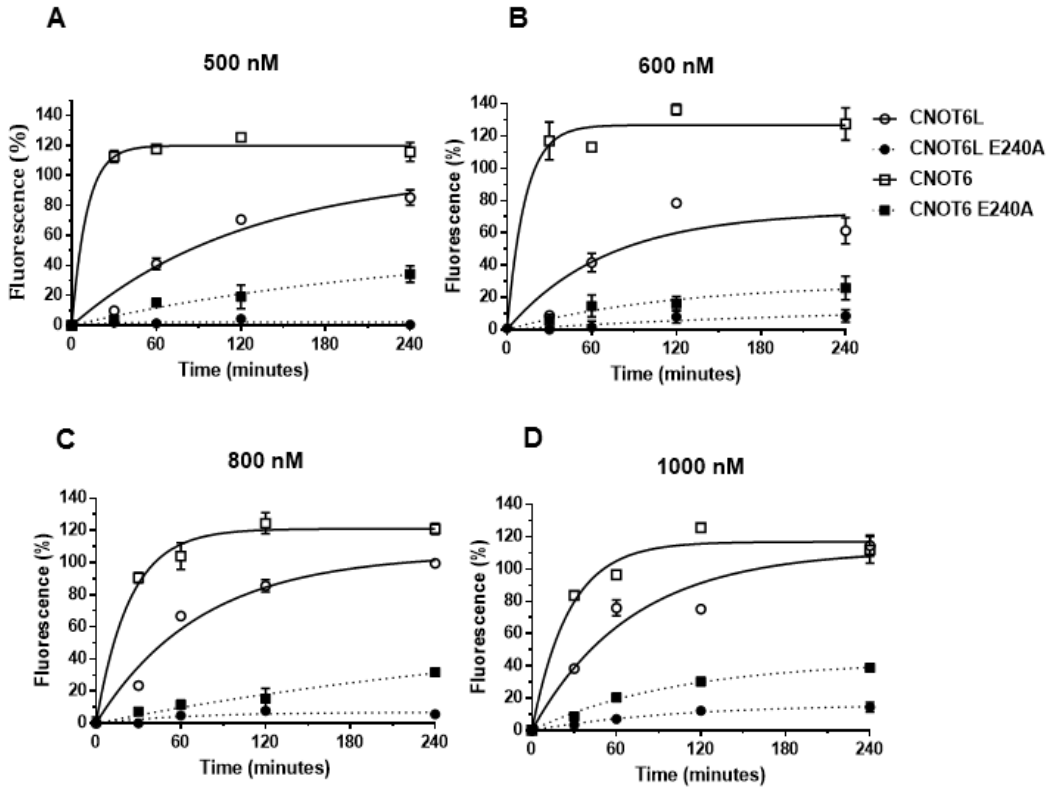

Figure 3.12. Comparison of the deadenylase activities of CNOT6ΔLRR and CNOT6LΔLRR. The activities of the enzymes at (A) 500 nM, (B) 600 nM, (C) 800 nM and (D) 1000 nM was measured as a function of time. The indicated amount of wild-type and inactive mutant (E240A) protein was incubated with Flc-labelled RNA substrate (1 μM). After incubation (60 min), a fivefold molar excess of the 3' TAMRA-labelled probe was added before fluorescence was measured. Error bars indicate the standard error of the mean (n=3).

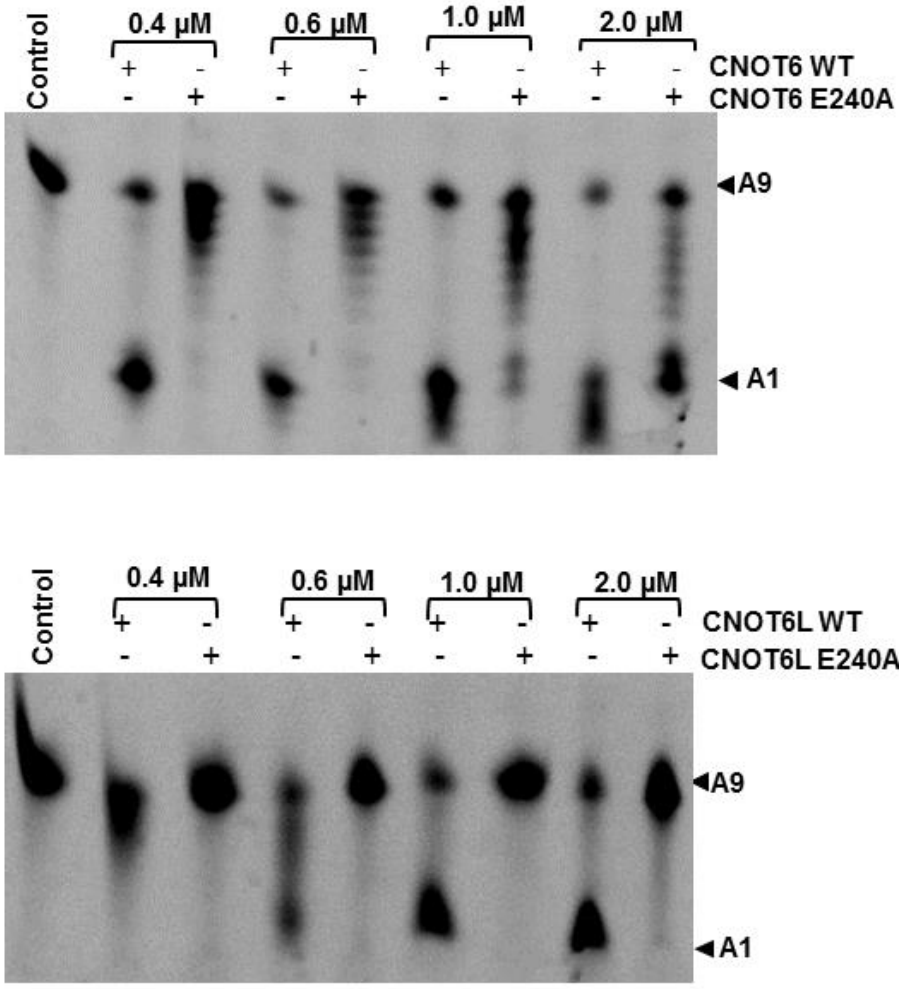

Figure 3.13. Deadenylation product analysis of Ccr4 proteins by PAGE. A fluorescent RNA containing nine adenosine (A9) residues was used as a substrate for purified CNOT6ΔLRR and CNOT6LΔLRR. Increasing amount of enzyme (0, 0.4, 0.6, 1.0 and 2.0 μM) was incubated with the RNA substrate (1.0 μM) at 30^0C for 60 min. The inactive E240A mutant and the positions of the intact RNA (A9) and degradation product (A1) are indicated.

Next, the effect of temperature on the CNOT6 and CNOT6L activity was investigated. The enzyme concentration (600 nM) of CNOT6 and CNOT6L was kept constant for this analysis. The enzyme reaction mix containing 1 µM fluorescently tagged RNA was incubated at varying time points (0-240 minutes), at 30^0C and 37^0C respectively. The results in Figure 3.14 indicates that deadenylase activities of the enzymes assays done at 30^0C and 37^0C were comparable. Therefore, 30^0C incubation condition was chosen for the assays. Taken together, the results demonstrate that the CNOT6 is more active than the highly similar CNOT6L.

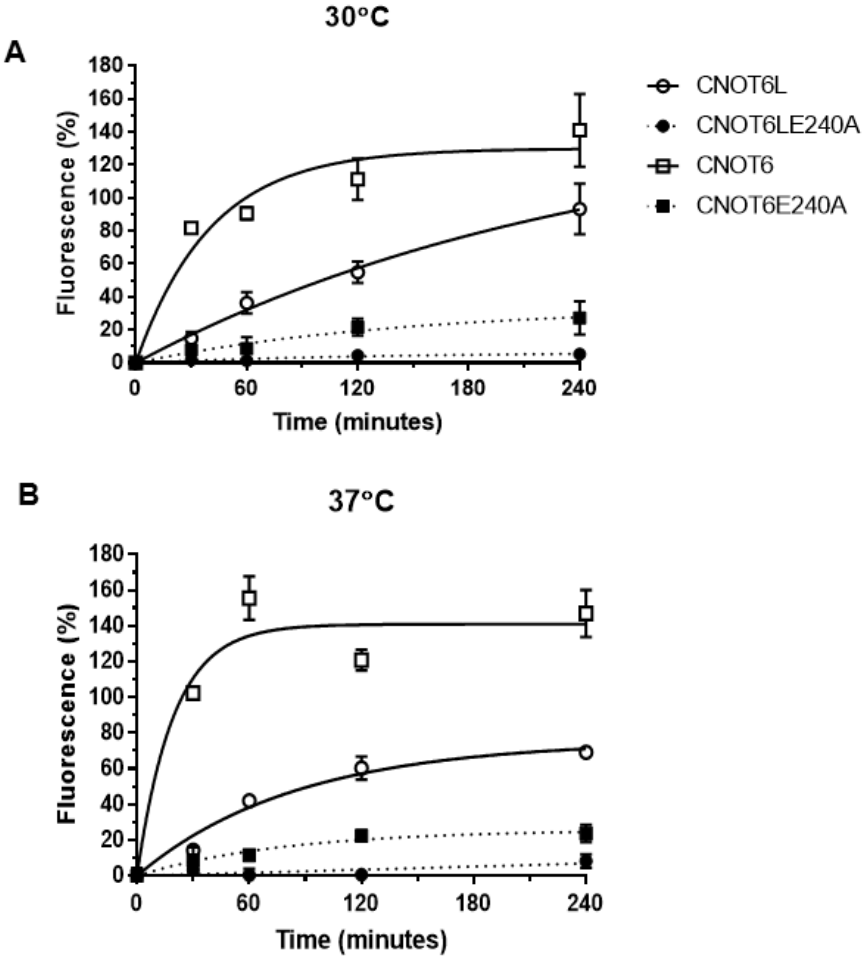

Figure 3.14. Comparison of CNOT6ΔLRR and CNOT6LΔLRR deadenylase activities at 30^0C and 37^0C. (A) Deadenylase activity measured at 30°C. (B) Deadenylase activity measured at 37°C. The wild type and catalytically inactive (E240A) versions of CNOT6ΔLRR and CNOT6LΔLRR (0.6 µM) were incubated with Flc-labelled substrate (1.0 µM). After the indicated time, a fivefold molar excess of the DNA probe was added before fluorescence was measured. Error bars indicate the standard error of the mean (n=3)

3.4.2 Evaluation of human Ccr4 activity using microwell plate-based formats

Next, the suitability of the fluorescence-based assay for use in micro-well plate-based formats was evaluated. Such formats would be useful for the screening of libraries of Ccr4 proteins with amino acid substitutions or the screening of compound libraries for the identification of inhibitors of the Ccr4 enzymes. Various factors may affect the suitability and reproducibility of microplate-based assays requiring the need to determine the efficiency and detection of changes in assay quality. This would help judge if the results from an assay is strong enough to warrant further attention. The evaluation of assay suitability for screening was determined by Z factor. The Z factor is a statistical parameter useful for evaluation of assay quality and gives a reflection on data variation associated with signal measurements. It is unitless and sensitive to factors affecting the dynamic range or variation in measured signal between groups of positive and negative controls. It can be calculated using the below formula:

$$\text{Z factor} = 1 - \frac{3SD \text{ of positive controls} + 3SD \text{ of negative controls}}{\text{Mean of positive controls} - \text{mean of negative controls}}$$

(where SD represents standard deviation).

Z factor is meaningful within the range ($-1 < Z \leq 1$) which implies that the larger the Z factor the higher the suitability of the enzymes or assay for identifying inhibitors (Zhang et al., 1999). To this end, 384-well plates (Greiner Bio-One) were used in combination with a four-step pipetting scheme. First a 20% dimethyl sulphoxide, DMSO solution was dispensed into selected wells on the microplate. 20% DMSO was used because it represents the concentration of compound diluent that does not interfere with assay signals or enzyme activity. This was based on preliminary optimisation work done to ascertain the amount of DMSO that would interfere with enzyme activity or assay signals (Maryati, 2014). Next, 0.8 µM concentration of CNOT6 and CNOT6L enzymes in elution buffer (20 mM Tris-HCl pH 7.9, 500

mM NaCl, 10% glycerol, 1 mM β-mercaptoethanol and 2 mM $MgCl_2$) was added and incubated for 15 minutes at room temperature. The RNA substrate (1 μM) was then added and incubated at 30^0C for 60 minutes. Finally, the reaction was terminated by the addition of a stop mixture containing 1% SDS and a fivefold molar excess of a TAMRA-labelled DNA probe. Thereafter fluorescent measurements were taken using a BioTek Synergy HT plate reader. Control reactions with no enzymes were dispensed into wells 1 and 2 containing 20% DMSO only and wells 23-24 contained 5% SDS in 20% DMSO (Figure 3.15A).

The results represented in Figure 3.15B and C indicate that the fluorescence-based assay was suitable for micro-well plate-based formats. Z factor analysis suggests that the assay is suitable for use with CNOT6 (Z factor, 0.71 ± 0.02, n=3) in a multiwell plate format. The signal to noise ratio was within acceptable range. However, the Z factor value determined when CNOT6L (Z factor, 0.05 ± 0.03, where n=3) was used for assay optimisation (Figure 3.15C and D) shows that the signal to noise ratio was low. It will not be possible to identify hits with confidence. As a result, the CNOT6L enzyme would be unsuitable for use in high throughput screening.

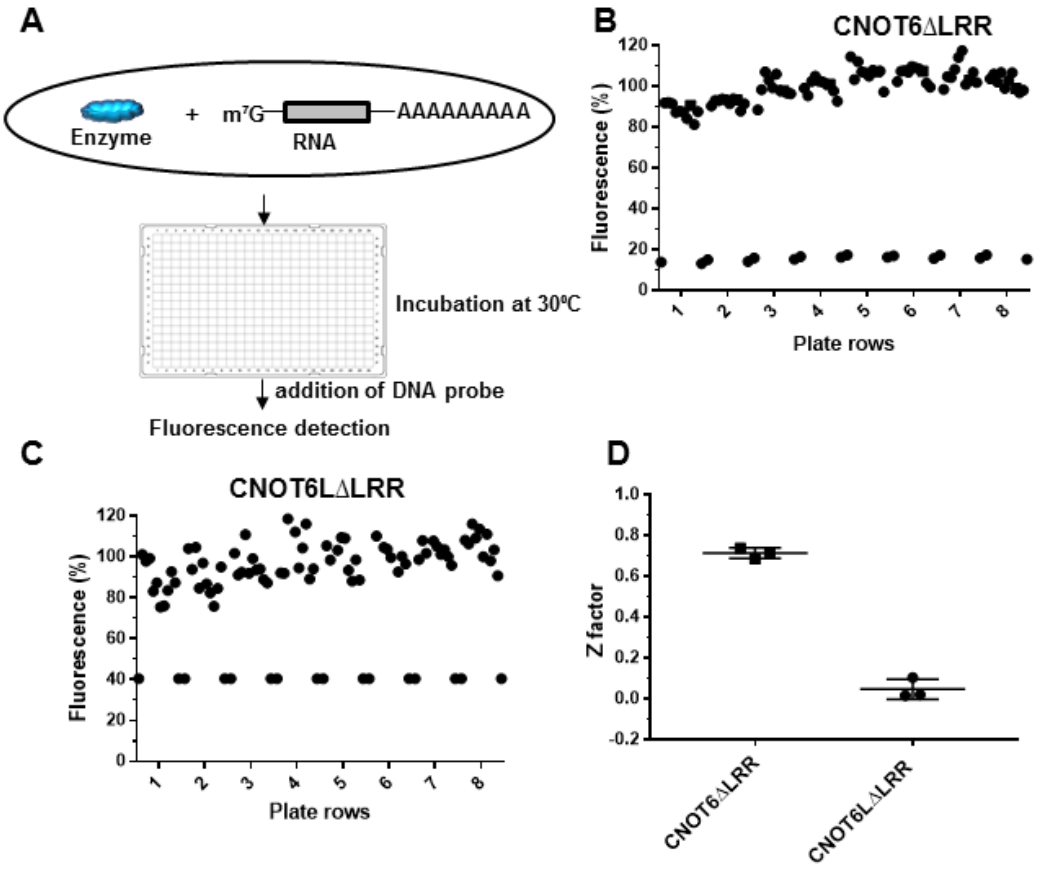

Figure 3.15. Evaluation of CNOT6ΔLRR and CNOT6LΔLRR activity using microwell plate formats. (A) A schematic representing the assay steps. Two microlitres of 20% DMSO was dispensed in a 384-well plate and pre-incubated with 0.8 µM CNOT6ΔLRR or CNOT6LΔLRR for 15 minutes at room temperature. RNA substrate (1.0 µM) was added to the reaction and incubated for 60 minutes. The reaction was stopped by the addition of 20 µl of a solution containing 1.0% SDS and a fivefold molar excess of a TAMRA-labelled DNA probe. Control reactions with no enzymes were dispensed into wells 1 and 2 containing 20% DMSO only and wells 23-24 containing 5% SDS in 20 % DMSO. (B-D) Evaluation of the feasibility of screening the CNOT6 and CNOT6L by fluorescence-based assay using Z factor analysis. The mean value of the Z factor using CNOT6ΔLRR was (0.71 ± 0.02, n=3) and (0.05 ± 0.03, n=3) using CNOT6LΔLRR. Dots indicate fluorescence of each well containing enzymes. Also indicated is the background fluorescence (black dots). Error bars indicate standard error of mean (n=3).

3.5 Conclusion/Discussion

In this chapter, the biochemical comparative analysis of the highly similar CNOT6 and CNOT6L is described. Previous studies show that the CNOT6L is a possible target in the regulation of energy metabolism (Morita et al., 2011). Also, the CNOT6 and CNOT6L are shown to have identical properties in cells (Mittal et al., 2011), regulate mRNA abundance of identical gene sets (Aslam et al., 2009) and are known to be 78% identical and 88% similar at the amino acid level. Though highly similar, it remains unclear whether the CNOT6 and the CNOT6L are biochemically interchangeable. The main aim of this chapter was to purify the enzymes and provide insight into their biochemical properties. This would contribute to the development of assays that screen for molecular inhibitors of the Ccr4-Not deadenylases. The findings of this study demonstrate that the CNOT6 and CNOT6L display differences in their enzymatic properties. This was based on the analysis of their deadenylase activities *in vitro* by a recently developed fluorescence-based assay (Maryati et al., 2014). The wild type and catalytically inactive variant of CNOT6 and CNOT6L ΔLRR versions were purified by immobilised-metal affinity chromatography and used for the analysis.

Protein purification results show a similarity in the elution profile of the CNOT6 and CNOT6L proteins purified by a one-step affinity purification with high protein yields. However, SDS-PAGE analysis also revealed that there were minor contaminants which may be due to bacteria native proteins (Figure 3.6B). Analysis of equal amounts (300 ng) of the wild type and catalytic inactive variant on SDS-PAGE to ascertain the level of contamination indicated that the proteins were of comparable purity and concentration. Nonetheless, to eliminate these contaminants, the enzymes were purified further by ion exchange chromatography. Interestingly, while the CNOT6L with a pI of 6.26 and overall negative charge was purified to homogeneity using a Hi-trap Q column (a strong anionic exchanger), pure samples of CNOT6 (pI, 6.82) were not obtained when purified under same conditions. It appeared the CNOT6 was weakly bound or did not bind to the column. Further attempts to optimise the purification of CNOT6 by ion exchange were

aborted. However, SDS-PAGE analysis (Figure 3.9) showed the pure CNOT6 protein in the unbound and wash fractions using Hi-trap SP XL columns, a strong cationic exchanger. It might be of interest to investigate the binding of Ccr4 (CNOT6/CNOT6L) proteins to SP XL columns and also explore other purification methods such as size exclusion chromatography in future work. The proteins purified by one-step affinity chromatography was used for characterisation and assay development.

Next, the enzymatic activities of CNOT6 and CNOT6L ΔLRR versions compared to controls were determined. The findings of this work demonstrate that the Ccr4 (CNOT6/CNOT6L) recognises and degrades poly (A) in agreement with previous studies(Wang et al., 2010b). Three independent approach using a fluorescence-based assay indicate that the enzyme activities of CNOT6 is higher than CNOT6L: (i) the analysis of enzyme concentration as a function of time; (ii) the use of denaturing polyacrylamide gel electrophoresis to analyse deadenylation products; and (iii) the determination of the effect of temperature and incubation time on enzyme activity. It was observed that the CNOT6 showed higher activity compared to CNOT6L in all experimental approaches. This was based on the minimal enzyme required for RNA substrate degradation.

A final evaluation of the feasibility of assessing the enzyme activity of the CNOT6 and CNOT6L in microwell plate-formats was carried out. This would be useful for the screening of libraries of Ccr4 proteins with amino acid substitutions or the screening of compound libraries for the identification of inhibitors of the Ccr4 enzymes. The suitability of the fluorescence-based assay for compound screening was specifically addressed by determining the Z factor. Z factor analysis, a statistical parameter useful for evaluation of assay quality, demonstrated that the fluorescence-based assay is of high quality and is suitable for screening the CNOT6 enzyme. By contrast, the lower activity of the CNOT6L enzyme precluded the use of this enzyme for compound screening as indicated by the low Z score (0.05).

Taken together, the conclusion that the CNOT6 and CNOT6L differ in their biochemical properties is surprising, based on previous findings that

employed a cell-based approach (Mittal et al., 2011). It may be that the differences observed may be caused by subtle differences in the amino acid linker between the N-terminal leucine-rich repeat domain and the EEP domain that are also present in the recombinant protein following the N-terminal His-tag.

The human Ccr4 enzymes are known to exist in association with other proteins in a nuclease complex in cells. Recent studies show a significant increase in enzymatic activity in a trimeric nuclease complex containing BTG2•CNOT7•Ccr4 (Maryati et al., 2015) when compared to monomeric Ccr4 (CNOT6 or CNOT6L) proteins. Further work involving the analysis of the human CNOT6 and CNOT6L enzyme activities will provide more insight into the findings from this study.

Chapter 4

Use of AMP detection as an activity assay for the human Caf1 and Ccr4 deadenylase enzymes

Chapter 4. Use of AMP detection as an activity assay for the human Caf1 and Ccr4 deadenylase enzymes

4.1 Introduction

Quantitative biochemical assays are useful for enzyme characterisation and they provide information on their catalytic activity, mechanisms, and structure. *In vitro* deadenylation assays have been used to study the deadenylases over the years. The advantages of these *in vitro* assays include their usefulness in determining enzyme kinetics and cofactor requirements of the enzyme (Chen et al., 2002, Viswanathan et al., 2003, Goldstrohm and Wickens, 2008, Andersen et al., 2009a). They are also useful in studying the effect of amino acid substitutions on enzymatic activity (Bianchin et al., 2005, Viswanathan et al., 2003).

In vitro assay methods currently available for studying deadenylases include colorimetric assays (Greiner-Stoeffele et al., 1996). Assays based on methylene blue colorimetry are quantified based on intercalation of methylene blue to RNA which will cause a shift of the absorbance maximum of methylene blue (Greiner-Stoeffele et al., 1996, Liu and Yan, 2008). However, they are insensitive and require high protein and substrate concentrations (Greiner-Stoeffele et al., 1996, Cheng et al., 2006). They are also time consuming and less suitable for quantitative analysis and screening. Gel assays based on substrates labelled with fluorescent or radioactive functional groups are also used to study deadenylase activity but are difficult to quantify and are quite laborious (Chen et al., 2002, Viswanathan et al., 2003). Quantitative assays based on size exclusion chromatography have also been used (He and Yan, 2012). This method allows for separation and quantification of product and substrate, after a reaction by size exclusion. However, it has disadvantages which include: limited sensitivity, requires large reaction volume, it is relatively time consuming and not suitable for high throughput screening (He and Yan, 2012). Generally, a good assay should be quick, simple to conduct, highly specific, sensitive and relatively inexpensive.

Recently, as described in previous chapter, a fluorescence-based quantitative assay suitable for high throughput screening in a multi-well plate format was recently developed (Maryati et al., 2014). The assay which is based on substrate detection using an oligonucleotide probe complementary to the RNA oligonucleotide substrate was used for characterisation of deadenylases. It was also used to screen small-molecule inhibitors (non-nucleoside *N*-hydroxyimide compounds) that selectively inhibit the enzyme activities of CNOT7 (Maryati et al., 2015, Jadhav et al., 2015). During the course of this work, an adenosine mono phosphate (AMP) based assay was used for kinetic characterisation of PDE12 and the CNOT6 and CNOT6L enzymes in a multiwell-plate based format (Wood et al., 2015, Steinberg and Kemp, 2009). Previous studies show that AMP is a reaction product of CNOT7 deadenylase (Bianchin et al., 2005). In this chapter, the main aim was to evaluate the use of the AMP product-based assay as an *in vitro* biochemical assay for characterisation of deadenylase enzymes. This would be useful to determine its suitability as a complementary assay to the fluorescence-based assay.

First, deadenylase enzymes for the evaluation of the AMP-based assay method were purified to homogeneity. This includes CNOT7, PARN, Ccr4 proteins and the human trimeric nuclease complex. A method of purifying the trimeric nuclease complex previously described (Maryati et al., 2015) was optimised. Next, the AMP detection assay method for characterising deadenylase enzymes was evaluated. Unlike the fluorescence-based assay method, the AMP detection assay is product-based. As described in the chapter 1, It is a homogeneous assay that generates a luminescent signal from any biochemical reaction that produces AMP as a reaction product (Figure 4.1). AMP-based assays quantitatively monitor the concentration of AMP in a biochemical reaction in a high-throughput format. The assay involves two steps: First, the termination of enzymatic reaction, simultaneous removal of adenosine triphosphate (ATP) and conversion of AMP produced to ADP by the enzyme polyphosphate AMP phosphotransferase (PAP) contained in AMP-Glo stop reagent 1. The second step involves the conversion of ADP to ATP by a second enzyme adenylate kinase (AK) contained in Kinase glo

detection solution and determining the amount of the ATP produced using a bioluminescent reaction utilizing a luciferase enzyme and a substrate for the luciferase enzyme. (Figure 4.1). The amount of ATP produced determines the amount of AMP present in the original solution. The amount of AMP produced by the reaction is proportional to the light measured using a Glomax luminometer and can be extrapolated using a standard curve.

Typically, in the presence of active enzyme, RNA substrate is degraded and deadenylase activity is measured by the quantity of AMP produced which is detected by luminescence. In the absence of enzymatic activity, there are no AMP products. The findings of this study demonstrate that the AMP product-based assay is a highly sensitive assay and is suitable for characterisation of deadenylase enzymes. It is also useful for screening molecular inhibitors and can be used as a complementary assay to the fluorescence-based assay.

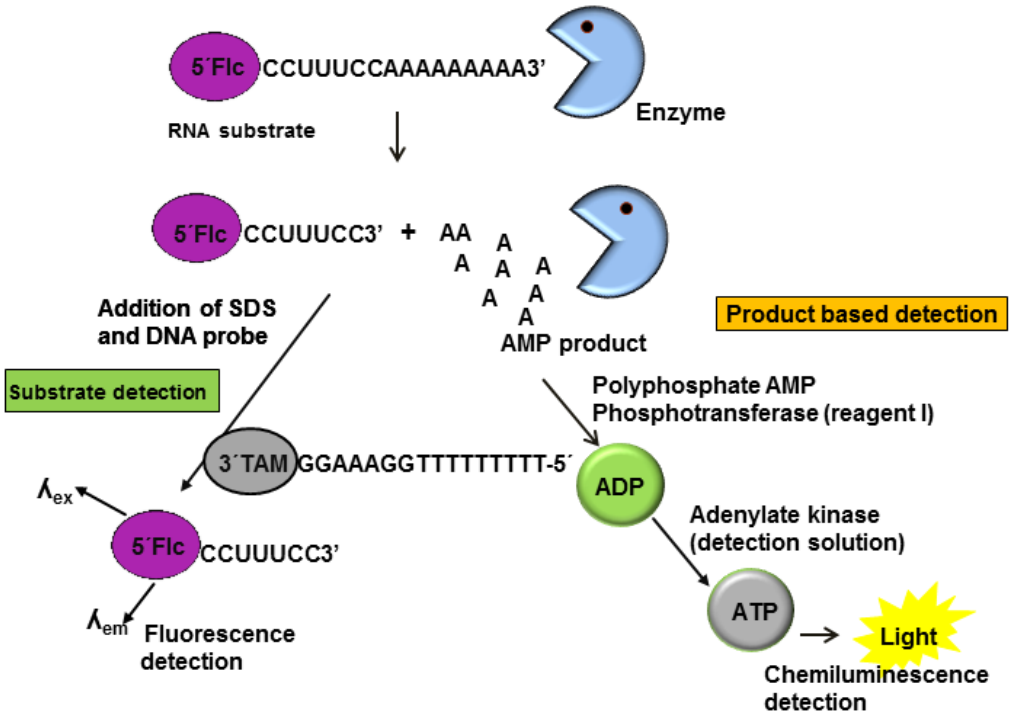

Figure 4.1. Principle of chemiluminescence and fluorescence-based deadenylase assay. A schematic representation of RNA substrate or AMP product-based measurements of enzyme activity. Deadenylase enzymes are incubated with 5´ Flc-labelled RNA oligonucleotide substrate for 60 minutes at 30^0C. Reactions for fluorescence-based measurements are terminated by the addition of SDS and DNA probe (left panel). In the presence of active enzyme, RNA substrate is degraded and fluorescence can be detected. Conversely, in AMP product-based quantification reactions are stopped by the addition of AMP-Glo reagent I containing polyphosphate AMP phosphotransferase for conversion of AMP to ADP. Then an AMP detection solution containing adenylate kinase is added for conversion of ADP to ATP. The amount of ATP is determined by a luciferase reaction. Enzyme activity is measured by chemiluminescence (right panel). In the absence of enzymatic activity, there are no AMP products.

4.2 Protein purification of deadenylases

4.2.1 Expression and purification of a minimal trimeric nuclease complex

4.2.1.1 Generation of plasmid expression vectors

Recently, a method of cloning, expression and purification of a human trimeric nuclease complex containing BTG2, CNOT7 and Ccr4 proteins from bacteria cells was developed and well established (Maryati et al., 2015). This method involved a two-step purification process by His-tag affinity purification and size exclusion chromatography. It also involved the use of plasmids pQE80L which consists of an ampicillin resistance gene and also CoIEI replication origin. Together these components are compatible with the chloramphenicol resistance gene and the P15A replication origin of the pACYCDuet-1 vector. The combination of the two vectors allow for co-expression of the trimeric nuclease complex in bacteria cells (Maryati et al., 2015). In this work, the trimeric nuclease complex containing the full-length CNOT6L was used. This was because it was easier to clone and express the full-length CNOT6L in the nuclease complex compared to the full-length CNOT6. In addition, previous work had also shown a significant increase in the activity of a nuclease complex containing CNOT6L when compared to monomeric proteins (Maryati et al, 2015). To optimise the purification of the trimeric nuclease sub-complex (His•BTG2-CNOT7-CNOT6L) previously described, plasmids containing the Strep-tag for co-expression in bacteria cells instead of a His-tag previously used, were generated. The Strep-tag was chosen based on their rather small size and near biochemically inert property. The tag offers the advantage of no interference with protein folding or their function in assays and also is advantageous in a one-step isolation of Strep-tagged proteins from bacterial crude lysates (Lichty et al., 2005, Schmidt and Skerra, 2007, Kimple et al., 2013). First, a modified bacterial expression vector pQE80L containing a Strep-tag (pQE80L-Strep) was constructed using standard procedures. A Strep-tag oligonucleotide (Table 2.6) containing an EcoRI at 5′ end and BamHI at the 3′ ends was annealed and cloned into EcoRI

and BamHI restriction sites of pQE80L replacing the His-tag sequence (Figure 4.2). Next, a PCR-generated human BTG2 fragment was cloned into the multiple cloning site of pQE80L plasmid encoded with a Strep-tag sequence using the BamHI and HindIII restriction sites. The plasmid modifications were verified by DNA sequencing.

Expression vector pACYCDuet-1 containing dual multiple cloning sites (MCS) and suitable for co-expression was used for dual expression of the full-length GST-tagged CNOT6L and CNOT7 in *E.coli* BL21 (DE3). pACYCDuet-1 plasmid contained CNOT6L at the MCS 1 and CNOT7 at MCS 2. Both CNOT6L and CNOT7 cDNAs were codon-optimised for expression in *E. coli* (Genscript).

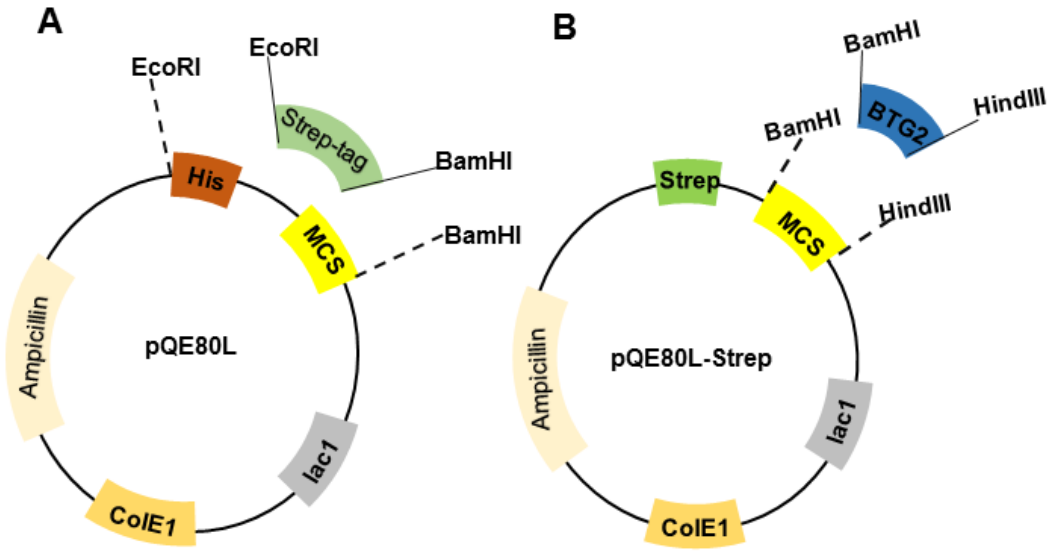

Figure 4.2 Generation of modified bacterial expression vector pQE80L-Strep. Plasmid pQE80L containing Strep-tag (pQE80L-Strep) was constructed using standard procedures. A strep-tag oligonucleotide containing an EcoRI at 5′ end and BamHI at the 3′ ends was annealed and cloned into EcoRI and BamHI restriction sites of pQE80L replacing the His-tag sequence. (B) Generation of pQE80L-Strep•BTG2. PCR generated human BTG2 fragment was cloned into the multiple cloning site of pQE80L plasmid encoded with a strep tag sequence using the BamHI and HindIII restriction sites.

4.2.1.2 Expression and purification of nuclease complex using Strep-tagged BTG2

To optimise the purification of the trimeric nuclease complex, Strep-tagged BTG2 was used for protein expression. First plasmid pACYCDuet-1 containing GST•CNOT6L at the MCS 1 and His•CNOT7 at MCS 2 was co-transformed with plasmid pQE80L-Strep•BTG2 in *E. coli* BL21 (DE3) cells. A GST-tag was chosen for expression of full-length CNOT6L based on optimisation of expression of the nuclease complex. It was difficult to express the full-length CNOT6L using His-tag in the nuclease complex. A single colony of *E. coli* BL21 (DE3) from transformation plates was used to inoculate a starter culture for protein expression. Pre-cultures were grown in Lysogeny Broth (LB) medium containing 34 µg/ml chloramphenicol and 100 µg/ml ampicillin at 37^0C with vigorous shaking until optical density was between 0.6 and 0.8. Protein expression (4 L culture) was induced by the addition of isopropyl β-D-1-thiogalactopyranoside (IPTG; 0.1 mM final concentration) overnight at room temperature. Cells were harvested by centrifugation (4200 rpm) for 30 minutes at 4°C and resuspended in lysis buffer (20 mM Tris-HCl pH 7.8, 250 mM NaCl, 5% glycerol, 1 mM β-mercaptoethanol). Subsequently, the bacterial cells were lysed by sonication and the lysate was made clear by centrifugation at 10000 rpm at 4°C for 30 minutes to remove insoluble material.

Thereafter, the protein complex was purified by gravity flow using Streptactin sepharose 50% gravity flow suspension. The column was loaded with the Streptactin resin and equilibrated with wash buffer (20 mM Tris-HCl pH 7.8, 250 mM NaCl, 5% (v/v) glycerol and 1 mM β-mercaptoethanol). The soluble lysate was loaded onto the column and washed with five column volumes of wash buffer. The trimeric nuclease complex (Strep•BTG2-CNOT7-GST•CNOT6L) was eluted with wash buffer containing 2.5 mM D-Desthiobiotin and collected in 0.5 ml fractions (Figure 4.3A). Protein purity was analysed by SDS-PAGE and visualised by staining with Coomassie Blue. The SDS-PAGE analysis indicates bands that correspond to CNOT6L, CNOT7

and BTG2 on the gel in agreement with predicted molecular weights. CNOT6L~80kDa, CNOT7~30 kDa and human BTG2~ 17 kDa. CNOT6L was observed as double bands (Figure 4.3B lane 3, 4 and 5). It was important to establish the stoichiometric ratio between proteins in the nuclease complex based on their molecular weight and band intensities. CNOT7 was more represented on the gel compared to the other proteins (Figure 4.3 lanes 4 and 5). Based on the apparent representation of the nuclease complex on gel, it is unlikely that this represents the predicted stoichiometric ratio.

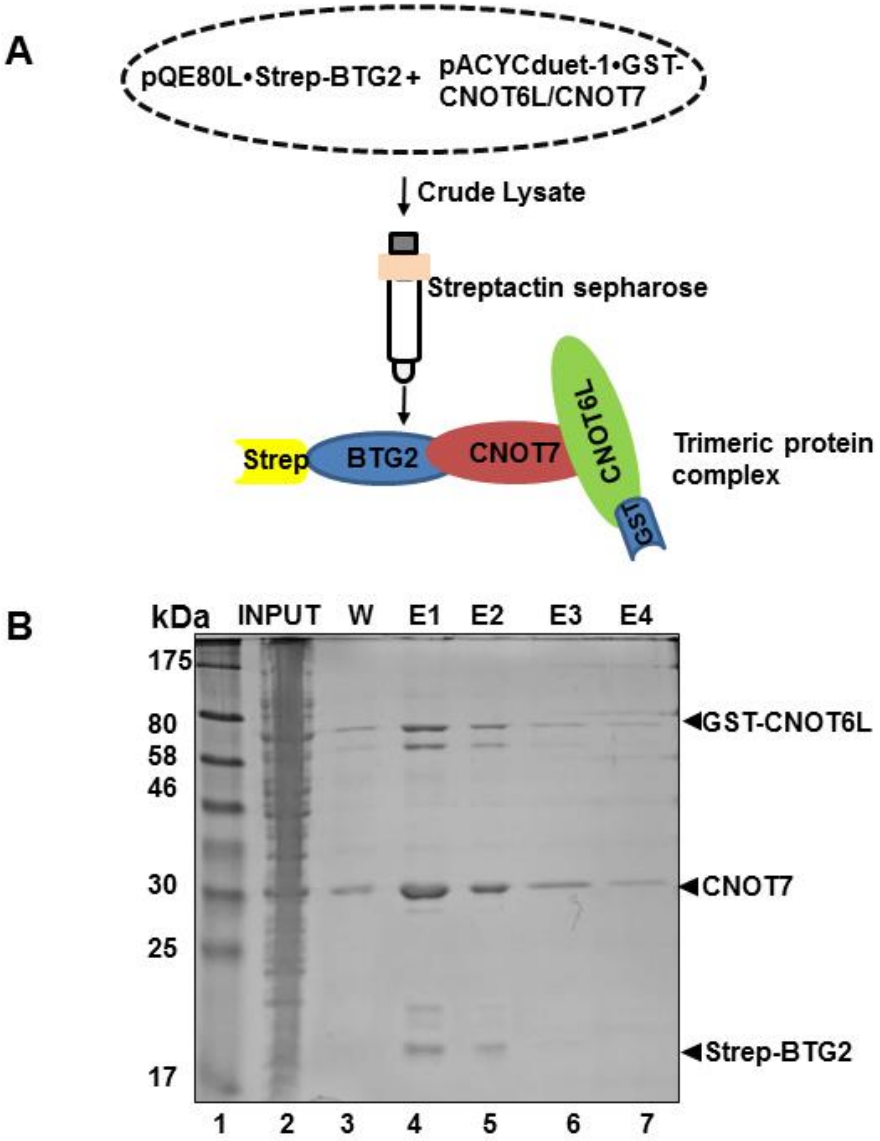

Figure 4.3. Single step affinity purification of Human BTG2-CNOT7-CNOT6L nuclease complex. (A) Purification strategy based on co-expression of Strep•BTG2, CNOT7 and GST•CNOT6L and a one-step affinity purification using Streptactin sepharose. (B) SDS gel analysis of purified Strep•BTG2-CNOT7-GST•CNOT6L. The crude lysate was loaded on a Streptactin column and washed. Protein complex was eluted with buffer containing 20 mM Tris-HCl pH 7.8, 5% glycerol, 2.5 mM D-Desthiobiotin and fractions were analysed on a 14% SDS-PAGE gel stained with Coomassie blue. The input, wash (W) and (E1-E4) elution fractions are indicated.

4.2.1.3 Purification of trimeric nuclease complex using Strep-tagged CNOT6L (His•BTG2-CNOT7-Strep•CNOT6L)

To further optimise the purification of the trimeric nuclease complex, an alternative approach using Strep-tagged CNOT6L instead of Step-tagged BTG2 was explored. First, dual expression plasmid pACYCDuet-1 containing Strep-tagged CNOT6L at MCS 1 and CNOT7 at MCS 2 was generated. CNOT7 cDNA (BamHI-SalI) was present at the multiple cloning site 2 of the pACYCduet vector. PCR-generated CNOT6L fragment was subcloned into vector pQE80L-Strep (BamHI-SalI). After confirmation of subcloning by digestion and DNA sequencing, PCR amplified CNOT6L fragments containing a Strep-tag DNA sequence and a 5′ NcoI site was generated and digested using NcoI and SalI endonucleases. The restriction digested fragment was subcloned into the NcoI and SalI sites of the MCS 1 of pACYCduet-1 replacing sequences encoding the histidine tag in MCS 1 (Figure 4.4).

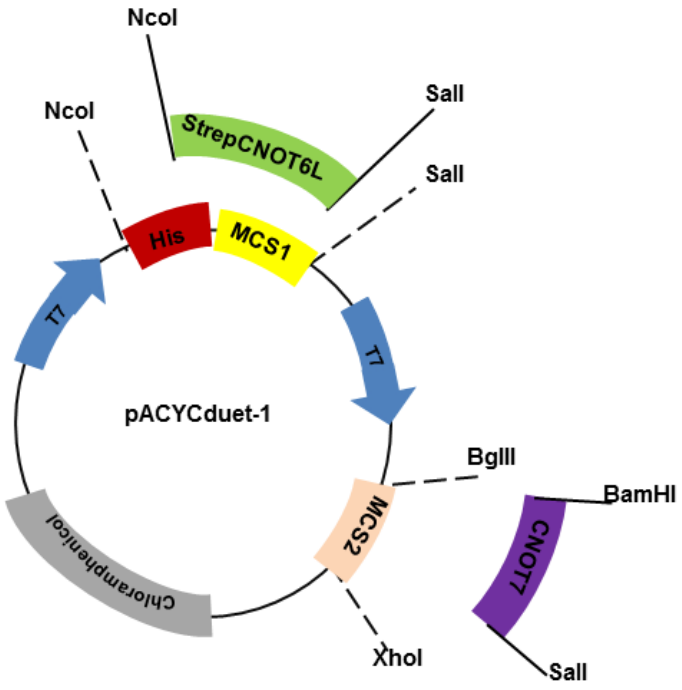

Figure 4.4. Generation of bacterial expression vectors containing CNOT7 and full length CNOT6L cDNAs. (A) CNOT7 cDNA (BamHI-SalI) was present in the multiple cloning site 2 of the pACYCduet vector. PCR amplified CNOT6L fragments containing a Strep tag DNA sequence and a 5′ NcoI site was digested using NcoI and SalI endonucleases. The restriction digested fragment was subcloned into the NcoI and SalI sites of the MCS 1 of pACYCduet-1 replacing sequences encoding the histidine tag in MCS1.

To express the trimeric nuclease complex, the newly generated plasmid pACYCDuet-1 containing Strep•CNOT6L at the MCS 1 and CNOT7 at MCS 2 was co-transformed with plasmid pQE80L-His•BTG2 in *E. coli* BL21 (DE3) cells. A single colony of *E. coli* BL21 (DE3) from transformation plates was used to inoculate a starter culture for protein expression. Pre-cultures were grown in Lysogeny Broth (LB) medium containing 34 µg/ml chloramphenicol and 100 µg/ml ampicillin at 37^0C with vigorous shaking until optical density was between 0.6 and 0.8. Protein expression (4 L culture) was induced by the addition of isopropyl β-D-1-thiogalactopyranoside (IPTG; 0.1 mM final concentration) overnight at room temperature. Cells were harvested by centrifugation for 30 minutes at 4°C and resuspended in lysis buffer (20 mM Tris-HCl pH 7.8, 250 mM NaCl, 5% glycerol, 1 mM β-mercaptoethanol).

The protein complex was purified by gravity flow using Streptactin sepharose 50% gravity flow suspension. The column was loaded with the Streptactin resin and equilibrated with wash buffer (20 mM Tris-HCl pH 7.8, 250 mM NaCl, 5% (v/v) glycerol and 1 mM β-mercaptoethanol). The soluble lysate (10 ml) was loaded onto the column and washed with five column volumes of wash buffer (Figure 4.5A). To improve yield, the elution step was modified by increasing the concentration of D-Desthiobiotin. The protein complex was eluted with buffer containing 10 mM D-Desthiobiotin and collected in 0.5 ml fractions. Protein purity was analysed by SDS-PAGE and visualised by staining with Sypro Ruby dye (Figure 4.5B). Sypro Ruby dye was used for easy detection of human BTG2 protein band on gel. The results show bands on the gel that correspond to CNOT6L, CNOT7 and BTG2 proteins based on molecular weight in kDa. Although the elution profile shows some impurities on the gel, the protein bands were represented on the gel in the expected ratio (4:2:1) based on their band intensities and overall molecular weight of each protein (Figure 4.5, lanes 4 and 5). Thus the single-step purification of the trimeric nuclease complex using Strep-tagged CNOT6L improved protein purification step, producing high yields compared to previous methods which required two or more purification steps and was quite laborious (Maryati et

al., 2015). The catalytic inactive double mutant His•BTG2-CNOT6LE240A-CNOT7D40A was also purified in parallel under same conditions.

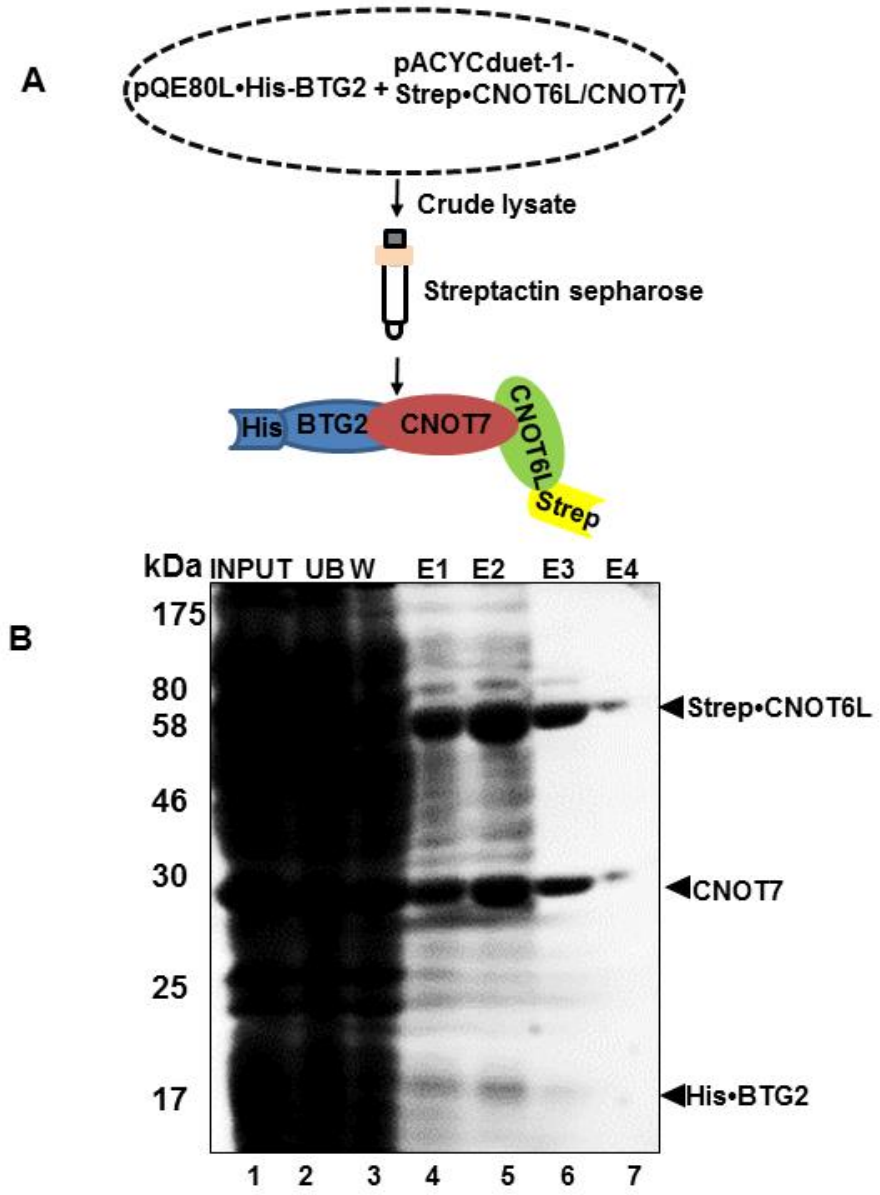

Figure 4.5. SDS-PAGE analysis of purified Human His•BTG2-CNOT7-Strep•CNOT6L nuclease complex. (A) Purification strategy based on co-expression of His•BTG2, CNOT7 and Strep•CNOT6L. Proteins were purified by a one-step affinity purification using Streptactin sepharose. (B) A 1 ml Streptactin column was loaded with crude protein lysate (10 ml) and washed. Proteins were eluted with buffer containing 10 mM D-Desthiobiotin. 0.5 ml fractions were collected and analysed on a 14% SDS-PAGE stained with Sypro Ruby dye. The input, unbound (UB), Wash (W) and Elution (E1-E4) fractions are indicated.

4.2.2 Purification of His•CNOT7 deadenylase

The wild type CNOT7 and catalytically inactive mutant CNOT7D40A were purified using pQE80L expression vector as described (Maryati et al., 2014). A 1 ml starter culture was inoculated with a single colony of *E.coli* BL21 containing His-tagged pQE80L-CNOT7 or pQE80L-CNOT7D40A respectively. The pre-culture was grown in 2 L of LB at 37°C until the optical density (600 nm) was between 0.6-0.8. Then 0.2 mM final concentration of isopropyl β-D-1-thiogalactopyranoside (IPTG) was added to the culture to induce protein expression.

CNOT7 was purified by immobilised metal affinity chromatography using a 1 ml His-trap HP column (GE healthcare). The protein lysate was applied to the column by a syringe and the column was washed with 10 ml of buffer (20 mM Tris-HCl pH 7.8, 500 mM NaCl, 5% (v/v) glycerol and 1 mM β-mercaptoethanol) containing 10 mM imidazole to remove impurities. CNOT7 was eluted with 6 ml buffer (20 mM Tris-HCl pH 7.8, 500 mM NaCl, 5% (v/v) glycerol, 1 mM β-mercaptoethanol and 250 mM imidazole) and collected in 0.5 ml fractions (Figure 4.6A). Protein purity was analysed by a 10% SDS-PAGE and visualised by staining with Coomassie Blue. The catalytic inactive mutant CNOT7D40A was purified in parallel under same conditions. SDS-PAGE analysis shows pure CNOT7 and inactive mutant CNOT7D40A. (Figure 4.6B). The purification step yielded a more than 95% pure protein.

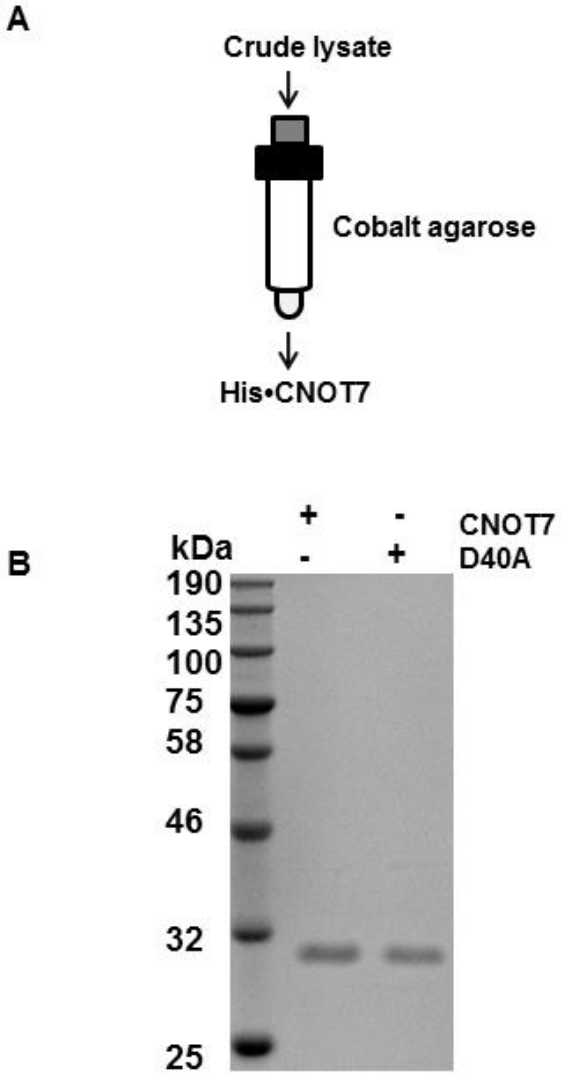

Figure 4.6. Purified CNOT7 deadenylase enzymes. (A) Overview of purification strategy by a one-step immobilised metal affinity chromatography using cobalt agarose. (B) A 10% Coomassie stained SDS-PAGE gel showing purified CNOT7 and inactive mutant D40A. Wildtype and inactive CNOT7 were expressed as His-tagged proteins in *E.coli.* The protein concentration was determined using Bradford assay and 300 ng proteins were analysed on gel. Numbers to the left indicate molecular masses of marker proteins (M) in kDa.

4.3 A comparison of substrate fluorescence and AMP product-based detection assay for activity measurements

4.3.1 Deadenylation activity of monomeric human CNOT7

To evaluate the sensitivity of the AMP product-based assay, the deadenylation activity of human CNOT7 was determined. First, the substrate fluorescence-based assay was used to evaluate CNOT7 activity as a standard for comparison. Enzyme concentrations (0, 100, 200, 400, and 600 nM) of CNOT7 and the catalytically inactive mutant D40A were incubated with RNA substrate (1 µM) for 60 minutes at 30^0C in a 10 µl reaction volume. The reaction was stopped by adding a stop/DNA probe mix containing 1% SDS, Tris-EDTA buffer and a fivefold molar excess of TAMRA-labelled DNA (5´TTTTTTTTTGGAAAGG-TAMRA-3´). Thereafter, enzyme activity was measured by substrate fluorescence using a Biotek plate reader (Figure 4.7A). The result indicates that the deadenylase activity is specific to the wild type CNOT7 compared to the control, D40A. There was a low level of fluorescence observed at all concentrations of D40A used for the reactions. Enzyme concentrations below 400 nM showed limited or no RNA degradation.

Next, the AMP product-based assay was used to evaluate the deadenylase activity of CNOT7. After incubation of the Flc-labelled RNA substrate (1 µM) with CNOT7 enzyme concentrations (0, 25, 50, 100, 200, 400 and 600 nM) for 60 minutes at 30^0C, the reaction was terminated by the addition of AMP-Glo reagent I. This was added for conversion of AMP to ADP for another 60 minutes. Then an AMP detection solution was added to the reaction for conversion of ADP to ATP. The reaction was incubated for a further 45-60 minutes and chemiluminescence was detected using a Glo-max luminometer. Interestingly, the results show a significant difference from the fluorescence-based assay as CNOT7 enzyme activity was detected at all concentrations used. The findings also indicated that enzyme concentrations below 400 nM would be optimal for the assay (Figure 4.7B). The signal/background ratio was also fivefold higher compared to the fluorescence-based detection assay.

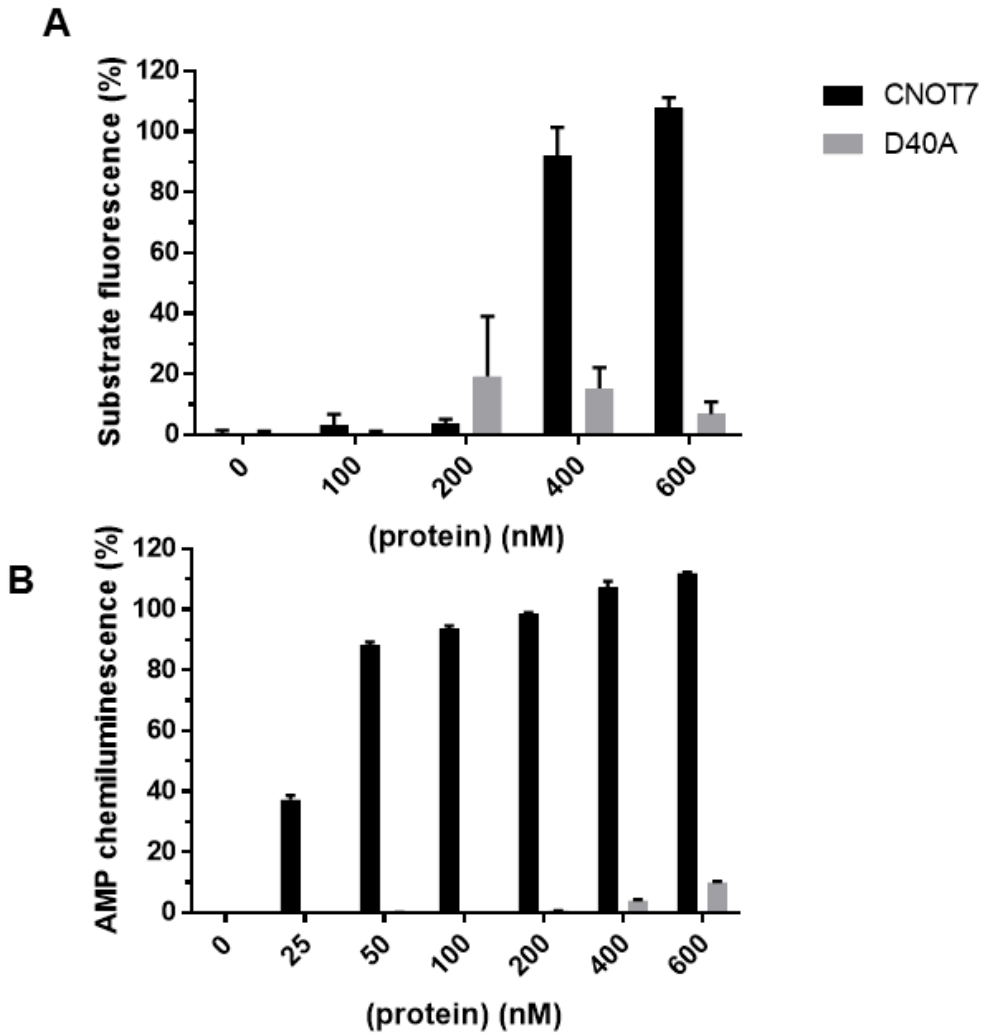

Figure 4.7. Comparison of assays based on substrate fluorescence or AMP product detection. (A) Increasing amounts (0, 100, 200, 400, 600, 800, 1000, 1200 nM) CNOT7 were incubated with RNA substrate (1 μM) for 60 minutes at 30^0C. The reaction was stopped by adding a stop/DNA probe mix. Enzyme activity was measured by substrate fluorescence. (B) A product based activity assay of CNOT7 measured by chemiluminescence. Enzyme concentrations (0, 25, 50,100, 200, 400 and 600 nM) were incubated with RNA substrate (1 μM) for 60 minutes. The reaction was stopped by adding AMP detection reagent I and II. The inactive mutant D40A is indicated. Error bars indicate standard error of mean (n=3).

4.3.2 Deadenylation activity of monomeric human Ccr4 proteins

Next, AMP product-based assay was tested using EEP-type deadenylases. The wild type CNOT6 and CNOT6L were used. In Chapter 3, a fluorescence substrate-based assay was used to compare the activity of both enzymes and CNOT6 was more active than the CNOT6L. CNOT6 enzyme activity was detected at concentrations <400 nM compared to the CNOT6L where activity was detected at concentrations >600 nM. Here, the AMP-based assay was used to determine enzymatic activity at very low concentrations. Optimisation work done using enzyme concentrations above 100 nM showed a saturation of assay signal. Therefore, a time course reaction using a range of enzyme concentrations was carried out. CNOT6 (0, 10, 30, 50 and 100 nM) concentrations and CNOT6L concentrations (0, 10, 30 and 100) respectively were incubated with fluorescent RNA substrate (1 μM) for 60 minutes at 30^0C. The reaction was terminated by the addition of AMP-Glo reagent I for conversion of AMP to ADP for another 60 minutes. Then an AMP detection solution was added to the reaction for conversion of ADP to ATP and incubated for a further 45-60 minutes. AMP product chemiluminescence was detected using a Glo-max luminometer. For controls, the catalytically inactive variant E240A was used. The results (Figure 4.8) show that the AMP-based assay detected deadenylase activity of the EEP-type enzymes. The sensitivity of the assay was striking as enzyme activity was detected at low CNOT6 and CNOT6L concentration (30 nM) compared to the previous findings were no enzyme activity was detected at < 400nM concentration by the fluorescence-based assay. Also, the assay showed similar activity for CNOT6 and CNOT6L in contrast to the fluorescence-based assay where CNOT6 had a higher activity compared to CNOT6L. This finding is surprising and remains unclear and should be further investigated. In addition, the background/signal ratio was high (> 10-fold) in agreement with the observation when CNOT7 was used for the evaluation of the AMP-based assay method. The inactive mutant E240A did not show any activity.

Subsequently, the AMP product-based assay was optimised using the CNOT6 enzyme. The most suitable RNA concentration for the reaction was determined. A fixed amount of RNA (0.25, 0.5 and 1 μM) was incubated with increasing human CNOT6 concentrations (0, 10, 25 and 50 nM). The result (Figure 4.9A) shows high signal for both wild type and mutant CNOT6 using 0.25 μM RNA concentration, suggesting there may have been an experimental error. This would need to be repeated. However, the results in figure 4.9B and C indicate that > 0.25 μM RNA is suitable for the AMP-based reactions.

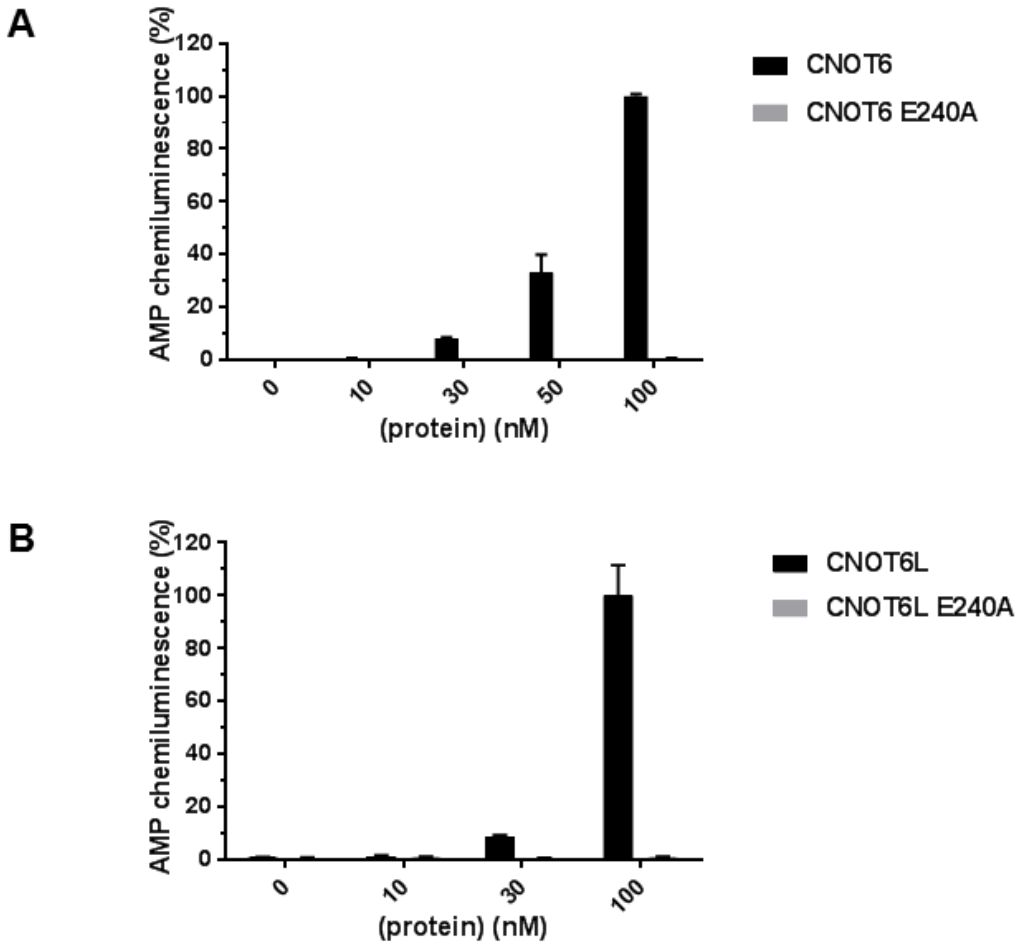

Figure 4.8. Evaluation of human Ccr4 enzyme activity by AMP detection
(A) Increasing enzyme concentrations (0, 10, 30, 50 and 100 nM) of human CNOT6 were incubated with RNA substrate (1 μM) for 60 minutes at 30^0C. The reaction was stopped and the AMP product was measured by chemiluminescence. (B) Increasing amounts (0, 10, 30, and 100 nM) of CNOT6L was incubated with RNA substrate (1 μM) as described in (A). The reaction was stopped and AMP product measured by chemiluminescence. Error bars indicate standard error of mean (n=3). The inactive mutant E240A was used for controls.

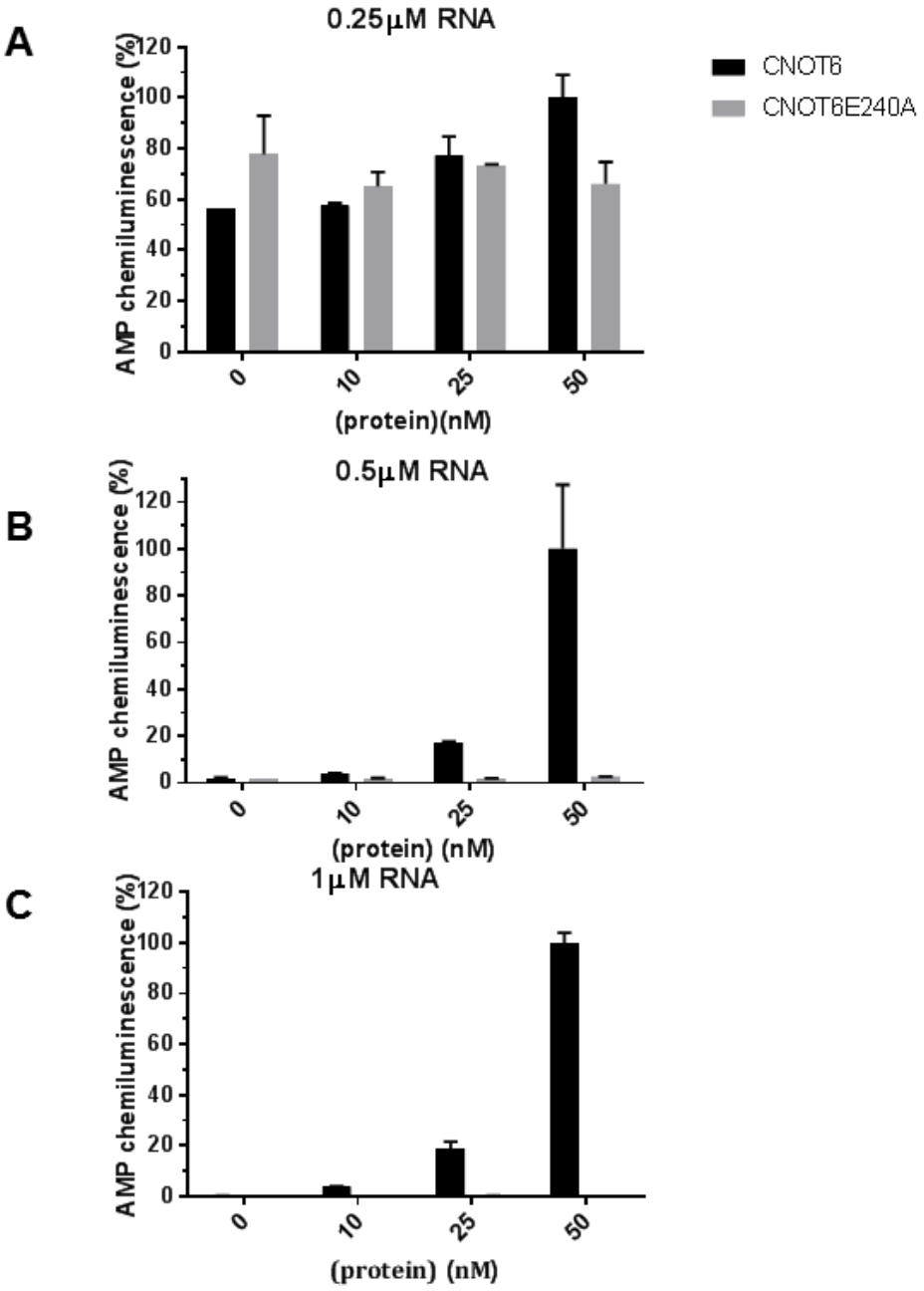

Figure 4.9. Determination of optimal RNA concentration using AMP chemiluminescence-based detection. (A-C) RNA substrate concentrations indicated were incubated with increasing amounts of CNOT6 (0, 10, 25 and 50 nM) for 60 minutes at 30^0C. The reaction was stopped and AMP product was measured by chemiluminescence. Error bars indicate standard error of mean (n=3).

4.3.3 Quantification of deadenylase activity of a trimeric nuclease complex

To evaluate the use of AMP product-based detection in comparison with fluorescence-based assay for quantification of deadenylase activity of a trimeric nuclease complex containing CNOT7, CNOT6L and BTG2, a concentration-dependent assay as a function of activity was carried out. Increasing concentrations (0, 100, 200, 300, 400, 600, 800 and 1000 nM) of wild type His•BTG2-CNOT7-Strep•CNOT6L and was used. For controls, the trimeric nuclease complex containing BTG2 and the double inactive mutants CNOT7D40A and CNOT6LE240A (His•BTG2-CNOT7D40A-Strep•CNOT6LE240A) were used. Thus, the enzymes were incubated with fluorescent RNA substrate (1 μM) for 60 minutes at 30^0C. Thereafter, the reaction was stopped by the addition of a stop DNA probe and substrate fluorescence was measured. The results in Figure 4.10A shows distinct enzymatic activity displayed by the wild type trimeric protein complex compared to the control. The reaction appeared to be saturating at 300 nM enzyme concentration. Subsequently, deadenylase activity was further determined by substrate fluorescence using lower enzyme concentrations (0, 5, 10, 15, 20, and 100 nM) (Figure 4.10B). No enzyme activity was observed, based on fluorescent signals as shown in the figure, comparing the wild type proteins with controls.

Next, the deadenylase activity of the trimeric nuclease complex (His•BTG2-CNOT7-Strep•CNOT6L) was further evaluated by the AMP-based assay. Enzyme concentrations (0, 5, 10 and 20 nM) were incubated with RNA (1 μM) for 60 minutes at 30^0C. Thereafter, the reaction was stopped by the addition of an AMP detection reagent and AMP-product chemiluminescence was measured. Interestingly, the result shows a detection of enzyme activity at the lowest concentration used (5 nM) (Figure 4.10C). This further confirmed that the AMP product-based assay is a more sensitive assay. Based on the results, 10 nM enzyme concentration was chosen for use in further compound screening assays.

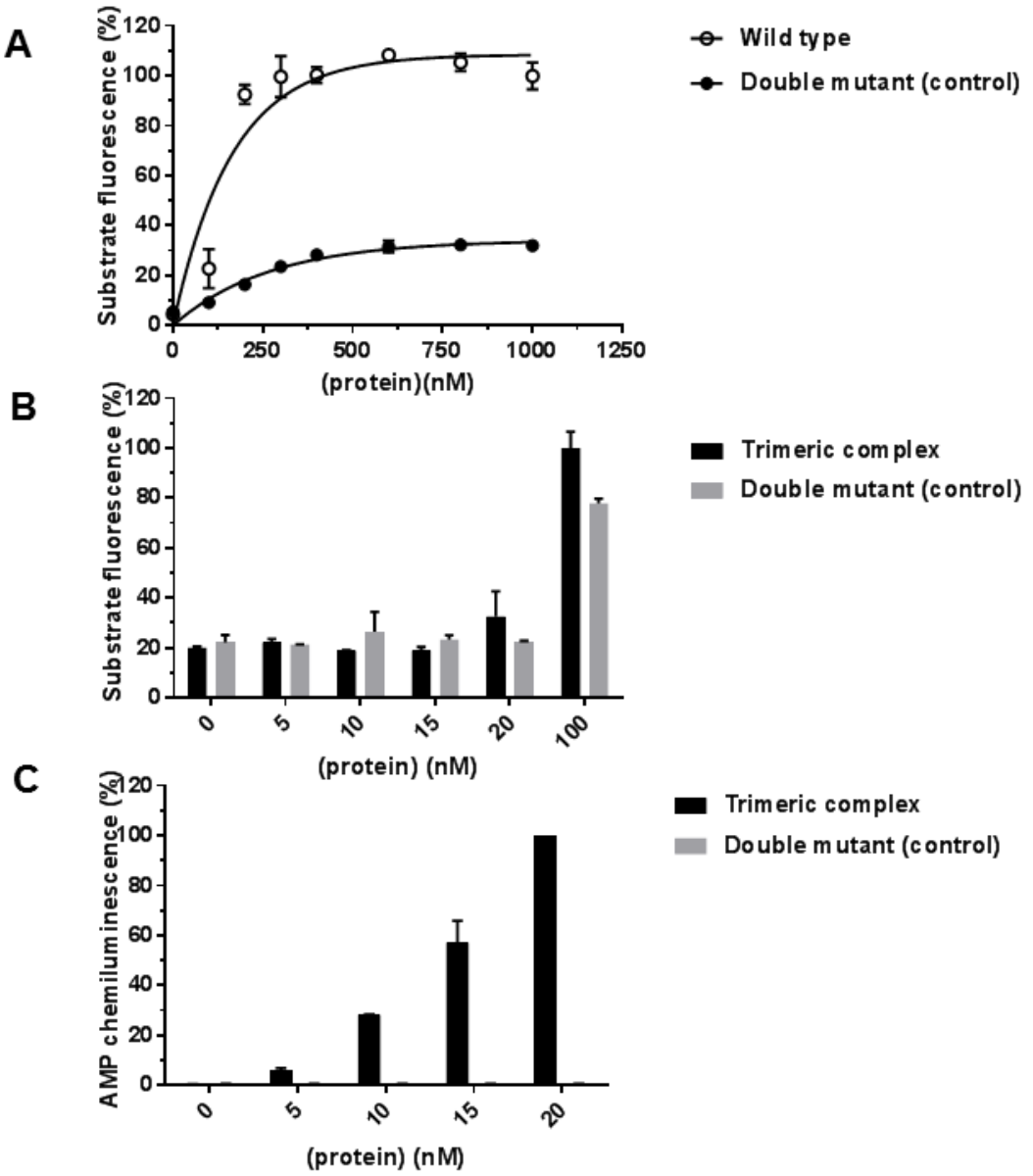

Figure 4.10. Comparison of trimeric complex His•BTG2-CNOT7-Strep•CNOT6L deadenylase activity based on substrate or AMP product detection. (A) Increasing enzyme concentrations (0, 100, 200, 400, 600, 800 and 1000 nM) of trimeric complex were incubated with RNA substrate (1 μM) for 60 minutes at 30^0C. The reaction was stopped and enzyme activity was measured by substrate fluorescence. (B) Increasing amount (0, 5, 10, 15, 20, and 100 nM) of trimeric complex was incubated with RNA substrate as in (A). The reaction was stopped and enzyme activity was detected by fluorescence. (C) AMP-based detection of trimeric complex activity at enzyme concentration (0, 5, 10, 20 nM). Proteins were incubated at 30^0C for 60 minutes. Control reactions contained the inactive double mutants CNOT7D40A and CNOT6LE240A. Error bars indicate standard error of mean. (n = 3)

4.3.4 Determination of PARN enzyme activity by AMP detection

To further evaluate the use of AMP product-based assay in comparison with fluorescence-based assay, the deadenylase activity of a different DEDD-type protein, PARN was assessed. Thus, increasing PARN concentrations (0, 1, 2, 5, 10, 20 and 40 nM) was incubated with RNA substrate (1 μM) for 60 minutes at 30^0C. The reaction was stopped by adding a stop/DNA probe mix containing 1% SDS, Tris-EDTA buffer pH 8 and a fivefold molar excess of TAMRA tagged DNA (5´TTTTTTTTTGGAAAGG-TAMRA-3´). Enzyme activity was measured by substrate fluorescence using a Biotek plate reader. The catalytic inactive mutant, D28A was used for controls. The results in Figure 4.11A depicts that there was no RNA substrate degradation observed with the inactive mutant D28A. PARN activity was detected at 20 nM concentration and seemed to degrade RNA completely at 40 nM concentrations. There was limited RNA degradation at concentrations <40 nM. However, when AMP detection assay was used to evaluate PARN deadenylase activity using enzyme concentrations (0, 1, 2, 5, 10 and 20 nM), PARN enzyme activity was detected at very low concentrations (1, 2 and 5 nM), (Figure 4.11B). Background signals were <100-fold lower compared to wild type. This observation is in line with previous findings and confirms that the AMP product-based assay method is highly sensitive and can detect enzyme activity at low enzyme concentration. Based on the result, 1 nM concentration was chosen for further use in compound screening assays.

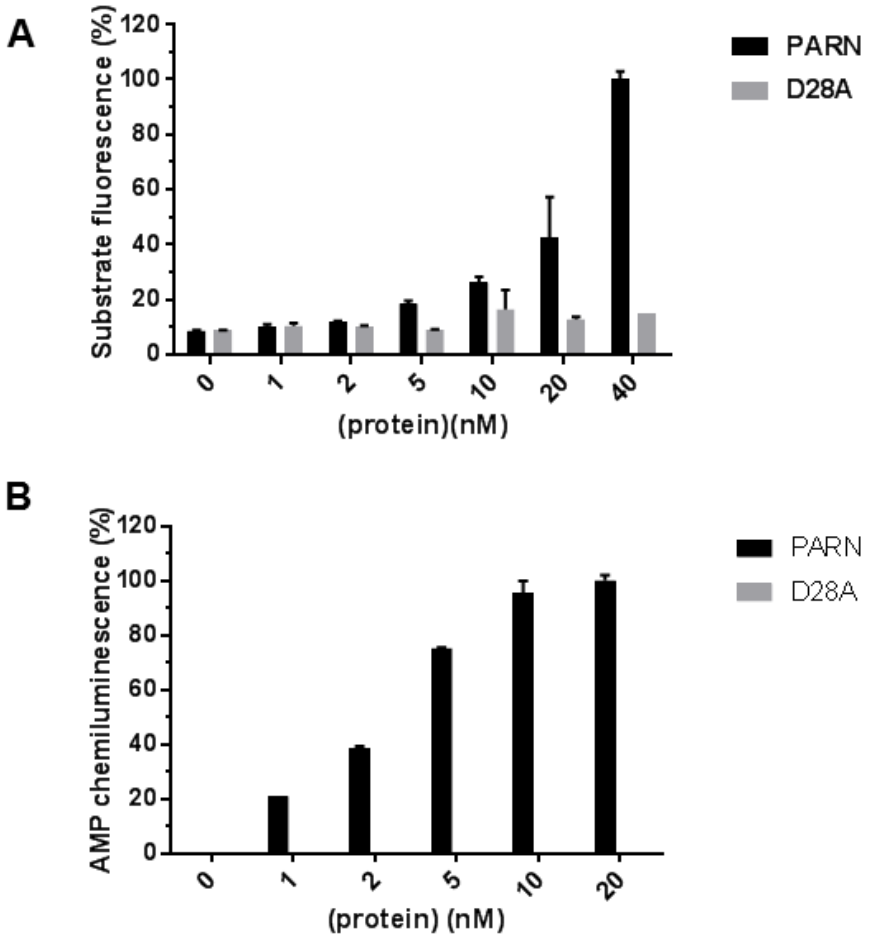

Figure 4.11. AMP based assay identifies PARN activity at low enzyme concentration. (A) Enzyme concentrations (0, 1, 2, 5, 10, 20 and 40 nM) of PARN and catalytic mutant D28A were incubated with RNA substrate (1 µM) for 60 minutes at 30^0C. The reaction was stopped and substrate fluorescence was measured. (B). Increasing amounts of PARN (0, 1, 2, 5, 10 and 20 nM) wild type and catalytic mutant D28A were incubated with RNA substrate (1 µM) for 60 minutes at 30^0C. The reaction was stopped and enzyme activity was measured by AMP product detection. Error bars indicate standard error of mean where (n=3).

4.4 Application of AMP detection assay for characterising small drug-like inhibitors of human CNOT7

4.4.1 Determination of IC_{50} value of compound 007 on human CNOT7 activity

Having established that the AMP product-based assay was highly sensitive and suitable for determining enzyme activity, its suitability for the characterisation of small drug-like inhibitors of CNOT7 was evaluated. Previously, cell permeable inhibitors that selectively inhibit CNOT7 were identified (Maryati et al., 2014, Jadhav et al., 2015). Therefore, compound 007, a benzylpurinedione identified as a lead compound and a well-characterised inhibitor of CNOT7 activity was used to test the validity of the AMP-based assay for enzyme inhibition compared with the fluorescence-based assay. Compound 007 is an analogue of FEN-1 nuclease inhibitor synthesised by Dr G. Jadhav and Prof. P.M Fischer at the school of Pharmacy, University of Nottingham (Maryati et al., 2014, Jadhav et al., 2015) (Figure 4.12). First, the IC_{50} value of compound 007 was determined by fluorescence-based assay. Serial concentrations of compound 007 (0, 0.1, 0.3, 1, 3, 10, 30, 100, 300, 500 and 1000 μM) was pre-incubated with 400 nM CNOT7 for 15 minutes at room temperature. After addition of RNA substrate (1 μM), the reaction mixture was incubated for 60 minutes at 30°C and then stopped by the addition of a DNA probe. Substrate fluorescence was measured using a Biotek plate reader. The IC_{50} value of compound 007 on CNOT7 activity was 14.6 ± 0.42 μM (Figure 4.13A). This was comparable with previously published IC_{50} value of 10.4 ± 0.4 μM using the fluorescence-based assay (Jadhav et al., 2015). Control reactions with no CNOT7 enzyme clearly showed no fluorescence signal.

Next, the IC_{50} value of compound 007 was determined by AMP product-based detection. Compound 007 was pre-incubated with a fixed amount of CNOT7 (25 nM) for 15 minutes at room temperature. RNA substrate (1 μM) was added to the reaction mixture and incubated for 60 minutes at 30°C. The reaction was stopped by adding AMP-glo reagent I and AMP product was detected by chemiluminescence. Interestingly, the IC_{50} value of compound

007 was 10.6 ± 1.1 μM which is comparable with the IC_{50} value determined by fluorescence-based detection method (Figure 4.13B). It also corroborates previously published data (Jadhav et al., 2015).

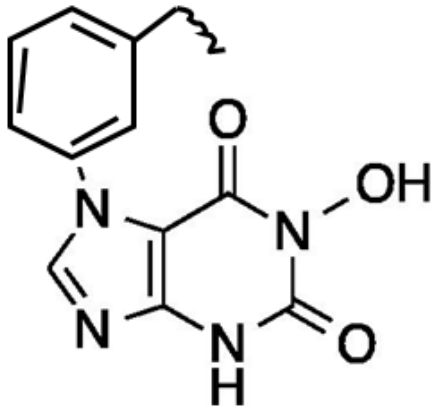

Figure 4.12. Structure of compound 007. A benzylpurine dione compound.

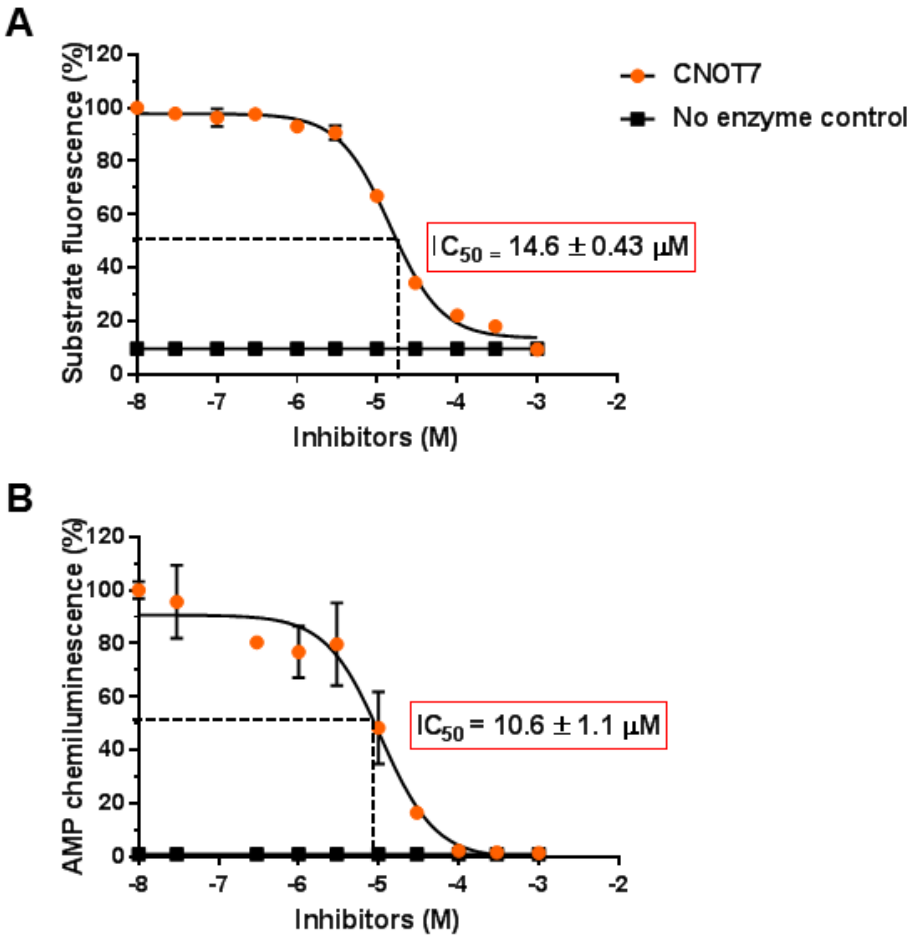

Figure 4.13. Comparison of IC_{50} values of CNOT7 inhibitor using substrate and AMP product-based detection. (A) Determination of IC_{50} values of compound 007. CNOT7 was pre-incubated with compound 007 for 15 minutes at room temperature followed by addition of RNA substrate. The reaction mixture was incubated at 30^0C for 60 minutes. A stop mix containing 10% SDS and fivefold molar excess of DNA probe was added to terminate the reaction and fluorescence was measured. (B) Graphical representation of AMP product based quantification of enzymatic activity in the presence of compound 007. The reaction was carried out as in (A) above and stopped by the addition of AMP reagent I and II. AMP product was measured by chemiluminescence. Error bars indicate standard error of mean where (n=3).

4.4.2 Evaluation of compound 007 inhibitory effect on trimeric nuclease complex

To further explore the use of AMP product-based assay for compound screening, the inhibitory effect of compound 007 on CNOT7 activity in a trimeric nuclease complex was determined. Studies show that the active sites of CNOT7 and CNOT6L are not close in an x-ray structure of a minimal nuclease module composed of the yeast MIF4G domain (Basquin et al., 2012). In addition, the enzyme activities of both CNOT7 and Ccr4 enzymes are required for deadenylation while BTG2 acts as positive regulator of mRNA deadenylation (Basquin et al., 2012, Horiuchi et al., 2009, Maryati et al., 2015, Mauxion et al., 2009, Winkler, 2010). It is speculated that the active sites are regulated by an allosteric interaction within the nuclease module and compound 007, a purine-2, 6 dione was demonstrated to selectively inhibit CNOT7 while the activity of Ccr4 was unaffected (Maryati et al., 2015). To this end, compound 007 was pre-incubated with trimeric nuclease complex (His•BTG2-CNOT7-Strep•CNOT6L) (300 nM) for 15 minutes at room temperature. After addition of RNA substrate (1 μM), the reaction mixture was incubated for 60 minutes at 30°C and then stopped by the addition of a stop DNA probe. Substrate fluorescence was measured using a Biotek plate reader. The results show that the compound 007 has inhibitory activity on the CNOT7nuclease complex. This was based on the IC_{50} value determined (9.58 ± 1.2 μM) (Figure 4.14A). As expected, the value was comparable with the IC_{50} of monomeric CNOT7 previously determined at 10.4 ± 0.4 μM concentration (Jadhav et al., 2015). For controls, a reaction with no enzyme was used.

To ensure that this observation was valid, the deadenylation reaction products were analysed on a denaturing PAGE and visualised by epifluorescence (Figure 4.14B). As expected, there was evidence of inhibition of substrate deadenylation by the nuclease complex in lanes 9-13. The minimal concentration range at which deadenylation appeared to be inhibited was between 10.0-30.0 μM which validates previous observation. The substrate was not degraded in control reactions that had no enzyme. Next,

AMP product-based assay was used to further evaluate the inhibitory effect of compound 007 on the activity of the nuclease complex. The IC_{50} value was determined. The trimeric nuclease complex (10 μM) was incubated with increasing concentrations of compound 007. Control reactions contained no compounds. As shown in Figure 4.14C, compound 007 displayed high affinity for the nuclease complex based on the IC_{50} value determined at 3.29± 1.7 μM. However, the graph does not represent a typical IC_{50} curve compared to Figure 4.14A as there were numerous outliers. This variance may be attributed to pipetting or measurement errors and there would be need for further repeats of this experiment. It was difficult to analyse the reaction product on a denaturing gel. This was a pointer to some of the possible limitations of the AMP product-based assay compared to the substrate fluorescence-based assay.

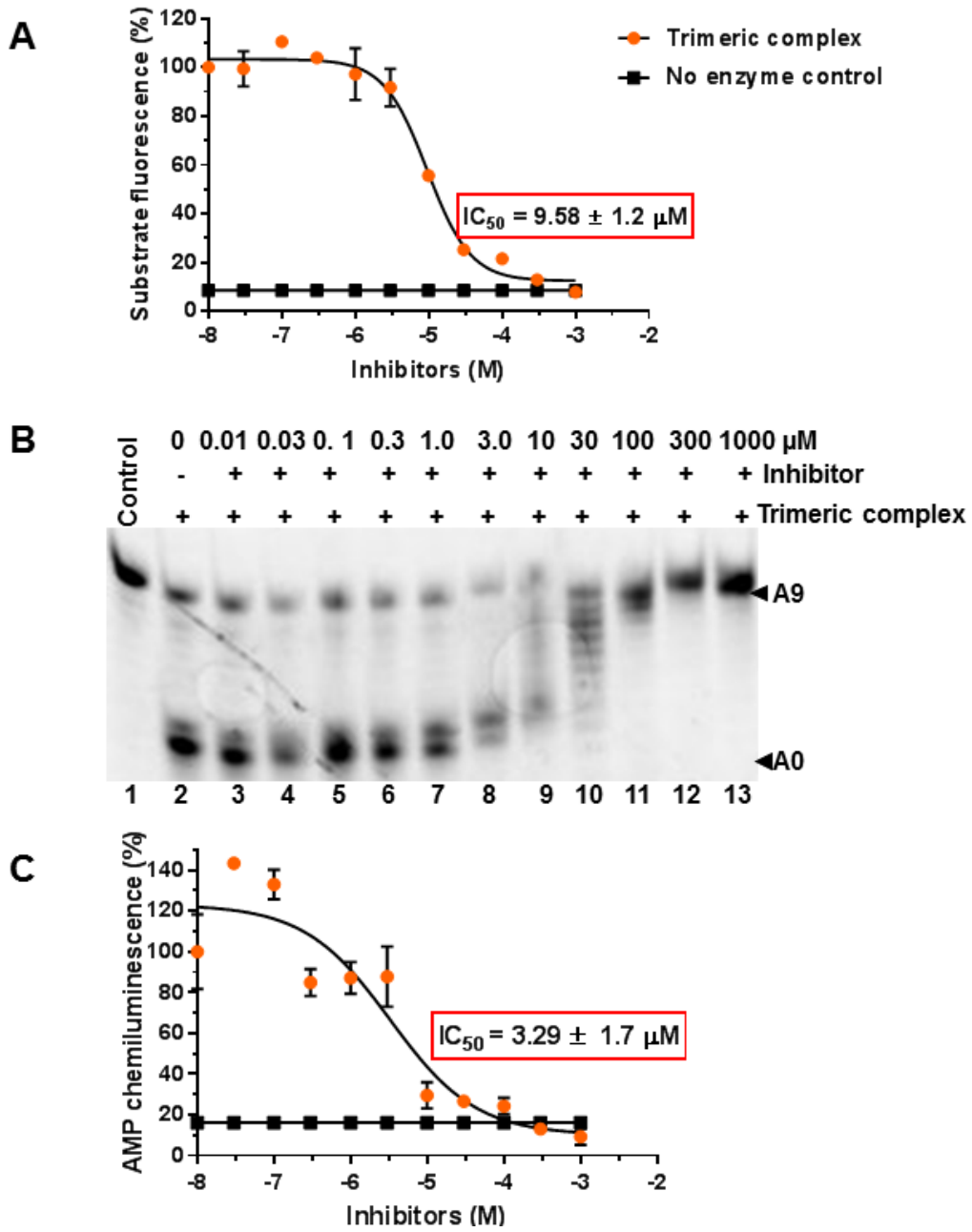

Figure 4.14. Screening of compound 007 inhibitory activity in a trimeric nuclease complex. (A) IC_{50} determination of compound 007 on trimeric nuclease complex activity using fluorescence detection. (B) PAGE analysis of reaction products in (A). Indicated are intact RNA substrates containing nine 3' adenine residues (A9) and the reaction product with no adenine residue (A0) (C) AMP based detection method was used to screen for inhibitory characteristics of compound 007.

4.5 Discussion

In this chapter, the evaluation of deadenylase activity by AMP product-based assay is described. Widely used *in vitro* assay methods available for studying deadenylases are laborious, time consuming, require high protein concentrations and are insensitive. Recently, a substrate-fluorescence assay based on end-point measurements and suitable for high throughput screening was developed and used for the screening of compound libraries (Maryati et al., 2014, Jadhav et al., 2015). The main aim of this chapter was to evaluate the use of an alternative AMP product-based assay as a secondary assay for deadenylase enzyme activity measurements. This would be useful to corroborate findings obtained using the substrate fluorescence-based assay. Wild type and inactive CNOT7, CNOT6, CNOT6L, PARN and a trimeric nuclease complex (His•BTG2-CNOT7-Strep•CNOT6L) were used to evaluate AMP product-based assay method. First, an efficient single-step purification method of the trimeric nuclease complex using Strep-tag was developed and proteins were purified. The results demonstrate that the AMP-based assay is highly sensitive and can be used for quantitative analysis of deadenylase enzymes in a micro-well plate format. This was judged by the enzymatic activities observed with CNOT7, CNOT6, CNOT6L, PARN and trimeric nuclease complex and majorly by the minimum enzyme concentration required for detection of degradation of the RNA oligonucleotide substrate. In addition, the signal/background ratio observed was relatively high across all measurements taken. These are desirable qualities of quantitative assays useful for enzyme characterisation and are advantages over existing assay methods such as methylene blue colourimetry, size exclusion chromatography and gel-based assays (Cheng et al., 2006, Greiner-Stoeffele et al., 1996, He and Yan, 2012). Enzymatic activity was detected at low enzyme concentrations and in small reaction volumes as compared with colourimetry, chromatography based assays or the recently developed fluorescence-based assay. Based on assay optimisation done, > 0.25 μM RNA substrate was optimal for the reactions which is comparable with the amount

of RNA required using fluorescence-based assay. It was noted that the AMP-based assay can be used as a secondary assay for the characterisation of small molecular inhibitors. Interestingly, the IC_{50} value of compound 007 determined by the fluorescence-based assay, validated by analysing gel products on a denaturing gel was comparable with the values obtained by AMP product-based assay. However, though the AMP based assay is advantageous in many ways, there were limitations observed. It was observed that chemiluminescence signals could only be measured immediately after adding the AMP detection reagent. Signals could not be measured hours after termination of the reaction unlike the fluorescence-based assay which has stable signals and can be measured hours and days after the addition of the probe. This suggests that an immediate access to a luminometer is required after the reaction is stopped. In addition, conducting the assay was more time consuming, required multiple steps before end point measurements compared with the fluorescence-based assay. This onerous task may be undesirable when carrying out large numbers of reactions in parallel. Furthermore, the AMP-based assay was more expensive to conduct as the reagents were quite costly compared to that required for the fluorescence-based assay. Finally, while the reaction products of deadenylation by substrate fluorescence-based assay could be easily analysed on denaturing PAGE, it was difficult to further analyse AMP reaction products on denaturing gel for evaluation of factors which may influence the assay.

In Conclusion, this chapter demonstrates an efficient purification method for a human nuclease trimeric complex. It also provides evidence that the AMP product-based assay is a highly sensitive assay for quantitative biochemical analysis of deadenylase enzymes. The findings of this study show that it can be used as a complementary assay to the fluorescence-based assay for characterisation of deadenylase enzymes and inhibitors useful for studying post-transcriptional gene regulation in diseases.

Chapter 5

Use of thermal shift assays to characterise small molecule inhibitors of the CNOT7 and CNOT6L deadenylase enzymes

Chapter 5. Use of thermal shift assays to characterise small molecule inhibitors of the CNOT7 and CNOT6L deadenylase enzymes

5.1 Introduction

The characterisation of small molecule interactions with their protein targets is a key step in drug discovery and the fragment-based drug design process. With the discovery of new therapeutic targets such as CNOT7 and the Ccr4 deadenylases and small molecular inhibitors of these targets, it becomes essential to rapidly identify and judge relative binding affinities of novel drug compounds to protein targets. Recently, cell permeable, small molecule which selectively inhibit CNOT7 were reported (Jadhav et al., 2015). These *N*-hydroxyimide compounds were characterised by a fluorescence-based enzyme assay and it was hypothesised that they inhibit enzyme activity by co-ordination of two divalent metal ions required for catalysis, based on the distance between the Mg^{2+} in the active site of CNOT7 enzyme (Petit et al., 2012a). Current trends in small molecule characterisation involve the analysis of biophysical properties of the protein targets for identifying small molecular weight ligands that bind to them (Pantoliano et al., 2001, Poklar et al., 1997, Lo et al., 2004, Niesen et al., 2007). It is well known that binding of small molecules, co-factors, metal ions, synthetic analogs of natural ligands result in conformational changes on proteins and provide enhanced stability (Brandts and Lin, 1990, Schellman, 1975, Pace and McGrath, 1980, Straume and Freire, 1992, Pantoliano et al., 2001). This stabilisation is a good indicator of interaction between components. Thermal shift assays (TSA) also referred to as differential scanning fluorimetry (DSF) allows the identification of conditions that affect protein stability. It is quick and has been demonstrated to be useful in a multiwell plate format for screening a large number of conditions (Vedadi et al., 2006, Wan et al., 2009, Senisterra et al., 2012). Typically, the TSA is conducted using a real-time PCR machine and it monitors unfolding of proteins from the native to denatured form in the presence of a

fluorescence dye which shows enhanced fluorescence in a hydrophobic environment. Proteins in their native form are folded, when exposed to a range of temperature the protein unfolds. As the protein unfolds, the hydrophobic pockets become exposed allowing binding of the SYPRO Orange dye, resulting in increased fluorescence (λ_{ex} = 492 nm, λ_{em} = 610 nm) and thus acts as reporter to monitor thermally induced protein unfolding. A gradual fall is observed following the peak fluorescent intensity mainly due to protein aggregation, precipitation and dye dissociation (Figure 5.1). The melting temperature (T_m) of the protein is determined by the transition midpoint (point at which 50% of the protein is denatured). Typically, the T_m value of the protein under each condition of the screen is compared with the reference T_m (Niesen et al., 2007).

In this chapter, the use of TSAs for the characterisation of small molecular inhibitors of CNOT7 and CNOT6L was evaluated. The main aim was to determine an alternative, quick and robust method of characterisation of small molecular inhibitors of these targets. First, as a proof of principle, the CNOT7 and CNOT6L deadenylases were used to identify conditions that stabilise the enzymes using TSAs. Next, an investigation into binding of compounds to the protein targets (CNOT7 and CNOT6L) and their effect on protein thermal stability was conducted. The findings of this study reveal that thermal shift assays is ideally suited for quantitative high throughput screening and evaluation of the CNOT7 and Ccr4 enzyme targets. In addition, the thermal shift assay unravelled the binding mode of small molecular inhibitors of CNOT7 enzyme specifically regarding the presence of the Mg^{2+} ions in the active site and a correlation was found between thermal shifts observed and the potency of compounds as determined by IC_{50} values.

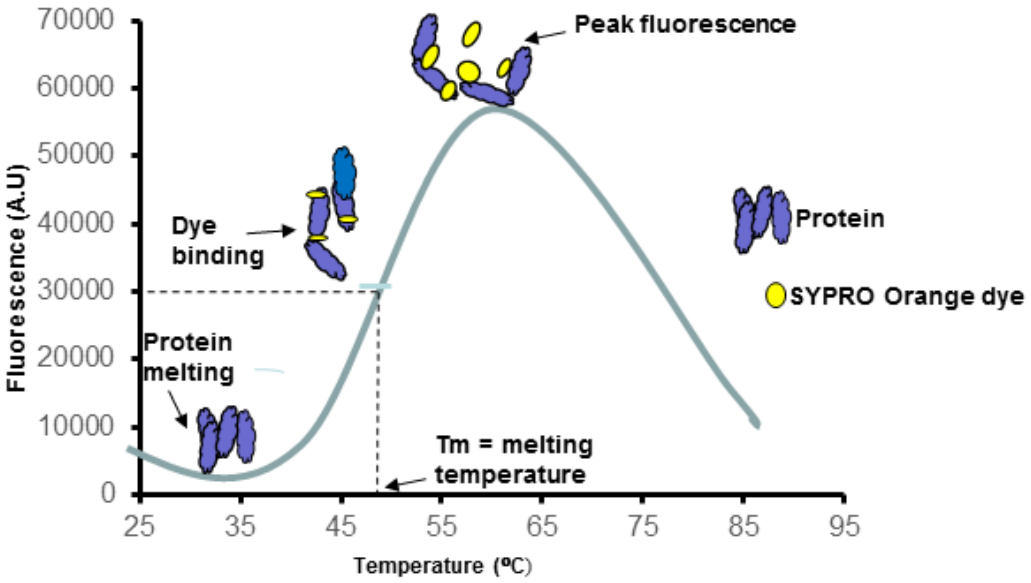

Figure 5.1. Principle of Thermal Shift Assays (TSA). A schematic showing typical unfolding of protein in the presence of the dye SYPRO Orange. As the protein unfolds, hydrophobic pockets become exposed allowing binding of the SYPRO Orange and resulting in increased fluorescence (λ_{ex} = 492 nm, λ_{em} = 610 nm). A gradual fall is observed following the peak fluorescent intensity mainly due to protein aggregation, precipitation and dye dissociation. The melting temperature(T_m) of the protein is determined by the transition midpoint between the native and unfolded state.

5.2 Thermal shift assays are tractable for use with the Ccr4 deadenylase.

5.2.1 Determination of optimal assay conditions

To evaluate the use of thermal shift assays for characterising the Ccr4 protein as a drug target, EPP type enzymes CNOT6 and CNOT6L lacking the LRR were used respectively. First, the thermal denaturation profile of the CNOT6 and CNOT6L proteins was determined. CNOT6 and CNOT6L enzyme concentrations (2, 5 and 10 μM) were used to show that the enzymes were amenable for use in TSAs. The protein/dye solutions were dispensed into each well in a 96-well plate format. All experiments were done in triplicates and reference wells had no enzyme. Subsequently, the plates were heated through a temperature range (25^0C-95^0C) at 1°C per minute and fluorescence intensity was measured at $\lambda_{excitation}$ = 492 nm and $\lambda_{emission}$ = 610 nm. The result show that the CNOT6 and CNOT6L undergo a two-state transition during thermal unfolding. The mean melting temperature (T_m) for CNOT6 (53.0 ± 0.6^0C) and CNOT6L (52.9 ± 0.1^0C) was observed to be comparable as similar thermal denaturation profiles were displayed (Figure 5.2). Also, the denaturation profile of the Ccr4 enzymes were comparable across all enzyme concentrations used (2, 5 and 10 μM) used. However, to ensure maximal efficiency and also to obtain more accurate results, 10 μM CNOT6 and CNOT6L enzyme concentrations were chosen for further use in the evaluations.

Next, TSA was used to ascertain if Mg^{2+} ions stabilise the CNOT6 and CNOT6L proteins. Reports have shown that divalent metal ions are crucial for the catalysis and stability of many enzymes (Beese and Steitz, 1991, He et al., 2011, Sissi and Palumbo, 2009). The Ccr4 (CNOT6 and CNOT6L) and CNOT7 are known to be dependent on Mg^{2+} ions for catalysis based on biochemical and structural analysis as EEP-type and DEDD type proteins respectively (Wu et al., 2005, Goldstrohm and Wickens, 2008). To this end, the denaturation profiles of the CNOT6 and CNOT6L were compared in the presence and absence of Mg^{2+} ions. A fixed amount of CNOT6 and CNOT6L (10 μM) proteins

mixed with SYPRO Orange dye respectively was incubated in the presence of (2 mM) Mg^{2+} ions. Thereafter, SYPRO Orange fluorescence was measured. The results show that Mg^{2+} ions increased thermal stability of the CNOT6 and CNOT6L compared to controls which did not contain Mg^{2+} ions (Figure 5.3). Based on the results, CNOT6L was chosen for further use in evaluation of thermal shift assays for small molecule characterisation because it displayed a greater ΔT_m value as compared to CNOT6.

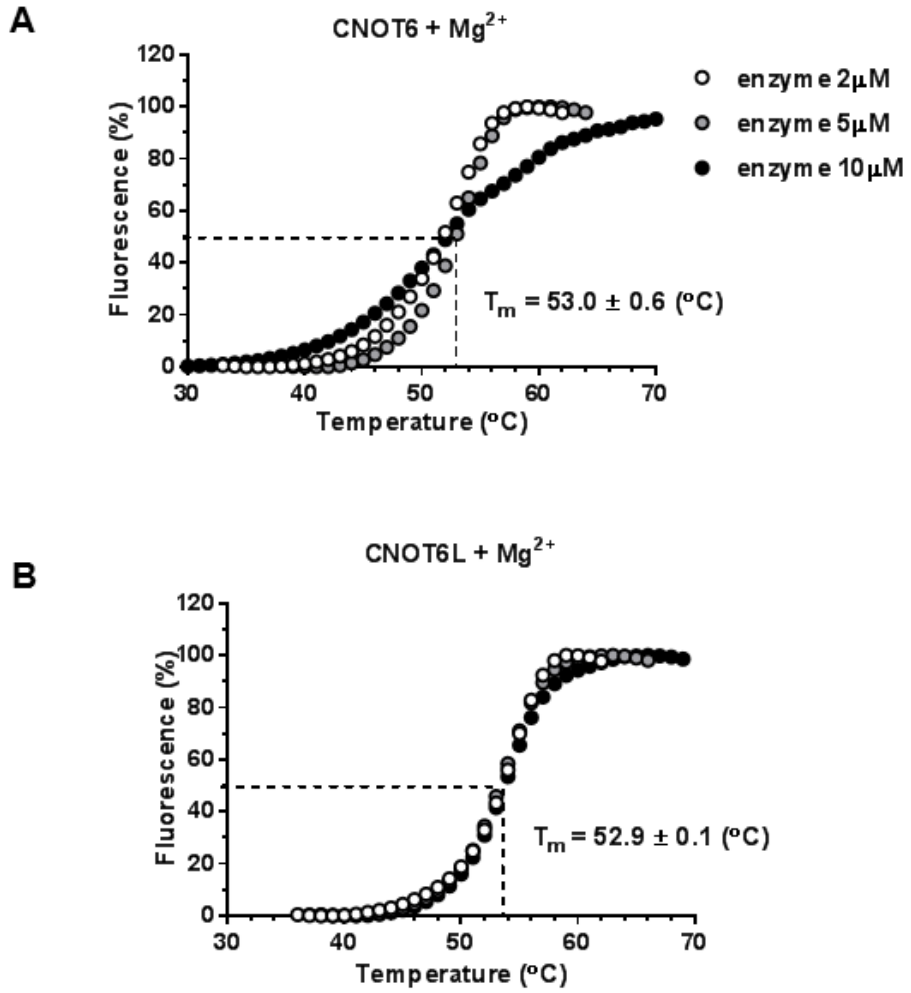

Figure 5.2. Determination of optimal enzyme concentration. (A) CNOT6 and (B) CNOT6L undergo a two-state transition denaturation profile. Proteins (2, 5 and 10 µM) were incubated in the presence of $MgCl_2$ (2 mM) and thermal denaturation was measured by SYPRO Orange fluorescence (λ_{ex}= 492 nm, λ_{em} = 610 nm). The experiment was done in triplicates. Error bars represent the standard error of mean (n=3).

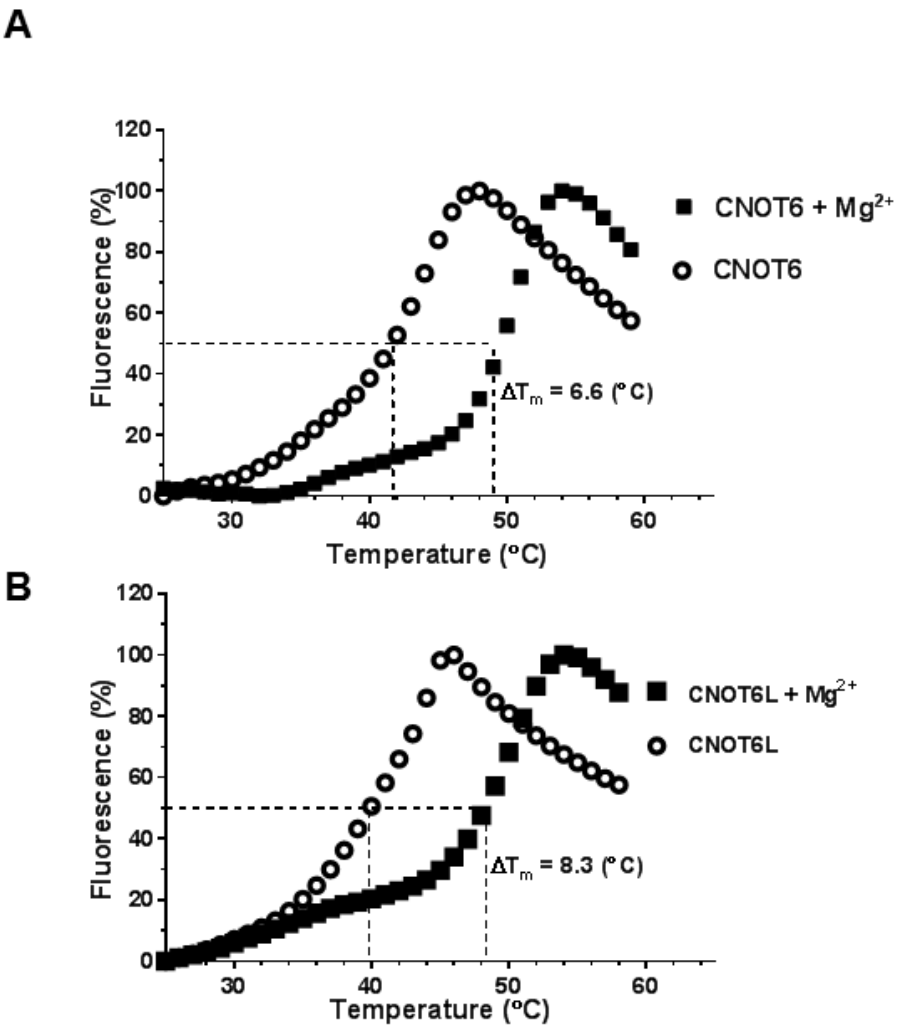

Figure 5.3. Mg^{2+} ions enhance the thermal stability of Ccr4 enzymes
(A-B) The CNOT6 and CNOT6L undergo a transition denaturation. CNOT6 and CNOT6L enzymes (10 μM) were incubated in the presence of $MgCl_2$ (2 mM) and thermal denaturation was measured by SYPRO Orange fluorescence (λ_{ex} = 492 nm, λ_{em} = 610 nm). Control reactions did not contain $MgCl_2$. The thermal shift (ΔT_m) was determined by the difference in transition midpoint in the presence of magnesium ions compared to control. Experiments were done in triplicates and melting temperature (T_m) values are represented as mean of an independent experiment. Error bars represent the standard error of mean (n=3).

5.2.2 Characterisation of ligands binding to Ccr4 protein by thermal shift assay

Next, thermal shift assays were used to evaluate ligand binding to CNOT6L. Previous studies to understand the structure of CNOT6L catalytic domain identified 3-pyridinium-1-ylpropane-1-sulfonate in the active site of the nuclease domain of the enzyme (Figure 5.4A) (Wang et al., 2010a, Winkler and Balacco, 2013)Previous studies to understand the structure of CNOT6L catalytic domain identified 3-pyridinium-1-ylpropane-1-sulfonate in the active site of the nuclease domain of the enzyme (Figure 5.4A) (Wang et al., 2010a, Winkler and Balacco, 2013). To obtain further insights into the potential of 3-pyridinium-1-ylpropane-1-sulfonate as an inhibitor of CNOT6L, this compound and four compounds with similarity to 3-pyridinium-1-ylpropane-1-sulfonate were obtained and used for further analysis. To obtain further insights into the potential of 3-pyridinium-1-ylpropane-1-sulfonate as an inhibitor of CNOT6L, this compound and four compounds with similarity to 3-pyridinium-1-ylpropane-1-sulfonate were obtained and used for further analysis. (Figure 5.4B)

A fixed concentration of CNOT6L (10 μM) was incubated with increasing concentrations (0.5, 1, 2, 5 and 10 μM) of compounds A, B, C, D and E in the presence of Mg^{2+} ions. Reactions which did not contain the compounds were used as a reference. The compound/enzyme mixture containing SYPRO Orange dye was subjected to thermal shift assay and SYPRO Orange fluorescence was measured. Thermal shifts were determined by the difference between mid-transition points in reaction that contained the compound relative to that which had no compounds. The results (Figure 5.5) show thermal shifts $<1^0$C in all the data analysed using compounds A, B, C, D and E. This indicates that the 3-pyridinium-1-ylpropane-1-sulfonate (compound A) and the other compounds did not stabilise the CNOT6L enzyme and are therefore not identified as possible inhibitors of the Ccr4.CNOT6L enzyme. Activity assays to evaluate inhibitory activity of compounds A-E by substrate fluorescence based assay (data not shown) showed no inhibition. Further investigation using AMP-based assay would be

necessary to ascertain if these compounds may be potential inhibitors of the Ccr4.

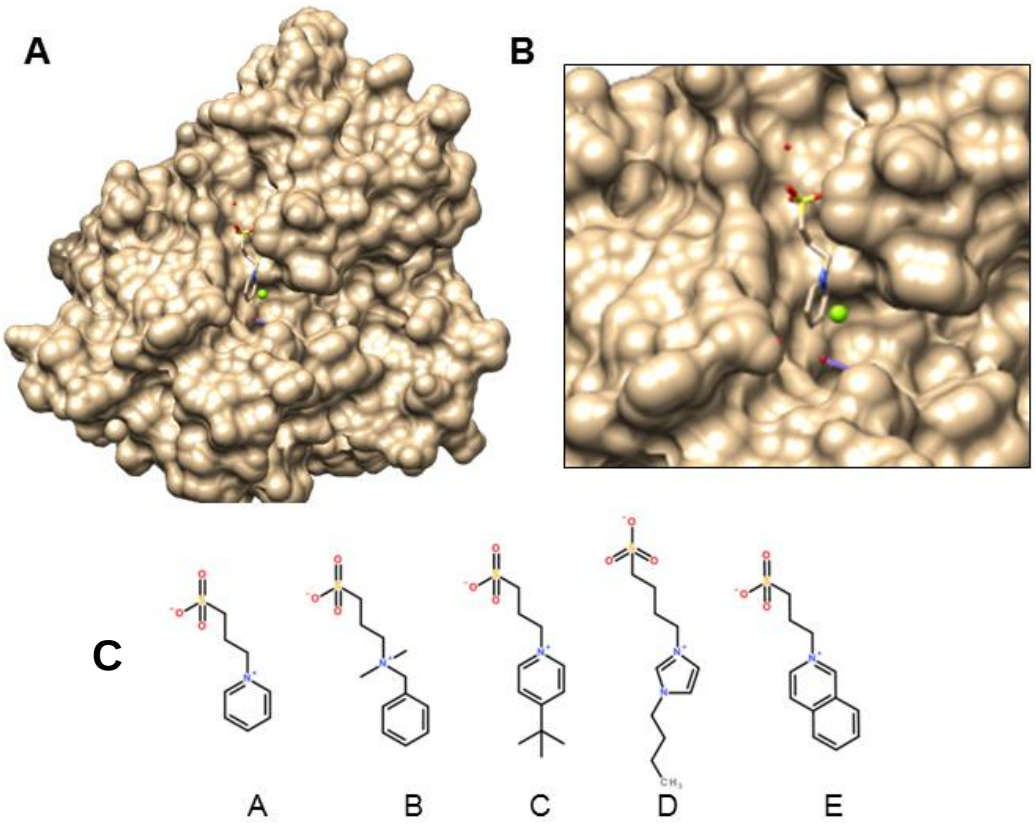

Figure 5.4. Application of thermal shift assay for the analysis of small molecule binding to CNOT6L. (A) Binding of 3-pyridinium-1-ylpropane-1-sulfonate to the catalytic domain of CNOT6L. (PDB accession number 3NGQ). (B) Enlarged view showing 3-pyridinium-1-ylpropane-1-sulfonate at CNOT6L active site. Structures were visualised using UCSF Chimera package (http://www.cgi.ucsf.edu/chimera;Pettersen et al, 2004). (C) Structures of 3-pyridinium-1-ylpropane-1-sulfonate and selected compounds with high similarity.

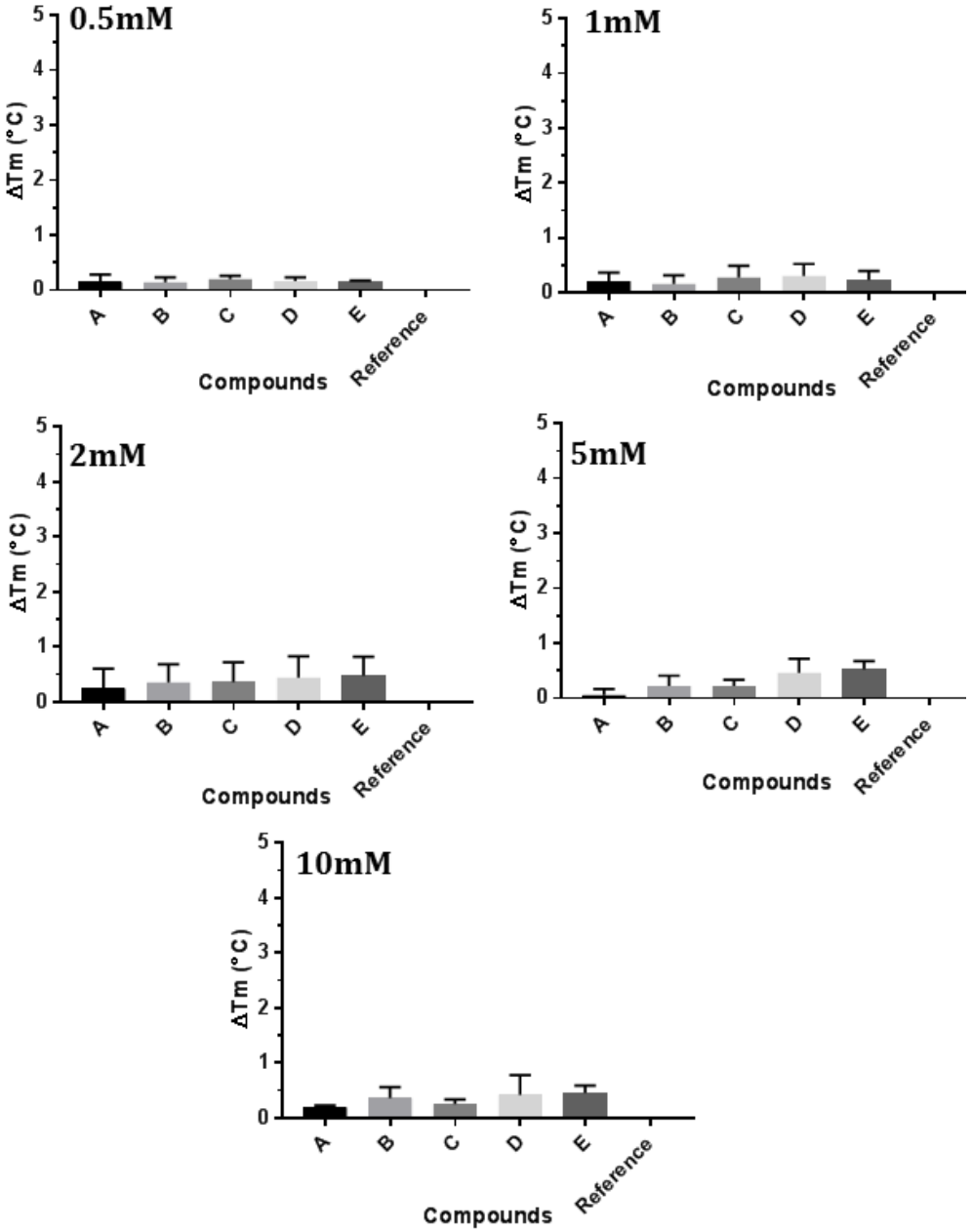

Figure 5.5. The effect of Compound A-E on thermal stability of CNOT6L. **The effect of Compound A-E on thermal stability of CNOT6L**. Compounds A-E at varying concentrations (0.5, 1, 2, 5 and 10 mM) were incubated with CNOT6L (10 μM) enzyme in the presence of $MgCl_2$ (2 mM) thermal denaturation was measured by SYPRO Orange fluorescence (λ_{ex}= 492 nm, λ_{em} = 610 nm). Compounds A-E at varying concentrations (0.5, 1, 2, 5 and 10 mM) were incubated with CNOT6L (10 μM) enzyme in the presence of $MgCl_2$ (2 mM) thermal denaturation was measured by SYPRO Orange fluorescence (λ_{ex}= 492 nm, λ_{em} = 610 nm). Control reactions (reference) did not contain the compounds. The resultant ΔT_m values was determined by the difference in melting temperature. Error bars indicate the standard error of the mean (n=3).

5.3 Identification of CNOT7 inhibitor binding modes by thermal shift assays

5.3.1 Characterisation of CNOT7 and small-molecule inhibitors by thermal shift assay

A series of *N*-substituted purine-2-6-diones (Jadhav et al., 2015) *N*-hydroxyimide compounds identified as CNOT7 inhibitors were readily available. Their inhibitory concentrations (IC_{50}) had been determined by a substrate fluorescence-based assay method (Maryati et al., 2014). Reports show that compounds which contain an *N*-hydroxy urea structure inhibited Flap Endonuclease-1 (FEN1) by coordination of the metal ions needed for FEN1 activity (Tumey et al., 2005). A similar mode of co-ordination of Mg^{2+} at the active site of CNOT7 was proposed for these *N*-substituted purine-2-6-diones compounds. The CNOT7 is a known Mg^{2+} dependent deadenylases and based on biochemical and structural analysis, it has been proposed that these enzymes use the two metal ions for their catalytic activity (Goldstrohm and Wickens, 2008). Based on these hypothesis, thermal shift assay was used to screen the binding mode of these *N*-substituted purine-2-6-diones CNOT7 inhibitors (Table 5.1).

First, assay conditions were optimised to ascertain the best CNOT7 enzyme concentration for use in the thermal shift assays. In addition, the influence of Mg^{2+} ions on CNOT7 enzyme stability was determined. To this end, a range of CNOT7 concentration (1, 2, 5 and 10 μM) was mixed with SYPRO Orange and $MgCl_2$ (2 mM). Control reactions did not contain MgCl2. The CNOT7 enzyme/SYPRO Orange mixture was subjected to a temperature range (25-95^0C) and SYPRO Orange fluorescence was measured. As shown in Figure 5.6, CNOT7 displayed a two-state transition: showing native proteins and thermally denatured and unfolded proteins. The thermal denaturation profile of CNOT7 was comparable for all concentrations used with the optimal ΔT_m observed at enzyme concentration of 5 μM. However, 2 μM enzyme concentration was chosen for further use as it gave a good thermal shift while using a slightly lower amount of enzyme. Together, the findings demonstrate that thermal shift assay is tenable for use with the CNOT7 enzyme. Conditions

to perform thermal unfolding experiments using potential small molecule inhibitors were established.

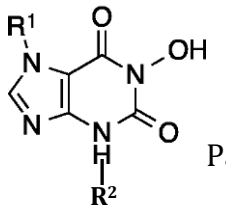

Parent compound

Cmpd	R^1	R^2	IC_{50} (μM)[a]
007	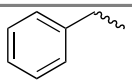	H	10.4 ± 0.4
066	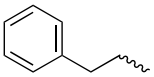	H	1.5 ± 0.3
071	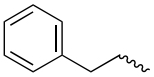	$CH_2(CH_2)_2Ph$	2.1 ± 0.3
086	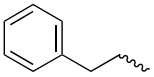	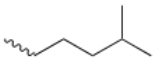	1.7 ± 0.4
108	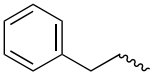	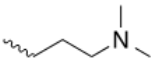	0.59 ± 0.11

Table 5.1 **Known CNOT7 inhibitors** IC_{50} values were determined in previous publication using a fluorescence-based biochemical assay. Jadhav et al. (2015) Discovery, synthesis and biochemical profiling of purine-2, 6-dione derivatives as inhibitors of the human poly (A)-selective ribonuclease Caf1. [a] Data is shown as Mean ± S.E.M (n=3).

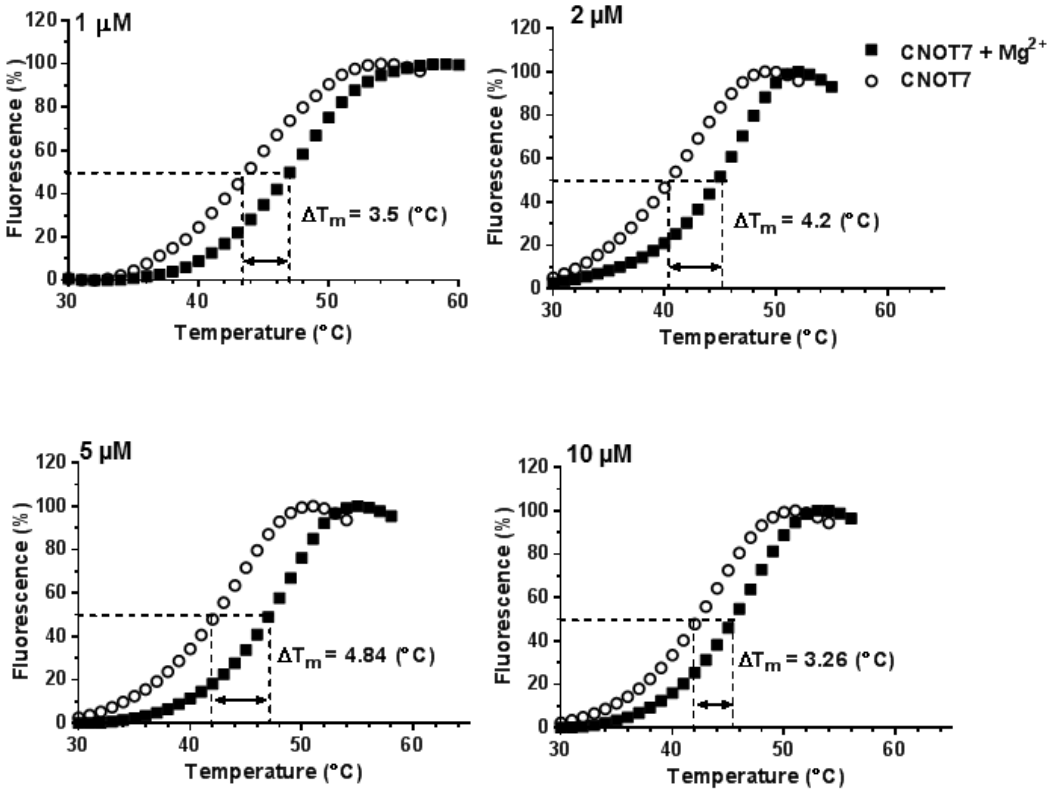

Figure 5.6. Magnesium ions stabilise CNOT7 deadenylase. A Graphical representation of CNOT7 denaturation profile. CNOT7 enzyme (1, 2, 5 and 10 µM) was incubated in the presence of $MgCl_2$ (2 mM). Thermal denaturation was measured by SYPRO Orange fluorescence (λ_{ex}= 492 nm, λ_{em} = 610 nm). Control reactions did not contain $MgCl_2$. The thermal shift (ΔT_m) was determined by the difference in transition midpoint in the presence and absence of $MgCl_2$.

5.3.2 Determination of CNOT7-inhibitor interactions by thermal shift assays

Having established conditions to perform thermal unfolding experiments using CNOT7, the assay was used to characterise the binding of five *N*-hydroxyimide compounds (007, 108, 066, 071, and 086) which are CNOT7 inhibitors. First, thermal shifts were determined in the presence and absence of $MgCl_2$ (2 mM). Typically, CNOT7 (2 μM) was mixed with SYPRO Orange dye in the presence $MgCl_2$ (2 mM). Compounds 007, 066, 071, 086 and 108 (100 μM) were added respectively into assigned wells and subjected to thermal denaturation. Thermal shifts were measured by SYPRO Orange fluorescence (λ_{ex}= 492 nm, λ_{em}= 610 nm). The thermal shift (ΔT_m) was determined by the difference in transition midpoint in the presence and absence of the inhibitory compounds.

The findings as shown in Figure 5.7 demonstrate that in the absence of $MgCl_2$, there was no difference between the thermal denaturation profile of CNOT7 enzyme in samples that contained only the enzyme and those which contained both the enzyme and compounds. However, in the presence of $MgCl_2$ there was a remarkable shift in the curve to the right indicating an increase in thermal stability of the enzyme in the wells that contained the compounds compared to the wells that contained only CNOT7 enzyme. In addition, TSA could discriminate between the different compounds (Figure 5.8). Each compound appeared to stabilise the CNOT7 enzymes to varying degree in the presence of $MgCl_2$ when compared to controls. Compound 108 was observed to stabilise CNOT7 by a thermal shift of 4.7^0C and compound 007 displayed the lowest thermal shift of 2.2^0C. These results indicate that the compounds require the presence of Mg^{2+} ions in the active site of CNOT7 for binding. It also confirms the hypothesis by Jadhav et al, on the binding mode of the inhibitors to CNOT7. In addition, the finding validates the use of thermal shift assays for characterising different small molecular inhibitors of deadenylase enzymes in a multiwell format.

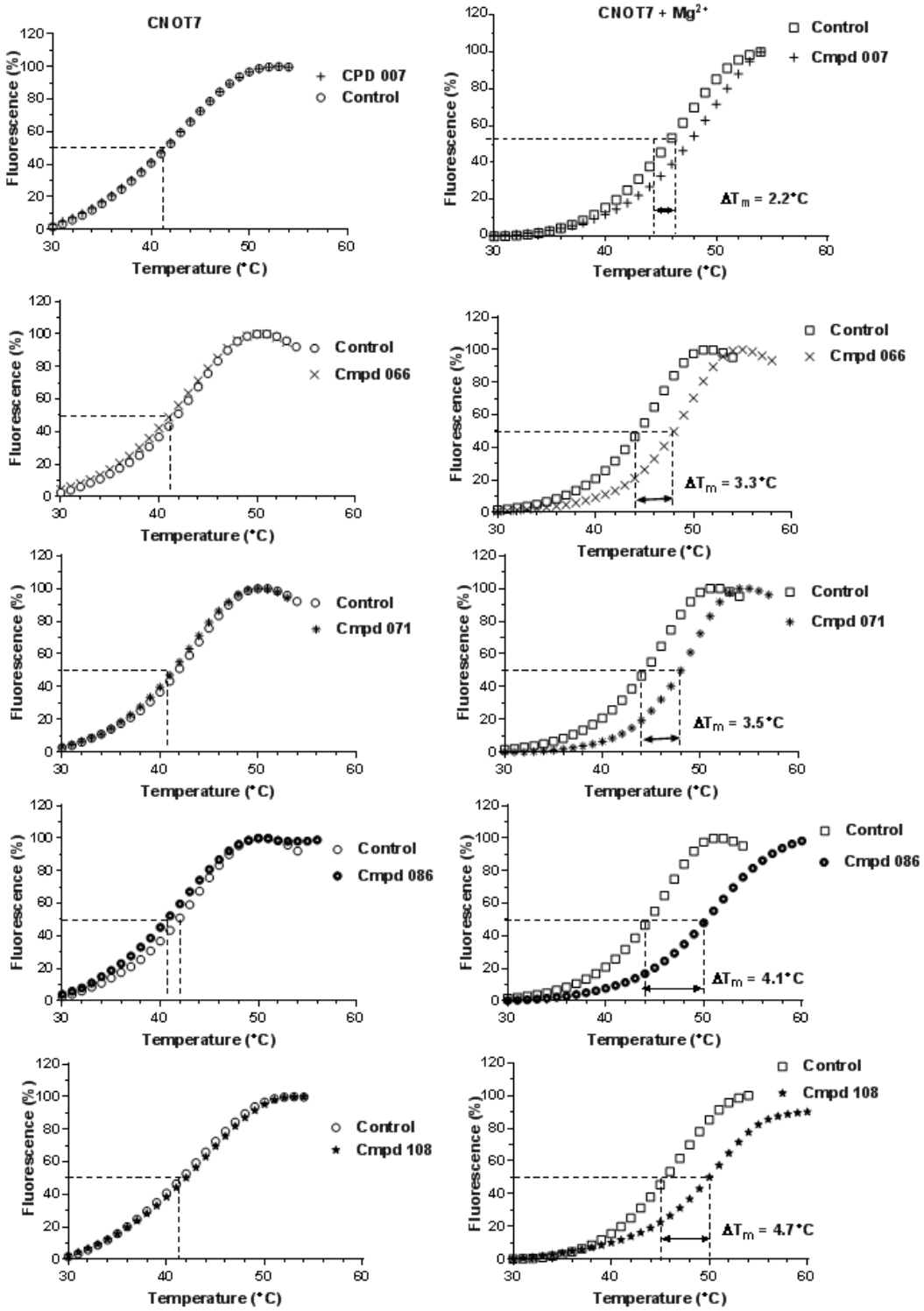

Figure 5.7. Thermal shift assay indicates the binding of CNOT7 inhibitors requires Mg^{2+} ions. CNOT7 (2 µM) was incubated in the presence and absence of $MgCl_2$ (2 mM). 100 µM of compounds 007, 066, 071, 086 and 108 were added. Thermal denaturation was measured by SYPRO Orange fluorescence (λ_{ex}= 492 nm, λ_{em}= 610 nm). The thermal shift (ΔT_m) was determined by the difference in transition midpoint in the presence and absence of the compounds (n=3).

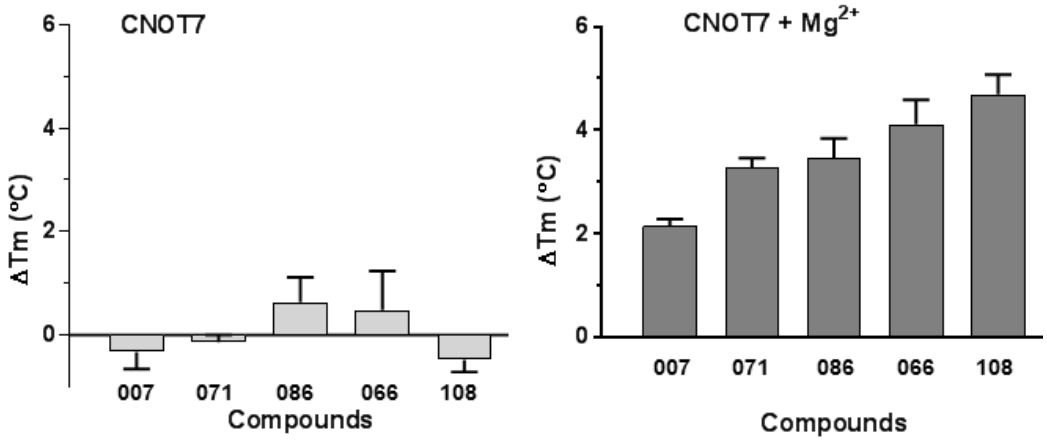

Figure 5.8. The effect of purine-2-6-dione compounds on the denaturation profile of CNOT7. Thermal shift values of CNOT7 inhibitors. Enzymes (2 μM) were incubated in the presence of $MgCl_2$ (2 mM). Compounds 007, 071, 086, 066 and 108 (100 μM) were added respectively and thermal denaturation was measured by SYPRO Orange fluorescence (λ_{ex}= 492 nm, λ_{em} = 610 nm). Control reactions did not contain $MgCl_2$. The thermal shift (ΔT_m) was determined by the difference in transition midpoint in the presence and absence of magnesium ions. Error bars represent standard error of mean (n=3).

5.3.3 Thermal shifts of CNOT7 inhibitors correlates with potency

To evaluate the use of thermal shift assays for determination of the potency of inhibitory compounds, a correlation analysis was determined. The IC_{50} of the N-hydroxyimide compounds previously determined (Jadhav et al., 2015) was compared with thermal shifts observed (Table 5.1). Interestingly, a linear relationship between thermal shifts and the potency of the compounds was observed (r^2 = 0.94.) As shown in Figure 5.9, more potent compounds displayed higher ΔT_m values. This result indicates the reproducibility, and validity of the thermal shift assay for characterising small molecules. In both fluorescence-based assay and thermal shift assay formats, the rank order of the CNOT7 inhibitory compounds was preserved.

was compared with thermal shifts observed (Table 5.1). Interestingly, a linear relationship between thermal shifts and the potency of the compounds was observed (r^2 = 0.94.) As shown in Figure 5.9, more potent compounds displayed higher ΔT_m values. This result indicates the reproducibility, and validity of the thermal shift assay for characterising small molecules. In both fluorescence-based assay and thermal shift assay formats, the rank order of the CNOT7 inhibitory compounds was preserved.

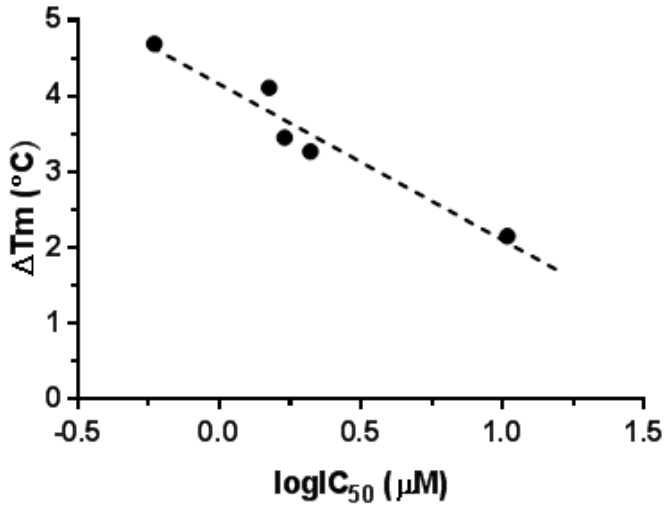

Figure 5.9. Comparison of thermal shifts and IC50 data from fluorescence-based assay. Graphical representation of the correlation analysis between thermal shifts and potency of CNOT7 inhibitors**.**

5.4 Discussion

In this section, the use of thermal shift assay for characterisation of small molecular inhibitors of CNOT7 and Ccr4 deadenylases is reported. The biophysical properties of protein targets have been used in recent times for identification of small molecular weight ligands that bind to them (Lo et al., 2004, Niesen et al., 2007, Pantoliano et al., 2001, Poklar et al., 1997). Thermal shift assays which operates on the principle that small molecule binding alters protein thermal stability and has been demonstrated to be useful in multi-well plate format was evaluated (Pantoliano et al., 2001, Senisterra et al., 2012, Vedadi et al., 2006). Having successfully characterised deadenylase enzymes and inhibitor compound using the fluorescence-based assay (chapter 3 and 4) and AMP product-based assay (Chapter 4), the main aim of this chapter was to determine an alternative, quick and robust method for characterisation of small molecular inhibitors. Not all proteins exhibit distinct phase transition or are amenable to thermal shift assays, therefore TSA was first evaluated for use in characterising CNOT6, CNOT6L and CNOT7. Interestingly, the results demonstrate that the assay is tractable for use with the purified CNOT6, CNOT6L and CNOT7 deadenylases. Next, optimal assay conditions that stabilise the enzymes were identified. It was observed that Mg^{2+} ions enhanced the thermal stability of all the enzymes. This is in agreement with the report that binding of small molecules, co-factors, metal ions, result in conformational changes on proteins and provide enhanced stability (Schellman, 1975, Pace and McGrath, 1980, Brandts and Lin, 1990, Pantoliano et al., 2001). Also, it confirms the report that the CNOT7 and Ccr4 deadenylases require two Mg^{2+} ions for catalytic activity (Petit et al., 2012b).

Once assay conditions were established thermal shift assays was used for characterisation of inhibitors compounds. The 3-pyridinium-1-ylpropane-1-sulfonate and its analogues used to screen for binding to CNOT6L did not confer thermal stability on the enzyme even at high compound concentrations., The 3-pyridinium-1-ylpropane-1-sulfonate and its analogues used to screen for binding to CNOT6L did not confer thermal stability on the enzyme even at high compound concentrations., It maybe that the compound

was weakly bound to the enzyme and the thermal shift assay could not detect the association between the enzyme and compounds tested.

In contrast, thermal shift assay was useful for the analysis of the *N*-hydroxyimide inhibitors of CNOT7. The requirement of Mg^{2+} ions for binding at the active site was determined. This is in agreement with the reports (Jadhav et al., 2015) that compounds which contain an *N*-hydroxy urea structure inhibited nucleases by coordination of the metal ions needed for activity (Tumey et al., 2005). It was quite intriguing to know that thermal shifts of the *N*-hydroxyimide compounds observed had a linear correlation with the potencies previously determined by a fluorescence-based deadenylase assay (Jadhav et al., 2015). The ranking of the compounds in their order of potency was preserved.

Together, the findings of this study demonstrate that thermal shift assays can be used for high throughput screening of small molecules in a multiwell plate format especially as a first line to narrow hits and save time. It is simple, robust, and quick. It is also a cheap way of analysing compounds as it requires little quantity of reagents for the assays. It is semi-quantitative and is useful for identifying binding mode of small molecules. However, it was noted that the assay may not be highly sensitive when compared with other biochemical assays (such as the fluorescence-based or AMP-product based assay) as it may give some false negatives. This may explain why there were no thermal shifts observed with the 3-pyridinium-1-ylpropane-1-sulfonate compounds used to determine stability of CNOT6 and CNOT6L. It would be of interest to further ascertain and also optimise the effect of these compounds on the Ccr4 proteins using AMP-based and fluorescence-based assays. Other disadvantages of the TSAs include the fact that interactions between dye and compounds may mask stabilization and give rise to artifacts. Also, coloured compounds may interfere with detection of fluorescence. Unlike the fluorescence-based assay which has stable signals and can be measured hours and days after the addition of the probe, thermal shifts can only be measured during protein unfolding.

Chapter 6

Analysis of BTG2 variants: effect on interactions with CNOT7 and CNOT8 subunit of the Ccr4-Not complex module

Chapter 6. Analysis of BTG2 variants: effect on interactions with CNOT7 and CNOT8 subunit of the Ccr4-Not complex module

6.1 Introduction

The BTG/TOB family are an antiproliferative gene family that consists of six members in human. Amongst the members of the BTG/TOB family, BTG1 and BTG2, TOB1 and TOB2 are highly similar. BTG3 and BTG4 are more distantly associated. Structurally, the conserved domain of BTG N-terminus consists of two regions: a box A and box B regions which are highly conserved compared to the other domains (Figure 6.1) (Boiko et al., 2006b, Horiuchi et al., 2009, Zhang et al., 2011, Winkler, 2010). Box A and box B regions mediate interaction with Caf1 catalytic subunit of the Ccr4-Not deadenylase complex (Duriez et al., 2004, Yang et al., 2008, Horiuchi et al., 2009, Aslam et al., 2009, Winkler, 2010) (Figure 6.1). The conserved BTG domain is shown to mediate protein-protein interactions as illustrated by the crystal structure of TOB1 in complex with CNOT7 (Horiuchi et al., 2009). In addition, the two highly similar TOB proteins contain a (Poly (A)-binding-protein-interacting Motif 2) PAM2 motif in their C-terminal regions which mediate interactions with poly (A)-binding protein PAPBCI (Ezzeddine et al., 2007, Mauxion et al., 2008, Funakoshi et al., 2007) Unlike the other family members, BTG1 and BTG2 have an additional box C region and reports show that they bind to the poly (A)-binding protein PABPC1 via the box C region (Yang et al., 2008, Stupfler et al., 2016). This interaction is sufficient to stimulate Caf1 deadenylase activity in vitro in the absence of other CCR4–NOT complex subunits. The interaction also plays a vital role in the control of cell proliferation and translational repression.

Recent studies have suggested that BTG2, the first identified family member is expressed in different body organs and tissues such as the spleen, thymus, lungs and stomach. It is also closely associated with tumour suppressor genes including p53, p73 and RB (Melamed et al., 2002, Zhang et al., 2011, Boiko et

al., 2006a, Rouault et al., 1996). BTG2 is also proposed to be a potential biomarker for cancer prognosis in patients (Wagener et al., 2013, Zhang et al., 2013, Takahashi et al., 2011, Choi and Lim, 2013). BTG2 expression is shown to be frequently at low levels in human cancers (Kawakubo et al., 2004, Struckmann et al., 2004) which correlates with tumour prognosis (Kawakubo et al., 2006). Although there is evidence supporting a role of BTG2 in cancer, the underlying mechanism or the BTG2 function in cancers is not fully understood. Recently, mutations in the BTG1 and BTG2 were identified in about 10-15% of Non-Hodgkin's lymphoma (NHL) cases (Morin et al., 2011, Lohr et al., 2012, Love et al., 2012), which suggested a direct involvement of BTG1 and BTG2 in lymphoma. In this chapter, the main focus was to determine the ability of lymphoma associated BTG2 variants to interact with the Caf1 subunit of the Ccr4-Not complex and to understand the effect on mRNA degradation using a reporter mRNA. To this end, 47 BTG2 variants were obtained from the Catalogue of Somatic Mutations in Cancer (COSMIC) database (Forbes et al., 2008). Each variant was tested using Sorting intolerant from tolerant (SIFT) and SuSPect analysis software to predict potential effect of these variants in protein function (Ng and Henikoff, 2003, Yates et al., 2014). Thereafter, the mutations were prioritized based on a comparison of SIFT and SuSPect score correlation and also by recent publications where lymphoma associated BTG2 variants were identified (Morin et al., 2011, Lohr et al., 2012). By using a yeast two-hybrid and RNA tethering assays, the ability of the BTG2 protein variants to interact with Caf1 catalytic subunits and the functional effect of BTG2 mutated proteins on mRNA degradation was assessed. The findings of this study identified three BTG2 variants that potentially regulate mRNA abundance in lymphoma via interaction with the Ccr4-Not deadenylase.

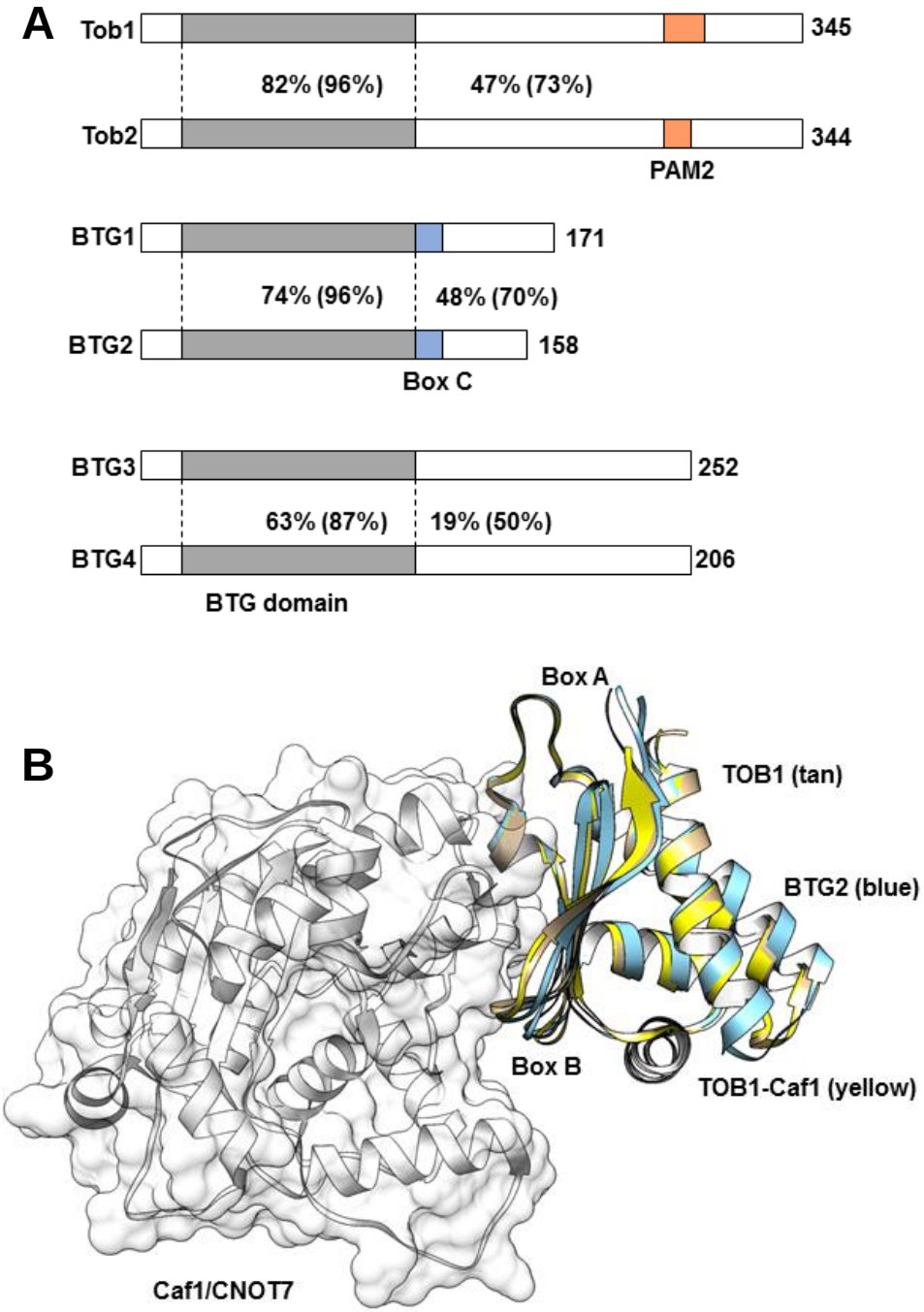

Figure 6.1. The structure of BTG2 is highly conserved to that of the N-terminal domain of TOB1. (A) The domain organisation of BTG/TOB family members and their percentage conservation is represented on this diagram based on amino acid sequence. BTG domain is shown in grey, the conserved PAM motif (orange) and box C motif is in blue. The size of amino acids and percentage of identical amino acids is also represented. (B) Indicated is a superimposition of the structures of BTG2 (blue; PDB accession number 3DJU), the N-terminal BTG domain of TOB1 (tan; PDB accession number 2Z15), and the N-terminal domain of TOB1 in complex with CNOT7 (TOB1, yellow; CNOT7, white; PDB accession number 2D5R). The Box A and Box B regions are indicated. Structure analysis was carried out using UCSF Chimera.

6.2 Computational analysis of lymphoma-associated BTG2 variants

To identify lymphoma associated variants, bioinformatic analysis was performed and 47 variants were obtained from the Catalogue of Somatic Mutations in Cancer (COSMIC) database using versions 65 and 81. Thereafter, each variant was tested using Sorting intolerant from tolerant (SIFT) prediction tool, a program that predicts whether an amino acid substitution affects protein function to help prioritize substitutions for further study and SuSPect (Disease-*Su*sceptibility-based single amino acids variants Phenotype *Pre*d*ict*ion) analysis software which predicts how likely single amino acid variants are associated with disease (Yates et al., 2014, Ng and Henikoff, 2003) (Table 6.1). Using the SIFT tool, amino acid substitutions submitted are based on calculation of the median conservation to obtain a score. The score is the normalized probability that the amino acid change is tolerated. SIFT predicts substitutions with scores less than 0.05 as deleterious. Suspect scores on the other hand ranges between 0 to 100, with a recommended cutoff of 50 for discriminating between neutral and disease-associated Single amino acid variants. This analysis was used to assess and predict the effect of the BTG2 variants on gene function such as the requirement for the interaction with CNOT7) and CNOT8).. Furthermore, a correlation analysis was performed to compare the SIFT and SuSPect prediction scores (Figure 6.2). As shown, the SIFT tool identified a greater number of variants that interfere with protein function as compared to the SuSPect tool. Based on the representation in Figure 6.2 eight (8) BTG2 variants were chosen for further investigation. The selected variants were a reasonable representation of identified variants in NHL cases (Lohr et al., 2012, Morin et al., 2011), During the course of this work, further variants were identified with some having higher SuSPect scores.

To further analyse the potential role of the BTG2 variants in mediating the CNOT7 and CNOT8 interaction, bioinformatic structural analysis was performed. The crystal structure of BTG domain of TOB1 in complex with CNOT7 (PDB accession number 2D5R) was aligned with crystal structure of BTG2 (PBD accession number 3DJU) and was used to map the eight BTG2

variants. The variants G117D, L100P, I70M and H49Y appeared to protrude towards the interface with the CNOT7 deadenylase. By contrast, S39N and L46F were located away from the interaction surface with CNOT7. S158I and S159C are not present in the BTG2 structure available. The structural alignments and analysis was performed using the UCSF Chimera molecular modelling package (http://www.cgi.ucsf.edu/chimera;Pettersen et al, 2004) (Figure 6.3).

BTG2 mutation	Prediction	SIFT score	SuSPect score
M1I	Affect protein function	0.00	6
G4V	Tolerated	0.16	16
K5T	Tolerated	0.36	14
T7S	Tolerated	0.63	15
A14V	Tolerated	0.26	27
S21C	Tolerated	0.16	11
R25K	Tolerated	0.22	16
G28D	Affect protein function	0.04	13
E32D	Tolerated	0.39	11
Q33H	Tolerated	0.18	15
R34S	Affect protein function	0.05	28
L35F	Affect protein function	0.01	63
K36R	Tolerated	0.29	15
L42V	Affect protein function	0.01	69
E44D	Tolerated	0.23	12
A45E	Tolerated	0.08	33
A45T	Tolerated	0.29	29
E48Q	Affect protein function	0.03	14
H53D	Damaging	0.002	76
G64S	Damaging	0.004	73
C67Y	Affect protein function	0.00	92
R69C	Affect protein function	0.00	68
I70V	Affect protein function	0.02	29
D75N	Affect protein function	0.00	65
S158S	**Affect protein function**	**0.00**	**0**
G86E	Affect protein function	0.01	11
Q91R	Tolerated	0.55	16
S158C	**Affect protein function**	**0.00**	**6**
P106L	Affect protein function	0.00	83
E108Q	Affect protein function	0.01	47

V109M	Affect protein function	0.00	82
Y111C	Affect protein function	0.00	20
T136I	Affect protein function	0.01	27
L100P	**Affect protein function**	**0.00**	**54**
P148R	Affect protein function	0.00	44
V153M	Tolerated	0.115	11
G117D	**Affect protein function**	**0.01**	**38**
R145Q	Tolerated	0.07	11
S147G	Affect protein function	0.02	42
C132S	Tolerated	0.76	9
A126S	Tolerated	0.99	8
S83R	Tolerated	0.54	14
S39N	**Tolerated**	**0.35**	**43**
L46F	**Affect protein function**	**0.01**	**43**
H49Y	**Affect protein function**	**0.01**	**43**
I70M	**Affect protein function**	**0.04**	**40**
G4R	Tolerated	0.57	15

Table 6.1 SIFT and SuSPect analysis of Human BTG2 mutations

Footnote: SIFT http://blocks.fhcrc.org/sift/SIFT.html, SuSPect http://www.sbg.bio.ic.ac.uk/suspect. The variants selected for further analysis are highlighted in bold.

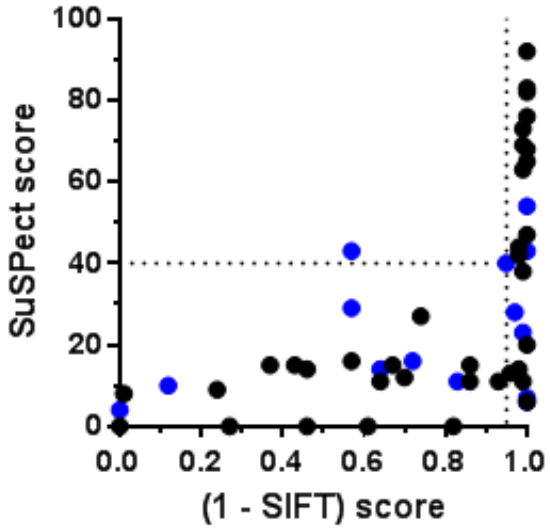

Figure 6.2. Relation between predictions of BTG2 function using SIFT and SuSPect analysis. Indicated are the relation between a modified SIFT score (1-SIFT score; 0-1) and SuSPect score (0-100). Variants selected based on the COSMIC database version 67 are indicated in blue; those present in COSMIC v.81 are indicated in black. Dotted lines indicate the cut-off scores for SIFT (0.95) and SuSPect (40).

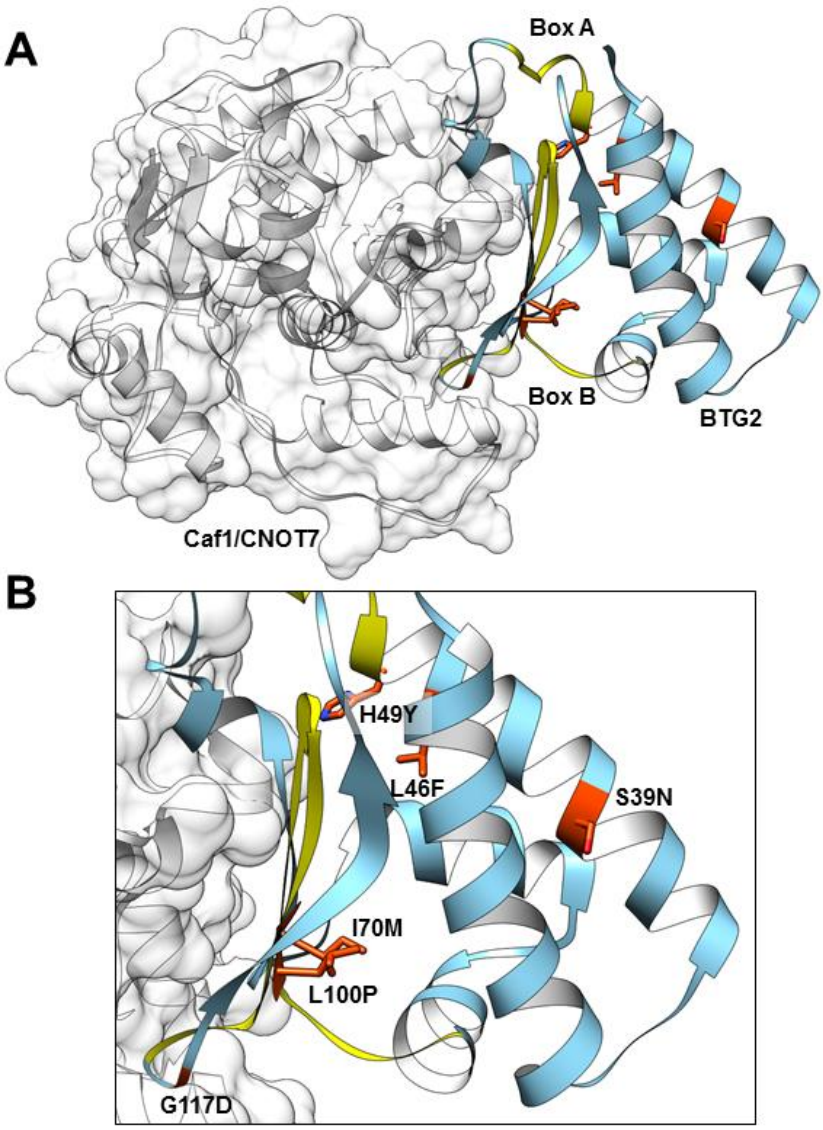

Figure 6.3. Structural view of Caf1-BTG2 complex. (A) A model of the CNOT7-BTG2 complex was prepared by superimposing the structure of BTG2 (blue) (PDB 3DJU) onto the structure of the BTG domain of TOB in complex with Caf1 (white) (PDB 2D5R). Highlighted are the highly conserved Box A and Box B regions (yellow) and a selection of lymphoma-associated BTG2 variants (orange red). (B) Detailed view of lymphoma-associated variant residues in BTG2. Structural analysis was carried out using UCSF Chimera.

6.3 Identification of BTG2 variants required for the interaction with CNOT7 and CNOT8 through the yeast-two hybrid system.

To assess the role of the identified BTG2 mutations in interaction with CNOT7, CNOT8, yeast two-hybrid analysis was performed. For yeast-two hybrid experiment, fusion proteins are constructed with either the activation domains (AD) or binding domains (BD). When there is an interaction between proteins, the AD and BD are brought together on the β-Galactosidase promoter thereby inducing transcription of the reporter gene. However, when there are no interactions, β-Galactosidase transcription is not initiated (Figure 6.4).

The plasmids containing BTG2 variants being investigated and plasmids containing CNOT7, CNOT8 cDNAs were readily available in our laboratory (Figure 6.5 A and B). Typically, the plasmid containing BTG2 cDNAs had the Gal4 DNA binding domain (BD) fused to the N-terminus of BTG2 and a HA epitope tag at the 5' end. The HA tag was introduced to enable western blot detection of BTG2 (Figure 6.5A). The yeast expression vector pAD-Gal4-2.1 containing CNOT7 and CNOT8 cDNA was also used (Figure 6.5B). The pAD-Gal4-2.1 which fused the Gal4 transcriptional activation domain (AD) to the N-terminus of CNOT7 or CNOT8 was detected by using antibodies against the Gal4 AD domain.

The appropriate vectors containing BTG2 variants and CNOT7 or CNOT8 cDNAs were transformed into yeast strain YRG2 and grown on media lacking leucine and tryptophan to select transformants. Thereafter, three colonies were subjected to the β-galactosidase assay for each BTG2 variant.

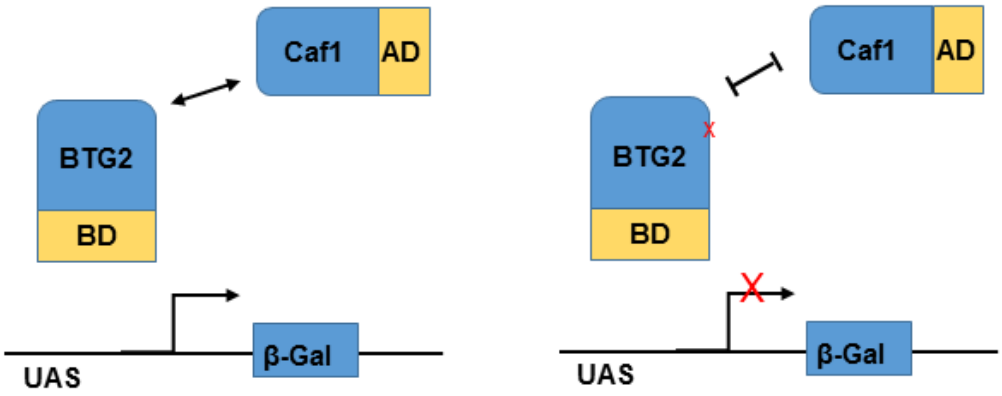

Figure 6.4. Yeast-two hybrid systems for analysis of BTG2/Caf1 interactions. Schematic showing yeast-two hybrid experiment. AD, Gal4 activation domains, BD, Gal4 DNA binding domain. When there is an interaction between CNOT7 and BTG2 the Gal4 BD and Gal4 AD are brought to close proximity on the β-Galactosidase promoter thereby inducing transcription of the reporter gene (left panel). When there are no interactions, β-Galactosidase transcription is not initiated (right panel).

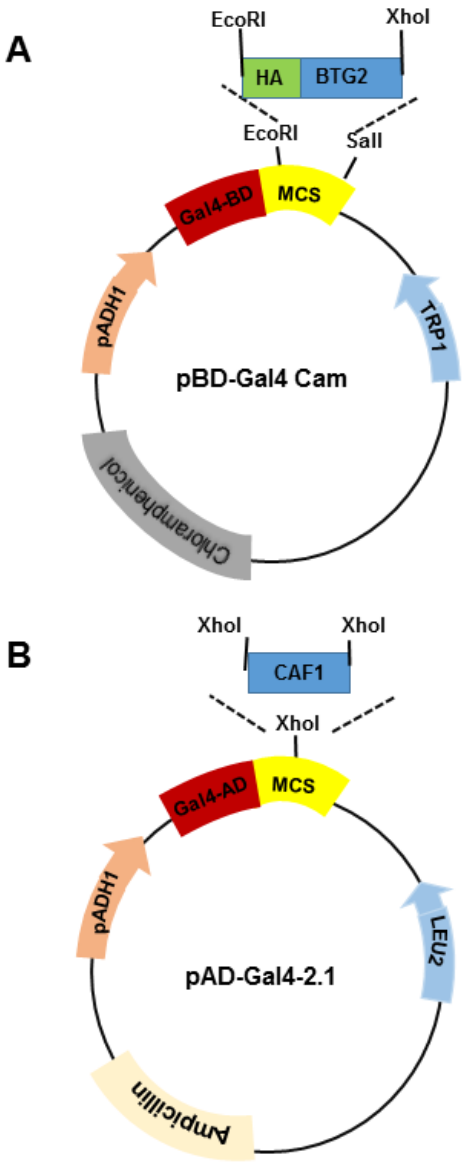

Figure 6.5. Plasmids used for yeast-two-hybrid analysis
(A) Gal4 DNA binding domain hybrids containing BTG2 cDNA and HA epitope tag to facilitate western blotting detection. (B) Gal4 activation domain hybrid. Expression vector pAD-Gal4-2.1 containing CNOT7 or CNOT8 cDNAs.

First, yeast-two hybrid analysis of the BTG2 variants and CNOT7 interaction was performed. Typically, transformation of the yeast with pAD-Gal4 and pBD-Gal4-HA confirmed the absence of background β-galactosidase activity. Transformation of pAD-Gal4 and pBD-Gal4-HA-BTG showed that the fusion to the BTG2 DNA binding domain was alone not capable of inducing β-galactosidase expression. Upon an interaction between BTG2 fused to the Gal4 DNA binding domain and CNOT7 fused to the Gal4 transcriptional activation domain, β-galactosidase expression was induced (Figure 6.6A). Of the eight BTG2 variants compared to BTG2 wild type protein (positive control), S39N, H49Y and S158I, retained the ability to interact with CNOT7 and stimulate β-galactosidase expression by >90% of wild type levels. There was a partial reduction (near 50%) in β-galactosidase expression observed with L46F and I70M BTG2 variants compared to wild type controls. The remaining L100P G117D and S158C BTG2 variants, did not induce β-galactosidase expression as judged by a < 50% reduction in β-gal activity and therefore were incapable of interacting with CNOT7 (Figure 6.6A). To confirm the expression of CNOT7 and the various BTG2 variants, proteins were extracted from yeast-cultures used in the β-Galactosidase assay and subjected to western blot analysis (Figure 6.6B).

Yeast two-hybrid analysis was also used to investigate the interaction between CNOT8 and the eight BTG2 variants. As expected the interaction between Gal4 BD-BTG2 and Gal4 AD-CNOT8 induced β-galactosidase expression (Figure 6.7A). Three of the eight BTG2 variants, S39N, H49Y and S158I retained the ability to interact with CNOT8 and stimulate β-galactosidase expression as observed with CNOT7 interaction results. Similar to the BTG2-CNOT7 interactions, there was a partial reduction in β-galactosidase expression observed with L46F and I70M BTG2 variants (near 50%). In addition, S158C displayed a partial reduction in β-galactosidase activity compared to wildtype positive control. The remaining three BTG2 variants L100P and G117D did not induce β-galactosidase expression and therefore were incapable of interacting with CNOT8 (Figure 6.7A). Thereafter, the expression of CNOT8 and the various BTG2 variants was confirmed by western blotting. Proteins were extracted from yeast cultures used in the β-

galactosidase assay (Figure 6.7B). Together, the findings of the yeast two hybrid experiments confirm the SIFT and SuSPect prediction for the L100P and G117D variants as essential for interaction with Caf1 deadenylase. The results also correlate with predictions based on structural alignment of Caf1-BTG2 complex where G117D and L100P variants appeared to protrude towards Caf1. S39N and L46F variants are located away from the Caf1 which may explain why they seem not to be necessary for interaction with Caf1 based on the yeast-two hybrid findings. However, I70M which appears to be in proximity to Caf1 was not found to be essential for interaction.

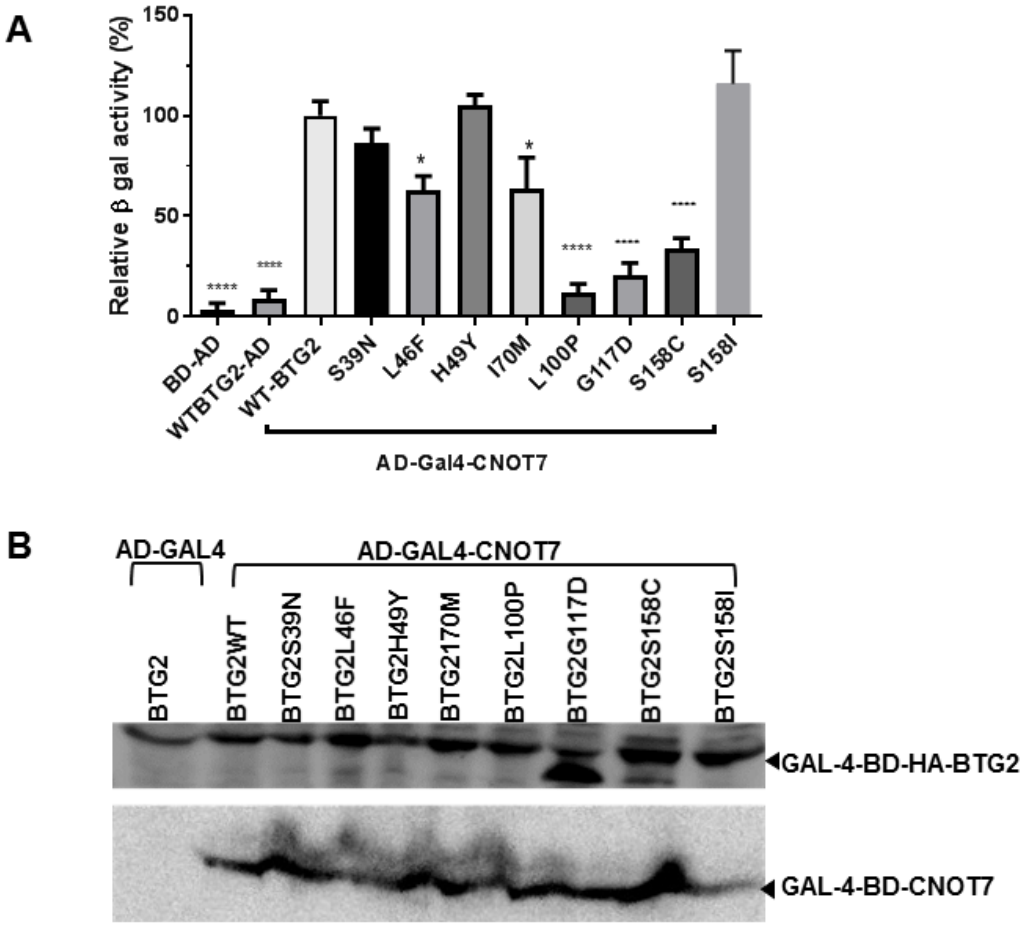

Figure 6.6. Yeast-two hybrid analysis of BTG2/CNOT7 interactions
(A) YRG2 yeast cells were transformed with the indicated vectors; pAD-Gal4 or pAD-Gal4-CNOT7 and pBD-Gal4-HA or pBD-Gal4-HA-BTG2. β-galactosidase activity was normalised using total protein concentration. Three independent experiments were done. Error bars represent the standard error of the mean (n=3). (B) Western blot analysis showing expression of Gal4-BD-HA-BTG2 and Gal4-AD-CNOT7. Anti-HA antibodies were used to detect Gal4-BD-HA-BTG2 and anti-Gal4-AD antibodies was used to detect Gal4-AD-CNOT7.

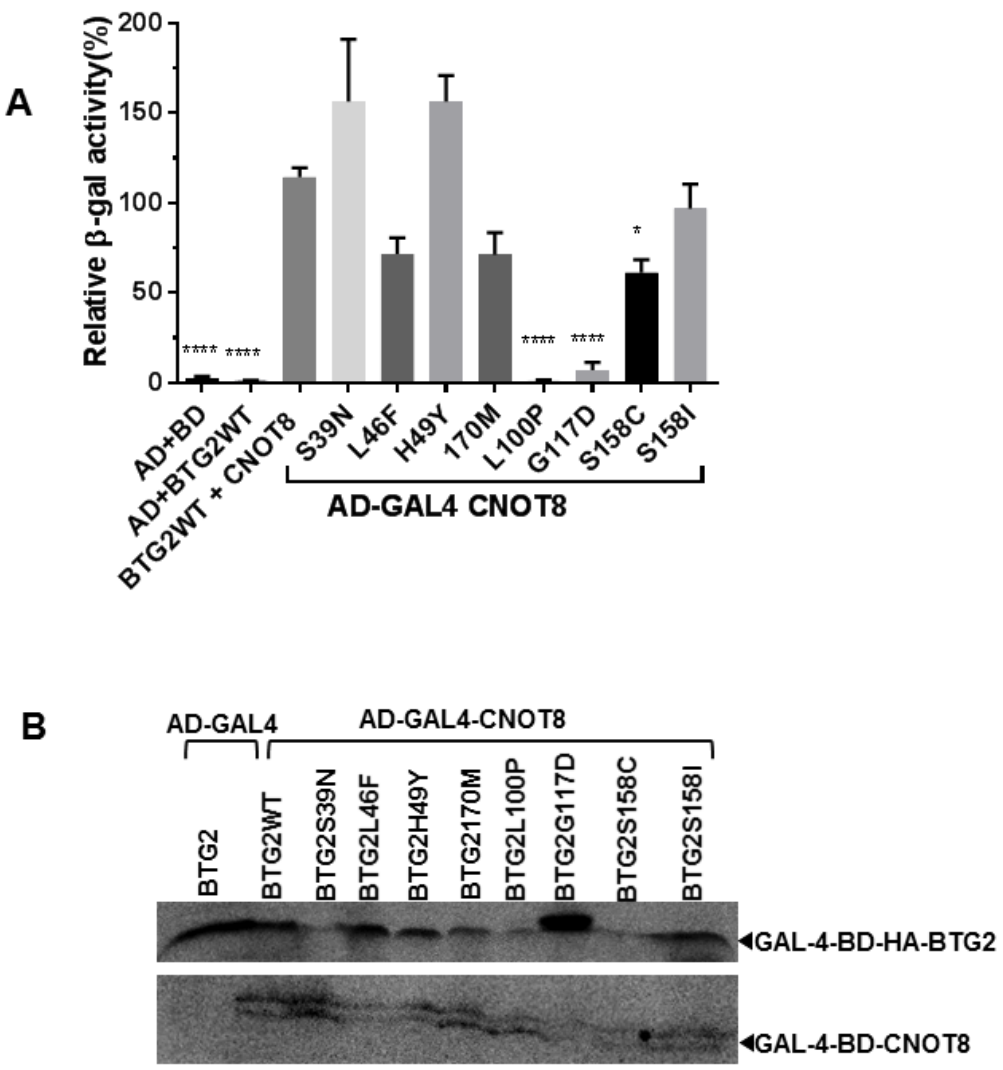

Figure 6.7. Yeast-two hybrid analysis of BTG2/CNOT8 interactions
(A) YRG2 yeast cells were transformed with the indicated vectors; pAD-Gal4 or pAD-Gal4-CNOT8 and pBD-Gal4-HA or pBD-Gal4-HA-BTG2. β-galactosidase activity was normalised against total protein. Experiment was carried out in triplicate. Error bars represent the standard error of the mean (n=3). (B) Western blot analysis showing expression of Gal4-BD-HA-BTG2 and Gal4-AD-CNOT8. Anti-HA antibodies were used to detect Gal4-BD-HA-BTG2 and anti-Gal4-AD antibodies was used to detect Gal4-AD-CNOT8.

6.4 Confirmation of amino acid required for BTG2 function by RNA tethering assay.

To confirm the effect of the BTG2 variants on protein function, RNA tethering assays were performed. The tethering assays were carried out to determine if the presence of BTG2 variants on the 3'UTR of a reporter mRNA alters its activity and to determine if any changes are dependent on the CNOT7 or CNOT8 interactions (Coller and Wickens, 2007). Typically, the reporter pRL-5box B motif present in the 3'UTR of a renilla luciferase mRNA and plasmids expressing fusions of the λN peptide containing wildtype BTG2 and the respective variant plasmids were co-transfected into cell lines. After transfection, total protein was extracted and luciferase activity was determined. The luciferase construct was used to determine changes that occur on mRNA when BTG2 is bound to it (Figure 6.8). To this end, the pCIλN RNA tethering vector containing BTG2 variants fused to N-terminal λN epitope was first constructed (Figure 6.9). The pCIλN plasmid containing the wildtype BTG2 was readily available and used for gene amplification. To generate plasmids the BTG2 cDNA was PCR amplified using primers with an HA tag sequence and XhoI at the 5' end. (Table 2.10) to include an XhoI restriction site and the HA tag 5' of the AUG start codon and an XhoI restriction site 3' of the termination codon. The HA tag was to facilitate western blotting detection. This PCR fragment was subcloned into plasmid pCIλN via the XhoI restriction site (Figure 6.9). All plasmid sequences were confirmed by DNA sequencing.

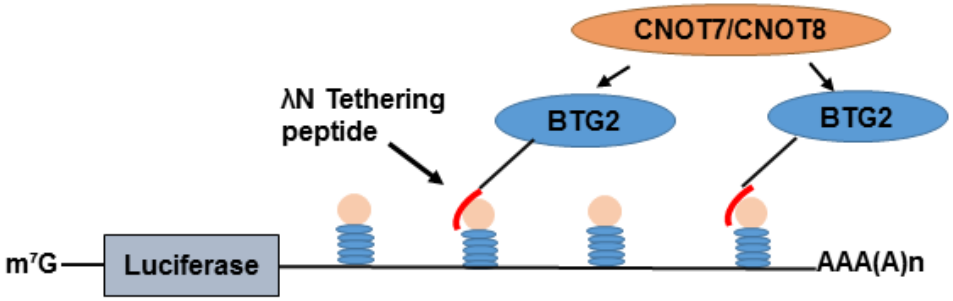

Figure 6.8. RNA tethering assay. (A) Schematic showing RNA tethering assay. The reporter pRL-5box B motif present in the 3'UTR of a renilla luciferase mRNA and plasmids expressing fusions of the λN peptide containing wildtype BTG2 and the respective variant plasmids are co-transfected into cell lines. The luciferase construct is used to determine changes that occur on mRNA when BTG2 is bound to it. Upon expression of protein BTG2 fused to the λN tethering peptide, it will bind to the 5 Box B motifs located in the renillia luciferase mRNA 3' UTR. BTG2 can then recruit other factors such as Caf1 to the mRNA 3' UTR that may affect mRNA translation or stability.

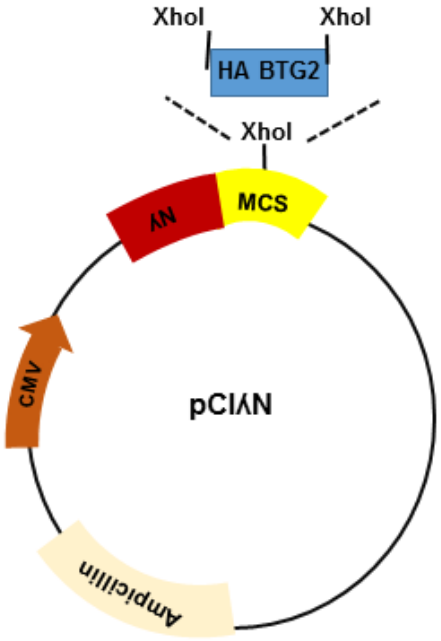

Figure 6.9. Plasmid λN-HA-BTG2 expression vector used for RNA tethering assay. The HA-BTG2 cDNA was generated by PCR amplification to include the XhoI restriction site 5' of the ATG start codon and 3' of the stop codon. This PCR fragment was subcloned into plasmid pCIλN.

After successful construction of the plasmids, RNA tethering assays were carried out. HEK293 cells were co-transfected with the reporter pRL-5boxB and plasmids expressing fusions of the λN peptide with HA-BTG2, HA-BTG2S39N, HA-BTG2L46F, HA-BTG2H49Y, HA-BTG2I70M, HA-BTG2L100P, HA-BTG2G117D, HA-BTG2S158C, and HA-BTG2S158I respectively. After transfection, total protein was extracted and luciferase activity was determined (Figure 6.10A). For controls, tethering of the empty vector and wildtype BTG2 fused to λN peptide (λN-HA-BTG2) were performed. As shown in Figure 6.10A, tethering of the empty vector did not cause a reduction of luciferase activity. However, tethering of wildtype BTG2 to the luciferase mRNA caused a reduction in luciferase activity. Compared to the controls, it was observed that tethering of five BTG2 variants (λN–HA-BTG2 S39N, λN–HA-BTG2 L46F, λN–HA-BTG2 I70M, λN–HA-BTG2 S158C and λN–HA-BTG2 S158I) to the luciferase mRNA caused a >80% reduction in luciferase activity. By contrast, expression of λN–HA-BTG2 H49Y, λN–HA-BTG2 L100P, and λN–HA-BTG2 G117D to the luciferase mRNA did not cause a reduction in luciferase activity. A near 60% increase in activity was observed compared to the empty vector control. (Figure 6.10B). Western blot analysis was then carried out to confirm the expression of BTG2 wildtype and variant proteins (Figure 6.10B). Clearly, there was the expression of the BTG2 variant proteins compared with the wildtype. However, the H49Y variant was not expressed. Together the results indicate that the reduction in luciferase protein activity was dependent on the interactions between BTG2 and the deadenylases CNOT7 and CNOT8 compared with the controls. Finally, a relation between SIFT and SuSPect predictions with observed effect on BTG2 function was determined (Figure 6.11). The finding confirms the SIFT, SuSPect predictions are valid to some degree based on the observed effects that also aligns with structural analysis predictions especially for L100P and G117D variants which protrude towards CNOT7 on the Caf1/BTG2 complex. The findings also consolidate the results obtained from yeast-two hybrid analysis where L100P and G117D were found essential for interaction with the Caf1 deadenylases. These BTG2 variants may potentially regulate mRNA abundance in lymphoma via interaction with the Ccr4-Not deadenylase.

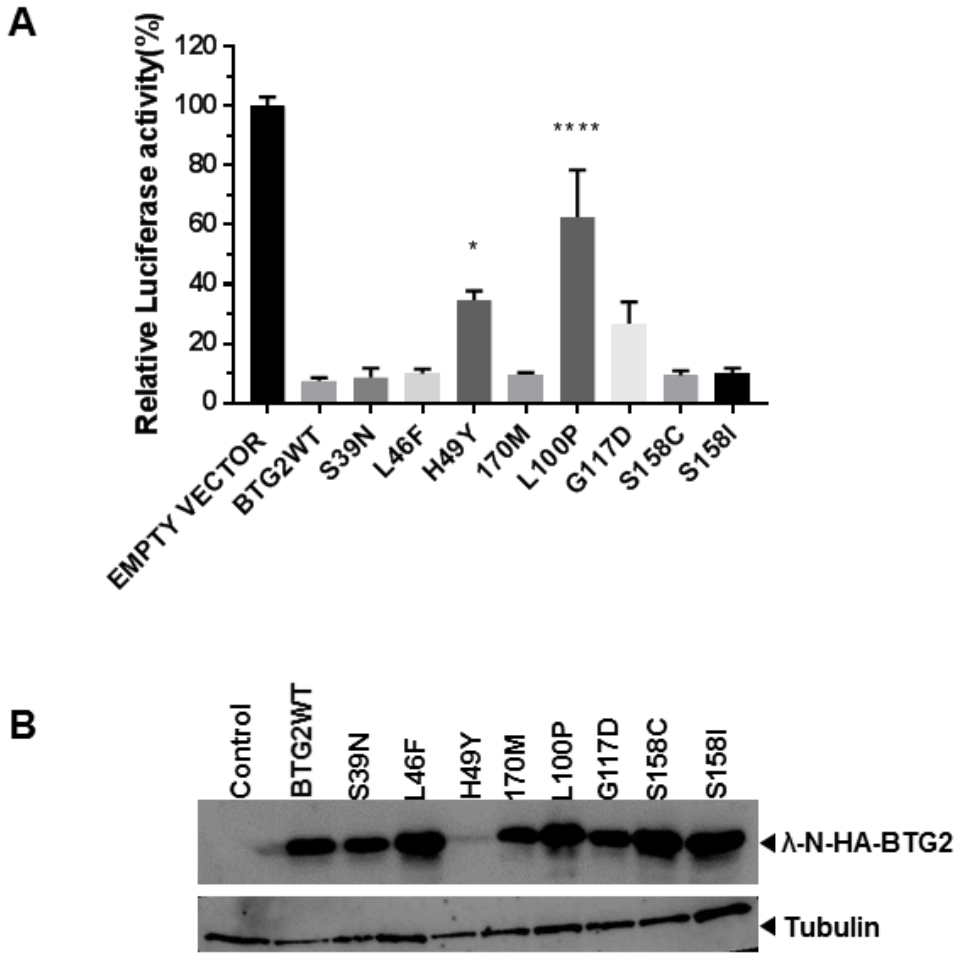

Figure 6.10. RNA tethering identifies BTG2 interactions required to reduce reporter activity. (A) Graph showing decreased reporter activity of BTG2 mutations; S39N, L46F, 170M, S18C, S158I but not H49Y, L100P, and G117D upon RNA tethering. HEK293 cells were transfected with empty vector or PCIλN containing the indicated BTG2 cDNA and the luciferase reporter plasmid pRL-5Boxb. Luciferase activity was measured 24hours after transfection. (B) Western blot analysis showing expression of λN-BTG wild type and mutations (S39N, L46F, H49Y, 170M, L100P, G117D, S158C, and S158I). λN fusion proteins were detected using anti-HA antibody. Tubulin was used as a loading control.

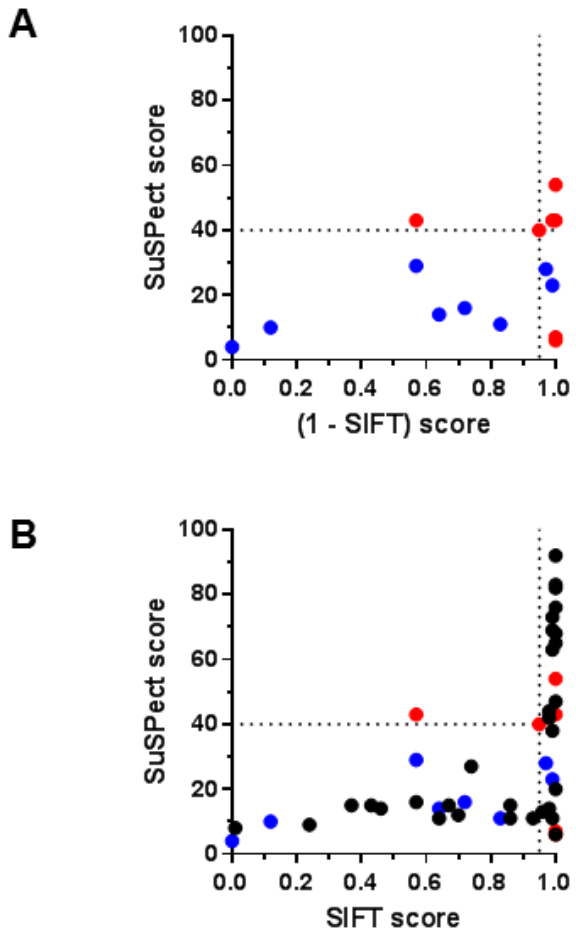

Figure 6.11. Relation between prediction and observed effect on BTG2 function. (A) Indicated are the relation between a modified SIFT score (1-SIFT score; 0-1), SuSPect score (0-100) and observed effect on BTG2 function. Variants with retained ability to interact with CNOT7 are indicated in blue; those unable to interact with CNOT7 are indicated in red. Dotted lines indicate the cut-off score for SIFT (0.95) and SuSPect (40). (B) Same as in (A). Also indicated are variants present in COSMIC v.81.

6.5 Discussion

The work described in this chapter identified three BTG2 variants that potentially regulate mRNA abundance in lymphoma by interaction with the CNOT7 and CNOT8 deadenylase. These BTG2 variants include G117D, L100P and H49Y. The BTG2 protein is a known antiproliferative protein that interacts with Caf1 catalytic subunit of the Ccr4-Not complex (Yang et al., 2008, Duriez et al., 2004). Recent studies identified BTG2 variants in Non-Hodgkin's lymphoma cases and suggested a direct involvement of these variants in the disease. Studies also show that amino acid substitution within the conserved BTG2 domains are capable of disrupting their interaction with Caf1 catalytic subunit (Horiuchi et al., 2009, Yang et al., 2008). The purpose of this section was to investigate the interactions between these BTG2 variants and the Caf1 catalytic subunit and also determine the effect of these mutations on mRNA abundance.

First, BTG2 variants frequently found in cancers were analysed using SIFT and SuSPect analysis tools to predict the scores and effect of the BTG2 variants on protein function. A correlation analysis was carried out to compare the SIFT and SuSPect prediction scores. BTG2 variants which had high SuSPect scores and low SIFT scores were predicted to be damaging. Based on the correlation analysis and recent findings where BTG2 variants were identified in lymphoma cases (Morin et al., 2011, Lohr et al., 2012). Eight BTG2 variants were chosen for further analysis and validation. Thereafter, a structural analysis of the amino acids being queried was performed to determine the location and potential requirement for interaction with Caf1. G117D, L100P and I70M were identified as potentially required for interaction with Caf1 while the others were protruded away from the Caf1 surface. Next, yeast two-hybrid analysis was used to determine interactions between the eight BTG2 variants-CNOT7 and CNOT8 respectively. The findings of the study show that of the eight BTG2 variants S39N, H49Y and S158I, retained the ability to interact with both CNOT7 and CNOT8 compared to the wildtype protein. Although there was a partial reduction in β-galactosidase expression observed with L46F, I70M and S158C BTG2 variants,

L100P and G117D BTG2 variants, did not induce β-galactosidase expression suggesting they were incapable of interacting with CNOT7 and CNOT8. Thus, implying that the amino acid residues, L100P and G117D are therefore essential for interaction with Caf1 as suggested by the BTG2/Caf1 structural alignment shown in Figure 6.3.

To further confirm the effect of these BTG2 variants on protein function using a mammalian cell system, RNA tethering assays were carried out. Intriguingly, the BTG2 variants L100P and G117D previously identified by yeast-two hybrid assays (as required for interactions with Caf1 catalytic subunit), did not cause a reduction in luciferase activity compared to controls. It was noted that H49Y which was not identified by yeast-two hybrid system as essential for interaction with Caf1 showed an increase in luciferase activity. Western blot analysis to ascertain protein expression showed that while it was difficult to express the H49Y variant, there was relative expression of the other seven BTG2 variants. Together, the findings of the study confirm SIFT and SuSPect analysis of the three variants (H49Y, L100P and G117D) which were predicted to be damaging and affect protein function. A relation analysis of the predictions of SIFT and SuSPect with the observed effects shows the validity of the predictions. Yeast two hybrid analysis identified and confirmed L100P, G117D but not H49Y as essential for interaction with Caf1. These variants also demonstrated increased luciferase activity which may be attributed to a lack of interaction between the BTG2 variants and CNOT7 and CNOT8 using a mammalian cell system. This finding suggests there may be some other factors involved in the interaction between BTG2 and the caf1 deadenylases. It is worthy of note that H49Y, L100P and G117D BTG2 variants may potentially regulate mRNA abundance in lymphoma via interaction with the Ccr4-Not deadenylase. Future work will involve further investigation into how Poly (A) binding proteins (PABPC1) may affect the association with the identified BTG2 variants. Future work will also involve further investigations into other variants predicted to be damaging to protein function. It will also involve a determination of how these variants affect other cell functions such as cell proliferation, amongst others.

Chapter 7

Concluding Remarks and Future Work

Chapter 7 Concluding remarks and Future work

The long-term goal of this work is to characterize the Ccr4-Not deadenylase as a potential drug target with a focus on the catalytic subunits of the Ccr4-Not complex (Ccr4 and Caf1). To facilitate the discovery, development, and characterisation of small drug-like inhibitors of the Ccr4-Not deadenylase enzymes, a biochemical approach was used. First, the biochemical properties of the highly similar CNOT6 and CNOT6L enzymes were investigated by a fluorescence-based assay method previously described (Maryati et al., 2014) as a starting point of screening for molecular inhibitors. Next, two biochemical assays were evaluated. The use of AMP product detection as a secondary assay to the fluorescence-based assay was evaluated. Furthermore, an alternative, quick and robust method for the characterisation of small molecular inhibitors by thermal shift assays was assessed. In addition, a cell based approach was used to study interactions between BTG2 (a part of the deadenylase module) and CNOT7 and CNOT8 deadenylases. The ability of BTG2 variants found in lymphoma to induce mRNA degradation using a reporter mRNA was also assessed.

7.1 Comparative analysis of the human CNOT6 and CNOT6L deadenylase enzymes

The human Ccr4-Not complex consists of catalytic (Ccr4 and Caf1) and non-catalytic subunits. The catalytic subunits Ccr4 (CNOT6 and CNOT6L) and Caf1 (encoded by the paralogues CNOT7 and CNOT8) are evolutionary conserved (Lau et al., 2009, Winkler and Balacco, 2013, Xu et al., 2014). Despite the high similarity and identity between the CNOT7 and CNOT8 paralogues (76% identical and 88% similar at the amino acid level) which have been well characterised, and the fact that the surface residues around the active site are completely conserved (Horiuchi et al., 2009, Jonstrup et al., 2007, Shirai et al., 2014, Thore et al., 2003, Winkler and Balacco, 2013, Xu et al., 2014), the

enzymatic activities of purified CNOT7 and CNOT8 proteins differ significantly when assessed *in vitro* (Bianchin et al., 2005). By contrast, cell studies show that the paralogues have overlapping roles (Aslam et al., 2009). Similarly, the human CNOT6 and CNOT6L are highly similar (78% identical and 88% similar at the amino acid level) and their surface residues in the active site are totally conserved. Cell studies show the CNOT6 and CNOT6L have largely similar properties (Mittal et al., 2011). However, relatively little is known about their biochemical properties. Given the differences observed with the Caf1 subunits in their characteristics *in vitro* compared to their cellular properties despite their high conservation, the biochemical properties of the CNOT6 and CNOT6L were investigated. To this end, the enzymatic activities of the human CNOT6 and CNOT6L were compared *in vitro* by a fluorescence-based assay method. Three independent approaches indicate that the enzyme activities of CNOT6 as an isolated EEP enzyme is higher than CNOT6L: (i) the analysis of enzyme concentration as a function of time; (ii) the use of denaturing polyacrylamide gel electrophoresis to analyse deadenylation products; and (iii) the determination of the effect of temperature and incubation time on enzyme activity. It was observed that the CNOT6 showed higher activity compared to CNOT6L in all experimental approaches. Based on these findings, the fluorescence-based assay was then adapted for use with a plate-based format, which allows the comparison of many reactions in parallel and may be useful for the screening of compound libraries or libraries of proteins with amino acid substitutions.

7.2 Use of AMP detection as an activity assay for the human Caf1 and Ccr4 deadenylase enzymes

Quantitative biochemical assays are useful for enzyme characterisation as they provide information on their catalytic activity, mechanisms, and structure. *In vitro* deadenylation assays have been used to study the deadenylases over the years. *In vitro* assay methods currently available for studying deadenylases include colorimetric assays (Greiner-Stoeffele et al., 1996, Cheng et al., 2006), gel assays based on substrates labelled with fluorescent or radioactive functional groups (Chen et al., 2002, Viswanathan et al., 2003), and assays based on size exclusion chromatography amongst others (He and Yan, 2012). The drawback of the colorimetric assay methods includes limited sensitivity, and the requirement of high protein and substrate concentrations. The gel based assays are difficult to quantify and quite laborious. The size exclusion chromatography assay method is relatively time consuming, has limited sensitivity, requires large reaction volume and is unsuitable for high throughput screening. Generally, a good assay should be quick, simple to conduct, highly specific, sensitive and relatively inexpensive. Recently, we developed a fluorescence-based quantitative assay suitable for high throughput screening in a multi-well plate format (Maryati et al., 2014). The assay was used for characterisation of deadenylases and also used to screen small-molecule inhibitors (non-nucleoside *N*-hydroxyimide compounds) that selectively inhibit the enzyme activities of CNOT7 (Maryati et al., 2015, Jadhav et al., 2015). During the course of this work, an AMP product-based assay was used for kinetic characterisation of PDE12 and the CNOT6 and CNOT6L enzymes in a multiwell-plate based format (Wood et al., 2015). Previous studies show that AMP is a reaction product of CNOT7 deadenylase (Bianchin et al., 2005). Therefore, the use of the AMP product-based assay as an *in vitro* biochemical assay for characterisation of deadenylase enzymes was evaluated. First,

deadenylase enzymes for the evaluation of the AMP-based assay method were purified to homogeneity: CNOT7, PARN, Ccr4 proteins and the human BTG2-Caf1-Ccr4 trimeric nuclease complex. A method of purifying the trimeric nuclease complex previously described (Maryati et al., 2015) was optimised and we developed an efficient, one-step purification method using Strep tag affinity purification. Next, by comparing the activities of the wild type and inactive CNOT7, CNOT6, CNOT6L, PARN and a trimeric nuclease complex (His•BTG2-CNOT7-Strep•CNOT6L) using the AMP product-based and fluorescence-based assay method, we demonstrated that the AMP product-based assay is a highly sensitive assay suitable for quantitative biochemical analysis of deadenylase enzymes. There was a high signal/background ratio (tenfold), enzymatic activity was detected at low enzyme concentrations, and in small reaction volumes as compared with colorimetry, and chromatography based assays or the recently developed fluorescence-based assay. In addition, the IC_{50} value of a small molecular compound (compound 007) determined by the fluorescence-based assay, and validated by analysing gel products on a denaturing gel was comparable with the values obtained by AMP product-based assay. However, though the AMP based assay is advantageous, there were limitations observed with its use. These include the need to measure signals immediately after the reaction is stopped, time consumption, and cost of reagents. By contrast the fluorescence-based assay displays stable signals up to 24 hours after reaction is stopped, it is quick and relatively cheap. Put together, the findings of this study demonstrate that AMP-product-based assays can be used as a secondary assay that is complementary to the fluorescence-based assay for characterisation of deadenylase enzymes and inhibitors.

7.3 Use of thermal shift assays to characterise small molecule inhibitors of the CNOT7 and CNOT6L deadenylase enzymes

The characterisation of small molecule interactions with their protein targets is a key step in drug discovery and the fragment-based drug design process. Current trends involve the analysis of biophysical properties of the protein targets for identifying small molecular weight ligands that bind to them (Pantoliano et al., 2001, Poklar et al., 1997, Lo et al., 2004, Niesen et al., 2007). It is known that binding of small molecules, co-factors, metal ions, confer changes on proteins and provide enhanced stability (Brandts and Lin, 1990, Schellman, 1975, Pace and McGrath, 1980, Straume and Freire, 1992, Pantoliano et al., 2001). This stabilisation is an indication of interaction between components. Recently, we reported cell permeable, small molecule which selectively inhibit CNOT7 (Jadhav et al., 2015). These *N*-hydroxyimide compounds characterised by a fluorescence-based enzyme assay were hypothesised to inhibit enzyme activity by co-ordination of two divalent metal ions required for catalysis, based on the distance between the Mg^{2+} in the active site of CNOT7 enzyme (Petit et al., 2012a). Having successfully characterised deadenylase enzymes and inhibitor compounds using the fluorescence-based assay (Chapter 3 and 4) and AMP product-based assay (Chapter 4), an alternative, quick and robust method of characterisation of small molecular inhibitors by TSAs was evaluated. First, as a proof of principle, the CNOT7 and CNOT6L deadenylases were used to identify conditions that stabilise the enzymes upon addition of $MgCl_2$ using TSAs. Next, an investigation into binding of compounds to the protein targets (CNOT7 and CNOT6L) and their effect on protein thermal stability was conducted. The findings of this study reveal that thermal shift assays are well suited for quantitative screening and evaluation of the CNOT7 and Ccr4 enzyme targets small molecules in a multiwell plate format especially as a first line to narrow hits and save time. In addition, the thermal shift assay was useful for the analysis of the *N*-hydroxyimide inhibitors of CNOT7. The requirement of Mg^{2+}

ions for binding at the active site was determined. A correlation was found between thermal shifts observed and the potency of compounds as determined by IC_{50} values. It is simple, robust, quick and is a cheap way of analysing compounds as it requires relatively little quantity of reagents for the assays. However, it was noted that the assay may not be highly sensitive when compared with other biochemical assays but is complementary to the fluorescence-based assay for screening.

7.4 Analysis of lymphoma-associated BTG2 variants: effect on deadenylation by the Ccr4-Not nuclease module

Having characterised the CNOT7 deadenylase as a potential drug target and determined biochemical methods of evaluating enzyme activity and screening for molecular inhibition (Chapter 4 and 5), a cell based approach was used to study interactions between lymphoma-associated BTG2 variants and CNOT7 and CNOT8. Studies show that the conserved domain N-terminal BTG domain consists of two regions: box A and box B which are highly conserved (Winkler, 2010, Mao et al., 2015). Box A and Box B regions mediate interaction with Caf1 catalytic subunit of the Ccr4-Not deadenylase complex (Duriez et al., 2004, Yang et al., 2008, Horiuchi et al., 2009, Aslam et al., 2009, Winkler, 2010). BTG2 expression is shown to be frequently at low levels in human cancers (Kawakubo et al., 2004, Struckmann et al., 2004) which correlates with tumour prognosis (Kawakubo et al., 2006). Although there is evidence supporting the association of BTG2 in cancer, the underlying mechanism or the BTG2 function in cancers is not fully understood. Recently, mutations in BTG2 were identified in about 10-15% of Non-Hodgkin's lymphoma (NHL) cases (Morin et al., 2011, Lohr et al., 2012, Love et al., 2012), which suggested a direct involvement of BTG2 in lymphoma. However, the effect of these BTG2 variants on protein function and on deadenylation is not fully understood. In Chapter 6, the ability of BTG2 variants found in lymphoma to interact with the Caf1 subunit of the Ccr4-Not complex and the

effect on mRNA degradation using a reporter mRNA was investigated. To this end, 47 BTG2 variants were obtained from the Catalogue of Somatic Mutations in Cancer (COSMIC) database. Each variant was tested using SIFT and SuSPect prediction tool to determine potential effect of these variants in protein function. Thereafter, the mutations were prioritized based a recent study where BTG2 variants were identified in NHL (Lohr et al., 2012, Morin et al., 2011). These BTG2 variants were S39N, L46F, H49Y, I70M, L100P, G117D, S158C, and S158I. From analysis of the crystal structure of BTG2 in complex with CNOT7, L100, I70 and G117 amino acids of BTG2 may form direct interactions with CNOT7. By using a yeast two-hybrid and RNA tethering assays, the ability of the BTG2 variants to interact with Caf1 catalytic subunits and the functional effect of BTG2 variants on mRNA degradation was assessed. The findings of this study identified three BTG2 variants: L100P, G117D, and H49Y that potentially regulate mRNA abundance in lymphoma via interaction with the Ccr4-Not deadenylase.

7.5 Future work

The findings reported in this thesis identifies two biochemical assay methods useful for the evaluation of the Ccr4-Not deadenylase activity and are complementary to the recently developed fluorescence-based assay method. These biochemical also assays work for a variety of enzymes. This is a significant and novel contribution to studies on the Ccr4-Not complex and also in work identifying small molecules that may inhibit the Ccr4-Not deadenylase as a drug target in disease conditions. Based on the findings of this study, we believe that both assays will be useful for characterisation and screening of potential CNOT6, CNOT6L inhibitors and further new inhibitors of CNOT7 useful for studying post-transcriptional gene regulation in diseases. It could also be useful in characterising BTG2 and variant proteins. While thermal shift assays can be used as first line screening assay method to narrow hits from a library of compounds, substrate fluorescence based assays

can be used to screen further compounds identified by TSAs. Next, the AMP assay method can be useful as a secondary assay to corroborate findings obtained by fluorescence-based method. Cell-based studies done that identified BTG2 variants involved that regulate messenger RNA abundance in NHL is also a starting point for further studies to determine potential molecular inhibitors for disease intervention.

Although an extensive work has been done in this thesis, there are still more fields to explore. Future work will involve the use of TSA to screen for conditions that affect stability of BTG2 and its variants associated with lymphoma (Chapter 6) to determine overall effect on the Ccr4-Not deadenylase and mRNA degradation. While three BTG2 variants: L100P, G117D, and H49Y that potentially regulate mRNA abundance in lymphoma via interaction with the Ccr4-Not deadenylase were identified in Chapter 6, future work will involve further investigation into how poly (A) binding proteins (PABPC1) may affect the association of the identified BTG2 variants (Stupfler et al., 2016). It will also involve a determination of how these variants affect other cell functions such as cell proliferation, protein stability amongst others. The use of mouse models to verify BTG2 as a tumour suppressor may provide more insight into its role. Furthermore, compounds A-E (chapter 4) could be evaluated by the AMP-based assay to determine possible inhibitory effect on the Ccr4 deadenylase.

References

ALBERT, T. K., HANZAWA, H., LEGTENBERG, Y. I., DE RUWE, M. J., VAN DEN HEUVEL, F. A., COLLART, M. A., BOELENS, R. & TIMMERS, H. T. 2002. Identification of a ubiquitin-protein ligase subunit within the CCR4-NOT transcription repressor complex. *Embo j,* 21**,** 355-64.

ALBERT, T. K., LEMAIRE, M., VAN BERKUM, N. L., GENTZ, R., COLLART, M. A. & TIMMERS, H. T. 2000. Isolation and characterization of human orthologs of yeast CCR4-NOT complex subunits. *Nucleic Acids Res,* 28**,** 809-17.

ANDERSEN, K. R., JONSTRUP, A. T., VAN, L. B. & BRODERSEN, D. E. 2009a. The activity and selectivity of fission yeast Pop2p are affected by a high affinity for Zn2+ and Mn2+ in the active site. *Rna,* 15**,** 850-61.

ASLAM, A., MITTAL, S., KOCH, F., ANDRAU, J. C. & WINKLER, G. S. 2009. The Ccr4-NOT deadenylase subunits CNOT7 and CNOT8 have overlapping roles and modulate cell proliferation. *Mol Biol Cell,* 20**,** 3840-50.

BAGGS, J. E. & GREEN, C. B. 2003. Nocturnin, a deadenylase in Xenopus laevis retina: a mechanism for posttranscriptional control of circadian-related mRNA. *Curr Biol,* 13**,** 189-98.

BARTLAM, M. & YAMAMOTO, T. 2010. The structural basis for deadenylation by the CCR4-NOT complex. *Protein Cell,* 1**,** 443-52.

BASQUIN, J., ROUDKO, V. V., RODE, M., BASQUIN, C., SERAPHIN, B. & CONTI, E. 2012. Architecture of the nuclease module of the yeast Ccr4-not complex: the Not1-Caf1-Ccr4 interaction. *Mol Cell,* 48**,** 207-18.

BAWANKAR, P., LOH, B., WOHLBOLD, L., SCHMIDT, S. & IZAURRALDE, E. 2013. NOT10 and C2orf29/NOT11 form a conserved module of the CCR4-NOT complex that docks onto the NOT1 N-terminal domain. *RNA Biol,* 10**,** 228-44.

BEESE, L. S. & STEITZ, T. A. 1991. Structural basis for the 3'-5' exonuclease activity of Escherichia coli DNA polymerase I: a two metal ion mechanism. *Embo j,* 10**,** 25-33.

BEHM-ANSMANT, I., REHWINKEL, J., DOERKS, T., STARK, A., BORK, P. & IZAURRALDE, E. 2006. mRNA degradation by miRNAs and GW182 requires both CCR4:NOT deadenylase and DCP1:DCP2 decapping complexes. *Genes & Development,* 20**,** 1885-1898.

BENTLEY, D. L. 2005. Rules of engagement: co-transcriptional recruitment of pre-mRNA processing factors. *Curr Opin Cell Biol,* 17**,** 251-6.

BHANDARI, D., RAISCH, T., WEICHENRIEDER, O., JONAS, S. & IZAURRALDE, E. 2014. Structural basis for the Nanos-mediated recruitment of the CCR4-NOT complex and translational repression. *Genes Dev,* 28**,** 888-901.

BIANCHIN, C., MAUXION, F., SENTIS, S., SERAPHIN, B. & CORBO, L. 2005. Conservation of the deadenylase activity of proteins of the Caf1 family in human. *RNA,* 11**,** 487-94.

BLACKSHEAR, P. J. 2002. Tristetraprolin and other CCCH tandem zinc-finger proteins in the regulation of mRNA turnover. *Biochem Soc Trans,* 30**,** 945-52.

BOIKO, A. D., PORTEOUS, S., RAZORENOVA, O. V., KRIVOKRYSENKO, V. I., WILLIAMS, B. R. & GUDKOV, A. V. 2006b. A systematic search for downstream mediators of tumor suppressor function of p53 reveals a major role of BTG2 in suppression of Ras-induced transformation. *Genes Dev,* 20**,** 236-52.

BONNEROT, C., BOECK, R. & LAPEYRE, B. 2000. The two proteins Pat1p (Mrt1p) and Spb8p interact in vivo, are required for mRNA decay, and are functionally linked to Pab1p. *Mol Cell Biol,* 20**,** 5939-46.

BRANDTS, J. F. & LIN, L. N. 1990. Study of strong to ultratight protein interactions using differential scanning calorimetry. *Biochemistry,* 29**,** 6927-40.

BRAUN, J. E., HUNTZINGER, E., FAUSER, M. & IZAURRALDE, E. 2011. GW182 proteins directly recruit cytoplasmic deadenylase complexes to miRNA targets. *Molecular Cell,* 44**,** 120-133.

BRAUN, J. E., TRUFFAULT, V., BOLAND, A., HUNTZINGER, E., CHANG, C. T., HAAS, G., WEICHENRIEDER, O., COLES, M. & IZAURRALDE, E. 2012. A direct interaction between DCP1 and XRN1 couples mRNA decapping to 5' exonucleolytic degradation. *Nat Struct Mol Biol,* 19**,** 1324-31.

BROWN, C. E., TARUN, S. Z., JR., BOECK, R. & SACHS, A. B. 1996. PAN3 encodes a subunit of the Pab1p-dependent poly(A) nuclease in Saccharomyces cerevisiae. *Mol Cell Biol,* 16**,** 5744-53.

CHEADLE, C., FAN, J., CHO-CHUNG, Y. S., WERNER, T., RAY, J., DO, L., GOROSPE, M. & BECKER, K. G. 2005a. Control of gene expression during T cell activation: alternate regulation of mRNA transcription and mRNA stability. *BMC Genomics,* 6**,** 75-75.

CHEADLE, C., FAN, J., CHO-CHUNG, Y. S., WERNER, T., RAY, J., DO, L., GOROSPE, M. & BECKER, K. G. 2005b. Stability regulation of mRNA and the control of gene expression. *Ann N Y Acad Sci,* 1058**,** 196-204.

CHEN, C. Y. & SHYU, A. B. 1995. AU-rich elements: characterization and importance in mRNA degradation. *Trends Biochem Sci,* 20**,** 465-70.

CHEN, J., CHIANG, Y. C. & DENIS, C. L. 2002. CCR4, a 3'-5' poly(A) RNA and ssDNA exonuclease, is the catalytic component of the cytoplasmic deadenylase. *EMBO J,* 21**,** 1414-26.

CHENG, Y., LIU, W. F., YAN, Y. B. & ZHOU, H. M. 2006. A nonradioactive assay for poly(a)-specific ribonuclease activity by methylene blue colorimetry. *Protein Pept Lett,* 13**,** 125-8.

CHLEBOWSKI, A., LUBAS, M., JENSEN, T. H. & DZIEMBOWSKI, A. 2013. RNA decay machines: the exosome. *Biochim Biophys Acta,* 1829**,** 552-60.

CHOI, J. A. & LIM, I. K. 2013. TIS21/BTG2 inhibits invadopodia formation by downregulating reactive oxygen species level in MDA-MB-231 cells. *J Cancer Res Clin Oncol,* 139**,** 1657-65.

CLARK, L. B., VISWANATHAN, P., QUIGLEY, G., CHIANG, Y. C., MCMAHON, J. S., YAO, G., CHEN, J., NELSBACH, A. & DENIS, C. L. 2004. Systematic mutagenesis of the leucine-rich repeat (LRR) domain of CCR4 reveals

specific sites for binding to CAF1 and a separate critical role for the LRR in CCR4 deadenylase activity. *J Biol Chem,* 279**,** 13616-23.

COLLART, M. A. 2003. Global control of gene expression in yeast by the Ccr4-Not complex. *Gene,* 313**,** 1-16.

COLLART, M. A. & PANASENKO, O. O. 2012a. The Ccr4--not complex. *Gene,* 492**,** 42-53.

COLLART, M. A., PANASENKO, O. O. & NIKOLAEV, S. I. 2013. The Not3/5 subunit of the Ccr4-Not complex: a central regulator of gene expression that integrates signals between the cytoplasm and the nucleus in eukaryotic cells. *Cell Signal,* 25**,** 743-51.

COLLART, M. A. & TIMMERS, H. T. 2004. The eukaryotic Ccr4-not complex: a regulatory platform integrating mRNA metabolism with cellular signaling pathways? *Prog Nucleic Acid Res Mol Biol,* 77**,** 289-322.

COLLER, J. & WICKENS, M. 2007. Tethered function assays: an adaptable approach to study RNA regulatory proteins. *Methods Enzymol,* 429**,** 299-321.

CONTI, E. & IZAURRALDE, E. 2005. Nonsense-mediated mRNA decay: molecular insights and mechanistic variations across species. *Curr Opin Cell Biol,* 17**,** 316-25.

COPELAND, P. R. & WORMINGTON, M. 2001. The mechanism and regulation of deadenylation: identification and characterization of Xenopus PARN. *Rna,* 7**,** 875-86.

COWLING, V. H. 2009. Regulation of mRNA cap methylation. *Biochem J,* 425**,** 295-302.

CZAPLINSKI, K., WENG, Y., HAGAN, K. W. & PELTZ, S. W. 1995. Purification and characterization of the Upf1 protein: a factor involved in translation and mRNA degradation. *Rna,* 1**,** 610-23.

DEHLIN, E., WORMINGTON, M., KORNER, C. G. & WAHLE, E. 2000. Cap-dependent deadenylation of mRNA. *EMBO J,* 19**,** 1079-86.

DOIDGE, R., MITTAL, S., ASLAM, A. & WINKLER, G. S. 2012a. The anti-proliferative activity of BTG/TOB proteins is mediated via the Caf1a (CNOT7) and Caf1b (CNOT8) deadenylase subunits of the Ccr4-not complex. *PLoS One,* 7**,** e51331.

DOIDGE, R., MITTAL, S., ASLAM, A. & WINKLER, G. S. 2012b. Deadenylation of cytoplasmic mRNA by the mammalian Ccr4-Not complex. *Biochem Soc Trans,* 40**,** 896-901.

DOMA, M. K. & PARKER, R. 2006. Endonucleolytic cleavage of eukaryotic mRNAs with stalls in translation elongation. *Nature,* 440**,** 561-564.

DOMINGUEZ, C., BONVIN, A. M., WINKLER, G. S., VAN SCHAIK, F. M., TIMMERS, H. T. & BOELENS, R. 2004. Structural model of the UbcH5B/CNOT4 complex revealed by combining NMR, mutagenesis, and docking approaches. *Structure,* 12**,** 633-44.

DRAPER, M. P., LIU, H. Y., NELSBACH, A. H., MOSLEY, S. P. & DENIS, C. L. 1994. CCR4 is a glucose-regulated transcription factor whose leucine-rich repeat binds several proteins important for placing CCR4 in its proper promoter context. *Mol Cell Biol,* 14**,** 4522-31.

DUPRESSOIR, A., MOREL, A. P., BARBOT, W., LOIREAU, M. P., CORBO, L. & HEIDMANN, T. 2001. Identification of four families of yCCR4- and Mg2+-dependent endonuclease-related proteins in higher eukaryotes, and characterization of orthologs of yCCR4 with a conserved leucine-rich repeat essential for hCAF1/hPOP2 binding. *BMC Genomics,* 2**,** 9.

DURIEZ, C., MOYRET-LALLE, C., FALETTE, N., EL-GHISSASSI, F. & PUISIEUX, A. 2004. BTG2, its family and its tutor. *Bull Cancer,* 91.

EULALIO, A., HUNTZINGER, E., NISHIHARA, T., REHWINKEL, J., FAUSER, M. & IZAURRALDE, E. 2009. Deadenylation is a widespread effect of miRNA regulation. *Rna,* 15**,** 21-32.

EZZEDDINE, N., CHANG, T. C., ZHU, W., YAMASHITA, A., CHEN, C. Y., ZHONG, Z., YAMASHITA, Y., ZHENG, D. & SHYU, A. B. 2007. Human TOB, an antiproliferative transcription factor, is a poly(A)-binding protein-dependent positive regulator of cytoplasmic mRNA deadenylation. *Mol Cell Biol,* 27**,** 7791-801.

EZZEDDINE, N., CHEN, C. Y. & SHYU, A. B. 2012. Evidence providing new insights into TOB-promoted deadenylation and supporting a link between TOB's deadenylation-enhancing and antiproliferative activities. *Mol Cell Biol,* 32**,** 1089-98.

FABIAN, M. R., FRANK, F., ROUYA, C., SIDDIQUI, N., LAI, W. S., KARETNIKOV, A., BLACKSHEAR, P. J., NAGAR, B. & SONENBERG, N. 2013. Structural basis for the recruitment of the human CCR4–NOT deadenylase complex by tristetraprolin. *Nat Struct Mol Biol,* 20**,** 735-739.

FAN, J., YANG, X., WANG, W., WOOD, W. H., BECKER, K. G. & GOROSPE, M. 2002. Global analysis of stress-regulated mRNA turnover by using cDNA arrays. *Proceedings of the National Academy of Sciences of the United States of America,* 99**,** 10611-10616.

FARAJI, F., HU, Y., WU, G., GOLDBERGER, N. E., WALKER, R. C., ZHANG, J. & HUNTER, K. W. 2014. An integrated systems genetics screen reveals the transcriptional structure of inherited predisposition to metastatic disease. *Genome Research,* 24**,** 227-240.

FARAJI, F., HU, Y., YANG, H. H., LEE, M. P., WINKLER, G. S., HAFNER, M. & HUNTER, K. W. 2016. Post-transcriptional Control of Tumor Cell Autonomous Metastatic Potential by CCR4-NOT Deadenylase CNOT7. *PLoS Genetics,* 12**,** e1005820.

FENGER-GRON, M., FILLMAN, C., NORRILD, B. & LYKKE-ANDERSEN, J. 2005. Multiple processing body factors and the ARE binding protein TTP activate mRNA decapping. *Mol Cell,* 20**,** 905-15.

FILIPOWICZ, W., BHATTACHARYYA, S. N. & SONENBERG, N. 2008. Mechanisms of post-transcriptional regulation by microRNAs: are the answers in sight? *Nat Rev Genet,* 9**,** 102-14.

FORBES, S. A., BHAMRA, G., BAMFORD, S., DAWSON, E., KOK, C., CLEMENTS, J., MENZIES, A., TEAGUE, J. W., FUTREAL, P. A. & STRATTON, M. R. 2008. The Catalogue of Somatic Mutations in Cancer (COSMIC). *Current protocols in human genetics / editorial board, Jonathan L. Haines ... [et al.],* CHAPTER**,** Unit-10.11.

FRISCHMEYER, P. A. & DIETZ, H. C. 1999. Nonsense-mediated mRNA decay in health and disease. *Hum Mol Genet,* 8**,** 1893-900.

FRISCHMEYER, P. A., VAN HOOF, A., O'DONNELL, K., GUERRERIO, A. L., PARKER, R. & DIETZ, H. C. 2002. An mRNA surveillance mechanism that eliminates transcripts lacking termination codons. *Science,* 295**,** 2258-61.

FUNAKOSHI, Y., DOI, Y., HOSODA, N., UCHIDA, N., OSAWA, M., SHIMADA, I., TSUJIMOTO, M., SUZUKI, T., KATADA, T. & HOSHINO, S. 2007. Mechanism of mRNA deadenylation: evidence for a molecular interplay between translation termination factor eRF3 and mRNA deadenylases. *Genes Dev,* 21**,** 3135-48.

GAO, M., FRITZ, D. T., FORD, L. P. & WILUSZ, J. 2000. Interaction between a poly(A)-specific ribonuclease and the 5' cap influences mRNA deadenylation rates in vitro. *Mol Cell,* 5**,** 479-88.

GARNEAU, N. L., WILUSZ, J. & WILUSZ, C. J. 2007a. The highways and byways of mRNA decay. *Nat Rev Mol Cell Biol,* 8**,** 113-26.

GATFIELD, D. & IZAURRALDE, E. 2004. Nonsense-mediated messenger RNA decay is initiated by endonucleolytic cleavage in Drosophila. *Nature,* 429**,** 575-8.

GIRALDEZ, A. J., MISHIMA, Y., RIHEL, J., GROCOCK, R. J., VAN DONGEN, S., INOUE, K., ENRIGHT, A. J. & SCHIER, A. F. 2006. Zebrafish MiR-430 promotes deadenylation and clearance of maternal mRNAs. *Science,* 312**,** 75-9.

GOLDSTROHM, A. C., SEAY, D. J., HOOK, B. A. & WICKENS, M. 2007. PUF protein-mediated deadenylation is catalyzed by Ccr4p. *J Biol Chem,* 282**,** 109-14.

GOLDSTROHM, A. C. & WICKENS, M. 2008. Multifunctional deadenylase complexes diversify mRNA control. *Nat Rev Mol Cell Biol,* 9**,** 337-44.

GREINER-STOEFFELE, T., GRUNOW, M. & HAHN, U. 1996. A general ribonuclease assay using methylene blue. *Anal Biochem,* 240**,** 24-8.

GUARDAVACCARO, D., CORRENTE, G., COVONE, F., MICHELI, L., D'AGNANO, I., STARACE, G., CARUSO, M. & TIRONE, F. 2000. Arrest of G(1)-S progression by the p53-inducible gene PC3 is Rb dependent and relies on the inhibition of cyclin D1 transcription. *Mol Cell Biol,* 20**,** 1797-815.

HE, G. J., LIU, W. F. & YAN, Y. B. 2011. Dissimilar roles of the four conserved acidic residues in the thermal stability of poly(A)-specific ribonuclease. *Int J Mol Sci,* 12**,** 2901-16.

HE, G. J. & YAN, Y. B. 2012. A deadenylase assay by size-exclusion chromatography. *PLoS One,* 7**,** e33700.

HESSE, M. & ARENZ, C. 2014. MicroRNA Maturation and Human Disease. *In:* ARENZ, C. (ed.) *miRNA Maturation: Methods and Protocols.* Totowa, NJ: Humana Press.

HOLBROOK, J. A., NEU-YILIK, G., HENTZE, M. W. & KULOZIK, A. E. 2004. Nonsense-mediated decay approaches the clinic. *Nat Genet,* 36**,** 801-8.

HOLLIEN, J. & WEISSMAN, J. S. 2006. Decay of endoplasmic reticulum-localized mRNAs during the unfolded protein response. *Science,* 313**,** 104-7.

HORIUCHI, M., TAKEUCHI, K., NODA, N., MUROYA, N., SUZUKI, T., NAKAMURA, T., KAWAMURA-TSUZUKU, J., TAKAHASI, K., YAMAMOTO, T. & INAGAKI, F. 2009. Structural basis for the antiproliferative activity of the Tob-hCaf1 complex. *J Biol Chem,* 284**,** 13244-55.

HOSODA, N., FUNAKOSHI, Y., HIRASAWA, M., YAMAGISHI, R., ASANO, Y., MIYAGAWA, R., OGAMI, K., TSUJIMOTO, M. & HOSHINO, S.-I. 2011. Anti-proliferative protein Tob negatively regulates CPEB3 target by recruiting Caf1 deadenylase. *The EMBO Journal,* 30**,** 1311-1323.

HOUSELEY, J. & TOLLERVEY, D. 2009. The many pathways of RNA degradation. *Cell,* 136**,** 763-76.

HU, G., KIM, J., XU, Q., LENG, Y., ORKIN, S. H. & ELLEDGE, S. J. 2009. A genome-wide RNAi screen identifies a new transcriptional module required for self-renewal. *Genes Dev,* 23**,** 837-48.

INADA, T. & AIBA, H. 2005. Translation of aberrant mRNAs lacking a termination codon or with a shortened 3′-UTR is repressed after initiation in yeast. *The EMBO Journal,* 24**,** 1584-1595.

INADA, T. & MAKINO, S. 2014. Novel roles of the multifunctional CCR4-NOT complex in post-transcriptional regulation. *Frontiers in Genetics,* 5.

ITO, K., TAKAHASHI, A., MORITA, M., SUZUKI, T. & YAMAMOTO, T. 2011. The role of the CNOT1 subunit of the CCR4-NOT complex in mRNA deadenylation and cell viability. *Protein Cell,* 2**,** 755-63.

JACKSON, R. J. & STANDART, N. 2007. How do microRNAs regulate gene expression? *Sci STKE,* 2007**,** re1.

JADHAV, G. P., KAUR, I., MARYATI, M., AIRHIHEN, B., FISCHER, P. M. & WINKLER, G. S. 2015. Discovery, synthesis and biochemical profiling of purine-2,6-dione derivatives as inhibitors of the human poly(A)-selective ribonuclease Caf1. *Bioorganic & Medicinal Chemistry Letters,* 25**,** 4219-4224.

JONAS, S. & IZAURRALDE, E. 2015. Towards a molecular understanding of microRNA-mediated gene silencing. *Nat Rev Genet,* 16**,** 421-433.

JONSTRUP, A. T., ANDERSEN, K. R., VAN, L. B. & BRODERSEN, D. E. 2007. The 1.4-Å crystal structure of the S. pombe Pop2p deadenylase subunit unveils the configuration of an active enzyme. *Nucleic Acids Research,* 35**,** 3153-3164.

KASHIMA, I., YAMASHITA, A., IZUMI, N., KATAOKA, N., MORISHITA, R., HOSHINO, S., OHNO, M., DREYFUSS, G. & OHNO, S. 2006. Binding of a novel SMG-1-Upf1-eRF1-eRF3 complex (SURF) to the exon junction complex triggers Upf1 phosphorylation and nonsense-mediated mRNA decay. *Genes Dev,* 20**,** 355-67.

KAWAKUBO, H., BRACHTEL, E., HAYASHIDA, T., YEO, G., KISH, J., MUZIKANSKY, A., WALDEN, P. D. & MAHESWARAN, S. 2006. Loss of B-cell translocation gene-2 in estrogen receptor-positive breast carcinoma is associated with tumor grade and overexpression of cyclin d1 protein. *Cancer Res,* 66**,** 7075-82.

KAWAKUBO, H., CAREY, J. L., BRACHTEL, E., GUPTA, V., GREEN, J. E., WALDEN, P. D. & MAHESWARAN, S. 2004. Expression of the NF-kappaB-

responsive gene BTG2 is aberrantly regulated in breast cancer. *Oncogene,* 23**,** 8310-9.

KIMPLE, M. E., BRILL, A. L. & PASKER, R. L. 2013. Overview of Affinity Tags for Protein Purification. *Current protocols in protein science / editorial board, John E. Coligan ... [et al.],* 73**,** Unit-9.9.

KORNBERG, R. D. 1999. Eukaryotic transcriptional control. *Trends Cell Biol,* 9**,** M46-9.

KORNER, C. G. & WAHLE, E. 1997. Poly(A) tail shortening by a mammalian poly(A)-specific 3'-exoribonuclease. *J Biol Chem,* 272**,** 10448-56.

KÖRNER, C. G., WORMINGTON, M., MUCKENTHALER, M., SCHNEIDER, S., DEHLIN, E. & WAHLE, E. 1998. The deadenylating nuclease (DAN) is involved in poly(A) tail removal during the meiotic maturation of Xenopus oocytes. *The EMBO Journal,* 17**,** 5427-5437.

LAU, N. C., KOLKMAN, A., VAN SCHAIK, F. M., MULDER, K. W., PIJNAPPEL, W. W., HECK, A. J. & TIMMERS, H. T. 2009. Human Ccr4-Not complexes contain variable deadenylase subunits. *Biochem J,* 422**,** 443-53.

LEE, T. I., WYRICK, J. J., KOH, S. S., JENNINGS, E. G., GADBOIS, E. L. & YOUNG, R. A. 1998. Interplay of positive and negative regulators in transcription initiation by RNA polymerase II holoenzyme. *Mol Cell Biol,* 18**,** 4455-62.

LEPPEK, K., SCHOTT, J., REITTER, S., POETZ, F., HAMMOND, M. C. & STOECKLIN, G. 2013. Roquin promotes constitutive mRNA decay via a conserved class of stem-loop recognition motifs. *Cell,* 153**,** 869-81.

LICHTY, J. J., MALECKI, J. L., AGNEW, H. D., MICHELSON-HOROWITZ, D. J. & TAN, S. 2005. Comparison of affinity tags for protein purification. *Protein Expr Purif,* 41**,** 98-105.

LIU, H., RODGERS, N. D., JIAO, X. & KILEDJIAN, M. 2002. The scavenger mRNA decapping enzyme DcpS is a member of the HIT family of pyrophosphatases. *Embo j,* 21**,** 4699-708.

LIU, H. Y., BADARINARAYANA, V., AUDINO, D. C., RAPPSILBER, J., MANN, M. & DENIS, C. L. 1998. The NOT proteins are part of the CCR4 transcriptional complex and affect gene expression both positively and negatively. *Embo j,* 17**,** 1096-106.

LIU, M., WU, H., LIU, T., LI, Y., WANG, F., WAN, H., LI, X. & TANG, H. 2009. Regulation of the cell cycle gene, BTG2, by miR-21 in human laryngeal carcinoma. *Cell Res,* 19**,** 828-37.

LIU, W. F. & YAN, Y. B. 2008. Biophysical and biochemical characterization of recombinant human Pop2 deadenylase. *Protein Expr Purif,* 60**,** 46-52.

LO, M. C., AULABAUGH, A., JIN, G., COWLING, R., BARD, J., MALAMAS, M. & ELLESTAD, G. 2004. Evaluation of fluorescence-based thermal shift assays for hit identification in drug discovery. *Anal Biochem,* 332**,** 153-9.

LOH, B., JONAS, S. & IZAURRALDE, E. 2013. The SMG5-SMG7 heterodimer directly recruits the CCR4-NOT deadenylase complex to mRNAs containing nonsense codons via interaction with POP2. *Genes Dev,* 27**,** 2125-38.

LOHR, J. G., STOJANOV, P., LAWRENCE, M. S., AUCLAIR, D., CHAPUY, B., SOUGNEZ, C., CRUZ-GORDILLO, P., KNOECHEL, B., ASMANN, Y. W., SLAGER, S. L., NOVAK, A. J., DOGAN, A., ANSELL, S. M., LINK, B. K., ZOU, L., GOULD, J., SAKSENA, G., STRANSKY, N., RANGEL-ESCAREÑO, C., FERNANDEZ-LOPEZ, J. C., HIDALGO-MIRANDA, A., MELENDEZ-ZAJGLA, J., HERNÁNDEZ-LEMUS, E., SCHWARZ-CRUZ Y CELIS, A., IMAZ-ROSSHANDLER, I., OJESINA, A. I., JUNG, J., PEDAMALLU, C. S., LANDER, E. S., HABERMANN, T. M., CERHAN, J. R., SHIPP, M. A., GETZ, G. & GOLUB, T. R. 2012. Discovery and prioritization of somatic mutations in diffuse large B-cell lymphoma (DLBCL) by whole-exome sequencing. *Proceedings of the National Academy of Sciences,* 109**,** 3879-3884.

LOVE, C., SUN, Z., JIMA, D., LI, G., ZHANG, J., MILES, R., RICHARDS, K. L., DUNPHY, C. H., CHOI, W. W., SRIVASTAVA, G., LUGAR, P. L., RIZZIERI, D. A., LAGOO, A. S., BERNAL-MIZRACHI, L., MANN, K. P., FLOWERS, C. R., NARESH, K. N., EVENS, A. M., CHADBURN, A., GORDON, L. I., CZADER, M. B., GILL, J. I., HSI, E. D., GREENOUGH, A., MOFFITT, A. B., MCKINNEY, M., BANERJEE, A., GRUBOR, V., LEVY, S., DUNSON, D. B. & DAVE, S. S. 2012. The genetic landscape of mutations in Burkitt lymphoma. *Nat Genet,* 44**,** 1321-5.

LYKKE-ANDERSEN, J. & WAGNER, E. 2005. Recruitment and activation of mRNA decay enzymes by two ARE-mediated decay activation domains in the proteins TTP and BRF-1. *Genes Dev,* 19**,** 351-61.

MAHADEVAN, S. & STRUHL, K. 1990. Tc, an unusual promoter element required for constitutive transcription of the yeast HIS3 gene. *Mol Cell Biol,* 10**,** 4447-55.

MAILLET, L. & COLLART, M. A. 2002. Interaction between Not1p, a component of the Ccr4-not complex, a global regulator of transcription, and Dhh1p, a putative RNA helicase. *J Biol Chem,* 277**,** 2835-42.

MAILLET, L., TU, C., HONG, Y. K., SHUSTER, E. O. & COLLART, M. A. 2000. The essential function of Not1 lies within the Ccr4-Not complex. *J Mol Biol,* 303**,** 131-43.

MALVAR, T., BIRON, R. W., KABACK, D. B. & DENIS, C. L. 1992. The CCR4 protein from Saccharomyces cerevisiae contains a leucine-rich repeat region which is required for its control of ADH2 gene expression. *Genetics,* 132**,** 951-62.

MANGUS, D. A., AMRANI, N. & JACOBSON, A. 1998. Pbp1p, a factor interacting with Saccharomyces cerevisiae poly(A)-binding protein, regulates polyadenylation. *Mol Cell Biol,* 18**,** 7383-96.

MAO, B., ZHANG, Z. & WANG, G. 2015. BTG2: a rising star of tumor suppressors (review). *Int J Oncol,* 46**,** 459-64.

MARTINEZ, J., REN, Y. G., NILSSON, P., EHRENBERG, M. & VIRTANEN, A. 2001. The mRNA cap structure stimulates rate of poly(A) removal and amplifies processivity of degradation. *J Biol Chem,* 276**,** 27923-9.

MARYATI, M., AIRHIHEN, B. & WINKLER, G. S. 2015. The enzyme activities of Caf1 and Ccr4 are both required for deadenylation by the human Ccr4-Not nuclease module. *Biochem J*.

MARYATI, M., KAUR, I., JADHAV, G. P., OLOTU-UMOREN, L., OVEH, B., HASHMI, L., FISCHER, P. M. & WINKLER, G. S. 2014. A fluorescence-based assay suitable for quantitative analysis of deadenylase enzyme activity. *Nucleic Acids Res,* 42**,** e30.

MATSUDA, S., ROUAULT, J., MAGAUD, J. & BERTHET, C. 2001. In search of a function for the TIS21/PC3/BTG1/TOB family. *FEBS Lett,* 497**,** 67-72.

MAUXION, F., CHEN, C. Y., SERAPHIN, B. & SHYU, A. B. 2009. BTG/TOB factors impact deadenylases. *Trends Biochem Sci,* 34**,** 640-7.

MAUXION, F., FAUX, C. & SERAPHIN, B. 2008. The BTG2 protein is a general activator of mRNA deadenylation. *EMBO J,* 27**,** 1039-48.

MAUXION, F., PREVE, B. & SERAPHIN, B. 2013. C2ORF29/CNOT11 and CNOT10 form a new module of the CCR4-NOT complex. *RNA Biol,* 10**,** 267-76.

MCMANUS, C. J. & GRAVELEY, B. R. 2011. RNA structure and the mechanisms of alternative splicing. *Curr Opin Genet Dev,* 21**,** 373-9.

MELAMED, J., KERNIZAN, S. & WALDEN, P. D. 2002. Expression of B-cell translocation gene 2 protein in normal human tissues. *Tissue Cell,* 34**,** 28-32.

MEYER, S., TEMME, C. & WAHLE, E. 2004. Messenger RNA turnover in eukaryotes: pathways and enzymes. *Crit Rev Biochem Mol Biol,* 39**,** 197-216.

MITTAL, S., ASLAM, A., DOIDGE, R., MEDICA, R. & WINKLER, G. S. 2011. The Ccr4a (CNOT6) and Ccr4b (CNOT6L) deadenylase subunits of the human Ccr4-Not complex contribute to the prevention of cell death and senescence. *Mol Biol Cell,* 22**,** 748-58.

MORAES, K. C., WILUSZ, C. J. & WILUSZ, J. 2006. CUG-BP binds to RNA substrates and recruits PARN deadenylase. *Rna,* 12**,** 1084-91.

MORIN, R. D., MENDEZ-LAGO, M., MUNGALL, A. J., GOYA, R., MUNGALL, K. L., CORBETT, R. D., JOHNSON, N. A., SEVERSON, T. M., CHIU, R., FIELD, M., JACKMAN, S., KRZYWINSKI, M., SCOTT, D. W., TRINH, D. L., TAMURA-WELLS, J., LI, S., FIRME, M. R., ROGIC, S., GRIFFITH, M., CHAN, S., YAKOVENKO, O., MEYER, I. M., ZHAO, E. Y., SMAILUS, D., MOKSA, M., CHITTARANJAN, S., RIMSZA, L., BROOKS-WILSON, A., SPINELLI, J. J., BEN-NERIAH, S., MEISSNER, B., WOOLCOCK, B., BOYLE, M., MCDONALD, H., TAM, A., ZHAO, Y., DELANEY, A., ZENG, T., TSE, K., BUTTERFIELD, Y., BIROL, I., HOLT, R., SCHEIN, J., HORSMAN, D. E., MOORE, R., JONES, S. J. M., CONNORS, J. M., HIRST, M., GASCOYNE, R. D. & MARRA, M. A. 2011. Frequent mutation of histone-modifying genes in non-Hodgkin lymphoma. *Nature,* 476**,** 298-303.

MORITA, M., OIKE, Y., NAGASHIMA, T., KADOMATSU, T., TABATA, M., SUZUKI, T., NAKAMURA, T., YOSHIDA, N., OKADA, M. & YAMAMOTO, T. 2011. Obesity resistance and increased hepatic expression of catabolism-related mRNAs in Cnot3+/− mice. 30**,** 4678-4691.

NASERTORABI, F., BATISSE, C., DIEPHOLZ, M., SUCK, D. & BOTTCHER, B. 2011. Insights into the structure of the CCR4-NOT complex by electron microscopy. *FEBS Lett,* 585**,** 2182-6.

NG, P. C. & HENIKOFF, S. 2003. SIFT: predicting amino acid changes that affect protein function. *Nucleic Acids Research,* 31**,** 3812-3814.

NIESEN, F. H., BERGLUND, H. & VEDADI, M. 2007. The use of differential scanning fluorimetry to detect ligand interactions that promote protein stability. *Nat Protoc,* 2**,** 2212-21.

OGAMI, K., HOSODA, N., FUNAKOSHI, Y. & HOSHINO, S. 2014. Antiproliferative protein Tob directly regulates c-myc proto-oncogene expression through cytoplasmic polyadenylation element-binding protein CPEB. *Oncogene,* 33**,** 55-64.

PACE, C. N. & MCGRATH, T. 1980. Substrate stabilization of lysozyme to thermal and guanidine hydrochloride denaturation. *J Biol Chem,* 255**,** 3862-5.

PANTOLIANO, M. W., PETRELLA, E. C., KWASNOSKI, J. D., LOBANOV, V. S., MYSLIK, J., GRAF, E., CARVER, T., ASEL, E., SPRINGER, B. A., LANE, P. & SALEMME, F. R. 2001. High-density miniaturized thermal shift assays as a general strategy for drug discovery. *J Biomol Screen,* 6**,** 429-40.

PARKER, R. & SONG, H. 2004. The enzymes and control of eukaryotic mRNA turnover. *Nat Struct Mol Biol,* 11**,** 121-7.

PASSERI, D., MARCUCCI, A., RIZZO, G., BILLI, M., PANIGADA, M., LEONARDI, L., TIRONE, F. & GRIGNANI, F. 2006. Btg2 enhances retinoic acid-induced differentiation by modulating histone H4 methylation and acetylation. *Mol Cell Biol,* 26**,** 5023-32.

PETIT, A.-P., WOHLBOLD, L., BAWANKAR, P., HUNTZINGER, E., SCHMIDT, S., IZAURRALDE, E. & WEICHENRIEDER, O. 2012a. The structural basis for the interaction between the CAF1 nuclease and the NOT1 scaffold of the human CCR4–NOT deadenylase complex. *Nucleic Acids Research,* 40**,** 11058-11072.

PETTERSEN, E. F., GODDARD, T. D., HUANG, C. C., COUCH, G. S., GREENBLATT, D. M., MENG, E. C. & FERRIN, T. E. 2004. UCSF Chimera--a visualization system for exploratory research and analysis. *J Comput Chem,* 25**,** 1605-12.

PICCIRILLO, C., KHANNA, R. & KILEDJIAN, M. 2003. Functional characterization of the mammalian mRNA decapping enzyme hDcp2. *RNA,* 9**,** 1138-1147.

POKLAR, N., LAH, J., SALOBIR, M., MACEK, P. & VESNAVER, G. 1997. pH and temperature-induced molten globule-like denatured states of equinatoxin II: a study by UV-melting, DSC, far- and near-UV CD spectroscopy, and ANS fluorescence. *Biochemistry,* 36**,** 14345-52.

PREVOT, D., VOELTZEL, T., BIROT, A. M., MOREL, A. P., ROSTAN, M. C., MAGAUD, J. P. & CORBO, L. 2000. The leukemia-associated protein Btg1 and the p53-regulated protein Btg2 interact with the homeoprotein Hoxb9 and enhance its transcriptional activation. *J Biol Chem,* 275**,** 147-53.

REN, Y. G., KIRSEBOM, L. A. & VIRTANEN, A. 2004. Coordination of divalent metal ions in the active site of poly(A)-specific ribonuclease. *J Biol Chem,* 279**,** 48702-6.

REN, Y. G., MARTINEZ, J. & VIRTANEN, A. 2002. Identification of the active site of poly(A)-specific ribonuclease by site-directed mutagenesis and Fe(2+)-mediated cleavage. *J Biol Chem,* 277**,** 5982-7.

RORBACH, J., NICHOLLS, T. J. J. & MINCZUK, M. 2011. PDE12 removes mitochondrial RNA poly(A) tails and controls translation in human mitochondria. *Nucleic Acids Research,* 39**,** 7750-7763.

ROSS, J. 1995. mRNA stability in mammalian cells. *Microbiol Rev,* 59**,** 423-50.

ROUAULT, J. P., FALETTE, N., GUEHENNEUX, F., GUILLOT, C., RIMOKH, R., WANG, Q., BERTHET, C., MOYRET-LALLE, C., SAVATIER, P., PAIN, B., SHAW, P., BERGER, R., SAMARUT, J., MAGAUD, J. P., OZTURK, M., SAMARUT, C. & PUISIEUX, A. 1996. Identification of BTG2, an antiproliferative p53-dependent component of the DNA damage cellular response pathway. *Nat Genet,* 14**,** 482-6.

SCHELLMAN, J. A. 1975. Macromolecular binding. *Biopolymers,* 14**,** 999-1018.

SCHMIDT, T. G. M. & SKERRA, A. 2007. The Strep-tag system for one-step purification and high-affinity detection or capturing of proteins. *Nat. Protocols,* 2**,** 1528-1535.

SCHOENBERG, D. R. & MAQUAT, L. E. 2012a. Regulation of cytoplasmic mRNA decay. *Nat Rev Genet,* 13**,** 246-259.

SEMOTOK, J. L., COOPERSTOCK, R. L., PINDER, B. D., VARI, H. K., LIPSHITZ, H. D. & SMIBERT, C. A. 2005. Smaug recruits the CCR4/POP2/NOT deadenylase complex to trigger maternal transcript localization in the early Drosophila embryo. *Curr Biol,* 15**,** 284-94.

SENISTERRA, G., CHAU, I. & VEDADI, M. 2012. Thermal denaturation assays in chemical biology. *Assay Drug Dev Technol,* 10**,** 128-36.

SHIM, J. & KARIN, M. 2002. The control of mRNA stability in response to extracellular stimuli. *Mol Cells,* 14**,** 323-31.

SHIRAI, Y.-T., SUZUKI, T., MORITA, M., TAKAHASHI, A. & YAMAMOTO, T. 2014. Multifunctional roles of the mammalian CCR4–NOT complex in physiological phenomena. *Frontiers in Genetics,* 5**,** 286.

SHYU, A. B., WILKINSON, M. F. & VAN HOOF, A. 2008. Messenger RNA regulation: to translate or to degrade. *The EMBO journal,* 27**,** 471-481.

SIMS, R. J., 3RD, MANDAL, S. S. & REINBERG, D. 2004. Recent highlights of RNA-polymerase-II-mediated transcription. *Curr Opin Cell Biol,* 16**,** 263-71.

SISSI, C. & PALUMBO, M. 2009. Effects of magnesium and related divalent metal ions in topoisomerase structure and function. *Nucleic Acids Res,* 37**,** 702-11.

SONG, M.-G., LI, Y. & KILEDJIAN, M. 2010. Multiple mRNA Decapping Enzymes in Mammalian Cells. *Molecular cell,* 40**,** 423-432.

STEIGER, M., CARR-SCHMID, A., SCHWARTZ, D. C., KILEDJIAN, M. & PARKER, R. O. Y. 2003. Analysis of recombinant yeast decapping enzyme. *RNA,* 9**,** 231-238.

STEINBERG, G. R. & KEMP, B. E. 2009. AMPK in Health and Disease. *Physiol Rev,* 89**,** 1025-78.

STRAUME, M. & FREIRE, E. 1992. Two-dimensional differential scanning calorimetry: simultaneous resolution of intrinsic protein structural energetics and ligand binding interactions by global linkage analysis. *Anal Biochem,* 203**,** 259-68.

STRUCKMANN, K., SCHRAML, P., SIMON, R., ELMENHORST, K., MIRLACHER, M., KONONEN, J. & MOCH, H. 2004. Impaired expression of the cell cycle regulator BTG2 is common in clear cell renal cell carcinoma. *Cancer Res,* 64**,** 1632-8.

STUPFLER, B., BIRCK, C., SERAPHIN, B. & MAUXION, F. 2016. BTG2 bridges PABPC1 RNA-binding domains and CAF1 deadenylase to control cell proliferation. *Nat Commun,* 7**,** 10811.

SUZUKI, T., J, K. T., AJIMA, R., NAKAMURA, T., YOSHIDA, Y. & YAMAMOTO, T. 2002. Phosphorylation of three regulatory serines of Tob by Erk1 and Erk2 is required for Ras-mediated cell proliferation and transformation. *Genes Dev,* 16**,** 1356-70.

TAKAHASHI, F., CHIBA, N., TAJIMA, K., HAYASHIDA, T., SHIMADA, T., TAKAHASHI, M., MORIYAMA, H., BRACHTEL, E., EDELMAN, E. J., RAMASWAMY, S. & MAHESWARAN, S. 2011. Breast tumor progression induced by loss of BTG2 expression is inhibited by targeted therapy with the ErbB/HER inhibitor lapatinib. *Oncogene,* 30**,** 3084-95.

THARUN, S., HE, W., MAYES, A. E., LENNERTZ, P., BEGGS, J. D. & PARKER, R. 2000. Yeast Sm-like proteins function in mRNA decapping and decay. *Nature,* 404**,** 515-8.

THARUN, S. & PARKER, R. 2001. Targeting an mRNA for decapping: displacement of translation factors and association of the Lsm1p-7p complex on deadenylated yeast mRNAs. *Mol Cell,* 8**,** 1075-83.

THORE, S., MAUXION, F., SERAPHIN, B. & SUCK, D. 2003. X-ray structure and activity of the yeast Pop2 protein: a nuclease subunit of the mRNA deadenylase complex. *EMBO Rep,* 4**,** 1150-5.

TIRONE, F. 2001. The gene PC3(TIS21/BTG2), prototype member of the PC3/BTG/TOB family: regulator in control of cell growth, differentiation, and DNA repair? *J Cell Physiol,* 187**,** 155-65.

TUCKER, M., STAPLES, R. R., VALENCIA-SANCHEZ, M. A., MUHLRAD, D. & PARKER, R. 2002. Ccr4p is the catalytic subunit of a Ccr4p/Pop2p/Notp mRNA deadenylase complex in Saccharomyces cerevisiae. *EMBO J,* 21**,** 1427-36.

TUCKER, M., VALENCIA-SANCHEZ, M. A., STAPLES, R. R., CHEN, J., DENIS, C. L. & PARKER, R. 2001. The transcription factor associated Ccr4 and Caf1 proteins are components of the major cytoplasmic mRNA deadenylase in Saccharomyces cerevisiae. *Cell,* 104**,** 377-86.

TUMEY, L. N., BOM, D., HUCK, B., GLEASON, E., WANG, J., SILVER, D., BRUNDEN, K., BOOZER, S., RUNDLETT, S., SHERF, B., MURPHY, S., DENT, T., LEVENTHAL, C., BAILEY, A., HARRINGTON, J. & BENNANI, Y. L. 2005. The identification and optimization of a N-hydroxy urea series of flap endonuclease 1 inhibitors. *Bioorg Med Chem Lett,* 15**,** 277-81.

VAN HOOF, A., FRISCHMEYER, P. A., DIETZ, H. C. & PARKER, R. 2002. Exosome-mediated recognition and degradation of mRNAs lacking a termination codon. *Science,* 295**,** 2262-4.

VEDADI, M., NIESEN, F. H., ALLALI-HASSANI, A., FEDOROV, O. Y., FINERTY, P. J., JR., WASNEY, G. A., YEUNG, R., ARROWSMITH, C., BALL, L. J., BERGLUND, H., HUI, R., MARSDEN, B. D., NORDLUND, P., SUNDSTROM, M., WEIGELT, J. & EDWARDS, A. M. 2006. Chemical screening methods to identify ligands that promote protein stability, protein crystallization, and structure determination. *Proc Natl Acad Sci U S A,* 103**,** 15835-40.

VISWANATHAN, P., CHEN, J., CHIANG, Y. C. & DENIS, C. L. 2003. Identification of multiple RNA features that influence CCR4 deadenylation activity. *J Biol Chem,* 278**,** 14949-55.

WAGENER, N., BULKESCHER, J., MACHER-GOEPPINGER, S., KARAPANAGIOTOU-SCHENKEL, I., HATIBOGLU, G., ABDEL-RAHIM, M., ABOL- ENEIN, H., GHONEIM, M. A., BASTIAN, P. J., MÜLLER, S. C., HAFERKAMP, A., HOHENFELLNER, M., HOPPE-SEYLER, F. & HOPPE-SEYLER, K. 2013. Endogenous BTG2 expression stimulates migration of bladder cancer cells and correlates with poor clinical prognosis for bladder cancer patients. *British Journal of Cancer,* 108**,** 973-982.

WAHLE, E. & WINKLER, G. S. 2013. RNA decay machines: deadenylation by the Ccr4-not and Pan2-Pan3 complexes. *Biochim Biophys Acta,* 1829**,** 561-70.

WAN, K. F., WANG, S., BROWN, C. J., YU, V. C., ENTZEROTH, M., LANE, D. P. & LEE, M. A. 2009. Differential scanning fluorimetry as secondary screening platform for small molecule inhibitors of Bcl-XL. *Cell Cycle,* 8**,** 3943-52.

WANG, H., MORITA, M., YANG, X., SUZUKI, T., YANG, W., WANG, J., ITO, K., WANG, Q., ZHAO, C., BARTLAM, M., YAMAMOTO, T. & RAO, Z. 2010a. Crystal structure of the human CNOT6L nuclease domain reveals strict poly(A) substrate specificity. *EMBO J,* 29**,** 2566-76.

WASHIO-OIKAWA, K., NAKAMURA, T., USUI, M., YONEDA, M., EZURA, Y., ISHIKAWA, I., NAKASHIMA, K., NODA, T., YAMAMOTO, T. & NODA, M. 2007. Cnot7-null mice exhibit high bone mass phenotype and modulation of BMP actions. *J Bone Miner Res,* 22**,** 1217-23.

WILUSZ, C. J., GAO, M., JONES, C. L., WILUSZ, J. & PELTZ, S. W. 2001. Poly(A)-binding proteins regulate both mRNA deadenylation and decapping in yeast cytoplasmic extracts. *RNA,* 7**,** 1416-24.

WINKLER, G. S. 2010. The mammalian anti-proliferative BTG/Tob protein family. *J Cell Physiol,* 222**,** 66-72.

WINKLER, G. S. & BALACCO, D. L. 2013. Heterogeneity and complexity within the nuclease module of the Ccr4-Not complex. *Front Genet,* 4**,** 296.

WOLF, J. & PASSMORE, L. A. 2014. mRNA deadenylation by Pan2-Pan3. *Biochem Soc Trans,* 42**,** 184-7.

WOOD, E. R., BLEDSOE, R., CHAI, J., DAKA, P., DENG, H., DING, Y., HARRIS-GURLEY, S., KRYN, L. H., NARTEY, E., NICHOLS, J., NOLTE, R. T., PRABHU, N., RISE, C., SHEAHAN, T., SHOTWELL, J. B., SMITH, D., TAI,

V., TAYLOR, J. D., TOMBERLIN, G., WANG, L., WISELY, B., YOU, S., XIA, B. & DICKSON, H. 2015. The Role of Phosphodiesterase 12 (PDE12) as a Negative Regulator of the Innate Immune Response and the Discovery of Antiviral Inhibitors. *The Journal of Biological Chemistry,* 290**,** 19681-19696.

WU, M., REUTER, M., LILIE, H., LIU, Y., WAHLE, E. & SONG, H. 2005. Structural insight into poly(A) binding and catalytic mechanism of human PARN. *Embo j,* 24**,** 4082-93.

WU, X. & BREWER, G. 2012. The regulation of mRNA stability in mammalian cells: 2.0. *Gene,* 500**,** 10-21.

XU, K., BAI, Y., ZHANG, A., ZHANG, Q. & BARTLAM, M. G. 2014. Insights into the structure and architecture of the CCR4–NOT complex. *Frontiers in Genetics,* 5**,** 137.

YAMASHITA, A., CHANG, T. C., YAMASHITA, Y., ZHU, W., ZHONG, Z., CHEN, C. Y. & SHYU, A. B. 2005. Concerted action of poly(A) nucleases and decapping enzyme in mammalian mRNA turnover. *Nat Struct Mol Biol,* 12**,** 1054-63.

YANG, W. H., YU, J. H., GULICK, T., BLOCH, K. D. & BLOCH, D. B. 2006. RNA-associated protein 55 (RAP55) localizes to mRNA processing bodies and stress granules. *Rna,* 12**,** 547-54.

YANG, X., MORITA, M., WANG, H., SUZUKI, T., YANG, W., LUO, Y., ZHAO, C., YU, Y., BARTLAM, M., YAMAMOTO, T. & RAO, Z. 2008. Crystal structures of human BTG2 and mouse TIS21 involved in suppression of CAF1 deadenylase activity. *Nucleic Acids Res,* 36**,** 6872-81.

YATES, C. M., FILIPPIS, I., KELLEY, L. A. & STERNBERG, M. J. E. 2014. SuSPect: Enhanced Prediction of Single Amino Acid Variant (SAV) Phenotype Using Network Features. *Journal of Molecular Biology,* 426**,** 2692-2701.

YONEDA, M., SUZUKI, T., NAKAMURA, T., AJIMA, R., YOSHIDA, Y., KAKUTA, S., KATSUKO, S., IWAKURA, Y., SHIBUTANI, M., MITSUMORI, K., YOKOTA, J. & YAMAMOTO, T. 2009. Deficiency of antiproliferative family protein Ana correlates with development of lung adenocarcinoma. *Cancer Sci,* 100**,** 225-32.

YOSHIDA, Y., NAKAMURA, T., KOMODA, M., SATOH, H., SUZUKI, T., TSUZUKU, J. K., MIYASAKA, T., YOSHIDA, E. H., UMEMORI, H., KUNISAKI, R. K., TANI, K., ISHII, S., MORI, S., SUGANUMA, M., NODA, T. & YAMAMOTO, T. 2003. Mice lacking a transcriptional corepressor Tob are predisposed to cancer. *Genes Dev,* 17**,** 1201-6.

YU, J. H., YANG, W. H., GULICK, T., BLOCH, K. D. & BLOCH, D. B. 2005. Ge-1 is a central component of the mammalian cytoplasmic mRNA processing body. *Rna,* 11**,** 1795-802.

ZHANG, J.-H., CHUNG, T. D. Y. & OLDENBURG, K. R. 1999. A Simple Statistical Parameter for Use in Evaluation and Validation of High Throughput Screening Assays. *Journal of Biomolecular Screening,* 4**,** 67-73.

ZHANG, J., SUN, X., QIAN, Y., LADUCA, J. P. & MAQUAT, L. E. 1998. At least one intron is required for the nonsense-mediated decay of

triosephosphate isomerase mRNA: a possible link between nuclear splicing and cytoplasmic translation. *Mol Cell Biol,* 18**,** 5272-83.

ZHANG, Y. J., WEI, L., LIU, M., LI, J., ZHENG, Y. Q., GAO, Y. & LI, X. R. 2013. BTG2 inhibits the proliferation, invasion, and apoptosis of MDA-MB-231 triple-negative breast cancer cells. *Tumour Biol,* 34**,** 1605-13.

ZHANG, Z., CHEN, C., WANG, G., YANG, Z., SAN, J., ZHENG, J., LI, Q., LUO, X., HU, Q., LI, Z. & WANG, D. 2011. Aberrant expression of the p53-inducible antiproliferative gene BTG2 in hepatocellular carcinoma is associated with overexpression of the cell cycle-related proteins. *Cell Biochem Biophys,* 61**,** 83-91.

ZHANG, Z., THELER, D., KAMINSKA, K. H., HILLER, M., DE LA GRANGE, P., PUDIMAT, R., RAFALSKA, I., HEINRICH, B., BUJNICKI, J. M., ALLAIN, F. H. & STAMM, S. 2010. The YTH domain is a novel RNA binding domain. *J Biol Chem,* 285**,** 14701-10.